



**TARGETING c-MET IN SONIC  
HEDGEHOG MEDULLOBLASTOMAS**

**SONIA MORLANDO**

**School of Science, Engineering and Environment,  
University of Salford, Salford, UK**

Submitted in partial fulfilment of the requirements for the Degree of  
Doctor of Philosophy, 2022

## Table of contents

LIST OF FIGURES.....	V
LIST OF TABLES .....	VIII
ACKNOWLEDGMENTS .....	IX
DECLARATION.....	X
RESEARCH PUBLICATIONS AND CONFERENCES.....	XI
LIST OF ABBREVIATIONS.....	XII
ABSTRACT.....	1
<b>CHAPTER 1: Introduction.....</b>	<b>3</b>
1.1 Fundamentals of cancer.....	4
1.2 Medulloblastoma: general overview.....	6
1.2.1 Medulloblastoma histological classification.....	7
1.2.2 Medulloblastoma molecular subgroups.....	8
1.2.3 Wingless (WNT) medulloblastomas.....	10
1.2.4 Sonic Hedgehog (SHH) medulloblastomas .....	10
1.2.5 Group 3 medulloblastoma .....	11
1.2.6 Group 4 medulloblastoma .....	12
1.2.7 Medulloblastoma diagnosis and therapeutic approaches .....	13
1.3 Receptor tyrosine kinases (RTKs) and their role in cancer.....	16
1.4 Scatter factor/Hepatocyte growth factor (SF/HGF)-c-MET signalling.....	18
1.4.1 SF/HGF-c-MET dysregulation in cancer .....	21
1.4.2 Therapeutic strategies against SF-HGF/c-MET kinase signalling.....	23
1.4.3 Role of c-MET pathway in cerebellar development and medulloblastoma .....	26
1.4.4 SF-HGF/MET signalling and Sonic Hedgehog medulloblastoma .....	28
<b>CHAPTER 2: Materials and methods.....</b>	<b>30</b>
2.1 Cell lines and culture methods .....	31
2.2 <i>In silico</i> analysis by querying R2 database.....	31
2.2 Inhibitors.....	32

2.3 Cell viability assay by MTT .....	34
2.3 Stimulation of SHH-MB cell lines with Hepatocyte Growth Factor (HGF).....	34
2.4 Long-term viability assay .....	35
2.5 Synergy study for combination treatments .....	35
2.5 Colony formation assay .....	36
2.6 Neurosphere formation assay .....	37
2.7 3-D spheroids model .....	37
2.8 Cell cycle analysis by Flow Cytometry .....	38
2.9 Apoptosis assay by Caspase 3/7 detection .....	39
2.10 siRNA transfection .....	39
2.11 Establishment of H2B-GFP stable cell lines .....	39
2.12 Cell fate analysis by automated time-lapse microscopy .....	40
2.13 Protein extraction and Western blot analysis .....	42
2.14 Data manipulation and Statistical analysis.....	43
<b>CHAPTER 3: Aims and Objectives.....</b>	<b>44</b>
<b>CHAPTER 4: Results.....</b>	<b>47</b>
4.1 c-MET kinase is a suitable RTK therapeutic target in SHH medulloblastoma .....	48
4.2 c-MET expression and prognostic significance in MB subtypes.....	51
4.2 c-MET kinase pathway activation in SHH MB cell lines .....	55
4.3 Tivantinib suppresses proliferation of SHH 2D and 3D models of MB cell lines.....	59
4.5 c-MET inhibitors differences in regulating cell cycle distribution .....	67
4.7 Tivantinib affects long-term cell viability, colony formation and stemness in SHH cell lines.....	71
4.8 Heterogeneous post-mitotic cell fate response to c-MET inhibitors in SHH MB cells .....	76
4.9 Tivantinib induces MCL-1 downregulation and PARP cleavage in DAOY cells.....	83
4.10 c-MET signalling in DAOY cells after treatment with crizotinib and tivantinib .....	86
4.11 Tivantinib synergises with vincristine in the killing of DAOY cells.....	89
4.12 Targeting BCL-2 family induces death in foretinib-treated cells.....	95
4.13 Enhanced MET signalling in vincristine-resistant MB cells.....	100

4.14 Tivantinib and mTOR inhibitors synergistically affect DAOY proliferation .....	104
<b>CHAPTER 5: Discussion.....</b>	<b>108</b>
5.1 General discussion.....	109
5.2 Conclusions and future directions.....	116
<b>Chapter 6: Supplementary .....</b>	<b>118</b>
Supplementary 1. Growth rate for ONS76-derived 3-D spheroids.....	119
Supplementary 2. Enlarged images for DAOY and ONS76 medullospheres.....	120
Supplementary 3. Cell fate analysis on UW228 treated with tivantinib and foretinib.....	121
Supplementary 4. Mitosis length in UW228 upon foretinib and tivantinib treatments.....	122
Supplementary Figure 5: MCL-1 downregulation in UW228 cells after tivantinib treatment.....	123
Supplementary Figure 6. CyclinB1 levels in DAOY serum-starved cells.....	124
Supplementary Figure 7. Unprocessed western blot showed in Figure 12 .....	125
Supplementary Figure 8. Unprocessed western blot showed in Figure 14 .....	126
Supplementary Figure 9. Unprocessed western blot showed in Figure 30 .....	127
Supplementary Figure 10. Unprocessed western blot showed in Figure 31 .....	128
Supplementary Figure 11. Unprocessed western blot showed in Figure 37 .....	129
Supplementary Figure 11. Unprocessed western blot showed in Figure 35 .....	130
Supplementary Figure 12. Unprocessed western blot showed in Figure 40 .....	131
<b>BIBLIOGRAPHY .....</b>	<b>132</b>

## LIST OF FIGURES

Figure 1: Number of cancer cases and deaths in UK estimated in 2020 .....	4
Figure 2: Timeline of hallmarks of cancer updates.....	6
Figure 3: Histological variants of medulloblastoma .....	8
Figure 4: Schematic representation of SF-HGF/MET pathway and signalling effects.....	20
Figure 5: Structures of selected inhibitors used in the study .....	33
Figure 6: Workflow of combinatorial treatments.....	36
Figure 7: Representative pictures of spheroids post-seeding and after 5 days .....	38
Figure 8: Schematic view of cell fate decisions upon drugs treatment.....	41
Figure 9: RTKs and MET gene expression in medulloblastoma .....	52
Figure 10: c-MET kinase association with survival in MB patients .....	53
Figure 11: Kaplan-Meier survival curves based on c-MET expression across MB subtypes ...	54
Figure 12: c-MET kinase activation study in MB SHH cell lines .....	57
Figure 13: Growth rate of SHH cell lines after HGF stimulation .....	58
Figure 14: siRNA-mediated c-MET knockdown impairs DAOY cell proliferation .....	58
Figure 15: Anti-proliferative effects of MET inhibitors on SHH cell lines .....	60
Figure 16: Bright-field pictures of DAOY and ONS76 upon treatment with tivantinib, foretinib and crizotinib .....	62
Figure 17: Proliferation rates upon treatment with tivantinib in SHH-MB cells .....	63
Figure 18: c-MET kinase inhibitors ability to hamper 3D spheroid's structure.....	65
Figure 19: Preliminary data on ONS76 3-D spheroids after 9 days treatment with c-MET inhibitors .....	66
Figure 20: Cell cycle analysis upon treatment with tivantinib, foretinib and crizotinib.....	68
Figure 21: Activation of apoptosis upon treatment with tivantinib, foretinib and crizotinib.	70
Figure 22: Caspase 3/7 activation in 3D DAOY spheroids treated with tivantinib .....	71

Figure 23: Long-term tivantinib effects on SHH cell lines.....	72
Figure 24: Tivantinib effects on colony formation ability in DAOY and ONS76 cells .....	74
Figure 25: Medullosphere formation upon tivantinib treatment in DAOY and ONS76 cells ..	75
Figure 26: Representative pictures of cell fate response visualized in H2B-GFB expressing DAOY and ONS76 .....	77
Figure 27: Cell fate decisions upon c-MET inhibitors treatment in DAOY.....	80
Figure 28: Cell fate profiles upon c-MET inhibitors treatment in ONS76.....	81
Figure 29: DAOY and ONS76 cell sizes upon 120h treatment with foretinib .....	82
Figure 30: Mitosis time length upon tivantinib, foretinib and crizotinib treatment .....	83
Figure 31: c-MET kinase inhibitors effects on PARP1, MCL-1 and Cyclin B1 expression.....	85
Figure 32: c-MET kinase role in tivantinib-induced effects on DAOY cells.....	87
Figure 33: Cell fate profiles upon c-MET kinase knockdown in DAOY.....	88
Figure 34: Synergistic effects of tivantinib and vincristine on DAOY and ONS76 cell proliferation .....	90
Figure 35: PARP1 cleavage upon combination treatment with vincristine and tivantinib .....	92
Figure 36: Combination treatment with vincristine and tivantinib on DAOY 3D spheroids ...	93
Figure 37: Caspase 3/7 activation in DAOY spheroids treated with vincristine and tivantinib combination .....	94
Figure 38: BH3-mimetics in combination with foretinib in ONS76 and DAOY cells .....	96
Figure 39: Anti-proliferative effects of BCL-2 family inhibitors on foretinib-treated DAOY and ONS76 .....	98
Figure 40: PARP cleavage upon treatment with navitoclax in DAOY and ONS76 pre-treated with foretinib .....	99
Figure 41: c-MET kinase pathway activation in vincristine resistant DAOY .....	101
Figure 42: c-MET kinase inhibitors effects on DAOY vincristine resistant.....	103
Figure 43: Tivantinib and BEZ235 synergistic effects on DAOY cell proliferation .....	106

Figure 44: Effects of dual combination with mTOR inhibitors and tivantinib in 3D spheroids  
.....107

## LIST OF TABLES

Table 1: Molecular features of MBs subgroups (Liu et al., 2017) .....	9
Table 2: RTKs inhibitors approved by FDA. List adapted from (Bhullar et al., 2018) .....	17
Table 3: List of small-molecules c-MET kinase inhibitors .....	25
Table 4: Gene expression datasets interrogated through R2 platform.....	31
Table 5: Literature review outputs on RTKs in medulloblastoma .....	49
Table 6: IC <sub>50</sub> values calculated for each c-MET inhibitor .....	61

## ACKNOWLEDGMENTS

I would like to thank all the people that shared this journey with me. This PhD has been an emotional roller-coaster and I was lucky enough not to be alone, but surrounded by amazing people:

Thanks to my supervisors: Dr. Gianpiero Di Leva for giving me the opportunity of joining his lab at very beginning, for guiding me and teaching me, for all the help and the advice during these challenging years; Dr. James Wilkinson and Dr. Caroline Topham, thank you for the support and for always being there when I needed.

Professor Divya Chari, thank you for giving me the chance to work with you. It has been an honour, and I am very grateful to have met you during my research and life path. All the NTEK laboratory at the University of Keele, with a special mention to Bushra, for being so kind with me.

Most of all, my entire family, my mum and dad for being always my safe place; if I have the chance to be here to discover myself and to explore all my possibilities away from home, it is only because of you two. My brothers, for loving me unconditionally.

Daniele, I feel so lucky for having you by my side. Thank you for being so loving and caring even if I am not the easiest person to deal with. I cannot wait to see what the future has reserved for us.

All my friends from Salford University (such a long list): Chiara, my little tuppino, thanks for being there all the time and for the strong “shaking” in my bad days, I am very lucky to be your friend; Filippo, no sweet words for you but only thanks for everything; Fanni, thanks for our “complain corner”, it saved most of my days in the lab, and for sharing this path with me from the very beginning; Camillo, Marco, Gloria, Toby, Grace, Somnya and all the people in Salford that supported me during these years.

Marta, thanks for being there until the end (almost), for helping me through the difficulties with your shoulder ready for my tears (Yes. I cry a lot under pressure). But most of all, thanks for all the beautiful things that we shared in these years.

All my friends from Italy, thanks because I understood that no distance is long enough if you care and love someone.

## **DECLARATION**

This research project has been funded by Kidscan for a period of three years in order to obtain the Award of the degree of Doctor of Philosophy at University of Salford. The experiments and the data presented in the study have been performed and collected by the author of this thesis. No parts of this thesis have been submitted to apply for other degrees neither in this nor other universities.

## RESEARCH PUBLICATIONS AND CONFERENCES

### RESEARCH PUBLICATIONS

- Marta Buzzetti \*, **Sonia Morlando** \*, Dimitrios Solomos, Ammara Mehmood, Alexander W.I.Cox , Mattia Chiesa, Yuri D’Alessandra, Michela Garofalo, Caroline Topham, Gianpiero di Leva: Pre-therapeutic efficacy of the CDK inhibitor dinaciclin in medulloblastoma cells. *Scientific Reports* (2020) <https://doi.org/10.1038/s41598-021-84082-3>
- Francesca Puca, Nadia Tosti, Antonella Federico, Yalcin Kuzay, Anna Pepe, **Sonia Morlando**, Teresa Savarese, Federica D’Alessio, Marianna Colomaio, Daniela Sarnataro, Sihana Ziberi, Marco De Martino, Alfredo Fusco, Sabrina Battista: HMGA1 negatively regulates NUMB expression at transcriptional and post transcriptional level in glioblastoma stem cells. *Cell cycle* (2019) <https://doi.org/10.1080/15384101.2019.1618541>

### CONFERENCES

- EACR Annual Congress (Seville 20-23<sup>th</sup>June 2022): Abstract accepted for poster presentation: “Heterogeneous response to c-MET inhibitors in SHH medulloblastoma cells”
- International PGR conference (University of Salford 5-7<sup>th</sup>April 2022): Oral presentation
- EACR Annual Congress (Virtual Attendance June 2020)
- Salford Postgraduate Annual Research Conference (SPARC) (July 2019): Poster presentation

## **LIST OF ABBREVIATIONS**

BCL-2: B-cell lymphoma 2

BET: Bromodomain and extra terminal proteins

CGH: Comparative Genomic Hybridization

CI: Combination index

CSC: Cancer stem cell

CNS: Central Nervous System

DMSO: dimethyl sulfoxide

ET: Embryonal tumour

FDA: Food and Drug Administration

GNP: Granule Cell Precursors

HGF: Hepatocyte Growth Factor

IC<sub>50</sub>: 50% inhibitory concentration effects

kDa: kilo Dalton

MAPK: mitogen-activated protein kinase

MB: Medulloblastoma

MCL-1: Myeloid cell leukemia 1

NGF: Nerve growth factor

OS: Overall Survival

PARP: Poly-ADP ribose polymerase

PI: Propidium Iodide

PI3K: Phosphoinositide 3-kinase

PVDF: Polyvinylidene difluoride

RTK: Receptor tyrosine Kinase

SD: Standard Deviation

SDS-PAGE: Sodium dodecyl-sulphate polyacrylamide gel electrophoresis

SF: Scatter Factor

siRNA: small interfering RNA

SHH: Sonic Hedgehog

SMO: Smoothened

WHO: World Health Organisation

WNT: Wingless

## ABSTRACT

Medulloblastoma (MB), a cerebellar tumour primarily diagnosed in children, is the most common malignant brain tumour consisting of four molecular subgroups: Wingless (WNT), Sonic Hedgehog (SHH), Group 3 and Group 4. Although the 70-75% of MB patients survive the disease, the current therapeutic regimen, which comprises surgical resection, chemotherapy and cranial irradiation, is worryingly associated with severe side effects in these young patients. Thus, identifying new and more precise therapeutic strategies is needed to overcome medulloblastoma progression and dissemination as well as the eradication of the disease. Over the last few years, various tyrosine kinase signalling pathways have been identified to play important roles in medulloblastoma tumorigenesis. Active c-MET kinase has been detected as a marker of SHH-driven MB and several inhibitors provided pre-clinical evidence for an effective therapy for SHH-MB patients.

In this PhD project, we firstly confirmed that c-MET is highly expressed in SHH MBs; next, the efficacy of multiple commercially available c-MET kinase inhibitors against several *in vitro* SHH-MB cell lines was evaluated to identify the most potent in the MB cells context and to provide a detailed explanation of how they induce cell death in MB cells.

We showed that the highly selective c-MET inhibitor tivantinib outperformed the c-MET inhibitors foretinib and crizotinib in impairing cell viability in both 2D and 3D cell models by inducing a strong apoptotic response, which was more prominent in *TP53*<sup>-/-</sup> MB SHH cells compared to *TP53*<sup>wt</sup> cells, where it showed primarily mitotic delay. We observed a complex and diverse pharmacological response to c-MET inhibitors; while tivantinib strongly induce mitotic cell death, through downregulation of MCL-1 protein, foretinib and crizotinib causes mitotic slippage, phenomenon frequently correlated to aneuploidy and drug-resistance. However, we demonstrated that use of BH-3 mimetics can reverse this effect and cause cell death. Taken together, this first set of data substantiate the rational use of c-MET inhibitors for SHH-driven MB but the pharmacological heterogeneity in response to c-MET inhibitors should be highly considered when designing novel effective therapies for MBs.

Finally, we demonstrated that tivantinib had synergistic anti-proliferative *in vitro* SHH-MB cells effects, when combined with either first-line chemotherapy for MB or small-molecule,

supporting the possibility of new therapeutic approaches aimed to lower doses of drugs and to limit drug toxicities as well as side effects.

# ***CHAPTER 1: Introduction***

## 1.1 Fundamentals of cancer

To date, according to the World Health Organization (WHO), cancer is the second leading cause of mortality around the world, and it accounted for nearly ten million deaths in 2020 (Ferlay et al., 2021). In the United Kingdom (UK), nearly 400,000 cases of cancer are diagnosed every year and the mortality rate is worryingly high (around 450 cancer-related deaths are registered every day) (Cancer UK Statistics, 2016-2018). Distribution and incidence of difference cancer types in UK are summarized in the pie charts in Figure 1.

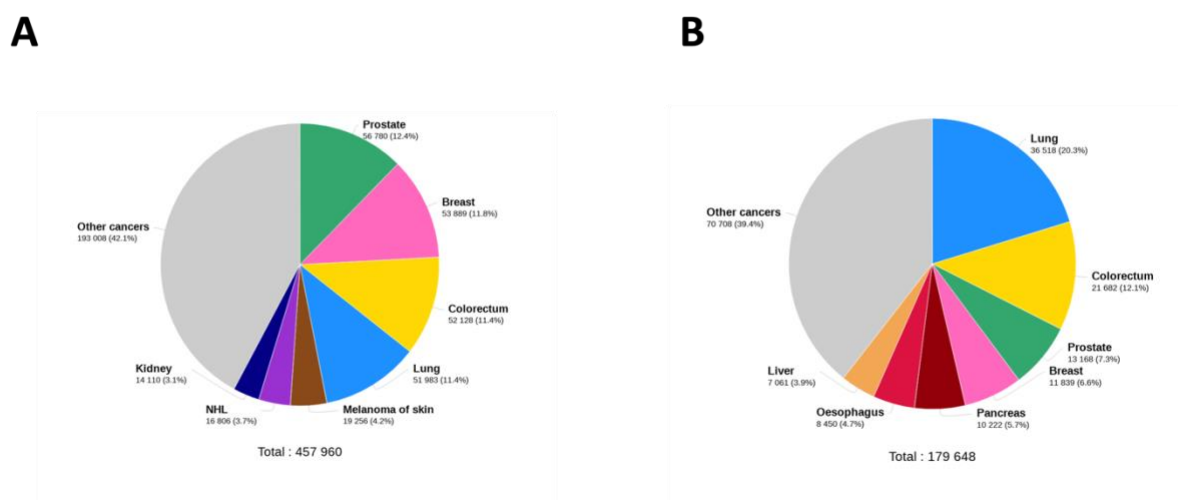


**Figure 1: Number of cancer cases and deaths in UK estimated in 2020**

A-B) Pie charts are referred to the estimated new cases (A) and number of deaths (B) in 2020 in UK. Graphs were generated on the International Agency for Research on Cancer website (<https://gco.iarc.fr/today/home>)(Ferlay et al., 2021)

The term cancer comprises almost 300 different types that arise from cell types and organs all over the body (Stratton et al., 2009). Generally, cancer initiation is a result of several genetic alterations that cause a single cell, the so-called malignant cell, to aberrantly proliferate and establish a population of tumour cells which can potentially invade tissues and metastasize. With the term “neoplasm” (from the Greek word “new growth”), we indicate both malign and benign tumours; benign tumours occur when the neoplastic cell does not acquire invasive phenotype otherwise, together with many other it is classified as malignant (Hassanpour & Dehghani, 2017).

As mentioned before, cancer is a final response to a series of mutations, named driver-mutations, which confer advantage in terms of cell growth. Passenger mutations were also identified within tumours by genome sequencing, but they do not contribute to cancer initiation and progression (Greenman et al., 2007). Mutations of two different groups of cancer-related genes, referred to as oncogenes and onco-suppressors, are implicated in malignant transformation and they arise in response to different factors, both exogenous (e.g. exposure to chemicals, ultraviolet (UV) light, viruses such as human papilloma virus or Epstein Barr virus) and endogenous (errors during mitosis, enzymatic deregulation of DNA repair or genome editing) (Martincorena & Campbell, 2015).

In terms of cellular phenotype, cancer cells can be described by a set of biological and functional capabilities, called the hallmarks of cancer, required to sustain the transformation from a normal to a malignant cell. Originally, only six hallmarks were proposed: sustaining proliferative signalling, resisting cell death, evading growth suppressors, inducing angiogenesis, enabling replicative immortality and activating invasion and metastasis) (Hanahan & Weinberg, 2000). However, in 2011 deregulated cellular energetics together with the avoiding of immune system were proved to play a crucial role in the development of cancer and thus, proposed as two emerging hallmarks of cancer (Hanahan & Weinberg, 2011). It is well known that cancer is an extremely complex disease and possibly, cancer research is a never-ending story, as clearly summarised in Figure 2. The remarkable progress made in the last decade in the understanding of cancer pathogenesis led to a further update of the hallmarks. In the 2022, the emerging hallmarks proposed in 2011 were confirmed as hallmarks of cancer and further, four new additions were advised as a new integration to the core hallmarks: cellular plasticity, nonmutation epigenetic reprogramming, microbiomes and senescent cells. Even though, these processes clearly contribute to malignancy progression, they are still considered emerging and not fully comprised in the classification (Hanahan, 2022). Nowadays, worldwide researchers are studying new effective approaches for cancer treatments. Unfortunately, as mentioned above, an upsettingly amount of people die from cancer every day. In most of the cases, cancer is treated with highly toxic drugs which affect long-term quality of life of patients; thus, targeted therapies aimed at affecting exclusively cancerous cells without affecting normal tissues are always needed to improve anti-cancer strategies.

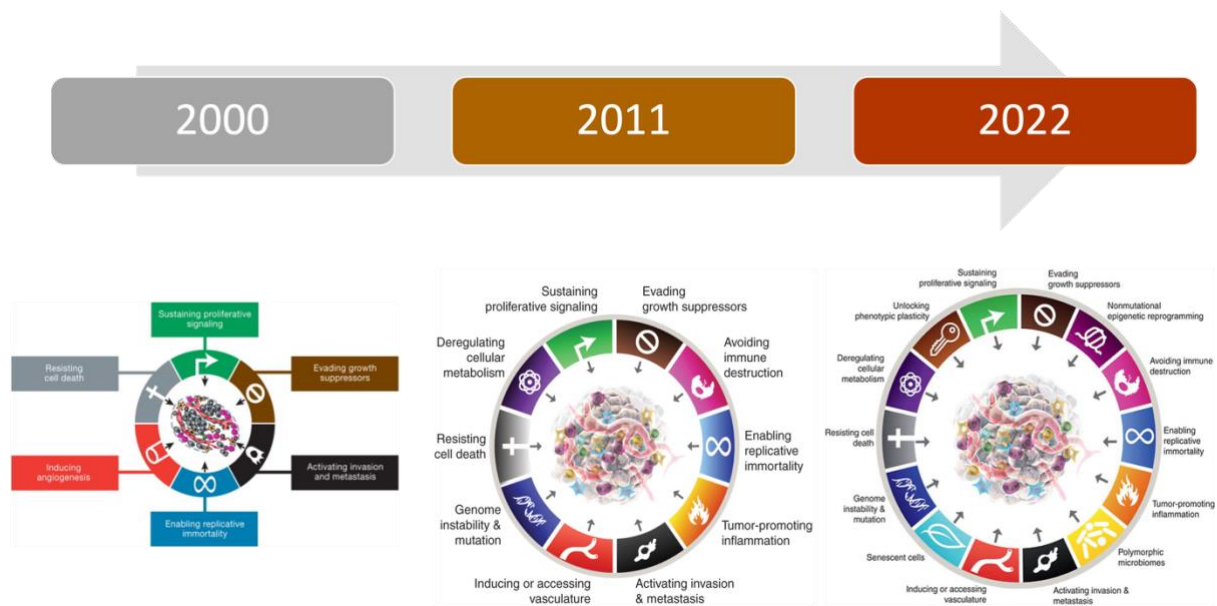


**Figure 2: Timeline of hallmarks of cancer updates**

Hallmarks of cancer were updated in the last two decades based on the latest discoveries in cancer research and graphically provided by Hanahan et al. Figure adapted from (Hanahan, 2022; Hanahan & Weinberg, 2000, 2011)

## 1.2 Medulloblastoma: general overview

Childhood tumours represent less than 1% of all the diagnosed tumours in UK (CRUK 2021, [www.cancerresearchuk.org/](http://www.cancerresearchuk.org/)). Only second to leukaemia in terms of incidence, embryonal tumours (ETs) of the Central Nervous System (CNS), are reported as nearly a third of all childhood cancer-related deaths (Zahnreich & Schmidberger, 2021). These high-grade malignancies include medulloblastomas, CNS neuroblastoma, pineoblastoma and others (Blessing & Alexandrescu, 2020).

Medulloblastoma (MB) is the most frequent high-grade embryonal brain tumour during childhood, and it accounts for 15-20% of all the diagnosed brain cancers in children (Thorbinson and Kilday, 2021). MB widely occurs in the first decade of life with a high incidence between 3 and 4 years of age and between 8 and 10 years; even though incidence of medulloblastoma significantly decreases with age, MB can rarely be diagnosed in adults. Furthermore, in concordance with the registered cases MB is slightly more common in males than in females (Millard et al., 2016). In the last decades, insights from epigenetic and

transcriptional analysis on medulloblastoma primary samples identified discrete molecular entities within medulloblastoma; in 2012 a consensus paper classified medulloblastoma in four distinct subgroups (Wingless, Sonic-Hedgehog, Group 3 and Group 4 MBs) based on molecular studies (Taylor et al., 2012). The high-level of intra-tumour heterogeneity emphasized the need to consider molecular signatures, together with the histology, when diagnosing and treating medulloblastoma. To date, according to the 2021 WHO classification of central nervous system (CNS) tumours medulloblastoma is classified based on histology (*MB histologically defined*) and molecular characteristics (*MB genetically defined*) (Louis et al., 2021).

### **1.2.1 Medulloblastoma histological classification**

Histologically, MBs is classified as classic medulloblastoma, desmoplastic/nodular medulloblastoma (D/N), medulloblastoma with extensive nodularity (MBEN) or large/anaplastic medulloblastoma (LCA) (Ellison, 2010; Louis et al., 2016; Millard & De Braganca, 2016). In detail, classic variant medulloblastomas are reported as the 72% of all the diagnosed MBs. They present small and round nuclei, minimal cytoplasm and low mitotic activity (Figure 3A). (Louis et al., 2016; Orr, 2020). In contrast to the classic variant, desmoplastic/nodular MB represents 10% of MBs. This variant presents nodular and reticulin-poor islands of neurocytic differentiation with highly active mitotic cells (Figure 3B) (Millard et al., 2016). Desmoplasia is defined as pericellular deposition of collagen and represents a reactive phenomenon when MB cells are spread in the leptomeninges. MBEN variant is defined as special variant of D/N MB, and it is dominated by nodules connected by neurocytic cells (Ellison, 2010; Millard et al., 2016; Orr, 2020). Finally, large cell and anaplastic MBs (Figure 3C) account for 17% of all the MBs (Ellison,2010). At the beginning those two variants were described as distinct. On one hand, large cells are described as increased in cell size and with round cell morphology. On the other hand, anaplasia is characterized by increased nuclear size, high number of mitoses and presence of apoptotic bodies (Giangaspero et al., 1992; Erhart et al., 2002). Regions of anaplasia can be observed in classic medulloblastoma and, rarely in desmoplastic medulloblastoma (Giangaspero et al., 2006). Given that anaplastic features, such as frequent mitotic activity and apoptosis, are commonly found associated with large cells, the two variants were combined according to the WHO classification (Gilbertson

and Ellison, 2008; Louis et al., 2016; (Louis et al., 2021). Identification of histological variants plays a crucial role in the MB diagnosis as well as in risk stratification.

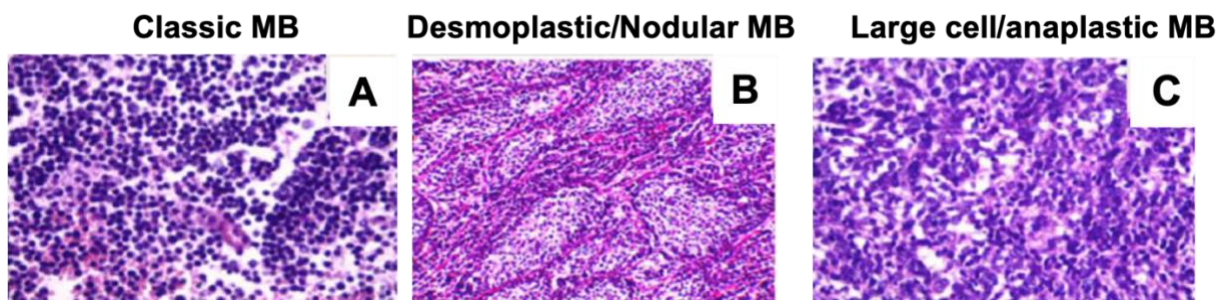


**Figure 3: Histological variants of medulloblastoma**

A-C) Hematoxylin/Eosin sections of MB samples A) Undifferentiated and small cells, characterize classic medulloblastoma. B) Nodules of cells and internodular desmoplasia define desmoplastic/nodular (D/N) MB C) Apoptotic bodies and enlarged cell phenotype are characteristic of large cell/anaplastic (LCA) MB. Figure was adapted from Eid & Heabah (Eid & Heabah, 2021)

### 1.2.2 Medulloblastoma molecular subgroups

One of the most remarkable features of medulloblastoma is the high intra-tumour heterogeneity. A high number of efforts are currently ongoing to better characterize medulloblastomas at molecular level. MBs are currently molecularly classified in: Wingless (WNT), Sonic Hedgehog (SHH), Group 3 and Group 4 (Louis et al., 2016; Louis et al., 2021; Ramaswamy et al., 2011; Taylor et al., 2012). The WNT and SHH account for 10% and the 30% respectively of all the MBs and are named after the activation of the WNT and SHH signalling pathways. The remaining 25% and 35% of all MB diagnoses are represented by Group 3 and Group 4 MBs which are indicated as non-WNT/non-SHH MBs (Hovestadt et al., 2020; Kool et al., 2012). Notably, a gene expression and DNA methylation study on a cohort of 763 medulloblastoma samples by Cavalli et al. allowed a further classification within MBs subgroups of different subtypes with unique clinical and molecular features (Cavalli et al., 2017). Interestingly, tumour location was observed to be predictive of molecular subgroups. WNT tumours tend to arise in the cerebellopontine angle (CPA), while SHH are frequently found in the cerebellar hemisphere. Group 3 and 4 MBs are mainly located in the fourth ventricle (Perreault et al., 2014). Importantly, the insight into the differences in epigenetic and transcriptional profiles between subgroups as well as the advent of single-cell RNA sequencing methods, suggested that different subgroups have different cellular origin (Azzarelli et al., 2018; Gilbertson & Ellison, 2008) further confirming the high degree of

heterogeneity within these tumours. Generally, MB is thought to have its origin in several neuronal stem and progenitor cells. (Northcott et al., 2019).

Each subgroup is well described in the following paragraphs and a detailed summary of MB subgroups features provided by Liu *et al.* is presented in Table 1 below (Liu et al., 2017).

**Table 1: Molecular features of MBs subgroups (Liu et al., 2017)**

	WNT	SHH	Group 3	Group 4
<b>Demographics</b>				
Percentage of cases	~10%	~30%	~25%	~35%
Age distribution				
Gender Ratio				
<b>Clinical features</b>				
Histology	Classic; rarely LCA	Classic; DNMB; LCA; MBEN	Classic; LCA	Classic; rarely LCA
Incidence of metastasis	5–10%	10–15%	40–45% (50% in infants)	35–40%
Prognosis/5-year survival	Very good/>95% (80% in adults)	Intermediate/~75%	Poor/50%	Intermediate/~70% (20% in adults)
Diagnostics	Nuclear $\beta$ -catenin; CTNNB1 mut; monosomy 6; DKK exp	SFRP1, YAP1 exp; 9q loss; GLI2 amp	NPR3 exp; MYC amp	KCNA1 exp
Risk stratification biomarkers	monosomy 6 (subgroup-driven)	GLI2 amplification; 14q loss; metastatic status	MYC amplification; Iso17q; metastatic status; FSTL5 exp	11 loss or 17 gain; metastatic status; FSTL5 exp
<b>Genomic features</b>				
Cytogenetics	chr 6 loss	chr 3q, 9p gain; 9q, 10q, 14q, 17p loss	chr 1q, 7, 17q, 18 gain; 8, 10q, 11, 16q, 17p loss; iso17q	chr 4, 7, 17q, 18 gain; 8, 10, 11, 17p, X loss; iso17q
Mutations (SNVs or indels)	CTNNB1, DDX3X, SMARCA4, TP53, KMT2D, CSNK2B, CREBBP, MLL2	PTCH1, SMO, SUFU, MLL2, DDX3X, KMT2D, TP53, BCOR, LDB1, NCOR2, TCF4, GABRG1	SMARCA4, MLL2, SPTB, CTDNEP1, LRP1B, TNXB, GPS2	KDM6A, MML3, HDAC2, ZMYM3, CBFA2T2, CTDNEP1
Somatic copy number alterations	No recurrent alteration	GLI1/2, MYCN, CCND2 amplification; PTCH1, TP53 deletion	MYC, OTX2 amplification; PVT1-MYC fusion	SNCAIP duplication; MYCN, CDK6, OTX2 amplification
Pathways	WNT signaling	SHH signaling	Photoreceptor/GABAergic; MYC and TGF $\beta$ signaling	Neuronal; glutamatergic; NF $\kappa$ B signaling

### 1.2.3 Wingless (WNT) medulloblastomas

WNT subgroup, as mentioned above, is the rarest subgroup of MB, and it is more common in children between 3 and 10 years and in adults rather than infants. Metastases are present in less than 10% of all the WNT diagnosed MBs and they usually exhibit classic histology. With a 98% 5-year overall survival rate, it represents a subgroup with an excellent prognosis and outcome (Kumar et al., 2020; Millard & De Braganca, 2016; Northcott et al., 2019). The first study suggesting that medulloblastoma subgroups have different cellular origins demonstrated that activating mutations of *CTNNB1* induced cells in the dorsal brain stem to aberrantly proliferate. Thus, WNT medulloblastomas are thought to originate from precursor cells in this region (Gibson et al., 2010). Genetically, nearly 90% of WNT tumours are driven by somatic activating mutation in the *CTNNB1* gene which encodes for  $\beta$ -catenin. The mutation prevents the  $\beta$ -catenin degradation by the Anaphase-promoting complex (APC) and aberrant activation of  $\beta$ -catenin leads to its constant accumulation in the nucleus resulting in up-regulation of WNT-responsive genes which causes uncontrolled cell growth and proliferation leading to cancerous phenotype (DeSouza et al., 2014; Northcott et al., 2017). In addition, the loss of one copy of the chromosome 6, also referred to as monosomy 6, is found in 83% of the WNT MB cases (Hovestadt et al., 2020; Northcott et al., 2017).

### 1.2.4 Sonic Hedgehog (SHH) medulloblastomas

SHH-driven medulloblastomas account for approximately 30% of the MB diagnoses with a peculiar and bimodal age distribution. It represents the most common subgroup in both infants and adults with events of metastasis registered in the 10-15% of the cases (Hovestadt et al., 2020). SHH-activated medulloblastomas can present different histological features; however they are mainly characterized by nodular/desmoplastic features but classic and anaplastic histology can be also frequent in these children (Table 1) (Ellison et al., 2011). SHH medulloblastomas arise from granule cell precursors (GNPs) in the external granule layer (EGL) (Schüller et al., 2008). The Hedgehog signalling pathway is a highly conserved pathway, crucial in embryonic development but mostly inactive in the adults (Skoda et al., 2018). Physiologically, SHH binds its receptor *PTCH1*, which then releases from suppression the Smoothed (SMO) protein. SMO is a transmembrane protein that promotes SUFU dissociation and activation of *GLI* genes to regulate cell growth (Ng & Curran, 2011).

Genetically, SHH MB tumours harbour somatic and germline mutations as well as copy-number alterations in the SHH pathway which lead to its hyperactivation and tumour initiation (Taylor et al., 2012). Several mutations are indicated as drivers of SHH medulloblastomas such as: germline mutations in either the patched-1 gene (*PTCH1*) or in the suppressor of fused gene (*SUFU*) in patients with Gorlin syndrome cause a genetic predisposition to medulloblastoma (Gilbertson & Ellison, 2008; Millard & De Braganca, 2016; Taylor et al., 2012) and activating mutations in Smoothed (SMO), *GLI1* or *GLI2* amplifications as well as *MYCN* amplifications. Interestingly, Northcott et al. reported alterations in the component of *TP53* signalling (such as *MDM2* amplifications and focal deletions of *TP53*) well known for its role in the control of DNA repair as well as cell cycle and apoptosis regulation (Northcott et al., 2019; Northcott et al., 2012). SHH subgroup is considered heterogenous in terms of molecular and clinical characteristics. Recently, Cavalli et al. performed a high-impact study of DNA methylation and gene expression analysis, and a high inter-tumours heterogeneity was pinpointed across SHH subgroups. Four distinct subtypes of SHH were identified (SHH $\alpha$ , SHH $\beta$ , SHH $\gamma$ , SHH $\delta$ ). SHH $\alpha$  tumours affect mostly children in the age between 3 and 16 years and are associated with poorer prognosis compared to SHH $\delta$ . These tumours are enriched for *MYCN* amplifications, *GLI2* amplifications and *TP53* mutations, all features previously related to very high-risk category of medulloblastomas (Cavalli et al., 2017; Louis et al., 2016; Ramaswamy et al., 2011). Generally, SHH $\beta$  occurs mostly in infants and it has the lowest 5-years overall survival (OS) (67%) compared to the other subtypes (Cavalli et al., 2017; Hovestadt et al., 2020).

### **1.2.5 Group 3 medulloblastoma**

Group 3 MB occurs primarily in infants and during childhood with LCA histology and metastases at the diagnosis (Taylor et al., 2012). One of the most important features of Group 3 MB is the *MYC* amplification which appears in nearly the 17% of MB patients and it is rarely detectable in other subgroups (Northcott et al., 2019; Taylor et al., 2012). Expression of *MYC* in animal models led to identification of stem-like cerebellar progenitors and GABAergic neuronal progenitors as putative cell of origins of these tumours (Azzarelli et al., 2018; Kawauchi et al., 2012; Pei et al., 2012). However, finding the exact cell of origin for Group 3 is still a challenge.

Initially, Group 3 MB was classified in two categories named 'C1' and 'C5' based on the genomic analysis of 194 tumours. Interestingly, C1 was exclusively associated with *MYC* amplification and more important, with poor outcome for these patients (Cho et al., 2011). Lately, three major studies classified Group 3 medulloblastoma in high and low risk (Schwalbe et al., 2017), in three different genetically subtypes (alpha, beta and gamma) (Cavalli et al., 2017) and finally, a study including both Group 3 and Group 4 tumours defining eight different subtypes (II, III and IV indicated as Group 3), each with distinct characteristics (Sharma et al., 2019). Importantly, all the subtypes associated with c-MYC aberrant activity were indicated as tumours with very poor-prognosis (5-years overall survival 50%) (Cavalli et al., 2017; Northcott et al., 2019; Schwalbe et al., 2017).

#### **1.2.6 Group 4 medulloblastoma**

Group 4 MB represents the most common MB subgroup and comprises almost 40% of all the patients. The age of incidence is recorded across all age groups with a prevalence in children (Hovestadt et al., 2020). Previously, Group 3 and Group 4 MBs were defined as a single mixed subgroup named non-SHH/WNT tumours (Ellison et al., 2011). Nowadays, according to the WHO classification these subgroups are considered distinct (Louis et al., 2016). Like Group 3, Group 4 cellular origin is still under debate. However, the finding that showed the transcriptional factor *Lmx1a* to be a regulator both in upper rhombic lip (URL) and in Group 4 MB tumours, suggested precursor cell in this region as putative cell of origin for this subgroup (Lin et al., 2016)

Group 4 MB patients present classic histology and are frequently diagnosed with metastatic disease. However, with an approximately 80% 5-year OS the prognosis is considered intermediate (Hovestadt et al., 2020; Kool et al., 2012). Group 4 represents the least understood subgroup; the most common driver event in this subgroup is the overexpression of *PRDM6* followed by loss of function (LOF) mutations in *KDM6A*, *ZMYM3*, and *KMT2C* as well as gene amplifications in *MYCN* and *CDK6* (Northcott et al., 2019).

### 1.2.7 Medulloblastoma diagnosis and therapeutic approaches

To date, diagnosis of medulloblastoma is not possible only with imaging methods and thus, surgical resection together with histopathological and molecular analysis are essential to exactly define the disease (Northcott et al., 2019). Generally, patients with medulloblastoma present increased intracranial pressure which causes typical brain tumour symptoms such as vomiting, nausea, headaches and irritability. Due to the existence of several tumours that can potentially arise in the posterior fossa (e.g. ependymoma), differential diagnosis by radiographic exams is necessary to confirm the diagnosis of medulloblastoma (Millard & De Braganca, 2016).

Historically, MB patients were classified as standard-risk or high-risk based on the tumour dimensions, age at diagnosis, histology and presence of metastasis or residual tumour (*Chang's classification*) (Chang et al., 1969). According to Chang's system, extent of metastasis is defined as: M0 in absence of metastasis, M1 when cancerous cells are detected in the cerebrospinal fluid (CSF), M2 and M3 when tumour spread either in the subarachnoid space, or third or lateral ventricle (M2), or in the spinal space (M3). Finally, M4 staging is assessed when metastases are found outside the brain and the spine (Dufour et al., 2012). According to this system, patients > 3 years age at diagnosis, with no metastatic disease and residual tumour < 1.5 cm<sup>3</sup> are classified as average-risk; patients that do not meet these parameters are all classified as high-risk (Gajjar et al., 2006). However, the biological understanding of medulloblastoma considerably increased in the last decade and that has led to integration of molecular criteria in order to diagnose and treat the disease. Commonly, patients between 3 and 17 years old belong to different risk groups: low-risk (Non-Metastatic; >90% survival), standard-risk (Non-metastatic; no *MYC* amplification or *TP53* mutation; 75-90% survival), high-risk (Metastatic; *MYCN* amplification; 50-75% survival), and very-high-risk (Metastatic; *TP53* Mutation <50% survival) (Juraschka & Taylor, 2019; Ramaswamy et al., 2016).

In the last decades the treatment scheme for medulloblastoma patients remained unchanged and consists of a combination of surgical maximal safe tumour resection, performed in almost all the patients, followed by radiation therapy (RT) and chemotherapy. Post-surgical RT represents the standard of care for patients older than 3 years whereas in younger patients is generally avoided due to severe effects on neurocognitive development (De Braganca & Packer, 2013). Average-risk children are treated with 23.4 Gy irradiation to the craniospinal

axis, while high-risk patients receive between 36 and 40 Gy craniospinal irradiation. Adjuvant chemotherapy with vincristine is weekly administered together with RT followed by eight cycles of a multidrug regimen with cyclophosphamide or lomustine, cisplatin and vincristine (Packer et al., 2006). There is still a little agreement about how to treat children younger than 3 years age which do not receive radiation therapy. Generally, very high dose of chemotherapy is the main choice for these patients (Packer & Vezina, 2008; von Bueren et al., 2011). Even though this regimen greatly improved survival in MB patients, with a 5-year overall survival rate registered at nearly 75% (Ellison, 2010), therapy-related side effects are devastating in terms of neurocognitive impairments, such as cerebellar mutism syndrome secondary to surgical resection, hearing loss, and vascular disease (Gurney et al., 2003; Robertson et al., 2006; Vieira et al., 2014). Worryingly, secondary malignancies, such as gliomas, can later develop as consequences of radiotherapy and chemotherapy (Packer et al., 2013). Altogether, this evidence suggests the poor quality of life of these young patients which led to the urgency of finding less toxic and more targeted therapies while improving survival. To date, tremendous efforts have been made in terms of genomic identification of new diagnostic and prognostic factors for medulloblastoma. The main goal now is to translate all these discoveries to the clinical strategies. Risk stratification schemes are now based on both molecular and histopathological features, and they are considered for the design of new clinical trials. When it comes to WNT MB patients, classified as low risk in most of the cases, a reduction both in the craniospinal irradiation dose and chemotherapy dosage is currently under evaluation in two distinct clinical trials (<https://www.clinicaltrials.gov/>: NCT04474964; NCT02724579). Interestingly, WNT MB are characterized by an aberrant blood-brain barrier (BBB) which allows accumulation of chemotherapeutic agents on the tumour site. On the contrary, patients diagnosed with SHH MB do not present defects in the BBB, and are less responsive to the therapy (Phoenix et al., 2016)

Therapeutic approaches to treat SHH MB patients have been largely investigated and, the most used strategy aims to target the Smoothed (SMO) receptor. The SMO antagonist vismodegib showed encouraging anti-tumoral effects and longer progression free survival (PFS) in both Phase I and Phase II clinical trials (LoRusso et al., 2011; Robinson et al., 2015). However, intra-tumour heterogeneity and overcoming resistance after repeated monotherapy administrations represent the major drawback of this therapy (Ransohoff et al.,

2015). A clinical trial, evaluating the combination of vismodegib in concomitance with standard cranial irradiation and chemotherapy, is currently on-going (NCT01878617). In the SHH context, also the protein kinase CK2, critical for the activation of GLI factors, showed to be a promising therapeutic target against SHH MB mouse models (Purzner et al., 2018) and a CK2 inhibitor is currently being evaluated in clinical trial recruiting recurrent SHH MB patients (NCT03904862). Furthermore, small molecule inhibitors of tyrosine receptor kinases were evaluated in several clinical trials. Interestingly, a clinical trial with volitinib, HGF receptor inhibitor, showed promising effects on Phase I on primary brain tumours and it is now recruiting (NCT03598244).

Given the poorly understood mechanisms underpinning Group 3 and Group 4 pathogenesis, there is a lack of targeted therapies. Considering that *MYC* is the driver event in Group 3 tumours and that it is not easy to target, alternative approaches are being evaluated. For instance, for *MYC*-amplified tumours, BET proteins, such as BRD4, are considered as potential therapeutic target (Luzzi et al., 2020). JQ1, BRD4 inhibitor, has been tested both *in vivo* and *in vitro* in *MYC*-amplified models; the use of this compound triggered cell cycle arrest and apoptosis in cell lines and prolonged survival of xenografts (Bandopadhyay et al., 2014). Interestingly, a combinatory approach with JQ1 and the PI3K/mTOR inhibitor BEZ235 recently showed to act synergistically to impair *MYC*-amplified cell proliferation and tumour growth (Chaturvedi et al., 2020).

Furthermore, immunotherapy has been evaluated for treating CNS tumours including medulloblastoma but immunosuppressive properties of these tumours are peculiar and often associated with treatment failures; oncolytic viruses as well as inhibitors of checkpoints are currently under clinical trials for brain tumour patients, comprising medulloblastoma (Kabir et al., 2020). The most novel and innovative type of immunotherapy is represented by Chimeric Antigen Receptor T (CAR T) cells therapy, where T-cells are taken directly from the patients and engineered in the laboratory to create specific receptors against antigens on the tumour cells before being administrated into the patients. Use of HER2-CAR-T as well as B7-H3-specific CAR-T cells are under clinical trials evaluation for paediatric tumours (NCT04185038; NCT03500991) (Voskamp et al., 2021).

### 1.3 Receptor tyrosine kinases (RTKs) and their role in cancer

Protein kinases are enzymes that catalyse the transfer of a  $\gamma$ -phosphate group from the ATP to another protein (Fabbro et al., 2015). When it comes to receptor tyrosine kinases (RTKs), they transfer the  $\gamma$ -phosphate group specifically to tyrosine residues substrates (Metibemu et al., 2019). RTKs represent a subclass of a larger family of protein tyrosine kinases (PTKs) which comprises non-receptor families and receptor families. (Robinson et al., 2000). Out of the 518 kinase genes encoded in the human genome, 58 are RTKs; among these, examples are the Epidermal Growth Factor Receptor (EGFR), Mesenchymal-epithelial transition factor (MET), Vascular endothelial growth factor Receptor (VEGFR). They all possess a similar structure with an extracellular portion which binds the specific ligand, a transmembrane domain (TM), juxta membrane region, a tyrosine kinase domain on the cytosolic side and a flexible C-terminal tail (Metibemu et al., 2019). RTKs are mostly activated by binding specific ligands, usually growth factors, in the extracellular regions of the receptors. Generally, ligand binding causes dimerization and resulting autophosphorylation of receptors which are now in their active conformation (Du & Lovly, 2018) and can activate downstream pathway such as MAPK, PI3K/AKT, and JAK/STAT. RTKs and activated downstream signalling are involved in a wide range of cellular processes such as cell proliferation, motility, differentiation (Blume-Jensen & Hunter, 2001). RTK activity is strictly regulated under physiological conditions; however, mutations in RTKs can disrupt balance between cell proliferation and cell death as well as deregulate mechanism of migration and invasion (Schlessinger, 2000). Deregulation of RTK activation, due to gain of function mutations, overexpression, gene re-arrangement or amplification, leads to aberrant signalling from RTK and further, to cancer initiation and progression (Takeuchi & Ito, 2011).

Thus, they were suggested as plausible targets for anti-cancer treatments. To date, RTKs inhibitors represent the predominant type of targeted therapies (Alexander & Wang, 2015). The Food and Drug Administration (FDA) has approved numerous protein kinase inhibitors, and in Table 2 below only inhibitors of tyrosine kinase receptors are listed.

However, beneficial effects of these compounds still represents a challenge due to the overcoming resistance and toxicity (Bhullar et al., 2018); in fact, pre-clinical and clinical evidences showed that treatment with tyrosine kinase inhibitors causes a selective pressure

on cancer cells which then acquire modifications to survive the drug inhibition (Jiao et al., 2018). Mechanisms of resistance can be related to the primary target and those are commonly single mutations occurring in the protein coding gene (e.g. the missense mutation T790M which substitutes a threonine in methionine in the EGFR which is found in almost 50% of lung cancers treated with EGFR inhibitors (Suda et al., 2009)).

Moreover, mechanisms of RTKs redundancy and compensation such as activation of other receptor tyrosine kinase via amplifications or translocation occur in the, so-called, secondary drug target (Alexander & Wang, 2015; Wood, 2015). c-MET amplifications are among the most frequent secondary events that confer resistance to primary therapies (Tartarone & Leroese, 2015). For examples, acquired resistance to EGFR inhibitors, such as erlotinib and osimertinib, in non-small lung cancers is related to c-MET amplification in almost the 25% of cases. Generally, c-MET overexpression and activation induces a constitutive activation of PI3K/AKT pathway which led to cell survival and proliferation (Wang et al., 2019).

To this instance, a full understand of mechanism of actions of these compounds, is essential to further investigate potential resistance mechanisms as well as to improve the development of more selective and effective inhibitors.

**Table 2: RTKs inhibitors approved by FDA. List adapted from (Bhullar et al., 2018)**

Target	Drug
ALK	Crizotinib, Ceritinib, Alectinib, Brigatinib
BTK	Ibrutinib
c-Met	Crizotinib, Cabozantinib
EGFR family	Gefitinib, Erlotinib, Lapatinib, Vandetanib, Afatinib, Osimertinib
JAK family	Ruxolitinib, Tofacitinib
PDGFR $\alpha/\beta$	Axitinib, Gefitinib, Imatinib, Lenvatinib, Nintedanib, Pazopanib, Regorafenib, Sorafenib, Sunitinib
RET	Vandetanib
VEGFR family	Axitinib, Lenvatinib, Nintedanib, Regorafenib, Pazopanib, Sorafenib, Sunitinib

## 1.4 Scatter factor/Hepatocyte growth factor (SF/HGF)-c-MET signalling

The N-methyl-N'-nitroso-guanidine human proto-oncogene (MET) was originally identified in a transformed osteosarcoma cell line (Cooper et al., 1984). MET transforming ability was related to a chromosomal rearrangement due to the fusion of sequences from the translocated promoter region (TPR) locus on chromosome 1 to sequences from MET locus on chromosome 7 (Park et al., 1986). Later, they observed that the proto-oncogene encodes for the so-called mesenchymal-epithelial transition tyrosine kinase receptor on the cellular surface (c-MET kinase) (Park et al., 1987), which binds the hepatocyte growth factor (HGF), also known as scatter factor (SF) (Bottaro et al., 1991; Naldini et al., 1991). To date, HGF represents the only known ligand for the c-MET receptor. It is located in the chromosome 7 and it is synthesized by mesenchymal cells as a single-chain inactive pro-peptide (pro-HGF); to be biologically active, HGF requires conversion to a functional  $\alpha$  and  $\beta$ -chain heterodimeric form (Gak et al., 1992) by extracellular proteases such as the serine protease activator (HGF-A), which acts by cleaving in certain residues of arginine and valine to generate the two different chains bonded by disulphide bridges (Miyazawa et al., 1993). Structurally, HGF in its active state is characterized by four Kringle domains (K1-K4), and amino (N) domain and a serine protease homology domain (SPH), which are all crucial for enabling receptor dimerization (Lokker et al., 1992). HGF acts in a paracrine manner with primary effects on epithelial cells that express c-MET receptor (Trusolino et al., 2010). The receptor c-MET is a heterodimer complex of 185-kDa consisting of a glycosylated extracellular  $\alpha$ -subunit linked by a disulphide bond to a transmembrane  $\beta$  subunit which contains an extracellular region, a membrane spanning segment and an intracellular catalytic region (Maulik et al., 2002).

As summarized in Figure 4, upon HGF binding at  $\alpha$ -subunit level, c-MET is activated by dimerization and trans-phosphorylation of two tyrosine residues (Tyr1234 and Tyr1235) located in the intracellular region (Birchmeier et al., 2003; Birchmeier & Gherardi, 1998). While phosphorylation of these residues is crucial for the receptor's activation (Longati et al., 1994), Tyr1349 and Y1356 phosphorylation in the C-terminal tail is important for adaptors recruitment such as Grb2 and Gab-1 (Growth factor receptor-bound protein 2 (Grb2) – associate binder 1) (Ponzetto et al., 1994). Moreover, phosphorylation sites in the juxta-membrane domain are required for endocytosis and degradation of the receptor; this

process is crucial to strictly regulate c-MET activity (Sattler & Salgia, 2009). After c-MET phosphorylation, adaptors are recruited to trigger activation of downstream pathways: mainly the mitogen-activated protein kinase (MAPK) and the phosphoinositide 3 kinase-AKT (PI3K-AKT) signalling.

c-MET dependent- MAPK cascade starts with c-MET and Grb2/SOS complex interaction followed by the small GTPase Ras. In its active state Ras associates with the serine/threonine Raf which acquires activity and phosphorylates the final effectors of the cascade, ERK1 and ERK2. Once activated, ERKs can translocate to the nucleus and stabilize transcription factors that play a role in the G1-S cell cycle transition (Trusolino et al., 2010). Activation of MAPKs regulate cell cycle as well as cell migration and degradation of extracellular matrix, all processes that can lead to tumorigenesis.

Furthermore, c-Met phosphorylation induces the activation of phosphatidylinositol-3-kinase (PI3K) and consequentially, the formation of phosphatidylinositol-3,4,5-triphosphate (PIP3). PIP3 recruits Akt to the plasma membrane where is phosphorylated at different residues and translocate to the nucleus. Here, AKT regulate several processes such as cell survival, by modulation of apoptotic proteins, and protein synthesis, by mTOR phosphorylation (Porta et al., 2014; Zhang et al., 2018).

Physiologically, HGF/c-MET is fundamental during the embryogenesis, development, and during adulthood, in wound healing processes when events of tissue and organs damage occur; however its deregulation has been strictly correlated to cancer (Comoglio et al., 2008).

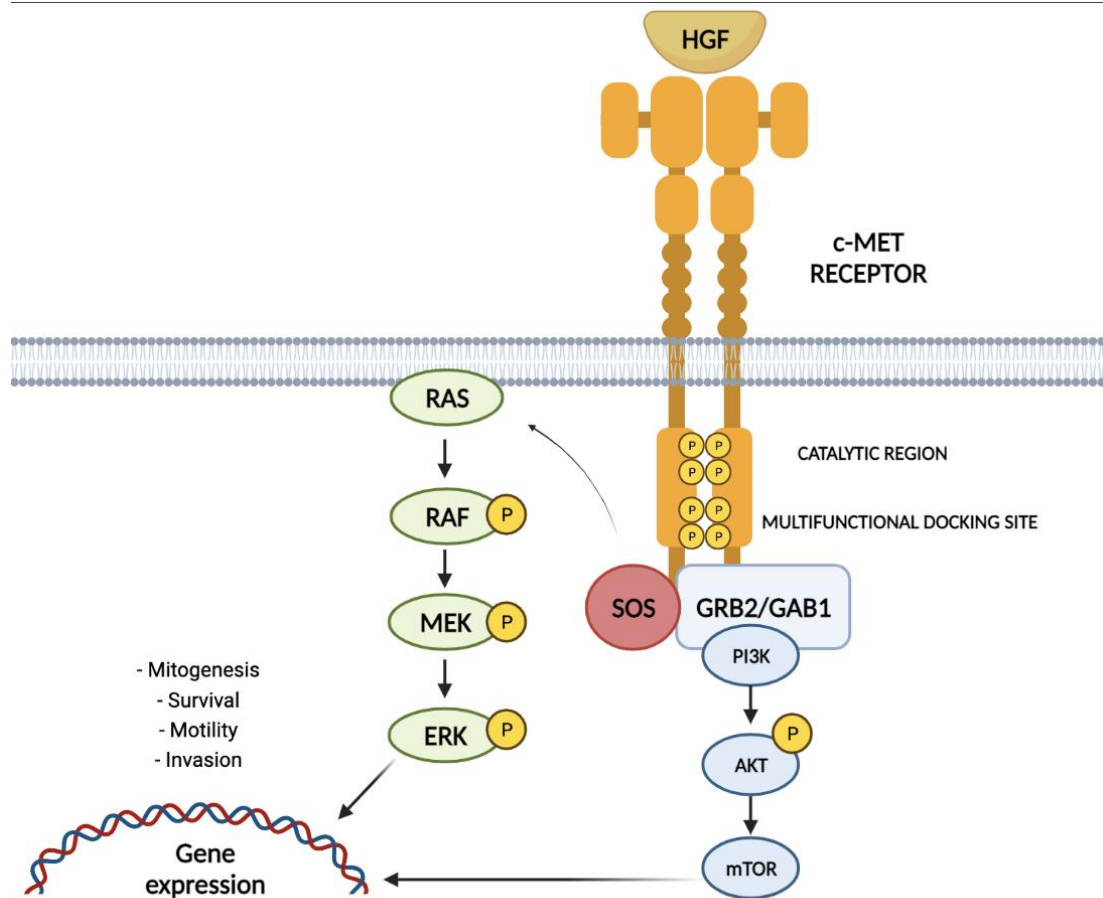


**Figure 4: Schematic representation of SF-HGF/MET pathway and signalling effects**

HGF binds to c-Met and causes receptor homodimerization and trans-phosphorylation of Tyr1234 and Tyr1235 in the catalytic intracellular region and Tyr1349 and Tyr1356 in the multifunctional docking site. Following MET activation, effectors such as GRAB2 and GAB1 are phosphorylated, and downstream signalling triggered. Activated Grb2 stimulates RAS and the ERK/MAPK signalling to modulate transcription factors for cell proliferation while Gab1 associated with c-Met trigger PI3K/Akt pathway to suppress apoptosis and stimulate cell growth (Pathway cascade was designed on Biorender (<https://biorender.com/>) and adapted from (Trusolino et al., 2010)).

#### 1.4.1 SF/HGF-c-MET dysregulation in cancer

In the last decades, both *in vivo* and *in vitro* evidence showed that SF/HGF-MET signalling is aberrantly expressed in a wide range of human carcinomas: lung, liver, colorectal, ovarian, gastric and metastatic head and neck cancers (Christensen et al., 2005; Gherardi et al., 2012; Maulik et al., 2002) and it is frequently associated with poor prognosis and outcome for cancer patients (Comoglio et al., 2008). In 1994, Rong *et al.*, demonstrated that human cell lines with ectopic overexpression of either SF-HGF or MET were transformed in tumorigenic cells with metastatic ability in athymic nude mice (Rong et al., 1994).

SF/HGF-MET aberrant activation occurs via several mechanisms such as receptor overexpression, amplification, mutations as well as ligand independent c-MET activation, due to constitutive phosphorylation of the receptor, or HGF-dependent autocrine and paracrine stimulation (Trusolino et al., 2010). Moreover, both germinal and somatic mutations, even though are rare events, have been associated with c-MET pathway dysregulation. For instance, skipping mutations in the *MET* exon 14 affect sites in the juxta membrane domain and causes inhibition of c-MET degradation (Christensen et al., 2005).

HGF plays also a crucial role in the tumour microenvironment by establishing a crosstalk between cancer-associated fibroblast (CAFs), the most predominant cell type in the tumour stroma, and tumour cells (Ding et al., 2018; Nakamura et al., 1997). This cross-talk lead to impairment of cellular processes such proliferation, survival, invasion, migration, and epithelial-mesenchymal transition (EMT), which all together play a major role in tumour progression, dissemination and metastatic spread (Owusu et al., 2017). Notably, stromal expression of HGF has been strictly correlated with mechanisms of drug resistance to RAF inhibitors by sustaining activation of ERK and AKT (Straussman et al., 2012); recently, HGF/c-MET pathway has been found responsible for the resistance to BRAF inhibitors in melanoma and further, targeting c-MET kinase with a selective inhibitor was needed to overcome this resistance (Caenepeel et al., 2017).

c-MET pathway also contributes to the growth of new blood vessels, process known as neo-angiogenesis (Comoglio et al., 2008), critical for both the sustainment of cancer cells and the metastatic process. It is well established that *MET* is highly expressed by endothelial cells and further, HGF induces growth and migration of endothelial cells as well as overexpression of

the vascular endothelial growth factor (VEGF) in cancer cells (Zhang et al., 2003). As support of this evidence, promising results of c-MET inhibitors in inhibiting tumour growth were correlated with a reduced angiogenesis (Piguet et al., 2015).

Given all these results, both HGF and c-MET have been pinpointed as suitable targets for cancer therapy.

#### 1.4.2 Therapeutic strategies against SF-HGF/c-MET kinase signalling

The role of SF/HGF-c-MET kinase pathway in tumorigenesis is now well defined. To date, different approaches are considered for disrupting this axis in order to inhibit cellular processes such as proliferation, migration, survival and invasion of cancer cells. Two major classes of SF/HGF-MET inhibitors were developed over the years: monoclonal antibodies and small molecule tyrosine kinase inhibitors (Scagliotti et al., 2013). The first category includes both anti-HGF (e.g. ficlatuzumab and rilotumumab) and anti-MET (e.g. onartuzumab) monoclonal antibodies which aim to neutralize c-MET activation by preventing HGF from binding to the receptor (Ariyawutyakorn et al., 2016). Small molecule tyrosine kinase inhibitors (TKIs) block intracellular signalling in tumour cells and are extensively studied as anti-cancer strategies (Steeghs et al., 2007). Generally, as many kinase inhibitors, c-MET inhibitors are classified, based on how the drug binds to the receptor, in: ATP competitive and non-ATP competitive. As suggested by the nomenclature, ATP-competitive inhibitors behave as ATP analogs; they compete with the intracellular ATP and recognize the receptor in its active conformation; those are further classified in class I ATP-competitive inhibitors which are selective for the ATP pocket of c-MET receptor and class II represented by multi-kinase inhibitors. Class III is represented by non-ATP competitive inhibitors which bind the receptor on its inactive conformation (e.g. tivantinib). (Lee et al., 2015; Puccini et al., 2019; Zhong et al., 2021). A brief description of examples of c-MET kinase inhibitors is provided below and structures, targets and mechanism of receptor inhibition are summarized in the Table 3 below.

*Crizotinib* (PF02341066) is a multi-kinase, non-selective ATP-competitive inhibitor targeting anaplastic lymphoma kinase (ALK), c-MET kinase receptor and the ROS proto-oncogene 1 (ROS1) (Cui et al., 2011; Puccini et al., 2019). In 2011, crizotinib was approved as ALK inhibitor by the Food and Drug Administration (FDA) for the treatment of non-small cell lung cancer (NSCLC). Later, its efficacy was also demonstrated in NSCLC patients harboring MET-exon 14 alterations (Drilon et al., 2020). Currently, crizotinib is under investigation in several other solid tumours (except NSCLC) either as monotherapy or in combination with other agents (NCT01121588, NCT02510001, NCT01524926) (Puccini et al., 2019)

*Foretinib* (GSK1363089) is also classified as ATP-competitive multi-kinase inhibitor with activity against c-MET receptor and the vascular endothelial growth factor receptor (VEGFR)

(Qian et al., 2009). Foretinib has been investigated, either as monotherapy or in combination, in clinical trials for different cancers, such as hepatocellular carcinoma (NCT00920192), breast cancer (NCT01138384), Papillary Renal-Cell carcinoma (NCT00726323).

*Cabozantinib* (XL184) inhibits both c-MET and ALK. It is an FDA approved small molecule inhibitor for patients with metastatic thyroid medullary carcinoma (Tomita et al., 2020).

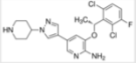
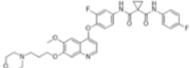
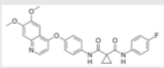
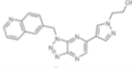
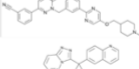
*Tivantinib* (ARQ197) is a selective non-ATP competitive c-MET inhibitor which binds to the dephosphorylated and inactive form of c-MET receptor (Munshi et al., 2010). The very first Phase I trial with tivantinib as monotherapy has been conducted in the UK recruiting patients with several types of solid tumours. This study confirmed its ability to inhibit c-MET signalling as well as safety and tolerability of the drug (Yap et al., 2011). Tivantinib reached Phase II and Phase III studies on hepatocellular carcinoma where patients with high-MET status showed a longer median overall survival (NCT01755767) (Santoro et al., 2013). To date, the debate regarding mechanism of action of tivantinib is still on-going. Despite its development as highly selective c-MET inhibitor, numerous studies concluded that its efficacy is not directly correlated with c-MET inhibition.

They demonstrated that tivantinib displayed cytotoxic activity in cell lines with lack of MET expression and suggested that its activity was mainly due to microtubule disruption (Basilico et al., 2013; Katayama et al., 2013; Remsing Rix et al., 2014). Nevertheless, during clinical studies patients with low-MET did not show significant advantages in the overall survival after administration of tivantinib compared to the high-MET status supporting the role of c-MET while using this compound (Pievsky & Pysopoulos, 2016). Interestingly, a recent study on glioblastoma patients demonstrated the positive association between c-MET expression and tumour size. Then, tivantinib was tested on glioblastoma cells to study its effects; the drug was able to repress the cell proliferation as well as colony formation through PI3K/Akt/mTOR signalling inhibition (Wu et al., 2019).

Overall, various c-MET inhibitors showed promising results in preclinical models and thus, entered clinical trials. Unfortunately, except for the non-selective inhibitors crizotinib and cabozantinib, whose effects are more related to ALK inhibition rather than c-MET, patients treated with c-MET inhibitors did not show significant improvement in the overall survival. It is likely that patient recruitment based on c-MET expression is often not sufficient to guarantee therapy success correlating with failure of many c-MET inhibitors. Importantly,

phosphorylation status of c-MET kinase is not evaluated when patients are selected to receive the treatment, and this may represent the major drawback for clinical trials evaluating c-MET inhibitors (Hughes & Siemann, 2018). Furthermore, the preclinical evaluation of c-MET inhibition employs the use of high concentration of HGF which does not mimic human levels in the serum; response to c-MET inhibitor resulted affected when tumour cells were stimulated with physiological concentrations of HGF compared to high concentrations, normally used in *in vitro* experiments (Hughes & Siemann, 2019).

**Table 3: List of small-molecules c-MET kinase inhibitors**

Drug name	Structure	Targets	Mechanism
Crizotinib (PF-2341066)		MET, ALK	Non selective – ATP competitive
Foretinib (GSK1363089)		MET, VEGFR, RET KIT, FLT3, TIE2	Non selective – ATP competitive
Cabozantinib (BMS-907351)		MET, VEGFR, RET	Non selective – ATP competitive
Tivantinib (ARQ197)		MET	Selective, ATP non-competitive
PHA-665752		MET, RON, FLK1, c-Abl	Non selective – ATP competitive
PF-04217903		MET	Selective ATP-competitive
Tepotinib		MET	Selective – ATP competitive
JNJ-38877605		MET	Selective – ATP competitive

### 1.4.3 Role of c-MET pathway in cerebellar development and medulloblastoma

As previously mentioned, SF-HGF/c-MET signalling pathway plays an important role during the embryogenesis, by controlling the proliferation and migration of cells during the establishment of several tissues, such as liver, placenta, muscle and nervous system (Trusolino et al., 2010). In the context of neuronal development, HGF has been demonstrated to be crucial as neurotrophic factor and to couple with nerve growth factor (NGF) in enhancing growth of axons in neurons (Maina et al., 1998). In line with this, HGF together with c-MET receptor was detected in the early embryonal stages of developing brain (Desole et al., 2021).

Medulloblastoma is an embryonal cerebellar tumour (Bailey & Cushing, 1925). Development of the cerebellum is a long and complex process that last until 2 years post-natal and it requires several steps such as organization and characterization of the cerebellar territory in the brain, establishment of two compartments for Purkinje cells and granule cells proliferation, migration of the granule cells to form several layers and finally, the formation of a cerebellar circuitry (ten Donkelaar et al., 2003).

Mechanisms of cell-cell interaction play a fundamental role in the formation of different cerebellar layers through a fine regulation of proliferation, migration and apoptotic processes. Those processes are normally controlled by different molecules, such as growth factors. Importantly, hepatocyte growth factor (HGF) and fibroblast growth factor 1 (FGF-1) were shown to have a similar neuroprotective role in cerebellar granule neurons when those were challenged with neurotoxic molecules and further, this process was correlated with the activation of the PI3K/AKT pathway (Hossain et al., 2002). Based on this evidence, in the same year Ieraci *et al.*, confirmed the expression of c-MET receptor in granule cell precursors and that the addition of HGF to the cerebellar cell cultures induced a strong increase in cell proliferation. They further proved the point *in vivo* by establishing an hypomorphic mutant of c-MET receptor which caused defects in the cerebellar size (Ieraci et al., 2002). Given that HGF/MET pathway is a well-known oncogenic pathway and that it plays a physiological role in the cerebellum development, its involvement in medulloblastoma pathogenesis was considered.

In 2004, MET gene amplifications were described for the first time by CGH analysis in 5 out of 14 primary medulloblastoma samples suggesting that amplification of this oncogene has a

role in medulloblastoma tumorigenesis (Tong et al., 2004). Expression of c-MET and HGF was then evaluated by RT-PCR and western blot analysis across CNS tumour samples and medulloblastoma cell lines. Both c-MET and HGF were largely expressed in MB samples and high-MET mRNA levels correlated with shorter survival compared with low MET patients' samples (Yunqing Li et al., 2005). Since c-MET autophosphorylation in response to HGF stimulation is essential to evaluate c-MET activity, *Li et al.* demonstrated that HGF induced activation of c-MET kinase as well as downstream proteins, such as AKT and ERK. An increase in cell proliferation was observed upon HGF stimulation in MB cell lines; in addition, they demonstrated that this effect was mediated by the activation of the Cyclin Dependent Kinase 2 (Cdk2) and the down-regulation of the tumour suppressor p27 (Yunqing Li et al., 2005). Later, HGF showed to regulate *MYC* expression both at transcriptional and post-transcriptional level in MB cell lines and MB primary tumours. c-Myc acted as potent mediator of HGF effects on cell cycle progression, proliferation and survival in MB cell suggesting that c-MET kinase pathway and c-Myc protein cooperates in MB development and growth (Li et al., 2008).

Furthermore, SF/HGF-c-MET kinase pathway was found to contribute to the chemoresistance to etoposide, a well-known cytotoxic agent, in medulloblastoma cells. Interestingly, experiments of knockdown demonstrated that HGF exploits cytoprotective effects in MB cells in correlation with higher expression of tissue factor (TF), suggesting that they couple in inducing resistance to etoposide in MB cells (Provencal et al., 2010). Moreover, higher sensitivity to c-MET kinase inhibition was found correlated with high expression of HGF in several cell lines derived from brain tumours, including medulloblastomas, suggesting that c-MET inhibition could be more efficient when tumours express high levels of the ligand (Zhang et al., 2013). Interestingly, exogenous HGF added to medulloblastoma cells treated with canertinib, a pan-erbB (RTKs) inhibitor, circumvented drug's effects in terms of cell viability, advising that a combination between RTKs inhibitors could be a better approach for MB treatment (Zomeran et al., 2015). Interestingly, promising results of targeting c-MET pathway in medulloblastoma were also provided with the use of flavonols, easily taken by dietary adjustments. In this instance, MB cells treated with low concentrations of quercetin showed a decrease phosphorylation of c-MET and AKT as well as an inhibitory effect of cell migration in response to HGF stimulation (Labbe et al., 2009).

The efficacy of targeting c-MET kinase in medulloblastoma was then investigated and confirmed by using a highly specific molecule against c-MET receptor (PHA665752) to inhibit cell proliferation as well as cell migration in *in vitro* medulloblastoma cell lines, representative both of SHH and Group 3 MB (Kongkham et al., 2010). Together with this finding, a different group demonstrated that the small molecule and orally bioavailable c-MET inhibitor (SGX523) was effective in halting MET-dependent cell proliferation and migration in medulloblastoma cells. SGX523 was tested in a range of glioma and medulloblastoma cells and it potently inhibited c-MET kinase phosphorylation as well as AKT and ERK phosphorylation. Interestingly, SGX523 was also effective in hampering intracranial tumour growth *in vivo* suggesting the capacity of this drug to cross the blood brain barrier (BBB) after oral administration (Guessous et al., 2010).

#### **1.4.4 SF-HGF/MET signalling and Sonic Hedgehog medulloblastoma**

Bearing in mind the molecular heterogeneity of medulloblastoma and the role of SF/HGF-MET in the cerebellum development, numerous studies investigated how SF/HGF-MET pathway was contributing to medulloblastoma pathogenesis. As previously mentioned, activation of SHH pathway was largely demonstrated to be contributing to medulloblastoma pathogenesis and several molecular signals contribute to SHH's ability to increase MB formation in mice (Rao et al., 2003; Weiner et al., 2002). Given the role of HGF/MET in cerebellum development and its correlation with medulloblastoma's poor-prognosis, Binning *et al.* decided to investigate whether ectopic expression of HGF enhances SHH-driven MB formation. A viral gene transfer system allowed them to establish a lineage of neural progenitors expressing both HGF and SHH. Results from this study confirmed the original hypothesis: HGF ectopic expression enhanced SHH-mediated cell proliferation and survival. In addition, the use of anti-HGF antibody prolonged survival of the mice, supporting the rationale behind the use of HGF/MET pathway inhibitors to stop MB growth (Binning et al., 2008).

Later, gene expression analysis on primary samples of medulloblastoma demonstrated that overexpression of c-MET receptor was more evident in SHH MBs compared to other subgroups and to healthy cerebella (Onvani et al., 2012). In addition, c-MET and expression were found significantly increased in the two distinct datasets of primary medulloblastomas. In the same study, single cell motility and invasion was observed to increase in response to c-

MET activation by HGF binding in SHH MB cell lines and that was confirmed using two different c-MET inhibitors which reverted HGF-mediated effects. Furthermore, MB cells dissemination in response to HGF stimulation was promoted by JNK activity and the Ser/Thr kinase MAP4K4, which regulates cytoskeleton dynamics driving cell motility and invasiveness (Santhana Kumar et al., 2015). Later, increase of MAP4K4 mRNA levels was found in medulloblastoma samples and associated with the subtype SHH  $\beta$ ; interestingly, tumours with high levels of MAP4K4 showed a high expression of c-MET. The authors revealed that activation of MAP4K4 controls ligand-dependent c-MET endocytosis which is crucial for its activation (Tripolitsioti et al., 2018).

Relying on these findings, Faria *et al.* observed that c-MET was highly expressed in SHH medulloblastoma in a cohort of primary medulloblastomas and both tumour recurrence and lower 5-year overall survival were associated with high expression of c-MET in SHH tumours. The efficacy of the orally available c-MET inhibitor foretinib was then investigated in SHH medulloblastoma cell lines. Foretinib was able to suppress c-MET as well as downstream pathways activation in SHH cell lines resulting in a strong anti-proliferative effect and apoptotic response. Additionally, intracranial drug injection both increased survival in transgenic mouse models of SHH MB and affected occurrence of metastases; this provided encouraging pre-clinical evidence for the use of foretinib in SHH MB treatment and it defined drug's ability of penetrating blood-brain barrier (Faria et al., 2015). Although the preclinical evidence was quite convincing, to date no clinical trials have evaluated the efficacy of foretinib in medulloblastoma patients. Interestingly, volitinib, a highly selective c-MET inhibitor is under Phase 1 clinical trial for treatment of childhood CNS tumours, including medulloblastoma, harbouring *MET* alterations (NCT03598244).

Altogether, this evidence endorses the idea that MET pathway plays a role in medulloblastoma progression and it represents a good candidate as therapeutic target to avoid treatment-related toxicity in young MB patients as well as to hamper MB metastasis. However, the mechanism of actions of many small molecule inhibitors are still not completely understood and it is crucial to characterize this before they can be proposed for the use in clinic.

# ***CHAPTER 2: Materials and methods***

## 2.1 Cell lines and culture methods

Human SHH medulloblastoma cell lines (DAOY, ONS76 and UW228) were either purchased from American Type Culture Collection (ATCC) (DAOY) or kindly provided by Dr Chris Jones (ONS76 and UW228). MB cell lines were maintained in RPMI-1640 growth medium (Biosera) with a supplement of 10% fetal bovine serum (FBS) (Gibco) and 1% penicillin/streptomycin (P/S) (Gibco) and placed in the incubator at 37°C and 5% CO<sub>2</sub>. Each cell line was subcultured twice a week: cells were washed with sterile phosphate buffered saline (PBS), detached with Trypsin-EDTA 0.25% (ThermoFisher Scientific, USA) and centrifuged at 1200rpm for 5mins. For seeding, cells were counted with a haemocytometer and plated dependent on the experimental design.

## 2.2 *In silico* analysis by querying R2 database

All data used to determine the RTKs expression and c-MET expression in both medulloblastoma samples and healthy cerebellum are accessible via R2 Genomic Analysis and Visualization platform (<http://r2.amc.nl/>). Kaplan Meier curves were generated on R2 considering only the first and last quartile of the patient cohort taken in consideration and the survival curves were downloaded as images from the software. Datasets interrogated in this study are listed in the table below (Table 4)

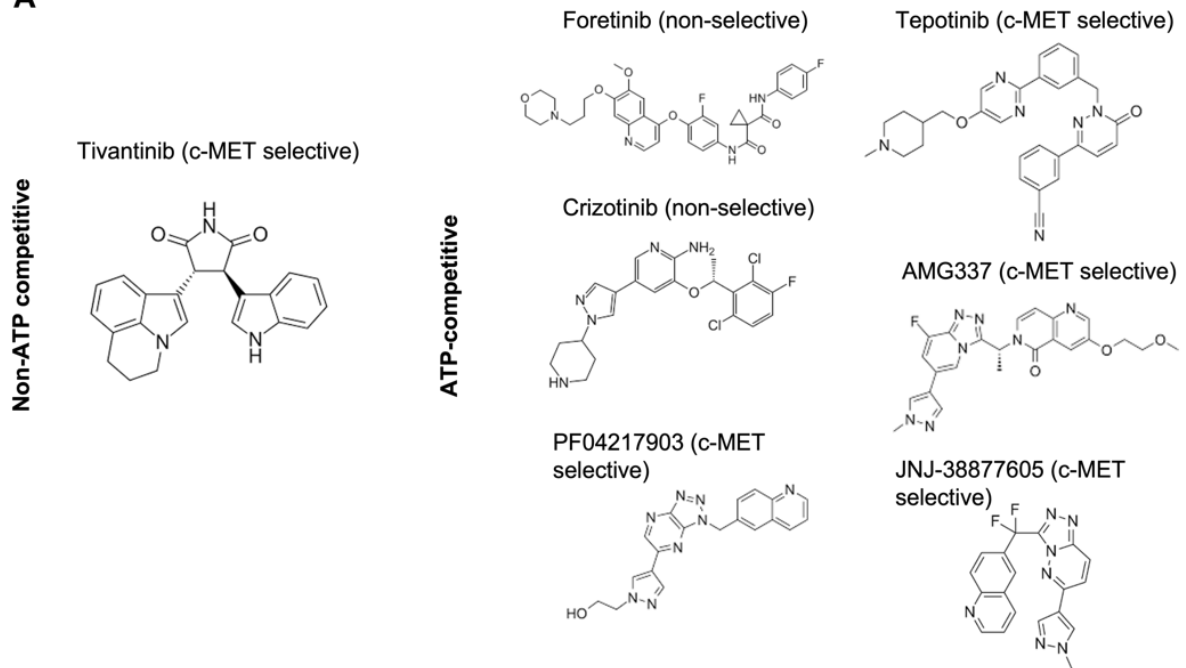
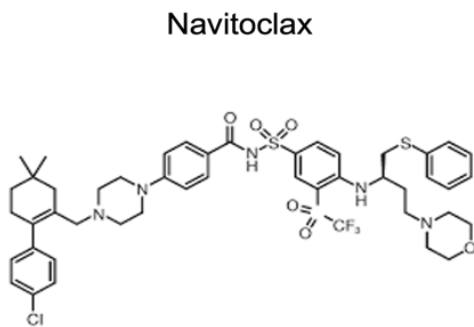
**Table 4: Gene expression datasets interrogated through R2 platform**

Tissue/Tumor	No of samples	Accession	Reference
Cerebellum	9	<a href="#">gse3526</a>	Roth et al., 2006
Medulloblastoma	76	<a href="#">gse37418</a>	Robinson et al., 2012
Medulloblastoma	763	<a href="#">gse85212</a>	Cavalli et al., 2017
Medulloblastoma	62	<a href="#">gse10327</a>	Kool et al., 2008
Medulloblastoma Ependymoma	51	<a href="#">gse74195</a>	De Bont, J.M., et al. 2008
Medulloblastoma	223	n/a	Northcott et al., 2017
Medulloblastoma	57	n/a	n/a
Medulloblastoma - ATRT	31	<a href="#">gse74195</a>	Ho et al., 2015

## 2.2 Inhibitors

Cells were treated with the following compounds (structures available in Figure5 ): c-MET kinase inhibitors both representative of ATP competitive and non-ATP competitive classes (tivantinib, crizotinib, foretinib, tepotinib, AMG337, PF-04217903, JNJ-38877605), BH3-mimetics (Navitoclax, Maritoclax), PI3K/mTOR inhibitor (BEZ235/Dactosilib), and the anti-microtubule agent Vincristine. They were purchased from Selleckchem (<https://www.selleckchem.com/>) with exception for AMG337 which was purchased from AdooQ Bioscience (<https://www.adooq.com/>).

Compounds were diluted in dimethyl sulfoxide (DMSO) (Fisher) at 10 mM stock concentration except for AMG337 (5 mM) and BEZ235 (1mM) and then aliquoted and stored at -20°C.

**A****B**

Maritoclax

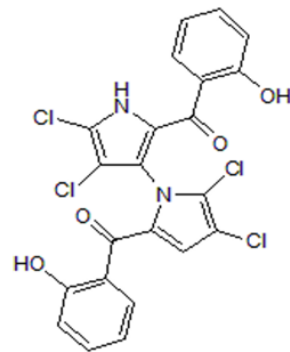
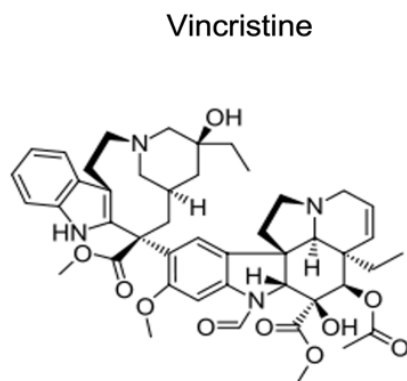
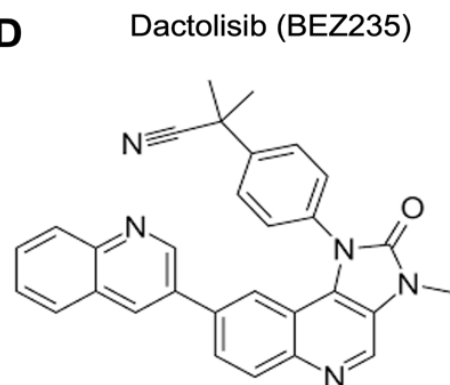
**C****D**

Figure 5: Structures of selected inhibitors used in the study

### **2.3 Cell viability assay by MTT**

DAOY (1500 cells/well), ONS76 (1000 cells/well) and UW228 (2000 cells/well) were seeded in 96 well plates and left for 24h in the incubator at 37°C and 5% CO<sub>2</sub> to allow adherence. After 24h, media was replaced with media containing different drugs at scalar concentrations (starting at 10 µM). Treatments were performed in technical quadruplicates for each condition. For short-term assay, cells were incubated for 72h with desired compounds. At the end point, Thiazolyl Blue Tetrazolium bromide (MTT) (Alfa Aesar) working solution was prepared by dissolving 150 mg of powder in 50 ml of phosphate saline buffer (PBS). Solution was aliquoted and stored at -20°C until use. At the experiment end point, 50 µl of MTT were added in each well and kept for 3h in the incubator at 37°C. DMSO was used to dissolve MTT crystals and absorbance was read after at 540 nM with Varioskan™ LUX multimode microplate reader (ThermoFisher Scientific, USA) to determine cell viability. Pictures post treatments were taken at 10X magnification with Evos FL Auto 2 microscope (ThermoFisher). Rate of proliferation was calculated relatively to the untreated cells. Results were plotted in GraphPad 8 software as non-linear regression curves. IC<sub>50</sub>, defined as the required concentration to cause a decrease of 50% of cell viability, was calculated in GraphPad 8 software for each drug.

### **2.3 Stimulation of SHH-MB cell lines with Hepatocyte Growth Factor (HGF)**

*Study of c-MET pathway activation by western blot analysis:* DAOY, UW228 and ONS76 were seeded in a 6-well plate at 150.000 cells/well density. After 24h, media was replaced with RPMI 1640 (Biosera) with no serum (0% FBS) and 1% penicillin/streptomycin (P/S) (Gibco) to allow cell starvation for 24h. After serum starvation, cells were pre-treated with c-MET inhibitor crizotinib (1µM) for 2h. c-MET kinase pathway was activated by adding human-recombinant HGF protein (10ng/ml) (SinoBiological) for 30 minutes according to the experimental design. Proteins were extracted as described in the paragraph 2.13 below.

*Proliferation assay by MTT:* DAOY (1500 cells/well) and ONS76 (1000 cells/well) were seeded in a 96-well plate in quadruplicates. One more plate (time 0) was seeded in parallel with the same cell density for each cell line. After a day, media was replaced with RPMI 0% FBS to starve the cells for 24 hours. MTT was added and absorbance was read after 24 hours for the time 0 plate to allow normalization. Cells were then treated with crizotinib (1 $\mu$ M) and HGF was added at 10ng/ml concentration for 24 hours. At the end point, MTT assay was performed as previously described. Growth rates were calculated by normalizing OD values at 24 hours on OD values at time 0. Graphs were plotted as Mean $\pm$ SD on GraphPad Prism 8 software and p-values were calculated by Student's student's t-test and values  $\leq 0.05$  were considered significant ( $p \leq 0.05 = *$ ,  $p \leq 0.01 = **$ ,  $p \leq 0.001=***$ )

## **2.4 Long-term viability assay**

For long-term viability assays, DAOY and ONS76 cells were seeded at low density (150 cells/well) in 96-well plate and left 24h in the incubator to allow adherence. The day after, cells were treated in technical quadruplicates every 3 days for a total of 9 days with tivantinib at scalar concentrations. After 9 days, Crystal Violet (0.5% w/v in methanol) was added to each well for 15 minutes at room temperature. Pure methanol was added to dissolve Crystal violet and plates were put on a shaker for 20 minutes to facilitate the dissolution. Absorbance was measured at 570 nm with Varioskan<sup>tm</sup> LUX multimode microplate reader (ThermoFisher Scientific, USA).

## **2.5 Synergy study for combination treatments**

DAOY and ONS76 cells were seeded in 96-well plate and treated the day after with either single agents or a combination of two drugs according to the experimental design. After 72 hours, MTT assay was performed (Figure 6A) as previously described. Drug dose and effect for each sample were computed using Compusyn Software to calculate Combination index values (Figure 6B). CI values reports were calculated and generated for each combinatorial treatment.

According to the Chou-Talalay method:  $CI < 1$  indicates synergistic effect;  $CI = 1$  indicates additive effects;  $CI > 1$  indicates antagonistic effects (Chou, 2010). CI values derived from for each combination treatment were plotted as heatmaps generated on R software (Figure 6C)

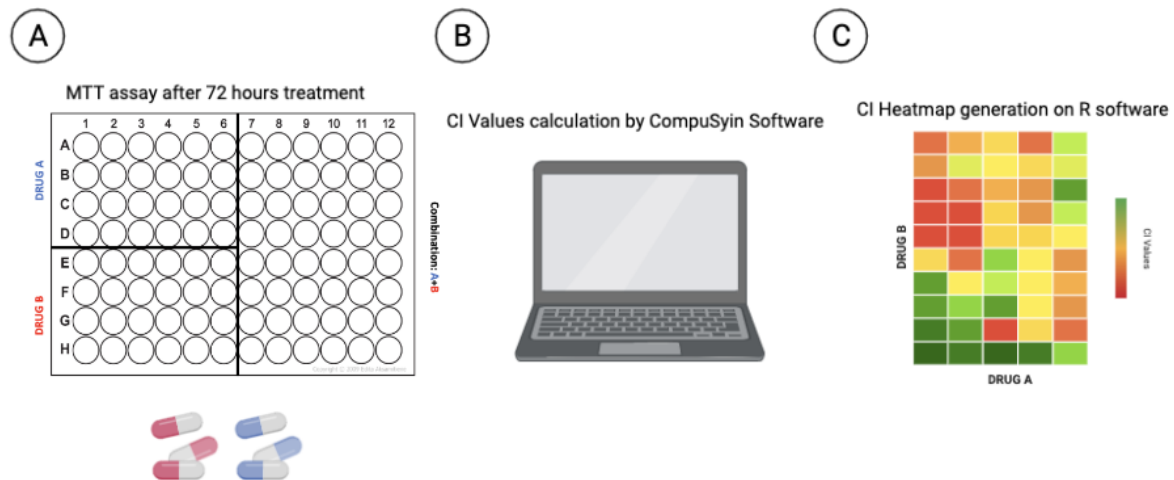


**Figure 6: Workflow of combinatorial treatments**

A) MB cells were seeded in 96-well plate and treated for 72 hours with single agents (Drug A and Drug B) and with combinations (Drug A+ Drug B). B) Dose and response for each condition were entered in CompuSyn software to calculate combination index values. C) Mean of three independent replicates were plotted as heatmap on R software. An example of the workflow as image was generated using Biorender (<https://biorender.com/>).

## 2.5 Colony formation assay

DAOY and ONS76 were seeded in a 6-well at 150.000 cells/well density and pre-treated for 24h with different concentrations of tivantinib. After 24h, cells were detached with trypsin, counted and seeded at low density (200 cells/well) in a 6 well plate. 15 days after, pictures of colonies were taken and staining with Crystal Violet (0.5%) was performed. Crystal Violet was dissolved in pure methanol. Plates were placed on a shaker for 20 mins to allow dissolution and absorbance was measured at 570 nm with Varioskan™ LUX multimode microplate reader (ThermoFisher Scientific, USA). Results were normalized to the untreated samples and plotted as Mean±SD in GraphPad Prism 8 software.

## 2.6 Neurosphere formation assay

DAOY and ONS76 were seeded in a 6-well plate and then, treated with tivantinib at different concentrations for 24h. After a day, cells were detached, washed with PBS and resuspended in fresh media. Single cell suspensions of DAOY and ONS76 were obtained by mechanical disaggregation using 25-gauge needle. Single cells were then seeded in technical replicates in 6-well plates (5000 cells/well) previously coated with 1.2% Poly 2-hydroxyethyl methacrylate (PolyHema, Sigma) and cultured in DMEM/F12 (Sigma) supplemented with B27 (50X) (ThermoFisher Scientific USA), bFGF (20 ng/ml) and EGF (20 ng/ml) EGF (ThermoFisher Scientific, USA). Spheres with a size above 50 µm were manually counted after 5 days at the Evos FL Auto 2 microscope (Invitrogen).

## 2.7 3-D spheroids model

DAOY adherent cells were detached, manually counted and centrifuged 100 x g for 10 min. Pellet was gently resuspended in 3ml of RPMI medium. 1500 cells/well were seeded as 100 µl in each well of the Nunclon Sphera 96-well microplate. (ThermoFisher Scientific, USA). The plate was centrifuged at 200xg for 2 minutes in order to allow single cells to aggregate in spheroids. Spheroids were left in the incubator at 37°C and 5% CO<sub>2</sub> for 5 days without any disturbance. After the incubation, formed spheroids were treated according to experimental designs. Pictures of spheroids were taken at the Evos FL Auto 2 microscope (Invitrogen) at different time points (day0-day3-day6-day9). Volumes were measured with ImageJ software and calculated with the formula:

$$Volume = \frac{(Length) * (Width)^2}{2} \text{ (Jensen et al., 2008)}$$

Each volume was normalized to the respective volume at time 0 and plotted on GraphPad Prism 8 software as Mean±SD.

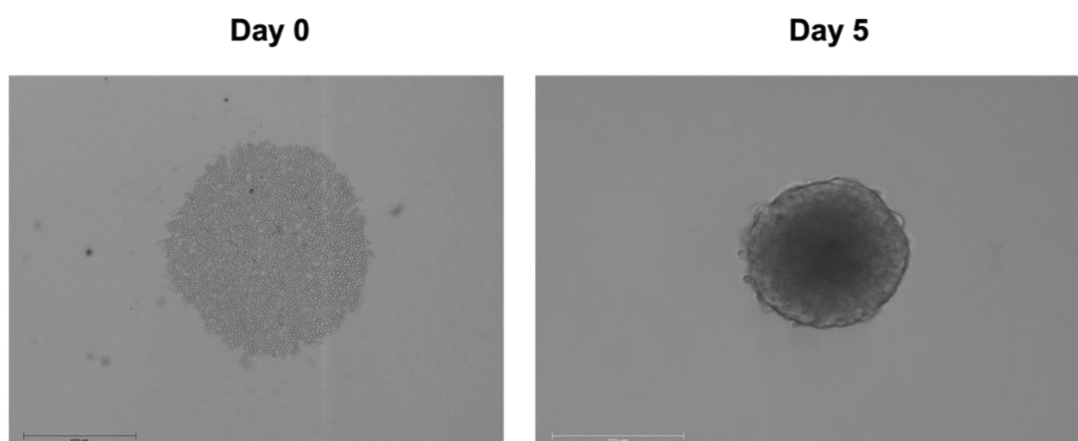


**Figure 7: Representative pictures of spheroids post-seeding and after 5 days**

DAOY were seeded at density of 1500 cells/well in Nunclon Sphera 96-well microplate. (ThermoFisher) and then centrifuged for 2mins at 200g. Spheroids were left for 5 days in the incubator to allow formation. Representative picture was taken right after the plating and after 5 days at the Evos FL Auto 2 microscope (Invitrogen).

## **2.8 Cell cycle analysis by Flow Cytometry**

DAOY, ONS76 and UW228 cells were seeded at 150.000 cells/well density and treated the day after with tivantinib, foretinib and crizotinib in technical duplicate. After 24 h, cells were detached with trypsin, washed twice with PBS and fixed in cold ethanol 70% overnight. Vortex was used to avoid cell clumps. Samples were then washed twice with cold PBS and bearing in mind that propidium iodide stains both RNA and DNA, 50  $\mu$ L of RNase A (Sigma-Aldrich) (stock concentration: 100  $\mu$ g/ml) was added for 15 mins at 37°C to digest RNA molecules. Propidium iodide (PI) solution (Stock concentration: 50  $\mu$ g/ml) (APEX-BIO) was then added for 15 mins in the dark at room temperature. By using BD FACSVerse flow cytometer (BD Biosciences), 10.000 events were analysed for each condition. FCS files were generated on the BD flow cytometer, and histograms and statistics were obtained by gating cells on for each sample on FlowJo software. Graphs with the percentage of cells in each phase were plotted with GraphPad Prism 8.

## 2.9 Apoptosis assay by Caspase 3/7 detection

Apoptotic pathway was studied by assessing the caspase 3/7 activation. For the 2D study, DAOY (1500 cells/well), ONS76 (1000 cells/well) and UW228 (2000 cells/well) were seeded in white bottom plate. Once cells were attached, treatment with c-MET inhibitors was performed for 24h at different concentration in technical duplicates. Activation of caspase 3/7 was evaluated by Caspase-Glo 3/7 Assay (Promega) following the manufacture's protocol. After 1 h of incubation, luminescence data were acquired with Varioskan<sup>™</sup> LUX multimode microplate reader (ThermoFisher) and results were normalized to untreated cells. Caspase 3/7 activation was analysed in 3D-DAOY spheroids model by adding CellEvent Caspase-3/7 Green Detection Reagent (final reagent concentration: 3 $\mu$ M) (ThermoFisher). After 30 min of incubation, fluorescence pictures were taken with Evos FL Auto 2 microscope (Invitrogen).

## 2.10 siRNA transfection

ON-TARGETplus siRNAs, SMARTpool siRNAs against MET (Cat.ID: L-003156-00-0005) and siGENOME non-Targeting siRNA Pool (Cat.ID: L-001810-01-05) were purchased from Dharmacon and resuspended in DNase/RNase-free water at 20 $\mu$ M stock concentration. Aliquots of 50 $\mu$ l were made to avoid degradation due to continue defrosting. DAOY cells were seeded in either 6-well plate (for protein extraction) or 96-well plate (for cell viability assay) and left for 24h to allow attachment. A day after, cells were transfected with siMET (100nM) and siCTR (100nM) using Lipofectamin 2000 (Invitrogen) and Reduced-Serum Medium Opti-MEM<sup>™</sup> (Gibco) in antibiotic-free media. 24h later media was replaced to avoid Lipofectamin-related toxicity, and assays were performed after 72h.

## 2.11 Establishment of H2B-GFP stable cell lines

H2B-GFP plasmid (neomycin resistance gene) (#11680) was purchased from Addgene as agar stab. Prior to transfection, plasmid was purified out of the bacteria using Qiagen Plasmid Midi Kit (Qiagen). Purified DNA was transfected with Lipofectamin 2000 (Invitrogen) at 2 $\mu$ g/ml concentration. A "kill-curve" with neomycin was performed on control cells to establish the

concentration of antibiotic needed to kill all the non-transfected cells in order to culture only cells that integrated the plasmid. Next, cells were kept in antibiotic selection with neomycin (G418) (Roche) at 1mg/ml concentration for 2 weeks and presence of GFP-positive cells was confirmed at the Evos FL Auto 2 microscope (Invitrogen) before performing further analyses.

## 2.12 Cell fate analysis by automated time-lapse microscopy

ONS76, DAOY and UW228 cells were seeded in technical quadruplicates in a 96-well plate and treated according to the experimental design, either with c-MET kinase inhibitors or with siRNA against MET. Cells were maintained at 37°C and 5% CO<sub>2</sub> in the Cytation 3 system (Biotek) where pictures were taken every 15 min for 72 h at 10X magnification to create time-lapse videos. Only cells in interphase, with a typical flattened morphology, were taken in consideration at time 0 before starting the analysis. Then, 40 cells for each condition were analysed by looking at cell's morphological changes (summarised in Figure 8 below) to define: entering in mitosis (cells round up when enter in mitosis), mitotic slippage and apoptotic cell death either in interphase or during mitosis. The term "slippage" defines an event when the cell does not complete the cellular division (cytokinesis) and comes back to the interphase forming tetraploid and multinucleated cells (Brito & Rieder, 2006; Sinha et al., 2019). Events of apoptosis were recognized by cell bubbling and presence of fragments.

Results of interphase duration, mitosis length, and time of cell death either in mitosis or interphase for each single cell were manually recorded and plotted with GraphPad Prism 8 as time in minutes and each bar colour corresponds to an event:

**Light grey** = Interphase

**Blue** = Slippage

**Black** = Mitosis

**Brown** = Death in interphase

**Orange** = Death in mitosis

To show percentages of cell fates derived from the manual analysis, pie charts were generated on GraphPad Prism 8 Software by plotting:  $\frac{\text{Number of cells in a certain fate}}{\text{Number of total cells tracked}}$ .

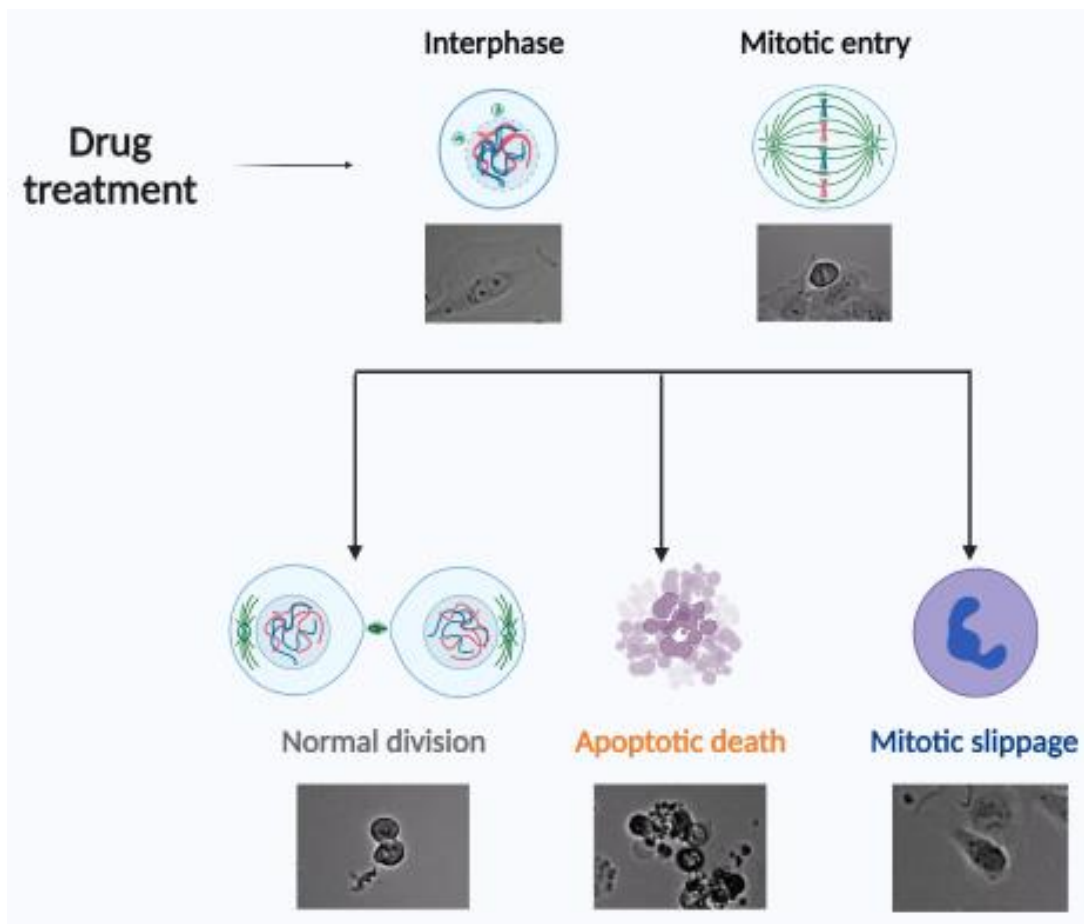


**Figure 8: Schematic view of cell fate decisions upon drugs treatment**

Treatments with different drugs lead to different responses in terms of cell fate decisions: single cell that enter mitosis can undergo normal division, mitotic cell death or death during interphase, and mitotic slippage. Representative pictures of DAOY cells are showed in the diagrams.

## 2.13 Protein extraction and Western blot analysis

Cells were seeded and cultured in 6-well plates. For proteins extraction, cells were washed with cold PBS and scraped. Homemade Triple Lysis Buffer containing 50 mM Tris-HCl (pH 7.5), 150 mM NaCl, 0.1 % SDS, 1% NP-40 and 0.5 % sodium deoxycholate, was added to the cells and collected in tubes. Prior to adding to the cells, Protease and Phosphates inhibitors cocktail were added to the buffer (Santa Cruz Biotechnology). After 30 mins in ice, lysates were centrifuged at 13000 rpm for 15 mins and then quantified with Bradford assay (Biorad). Absorbance was measured at 595nm using a spectrophotometer. Protein lysates were diluted using distilled water and Loading Dye (6X) (Fisher Scientific). To avoid protein denaturation, lysates were boiled at 99° for 10 minutes. Equal amounts of lysates (40 µg) were loaded on 4-10% SDS polyacrylamide gels before starting electrophoresis. Either PageRuler Prestained Protein Ladder (ThermoFisher) or Precision Plus Protein Kaleidoscope (Biorad), was loaded into the gel as molecular weight reference. Gels were then transferred to polyvinylidene difluoride (PVDF) membrane (Merck Millipore) for 1 hour and 30 minutes at constant amperage (400 mA). Ponceau S (Biorad) staining was used to assess successful protein transfer. Filters were blocked with 5% milk solution in PBS supplemented with Tween 0.1% (Biorad) (T-PBS) and incubated with primary antibodies overnight in a cold room. Next, filters were washed 3 times with T-PBS and incubated for 1 hour with secondary antibodies. Finally, signals for proteins of interests were detected by mixing equal parts of West Femto Chemiluminescent Substrate (ThermoFisher), added on the membranes for 60 seconds in the dark. Images were taken with G: BOX SynGene software. Densitometric analysis was performed by measuring band intensity with ImageJ software and each band was normalized to the loading control (GAPDH/Vinculin). Graphs were generated on GraphPad Prism 8 software.

Primary and secondary antibodies used in this study are listed below:

- **MET Rabbit mAb** (Cell signalling Technology) – 1:1000
- **Phospho-MET Rabbit (Tyr1234/1235) mAb** (Cell signalling Technology) – 1:1000
- **AKT Rabbit mAb** (Cell signalling Technology) – 1:1000
- **Phospho-AKT (Ser473) mAb** (Cell signalling Technology) – 1:1000
- **p44/42 MAPK (Erk1/2) Rabbit mAb** (Cell signalling Technology) 1:1000

- **Phospho-p44/42 (Thr202/Tyr 204) MAPK Rabbit mAb** (Cell signalling Technology) 1:1000
- **PARP (46D11) Rabbit mAb** (Cell signalling Technology) 1:1000
- **Mcl-1 Antibody Rabbit mAb** (Cell signalling Technology) 1:1000
- **Cyclin B1 Antibody Rabbit mAb** (Cell signalling Technology) 1:1000
- **P70 S6 Kinase (49D7) Rabbit mAb** (Cell signalling Technology) 1:1000
- **Phospho-p70 S6 Kinase (Thr389) Rabbit mAb** (Cell Signalling Technology) 1:1000
- **GAPDH Mouse mAb** (EMD Millipore) 1:10000
- **Vinculin Mouse mAb** (SantaCruz Biotechnology) 1:1000
- **Secondary Ab anti-Rabbit IgG**, HRP-linked (Cell signalling) (1:5000)
- **Secondary Ab anti-Mouse IgG**, HRP-linked (GE Healthcare) (1:3000)

## 2.14 Data manipulation and Statistical analysis

Data are presented as Mean±SD and p-values were calculated by Student's t-test and values less than 0.05 were considered significant ( $p \leq 0.05 = *$ ,  $p \leq 0.01 = **$ ,  $p \leq 0.001 = ***$ , ns= no significant). Graphs presented in this study were generated with GraphPad Prism Software (Version 8.0) with the exception for Violin plots and Heatmaps which were generated with R software (<https://www.R-project.org/>). Kaplan-Meier curves were generated on R2 Genomic and Visualization Platform (<http://r2.amc.nl/>).

# ***CHAPTER 3: Aims and Objectives***

Medulloblastoma (MB) is a highly heterogeneous disease, and it is currently classified in four subgroups on molecular basis (WNT, SHH, Group 3 and Group 4). Each subgroup is then subclassified in subtypes which can have important differences in prognosis and outcome. To date, MB is treated with a strong combination of surgical resection, chemo and radiotherapy. Side effects linked with this regimen are worrying and there is an urgent need to find and to characterize new targeted therapies. SF/HGF-c-MET pathway has been correlated with SHH MB pathogenesis and it has been proposed as potential MB treatment target. Various c-MET kinase inhibitors have been described as effective in hampering MB growth and dissemination. However, understanding mechanisms of action underlying their effects can be quite challenging.

The aims of this PhD project are to:

**AIM 1:** confirm the importance of c-MET kinase as potential target in SHH medulloblastoma, test commercially available c-MET kinase inhibitors and identify the most effective inhibitors in suppressing SHH MB cell lines proliferation in both 2D and 3D cultures.

**AIM 2:** define differences in how c-MET inhibitors cause SHH MB cell death and characterise the molecular changes that may be involved in the drug's effects.

**AIM 3:** perform combinatorial treatments with the most effective c-MET kinase inhibitor and chemotherapeutic drugs used to treat MB patients, or other small molecule drug inhibitors linked to HGF-c-MET pathway to investigate the possibility to lower the concentrations of chemotherapeutic drugs curtailing drug-resistance and toxicity.

#### **OBJECTIVES:**

- A panel of commercially available c-MET kinase inhibitors was tested *in vitro* on SHH-MB cell lines to evaluate their ability to impair cell proliferation in 2D and then in 3D models of SHH MB cells
- Cell cycle distribution and apoptotic activation was investigated upon treatments with effective c-MET kinase inhibitors to define possible mechanisms of anti-proliferative activity.
- To use high-throughput automated time-lapse microscope to create the cellular profiles (mitotic death, death during interphase, mitotic slippage, mitotic delay) of

SHH MB cell lines in response to effective c-MET kinase inhibitors and assessing the pharmacological variation to c-MET inhibitors.

- Western blot analyses were performed to identify the molecular determinants that dictate cellular cell fate changes in SHH MB cell lines treated with effective c-MET kinase inhibitors.
- Combinatorial strategies between chemotherapeutic drugs and c-MET kinase inhibitors were established to check their effectiveness *in vitro* to suppress SHH MB cell proliferation in 2D and 3D cellular models.

# ***CHAPTER 4: Results***

## 4.1 c-MET kinase is a suitable RTK therapeutic target in SHH medulloblastoma

In cancer tissues, RTKs are constitutively and aberrantly activated to promote uncontrolled proliferation, metastatic spreading and resistance to therapeutic interventions. For this reason, blunting the activity of RTK proteins has become an elective strategy in oncology (Takeuchi & Ito, 2011). To identify possible RTKs that perpetuate the malignant phenotype and representing a prime druggable targets in MB, first we assessed the expression of the 57 members of the RTK gene family in MB tumour samples compared to normal adult cerebella from patients with an age ranging between 23 to 50 years. By interrogating seven different dataset (Table 4; Figure 9A), obtained from R2: Genomic analysis and Visualisation Platform (<http://r2.amc.nl/>), which comprehend 500 MB primary tumour samples and 9 normal cerebella (Table 4), we found that only 36 RTK genes were significantly modulated in MB tumours when compared to normal adult cerebella (p-value < 0.05). Of these, only 8 candidate genes were significantly overexpressed in MB tumours: MET, PTK7, ROR1 and 2, RYK, EPHA3, EPHA8 and EPHB2. To further refine our initial list of gene targets, we completed a literature search to verify a possible implication of these genes in MB tumorigenesis and evaluate the availability of commercial inhibitors that can be repurposed for therapeutic strategy in MB. A literature search was generated with archived articles from PUBMED (<https://pubmed.ncbi.nlm.nih.gov/>) using as a query the keywords “medulloblastoma AND (official gene target name)”. Only primary research articles were selected for critical analyses and the number of outputs is reported in Table 5 below.

Table 5: Literature review outputs on RTKs in medulloblastoma

RTK	OUTPUTS	REFERENCES	INHIBITORS	
			Medchem Express	Selleckchem
MET	18	Tripolitsioti et al., 2018; Sharma et al., 2016; Zomeran et al., 2015; Kumar et al., 2015; Faria et al., 2015; D'Asti et al., 2014; Zhang et al, 2013; Onvani et al., 2012; Guessous et al., 2012; Guessous et al., 2010; Guessous et al., 2010; Provencal et al., 2010; Labbe et al., 2009; Kongkham et al., 2008; Li et al., 2008; Binning et al., 2008; Li et al., 2008; Li et al., 2005	66	43
ROR1	0		0	0
ROR2	1	Lee et al., 2013	0	0
RYK	0		0	1
PTK7	1	Messerli et al., 2017	0	0
EPHA3	1	Haeberle et al., 2012	0	3
EPHA8	1	McKinney et al., 2015	0	3
EPHB2	3	Bathia et al., 2017; Sikkema et al., 2012; McKinney et al., 2015	9	3

The highest number of outputs were identified for c-MET kinase and all studies assessed the oncogenic role of HGF/c-MET axis supporting the proliferative and invasive phenotype of MB cells. Contrasting evidence was instead identified for EPHB2. If Bhatia et al., corroborated our data and found that EPHB2 is upregulated in MB samples compared to normal cerebella and its siRNA-mediated knockdown sensitises MB cells to radiation (Bhatia et al., 2017), McKinney et al. found that EPHB2 is also strongly expressed in fetal cerebella (McKinney et al., 2015). No literature outputs were identified for RYK and ROR1 and limited evidence (a single article) were found for all other genes. Then, availability of small molecule inhibitors was assessed for all the identified receptors by using two of the leading suppliers of small molecule inhibitors with validated biological and pharmacological activities confirmed through pre-clinical and clinical research (<https://www.selleckchem.com/>; <https://www.medchemexpress.com/>). To date, no inhibitors are commercially available for ROR1, ROR2 and PTK7 receptors. A naturally occurring bioactive furochromone, named Khellin, is reported in Selleckchem as RYK inhibitor but it has aspecific activity and low potency against RTK receptors is instead reported in Selleckchem as RTK inhibitor. Up to 9 inhibitors are available against the Eph receptors, but they have been developed only to target EPHA2, EPHB4, EPHA4. As expected, up to 66 small molecule inhibitors have been developed against c-MET kinase and several of them, including crizotinib and foretinib, have been also tested against medulloblastoma cell lines showing a potent anti-proliferative effect (Faria et al., 2015; Zomerman et al., 2015). Overall, these initial data identified c-MET kinase as the most ideal therapeutic RTK in MB.

## 4.2 c-MET expression and prognostic significance in MB subtypes

To support this initial finding that c-MET kinase is a promising RTK target in MB, we further ascertained the expression of c-MET kinase across an independent validation cohort that comprehends 763 primary MB tumour specimens with available clinical data related to 612 patients (Cavalli et al., 2017) (Figure 9B-C). Firstly, we considered c-MET expression across the four main MB subgroups, and we found that c-MET kinase is preferentially expressed in SHH MB compared to the other subgroups (Figure 9B). This trend has been already reported by Faria et al., (2015) showing in two large nonoverlapping cohorts of MB patients that c-MET kinase is a biomarker of SHH-driven MB (Faria et al., 2015).

In addition to this, we also evaluated c-MET expression across the different MB subtypes which bear distinct patient demographics, genetic abnormalities and clinical progression (Cavalli et al., 2017). We found that c-MET kinase is robustly expressed in the SHH- $\alpha$  subtype (Figure 9C) which affects non-infant children (>3 years old), and it is defined by accumulation of both germline and somatic TP53 mutations, amplification of MYCN or GLI2 and pathogenic germline alterations in ELP1 (Cavalli et al., 2017; Garcia-Lopez et al., 2021). Interestingly, the other three SHH subtypes (Shh- $\beta$ : infants with a poor prognosis; Shh- $\gamma$ : infants with a good prognosis; Shh- $\delta$ : adults) still expressed higher levels of c-MET kinase compared to all other MB subtypes (Figure 9C).

Next, we interrogated the dataset to explore the correlation between c-MET expression and the overall survival of MB patients. Initially, the total specimens (n=612) were divided in high and low-c-MET expression and the Kaplan-Meier curve was generated only by using the first and the last quartile of the patient cohort. Survival differences could not be determined according to c-MET expression across the full cohort or subgroups of MB patients (Figure 10A). Interestingly, a trend toward a poor survival was observed for high c-MET patients in the Group 3 population which displays a refractory phenotype to multimodal therapies and the worst prognosis across all MB subgroups (Northcott et al., 2019) (Figure 10D).

We also assessed the correlation of c-MET expression with the overall survival of MB patients according to their molecular subtypes (Figure 11). High c-MET expressing cohort displayed the lowest survival rates in the MB subtypes associated with the poorest survival, with the exception of WNT group which is usually related with good outcomes, (WNT- $\alpha$ : p-value =

0.033; SHH- $\beta$  : p-value = 0.038; G4- $\alpha$ : p-value = 0.018) (Figure 11 A-B-D); interestingly, a trend toward poor survival was also identified for all three subtypes of Group 3 MBs (Figure 11C). However, statistical significance was not reached for any of these subtypes, possibly due to the small number of patients in the cohorts. Altogether, these results provide evidence that c-MET kinase exert an oncogenic role in MB and a strong rationale to explore the targeting of c-MET kinase in SHH-MB.

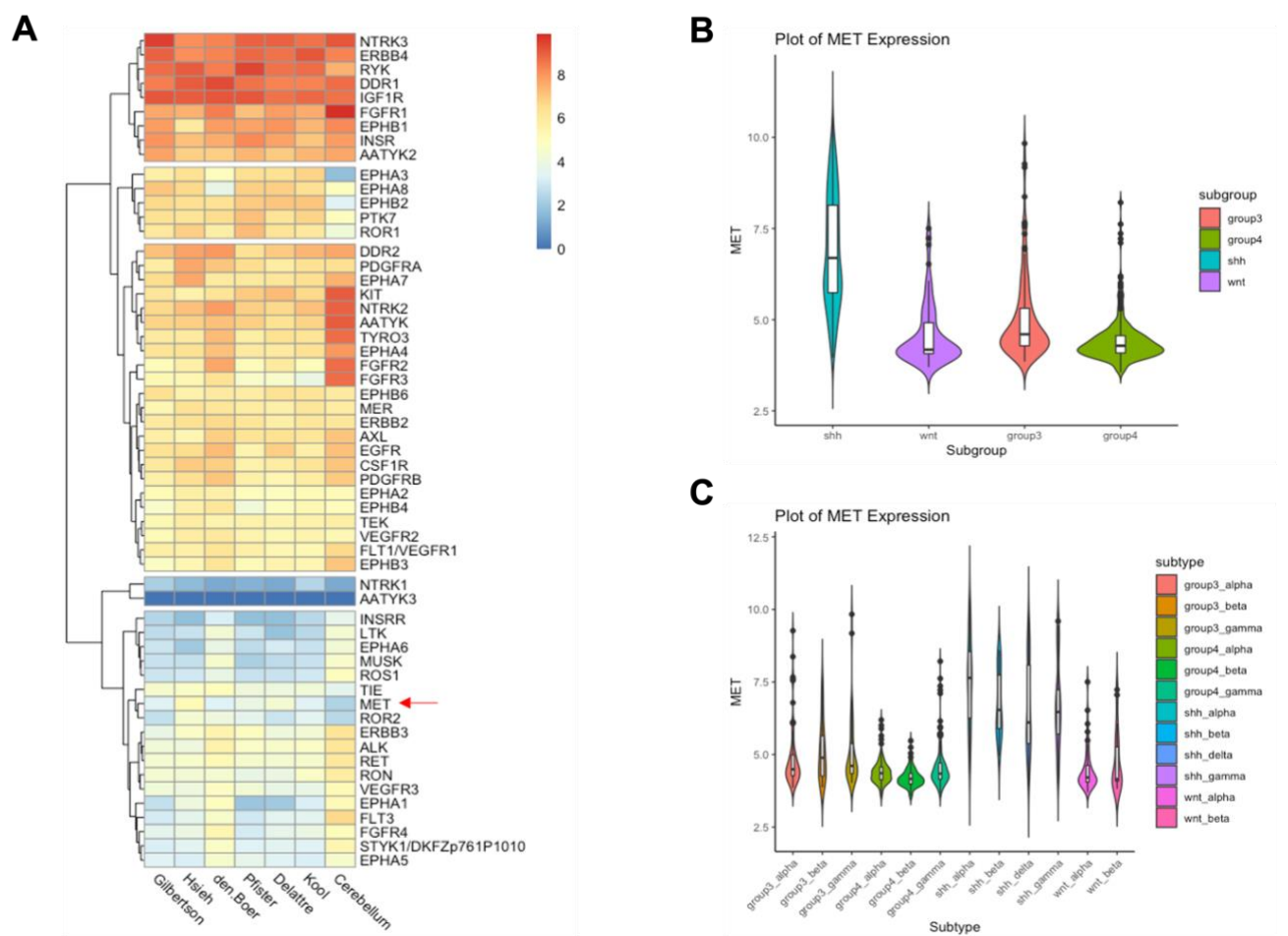


**Figure 9: RTKs and MET gene expression in medulloblastoma**

A) Gene expression analysis of tyrosine kinase receptors from six different medulloblastoma datasets compared with expression in healthy cerebellum. Heatmap was generated by plotting gene expression values on R software. B-C) MET gene expression in Cavalli dataset (MB samples=612) across medulloblastoma subgroups (p-value = 1.01e-115) (no of samples: WNT=70; SHH=223; Group 3= 144; Group 4= 326) (B) and subtypes (p-value = 3.75e-115) (no of samples: WNT $\beta$ =21; WNT $\alpha$ =49; SHH $\alpha$ =65; SHH $\beta$ =35; SHH $\delta$ = 76; SHH $\gamma$ =47; Group 3 $\alpha$ =67; Group 3 $\beta$ = 37; Group 3 $\gamma$ =40; Group 4 $\alpha$ =98; Group 4 $\beta$ = 109; Group 4 $\gamma$ =119) (C). All the data were visualized and analysed by R2 genomics analysis and visualization platform. References to each interrogated dataset are listed in Table 4 (Chapter 2).

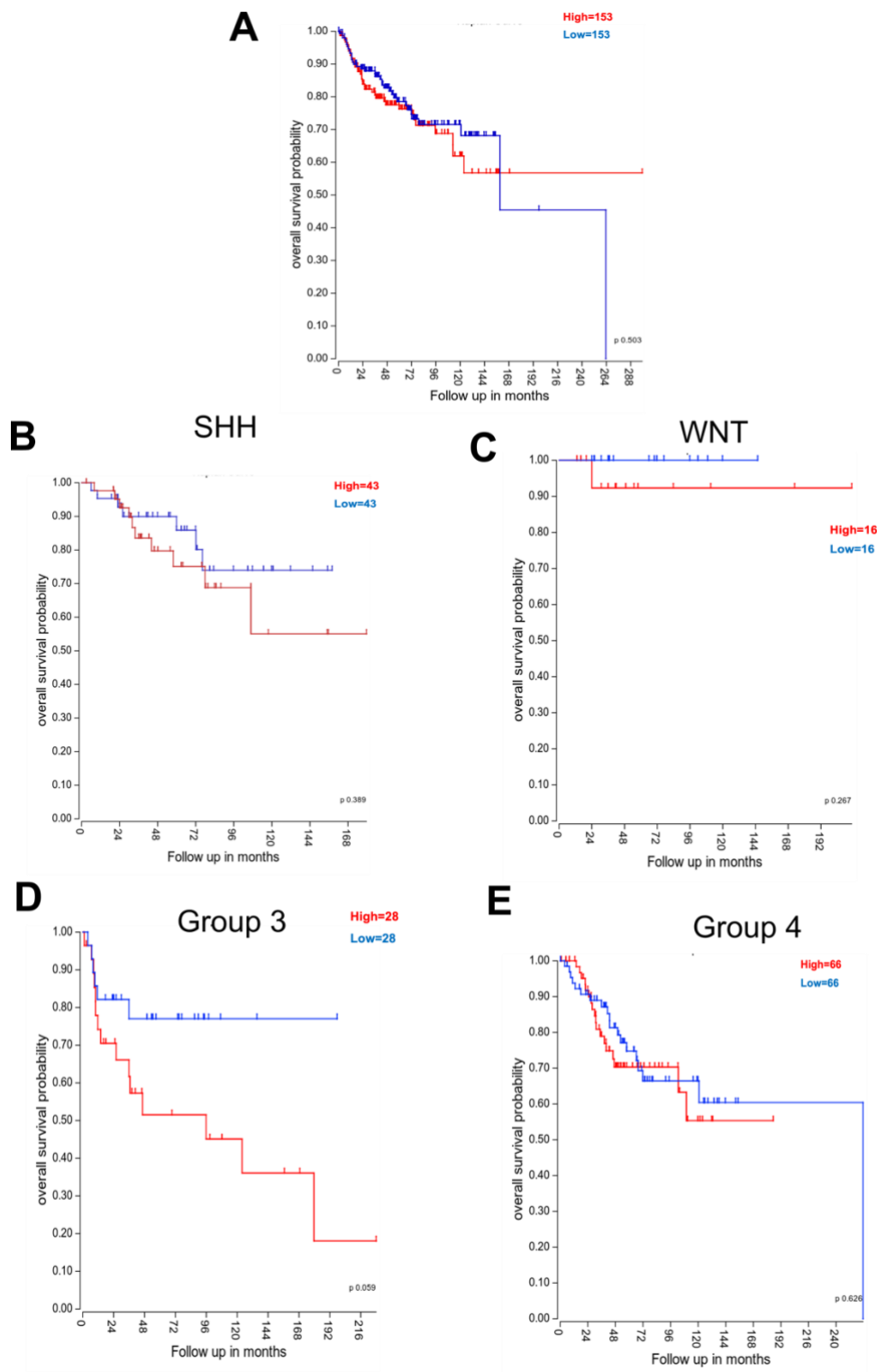


**Figure 10: c-MET kinase association with survival in MB patients**

A-E) Kaplan-Meier survival curves correlated to MET expression in medulloblastoma primary tumours (Cavalli et al., 2017). Survival rates based on MET expression were generated on R2 software across the whole cohort of MB patients (A) and for each MB subgroup: SHH (B), WNT (C), Group 3 (D), Group 4 (E). Statistical significance is indicated as p-value in each graph (bottom right corner).

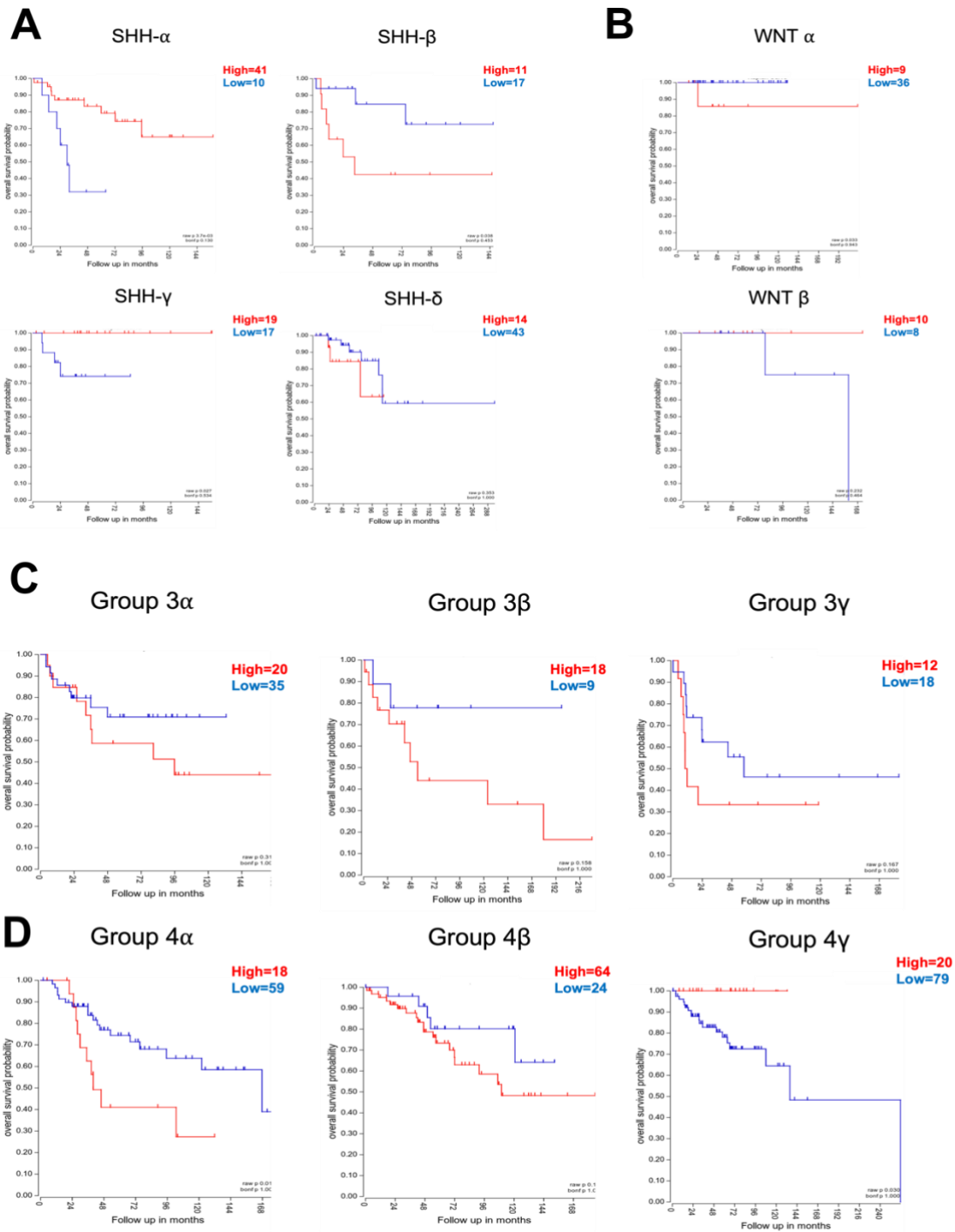


**Figure 11: Kaplan-Meier survival curves based on c-MET expression across MB subtypes**

A-D) Survival analysis of c-Met kinase expression for each subtype of medulloblastoma: A) SHH  $\alpha$  (n=51), SHH $\beta$  (n=28), SHH $\gamma$  (n=36) SHH $\delta$  (n=57). B) WNT  $\alpha$  (n=55), WNT  $\beta$  (n=18). C) Group 3 $\alpha$  (n=55), Group 3 $\beta$  (n=27), Group 3 $\gamma$  (n=30). D) Group 4 $\alpha$  (n=77), Group 4 $\beta$  (n=88), Group 4 $\gamma$  (n=99) (Cavalli et al., 2017). Kaplan-Meier curves displaying overall survival probability correlating to c-MET expression were generated by only using the first and the last quartile of the patient's cohort on R2 software and retrieved significance values are indicated as raw p-values in each graph.

## 4.2 c-MET kinase pathway activation in SHH MB cell lines

HGF dependent – c-MET kinase activation promotes the modulation of many downstream signalling pathways, such as ERK1/2 and PI3K/AKT, that affect tumour growth by stimulating proliferation, anti-apoptosis, invasion and angiogenesis in multiple tumour types (Birchmeier et al., 2003). To assess the integrity of the c-MET signalling pathway in SHH-driven MB cells, we first investigated the biochemical responsiveness of c-MET kinase to HGF stimulation on three different SHH MB cell lines (DAOY, UW228 and ONS76) (Figure 12). These cell lines were selected because harbouring different genetic abnormalities in the *TP53* gene, which has been reported to be highly prognostic for SHH MB patients and prioritised by the WHO for the design of new therapies (Ramaswamy et al., 2016): DAOY and UW228 are typical representative of a *TP53* mutant MB cell lines, whilst ONS76 cells are derived from a classic medulloblastoma tumour harbouring a *TP53* wildtype gene (Ivanov et al., 2016).

Analysis of activated c-MET signalling pathway was initially performed by measuring the level of phosphorylation of c-MET kinase following stimulation with exogenous human recombinant HGF and c-MET kinase inhibitor crizotinib (Rodig & Shapiro, 2010). Western blot analysis revealed that c-MET autophosphorylation was similarly induced by short time exposure to HGF (30 minutes) in both DAOY and UW228 cell lines (Figure 12). As expected, pre-incubation with the crizotinib abolished the tyrosine phosphorylation of c-MET in response to HGF. Despite HGF stimulation prompted the phosphorylation of c-MET, that was equally ablated by crizotinib, ONS76 cells were 10-fold less responsive to the HGF treatment. Interestingly, a limited reduction in the levels of c-MET phosphorylation was observed in the ONS76 cells after serum starvation, suggesting a ligand-independent stimulation of c-MET phosphorylation, possibly due to the activity of other RTK receptors or cellular adhesion (Varkaris et al., 2013). No differences were measured in the levels of total c-MET kinase after serum-starvation, HGF treatments or crizotinib pre-treatments in all SHH cell lines (Figure 10). Similar results were obtained when we assessed the ability of c-MET kinase to activate the downstream signalling cascades (pERK and pAKT). Of note, ONS76 cells still exhibited the highest levels of pERK and pAKT at baseline followed by a minimal stimulation upon treatment with HGF (Figure 12). Inappropriate activation of the signalling pathway of c-MET kinase or its HGF ligand has been shown to support MB malignancy (Li et al., 2008).

To further corroborate the role of c-MET kinase in supporting the proliferation of our SHH models, we first assessed cell proliferation of MB cell lines upon stimulation with c-MET ligand HGF. DAOY and ONS76 cell lines were subjected to serum starvation prior to HGF stimulation (Figure 13 A-B); whereas DAOY cells grew under normal serum conditions, proliferation assays showed that 10 ng/ml recombinant HGF increased significantly DAOY cell numbers relative to starved control cells. Co-treatments of DAOY cells with the c-MET inhibitor crizotinib halted the effect of HGF stimulation on proliferation for this cell line (Figure 13A). Interestingly, 24 hours stimulation with HGF did not promote a significant increase in the proliferation of ONS76 cells that also continued to grow under serum starvation (Figure 13B). Next, we employed siRNA-mediated knockdown of c-MET kinase in DAOY cells and assessed the effect of its silencing on cell proliferation. Transfection of DAOY cells with a siRNA directed against c-MET kinase resulted in the suppression of protein levels of c-MET (Figure 14A). When compared to siRNA control transfected cells, *MET* siRNA transfected cells showed a significant reduction in survival after 72 hours from transfection (Figure 14B), confirming that the direct inhibition of c-MET kinase can affect the growth of MB cells. Taken together, these data confirm the ability of SHH-driven MB cells to fully activate c-MET kinase upon stimulation with HGF and regulate the downstream signalling cascades that are responsible for most of the oncogenic properties of c-MET kinase (Gherardi et al., 2012). According to our data, activation of c-MET signalling pathway preferentially enhances the proliferation of mutant *TP53* MB cells whilst wild-type *TP53* cells only showed a minimal responsiveness to c-MET biochemical and proliferative stimulation when compared to *TP53* mutant cells.

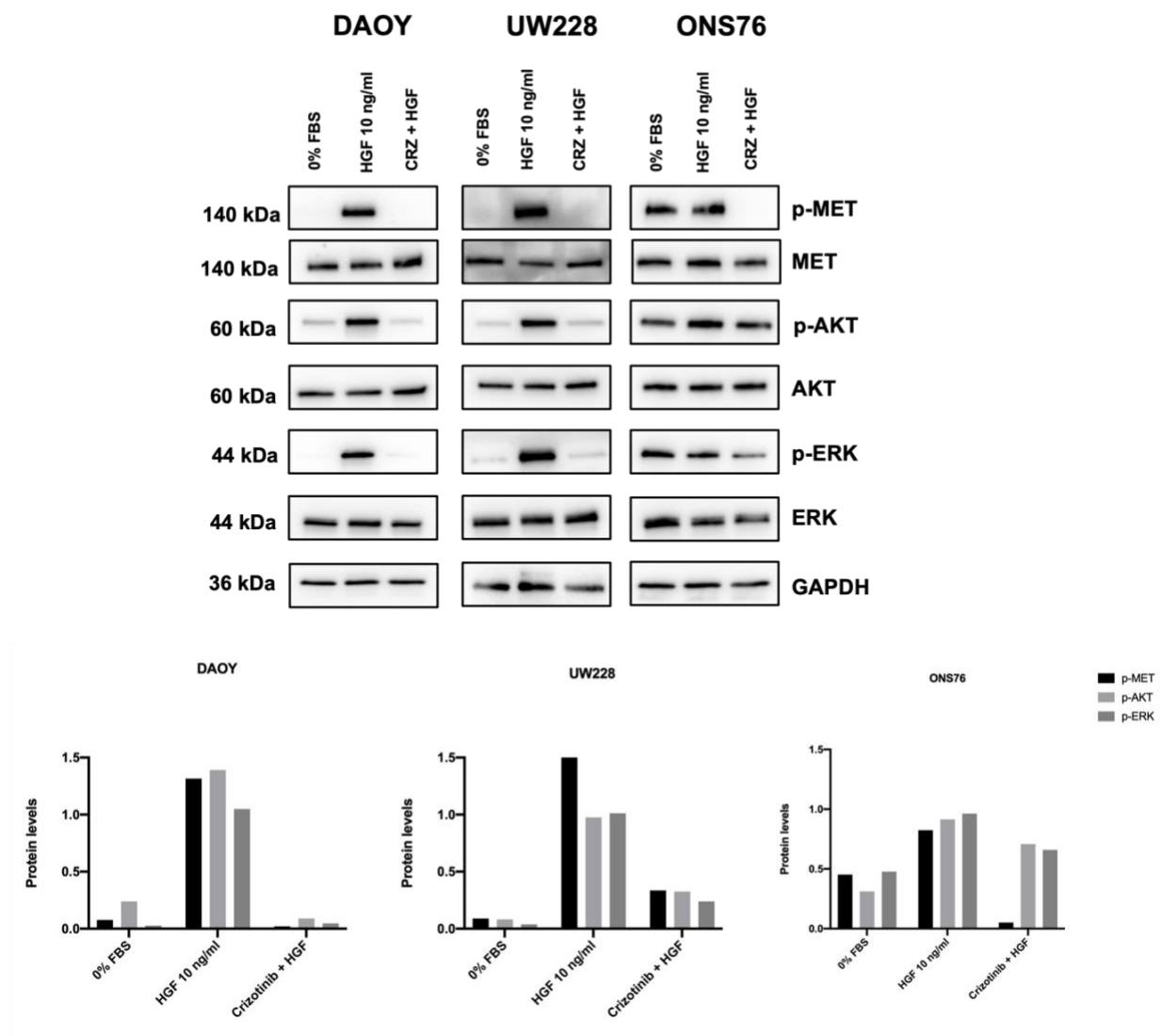


**Figure 12: c-MET kinase activation study in MB SHH cell lines**

Phosphorylation of c-MET kinase and its downstream signalling pathway activation was investigated in SHH cell lines via western blot analysis. Cells were starved for 24h followed by stimulation with human recombinant HGF (10 ng/ml) for 30 minutes. Pre-treatment with c-MET kinase inhibitor crizotinib (CRZ) was performed for 2hours before HGF-stimulation. GAPDH was used as loading control. Densitometric analysis was performed with ImageJ software and graphs are representative of phospho/total protein ratio for the representative experiment in the figure.

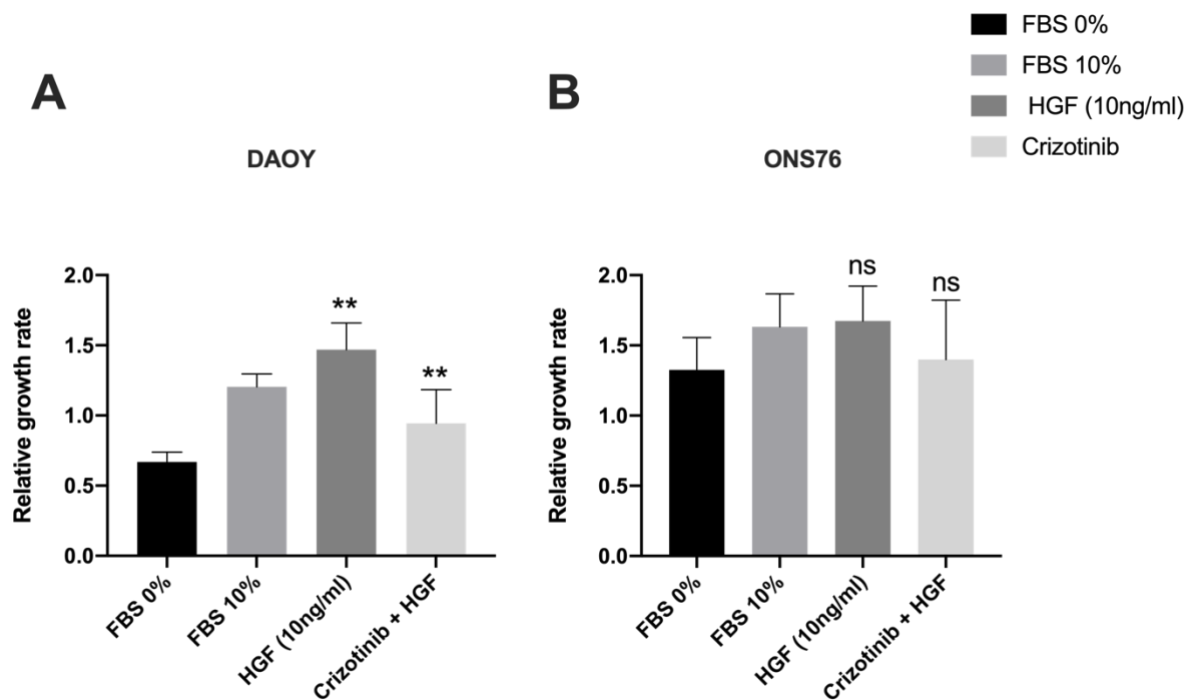


**Figure 13: Growth rate of SHH cell lines after HGF stimulation**

DAOY (A) and ONS76 (B) were seeded in 12-well plate and after 24h media was replaced with 0% FBS medium to starve cells. HGF (10 ng/ml) and crizotinib (1 $\mu$ M) were added for 24h. At the end point, MTT assay was performed, and results were normalized to absorbance read at time 0. Statistical significance was calculated with student's t-test between FBS 0% and HGF and between HGF and crizotinib ( $p \leq 0.05 = *$ ,  $p \leq 0.01 = **$ ,  $p \leq 0.001 = ***$ , ns= non-significant). Results (n=3) are showed as Mean $\pm$ SD were generated on GraphPad Prism 8 software.

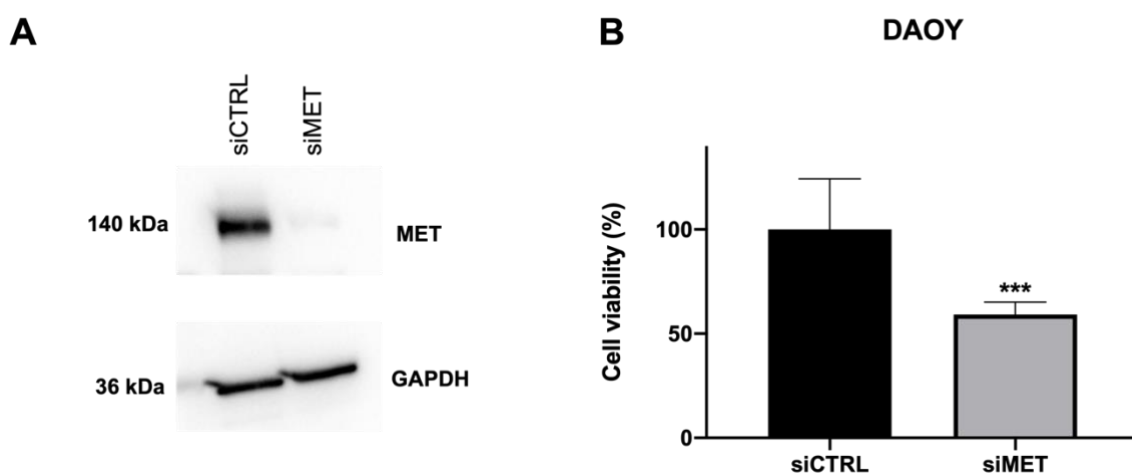


**Figure 14: siRNA-mediated c-MET knockdown impairs DAOY cell proliferation**

A) Western blot analysis was performed to verify c-MET kinase knockdown, 72h B) DAOY cells were transfected with siRNA scramble (siCTRL) and siRNA directed against c-MET at concentration of 100nM. After 72h, cell viability was assessed by MTT assay. Results are shown as Mean $\pm$ SD of two

independent biological replicates each performed in four technical replicates (n=2). Significance between siMET and siCTRL was calculated with student's t-test ( $p \leq 0.05 = *$ ,  $p \leq 0.01 = **$ ,  $p \leq 0.001 = ***$ ).

### **4.3 Tivantinib suppresses proliferation of SHH 2D and 3D models of MB cell lines**

To confirm that c-MET kinase confers proliferative advantages to SHH MB cell lines, we investigated the anti-proliferative efficacy of c-MET kinase inhibitors against SHH MB cells. To this aim, SHH MB cells were treated with linear dilutions of seven different c-MET inhibitors, with ATP or non-ATP competitive activity (Figure 5). MTT proliferation assays were performed 72h after treatment, and tivantinib was found to be the most effective drug in impairing cell proliferation of SHH MB cell lines (Figure 15 A-D). DAOY cells resulted to be the most sensitive cell line to tivantinib whilst ONS76 and UW228 showed around 20% residual cell viability when treated with the drug (Figure 15 B-C, Table 6). Both crizotinib and foretinib were effective in suppressing the proliferation of all SHH MB cell lines but at much higher concentration compared to tivantinib. With the exception of tepotinib, which showed ability to suppress proliferation only at a concentration forty times higher than tivantinib, the other three c-MET inhibitors did not present any anti-proliferative activity in the range of the concentrations we tested (Figure 15, Table 6). Given the sensitivity of SHH cell lines to tivantinib, we focused our attention on comparing the effects of tivantinib with foretinib and crizotinib, both previously shown to be effective against medulloblastoma cells (Endersby et al., 2021; Faria et al., 2015). Representative pictures of DAOY (*TP53* mutant) and ONS76 (*TP53* wild-type) cells were taken 72h after treatments to investigate the presence of any morphological changes upon treatment with the three drugs (Figure 16 A-B). Cells treated with tivantinib clearly showed accumulation of apoptotic bodies preferentially in DAOY (Figure 16A) rather than ONS76 (Figure 16B) cells. Interestingly, a consistent increase in cell size was observed for both cell lines when treated exclusively with crizotinib or foretinib (Figure 16 A-B).

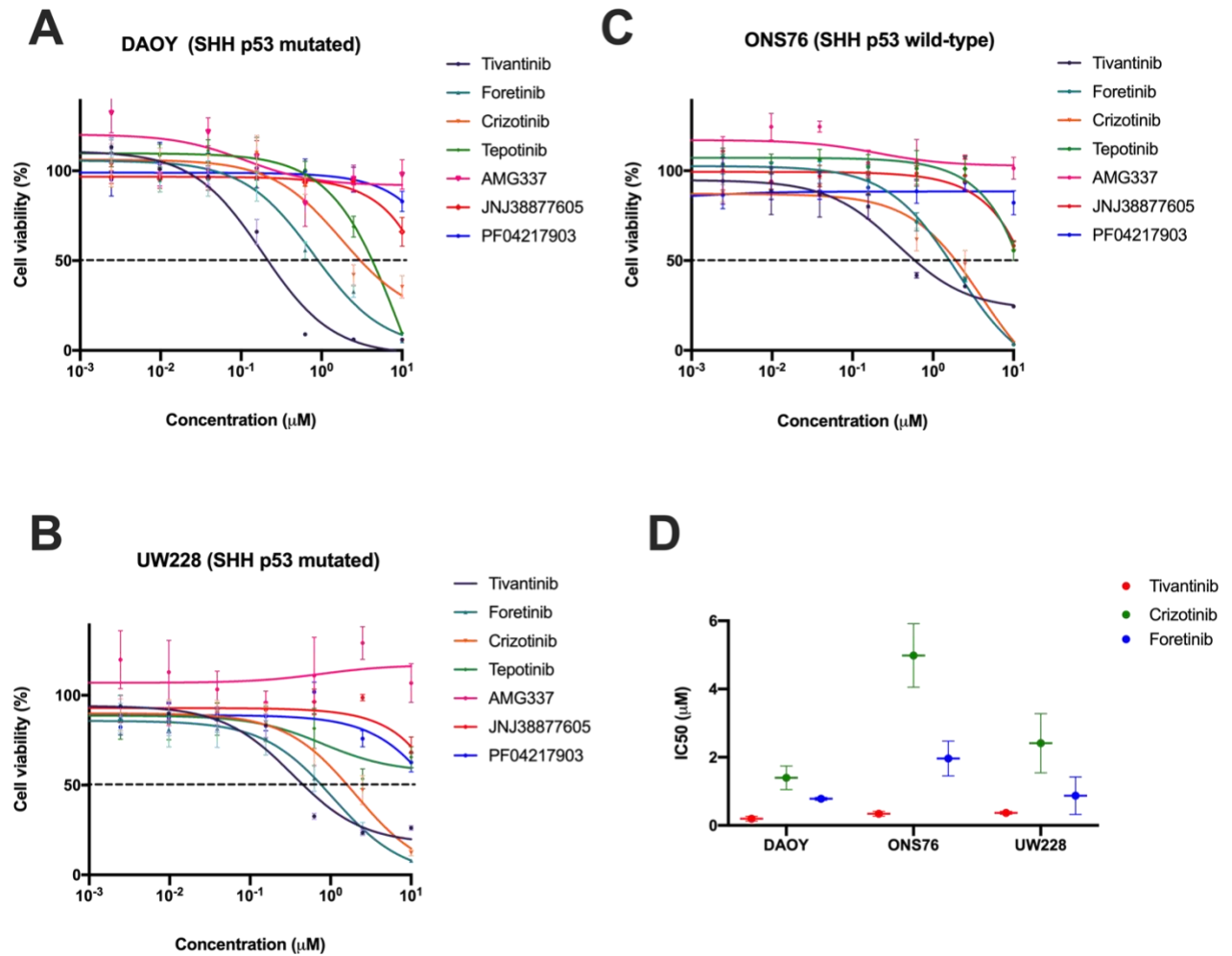


**Figure 15: Anti-proliferative effects of MET inhibitors on SHH cell lines**

A-D) SHH medulloblastoma cell lines DAOY (A), UW228 (B) and ONS76 (C) were treated for 72h with increasing concentration (fold dilution=1:4) of different c-MET inhibitors and cell viability was assessed by MTT assay. Results were relative to untreated cells and are shown as Mean±SD (n=3). (D) IC50 values for tivantinib, foretinib and crizotinib were calculated with GraphPad 8 software and shown as Mean±SD of the three independent experiments.

**Table 6: IC<sub>50</sub> values calculated for each c-MET inhibitor**

IC<sub>50</sub> for each compound tested was calculated on GraphPad Prism 8 Software is represented in the table as Mean±SD of three independent experiments and N.D indicates the drugs were calculation of IC<sub>50</sub> was not possible.

<b>IC50 (μM)</b>	<b>DAOY</b>	<b>UW228</b>	<b>ONS76</b>
<b>Tivantinib</b>	0.19±0.06	0.36±0.04	0.34±0.07
<b>Crizotinib</b>	1.39±0.34	2.41±0.86	4.98±0.93
<b>Foretinib</b>	0.78±0.04	0.87±0.55	1.96±0.51
<b>Tepotinib</b>	5.88±4.20	N.D	N.D
<b>AMG337</b>	N.D	N.D	N.D
<b>JNJ38877605</b>	N.D	N.D	N.D
<b>PF0421793</b>	N.D	N.D	N.D

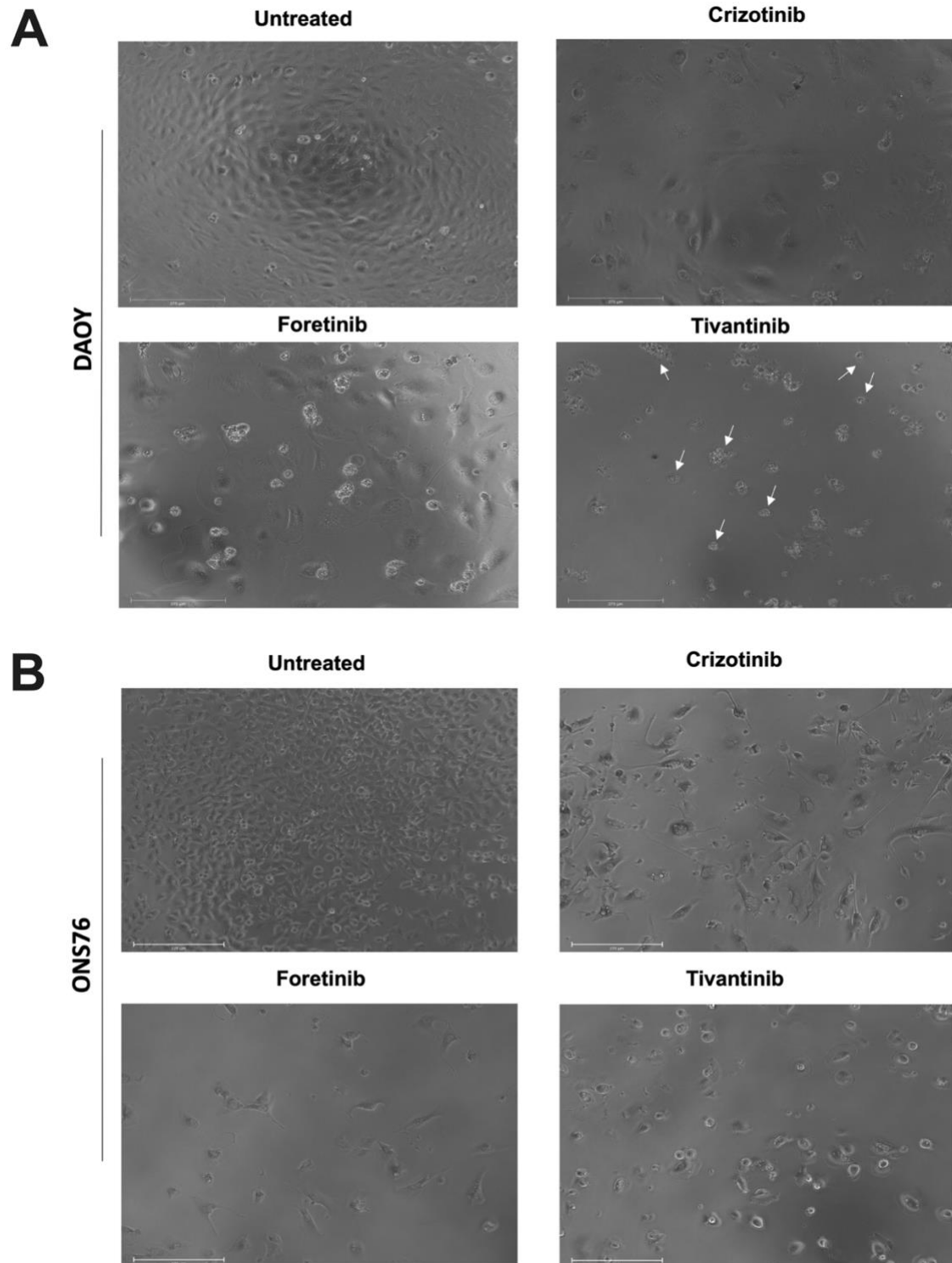


**Figure 16: Bright-field pictures of DAOY and ONS76 upon treatment with tivantinib, foretinib and crizotinib**

Pictures of DAOY and ONS76 treated with crizotinib, foretinib and tivantinib (2.5  $\mu$ M) were taken after short-term viability assay (72 h) with Evos FL Auto 2 microscope (Invitrogen) at 10X magnification (scale bar = 275  $\mu$ m).

Furthermore, we evaluated the time-dependent response, in terms of cellular proliferation, to tivantinib over a period of 72h in DAOY and ONS76 cells. MTT assays results showed that tivantinib exploited its anti-proliferative effects already at 24h in both SHH-MB cell lines. However, treatment with tivantinib caused a significant and dose-dependent reduction of cell proliferation in DAOY cells (Figure 17A). Even though ONS76 cells treated with tivantinib showed a significant time and dose-dependent decrease in proliferation rates compared to untreated cells, a complete suppression of cell growth was not evident in these cells when compared to DAOY (Figure 17B).

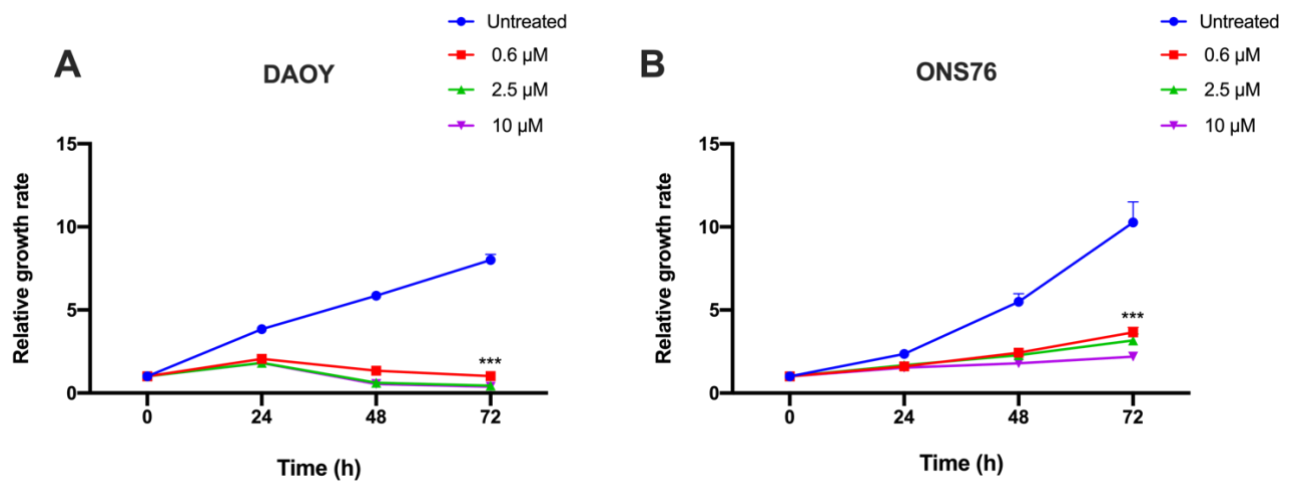


**Figure 17: Proliferation rates upon treatment with tivantinib in SHH-MB cells**

A-B) DAOY (A) and ONS76 (B) cells were seeded in 96-well plates and treated with tivantinib at different concentrations for 72h. A reference plate after the seeding was read for each cell lines (Time 0 plate). MTT assay was performed at 24, 48 and 72h and absorbance at each time point were normalized to absorbance at time 0 to establish growth rates in both cell lines. Student's t-test ( $p \leq 0.05 = *$ ,  $p \leq 0.01 = **$ ,  $p \leq 0.001 = ***$ ) was performed to statistically compared viability at time 0 vs viability at 24, 48 and 72h for both cell lines (n=3).

Sensitivity to the tivantinib was then tested by using 3D tumour spheroids, a tumour model previously established in the laboratory and that better mimics the biological features of the original tumour (Buzzetti et al., 2021; Edmondson et al., 2014). Thus, we challenged DAOY 3-D spheroids for 9 days treatments with tivantinib at 1 and 10 $\mu$ M concentrations and results were compared to the effects of crizotinib and foretinib at the same concentrations. As shown in Figure 18, treatment with tivantinib was effective in hampering spheroid growth over time and started to be effective at 1 $\mu$ M after only three days of treatment (Figure 18 A-B); spheroid structures were completely dissociated when treated with both concentrations of tivantinib with the maximum effect after 9 days of treatment (Figure 18A). When compared to tivantinib, 1 $\mu$ M treatments with foretinib and crizotinib did not induce any significant reduction in the spheroid volumes (Figure 18B); 10  $\mu$ M concentration of foretinib was required to significantly reduce spheroid volumes to the same extent as tivantinib at 1  $\mu$ M (Figure 18A-B). No reductions in volume were observed for crizotinib treatments and even 10 $\mu$ M concentration only showed limited reduction when compared to tivantinib. To summarise, SHH MB cell lines showed a time- and dose-dependent sensitivity to c-MET kinase inhibitors with tivantinib outperforming all inhibitors including foretinib and crizotinib.

In addition, we preliminarily tested the c-MET kinase efficacy (1 and 10 $\mu$ M) in ONS76-derived 3D spheroids. Here, we firstly observed that, in contrast with DAOY 3D spheroids, untreated spheroids generated from ONS76 cells did not show evidence of growth over a period of 9 days (Supplementary 1). We then evaluated the spheroids volume after 9 days of treatment with c-MET inhibitors in comparison with the untreated and we showed that tivantinib and crizotinib at both 1 and 10 $\mu$ M did not significantly affect the spheroids volume (Figure 19 A-B). Interestingly, treatment with foretinib at 10 $\mu$ M caused a significant increase in ONS76 spheroids volume after 9 days treatment (Figure 19 A-B)

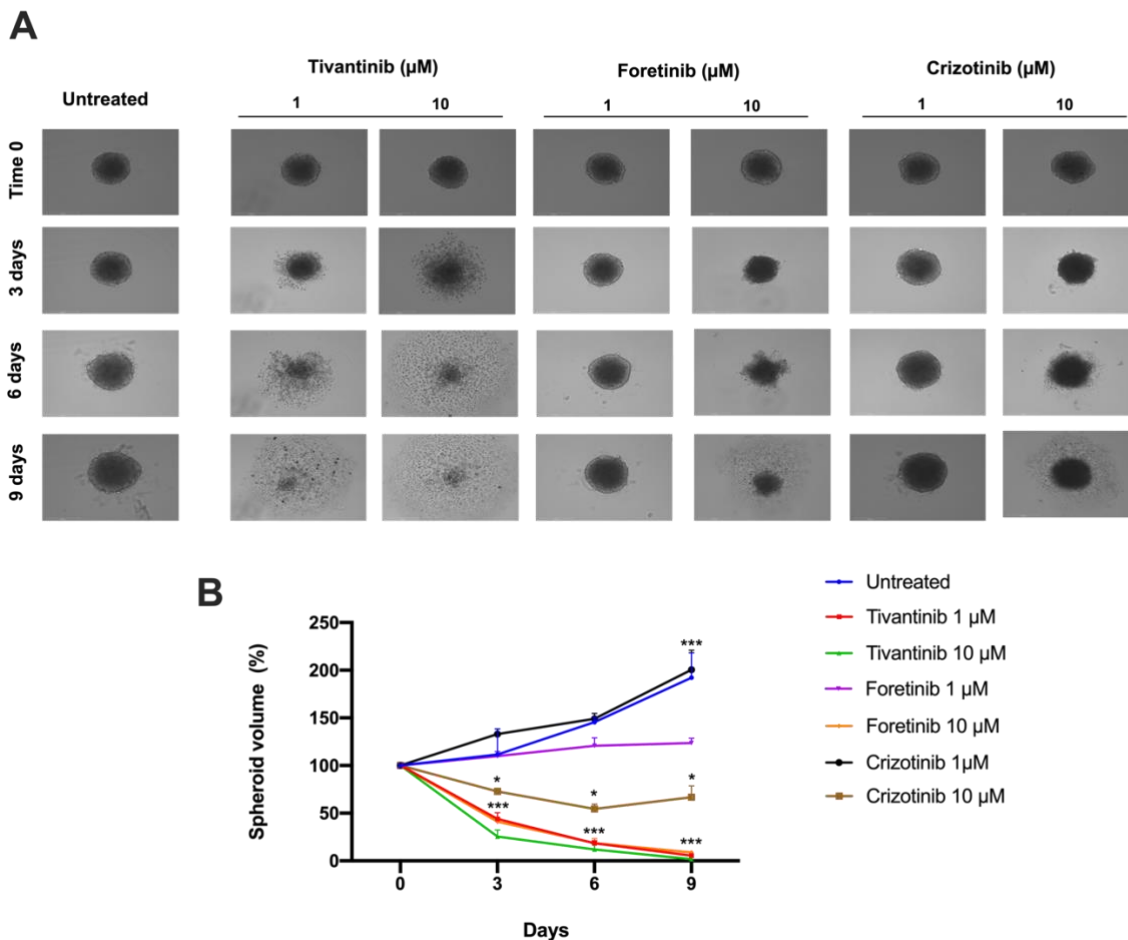


**Figure 18: c-MET kinase inhibitors ability to hamper 3D spheroid's structure**

A-B) DAOY (1500 cells/well) cells were seeded in U-bottom 96-well plate and left for 5 days to allow spheroids formation. Spheroids were treated with c-MET kinase inhibitors at 1 and 10 $\mu$ M concentration every 3 days for 9 days. A) Pictures of DAOY spheroids were taken at time 0 and after 3, 6, and 9 days with Evos FL Auto 2 microscope (Invitrogen) at 10X magnification (scale bar = 275  $\mu$ m) B) Volume of each spheroid was calculated at the end point and results were normalized to time 0 for the respective spheroid; relative growth rates were plotted on GraphPad Prism Software and are showed as Mean $\pm$ SD (n=3) Student's t-test ( $p \leq 0.05 = *$ ,  $p \leq 0.01 = **$ ,  $p \leq 0.001 = ***$ ) was performed to statistically compared volume at time 0 vs volume at 3, 6, and 9 days for each treatment.

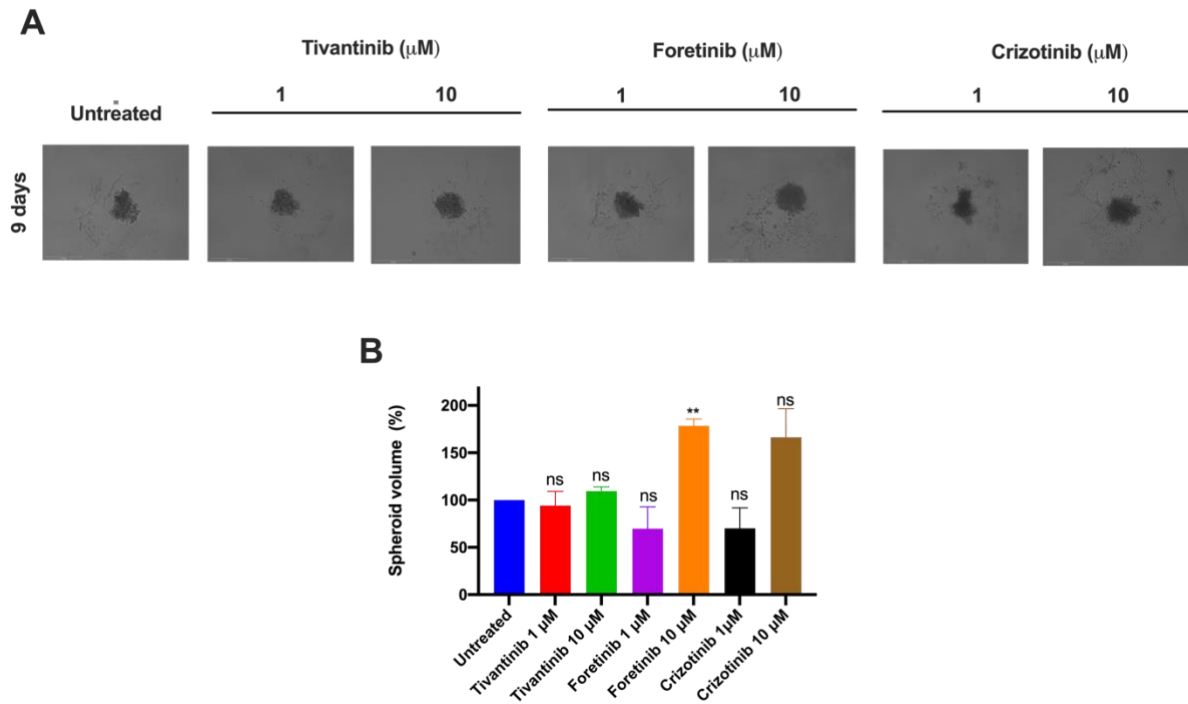


**Figure 19: Preliminary data on ONS76 3-D spheroids after 9 days treatment with c-MET inhibitors**

A-B) ONS76 (1500 cells/well) cells were seeded in U-bottom 96-well plate and left for 5 days to allow spheroids formation. Spheroids were treated with c-MET kinase inhibitors at 1 and 10 $\mu\text{M}$  concentration every 3 days for 9 days. A) Pictures of ONS76 spheroids were taken after 9 days with Evos FL Auto 2 microscope (Invitrogen) at 10X magnification (scale bar = 275  $\mu\text{m}$ ) B) Volume of each spheroid was calculated at the end point and results were normalized to untreated spheroids after 9 days; Volumes were plotted on GraphPad Prism Software and are showed as Mean $\pm$ SD (n=3, technical replicates). Student's t-test ( $p \leq 0.05 = *$ ,  $p \leq 0.01 = **$ ,  $p \leq 0.001 = ***$ ) was performed to statistically compared volume of untreated vs treated.

#### 4.5 c-MET inhibitors differences in regulating cell cycle distribution

To further investigate how tivantinib inhibits SHH MB cell proliferation, cell cycle distribution of DAOY, ONS76 and UW228 cell lines was assessed by flow cytometry 24h after treatments with tivantinib, foretinib and crizotinib. Treatment with tivantinib induced a dose-dependent accumulation of cells in sub-G1 in all the SHH-MB cell lines (Figure 20 A-C). DAOY cells resulted again significantly more sensitive to tivantinib when compared to ONS76: an average of 45% of DAOY cells accumulated in Sub-G1 when treated with 1 $\mu$ M of tivantinib, whilst ONS76 cells showed a 20% significant accumulation of cell in Sub-G1 (Figure 20 A-B). When treated with tivantinib UW228 cells showed a G2/M arrest still coupled with nearly 20% of cells accumulating in Sub-G1 (Figure 20 C). Treatment with foretinib altered the Sub-G1 population of both cell lines to a limited extent and only when cells were treated with 1 $\mu$ M concentration of the drug (Figure 20 A-C). Specifically, DAOY and ONS76 cells showed an average of 7% and 6% respectively, of cells accumulated in Sub-G1. In sharp contrast to tivantinib, foretinib preferentially induced a G2/M arrest in all the three cell lines with more than 50% of the cells accumulated in G2/M after 24h treatment with the drug. At the same time, foretinib also caused the specific appearance of a polyploid population in both DAOY and ONS76 cell lines (Figure 20 A-B). No significant differences in cell cycle distribution were observed when SHH-MB cells were treated with crizotinib at 0.5 and 1 $\mu$ M concentrations for 24h, highlighting the low potency of the drug ( $IC_{50} > 1\mu$ M) when compared to tivantinib and foretinib (Figure 15 D Table 6).

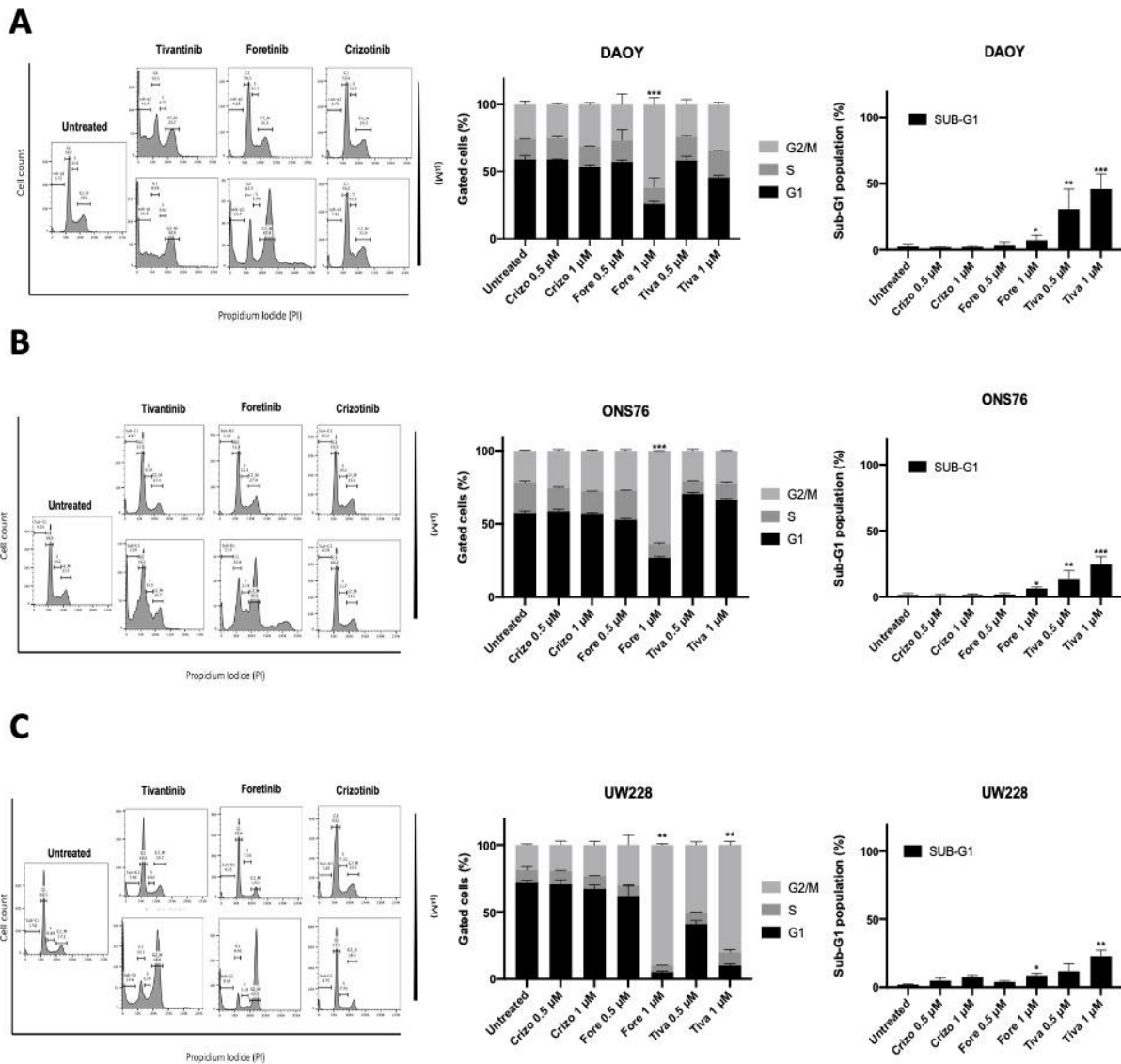


**Figure 20: Cell cycle analysis upon treatment with tivantinib, foretinib and crizotinib**

A-C) Cell cycle analysis with 24h c-MET inhibitors treatment on DAOY (A), ONS76 (B) (n=3) and UW228 (C) (n=2). Cell cycle phases were determined based on DNA content by propidium iodide staining with flowcytometry. Representative histograms are shown and were obtained by gating cells on FlowJo Software. Representative G1, S and G2/M populations are plotted as percentages Mean±SD. Sub-G1 populations were separately calculated, and results are presented as Mean±SD. Statistical comparison for both Sub-G1 and G2/M phases was calculated with Student's t-test ( $p \leq 0.05 = *$ ,  $p \leq 0.01 = **$ ,  $p \leq 0.001 = ***$ ) between treated and untreated cells.

To further support these results, we investigated whether tivantinib, foretinib and crizotinib specifically induce apoptotic cell death in SHH MB cells. To this aim, activation of Caspase 3/7, an essential event in the onset of cellular apoptosis (Shi, 2004), was evaluated upon 24h treatment with the three drugs. As expected from the cell cycle results, in both DAOY and UW228 cell lines, tivantinib was able to induce a strong dose-dependent increase in the activity of the Caspase 3/7 when compared to foretinib and crizotinib (Figure 21 A-B). Despite

the Caspase 3/7 activation, at the concentration and time chosen for the treatments, ONS76 cells resulted to be also less sensitive to the effect of tivantinib in the induction of apoptosis when compared to the DAOY and UW228 cells (Figure 21C).

Finally, treatments with foretinib and crizotinib did not consistently alter Caspase 3/7 activity in any of the cell lines, further validating the previous results on the cell cycle. To further confirm the apoptotic induction by tivantinib in DAOY cells, we also assessed the Caspase 3/7-mediated apoptotic activation in DAOY 3D spheroid models. DAOY spheroids were treated with tivantinib at 0.5 and 1 $\mu$ M concentration and Caspase 3/7 activity was measured after 24h. As shown in Figure 22, tivantinib significantly induced apoptosis in DAOY spheroids in a dose-dependent manner compared to the untreated spheroids (Figure 22).

Altogether, these results suggested that tivantinib is effective in suppressing proliferation of SHH MB cells by inducing apoptotic death in both 2D and 3D culture models. This effect is particularly consistent in the *TP53* mutant SHH-MB cells, DAOY and UW228, where a prominent accumulation of cells in sub-G1 (Figure 20A) was measured coupled with induction of caspase 3/7 activity in both 2D and 3D models (Figure 21A-B; Figure 22).

Conversely, neither foretinib nor crizotinib treatments caused a consistent accumulation of cells in sub-G1 or a Caspase 3/7 activation, with foretinib inducing a major cell cycle arrest in G2/M and appearance of cells with polyploidy.

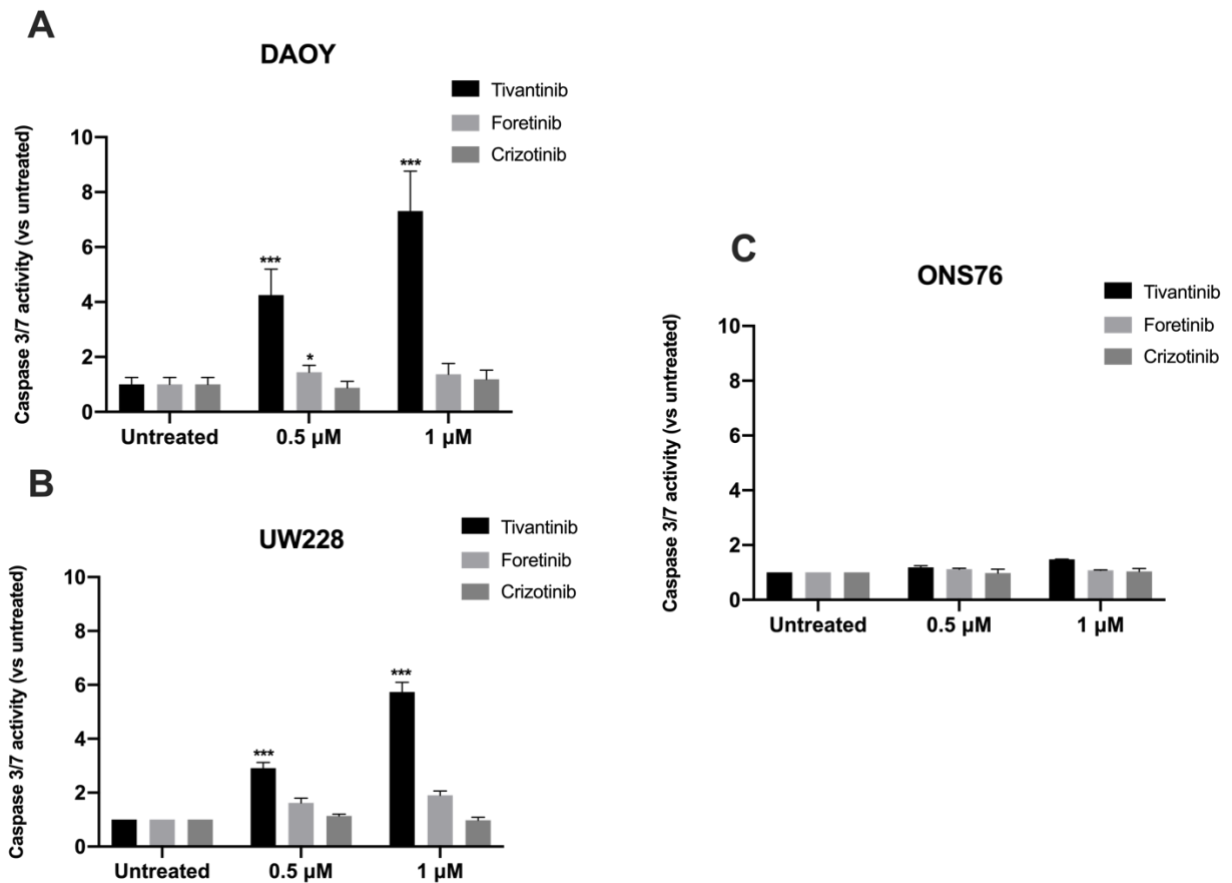


**Figure 21: Activation of apoptosis upon treatment with tivantinib, foretinib and crizotinib**

DAUY (A), UW22 (B) and ONS76 (C) were treated with tivantinib, foretinib and crizotinib (0.5 and 1 μM). After 24h, apoptotic activation was assessed by Caspase Glo luminescence assay. Results are presented as Mean±SD (n=2, each performed in technical replicates). Student's t-test ( $p \leq 0.05 = *$ ,  $p \leq 0.01 = **$ ,  $p \leq 0.001 = ***$ ) was performed to statistically compare treated samples vs untreated.

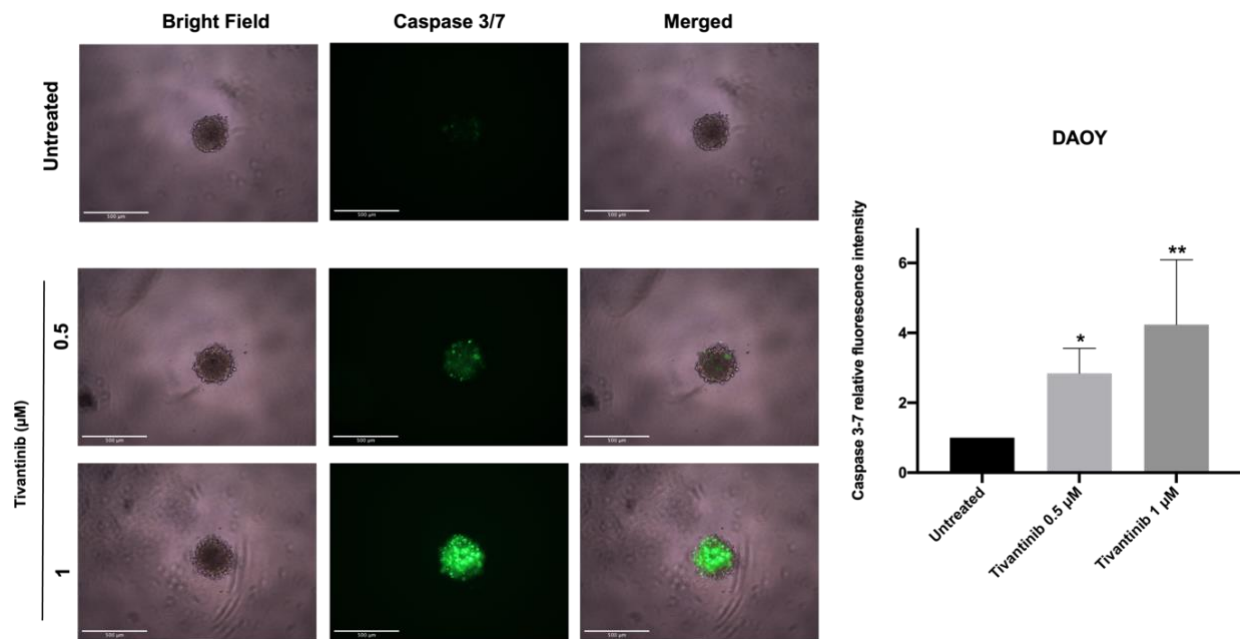


**Figure 22: Caspase 3/7 activation in 3D DAOY spheroids treated with tivantinib**

DAOY spheroids were treated with tivantinib at 0.5 and 1  $\mu\text{M}$  concentration for 24h. Apoptotic activation was assessed by adding CellEvent Caspase 3/7 detection reagent. Apoptotic cells are showed in green. Pictures were taken with Evos FL Auto 2 microscope (scale bar = 500  $\mu\text{m}$ ). Fluorescence intensity data are plotted as Mean $\pm$ SD (n=3), and statistical analysis untreated vs treated was performed with Student's t-test ( $p \leq 0.05 = *$ ,  $p \leq 0.01 = **$ ,  $p \leq 0.001 = ***$ ).

#### **4.7 Tivantinib affects long-term cell viability, colony formation and stemness in SHH cell lines**

Tivantinib is the most effective c-MET kinase inhibitor in suppressing cell proliferation of SHH MB cells when compared to other tested c-MET inhibitors. To further investigate its anti-proliferative potential, we first assessed its ability to curtail MB cells viability when SHH MB cells were exposed to multiple doses of the drug. SHH MB were challenged for 9 days with linear dilutions of tivantinib, and drug was refreshed every three days. At the end point, staining with crystal violet was performed to assess cellular viability and results showed that multiple treatments with tivantinib affect cell proliferation of all SHH MB cells with preferential inhibition of DAOY cells (Figure 23A). Interestingly, multiple treatments with tivantinib increased the drug sensitivity of all SHH MB cells as measured by the reduction of the relative  $\text{IC}_{50}$  values for the long-term treatments (DAOY = 0.04  $\mu\text{M}$ ; UW228 = 0.19 $\mu\text{M}$ ;

ONS76 = 0.14 $\mu$ M) when compared to single dose 72h treatments (DAOY = 0.19 $\mu$ M; UW228 = 0.36  $\mu$ M; ONS76 = 0.36  $\mu$ M) (Figure 23B; Table 6)

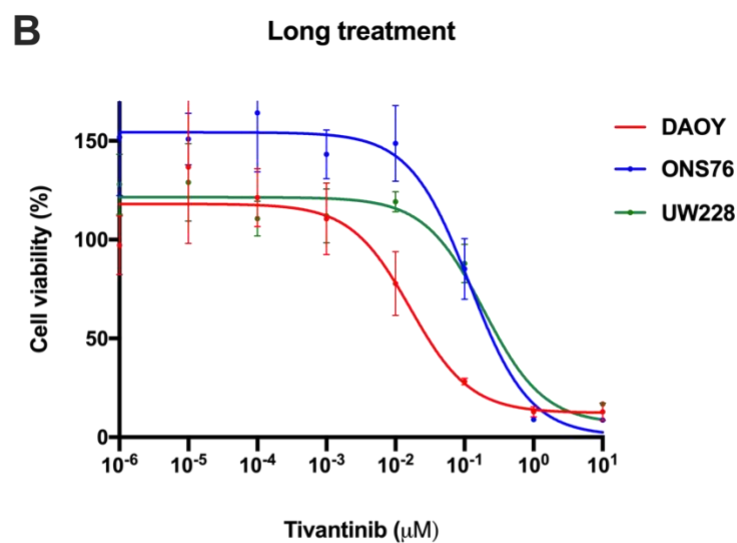
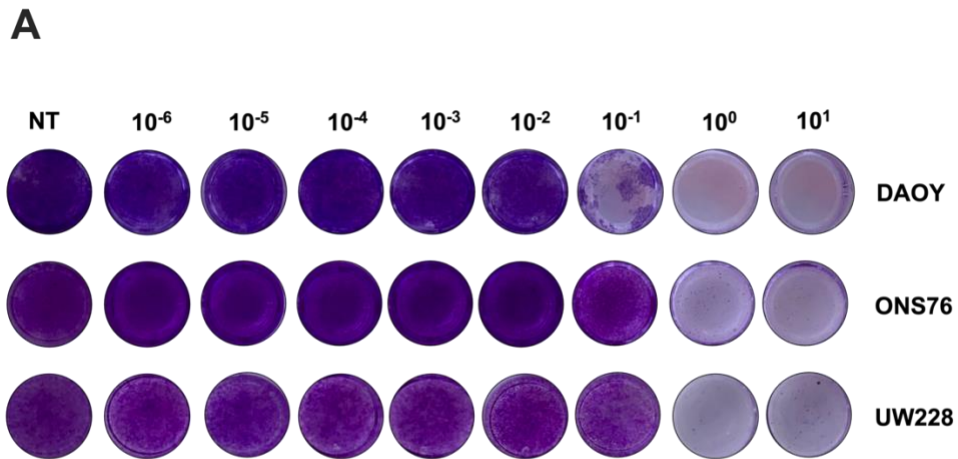


**Figure 23: Long-term tivantinib effects on SHH cell lines**

A) Representative crystal violet pictures of long-term treatment with tivantinib (n=3). DAOY, UW228 and ONS76 were seeded in 96-well plate at low-density (150 cells/well) and treated with tivantinib at linear dilutions starting from 10  $\mu$ M and with drug refreshed every three days for a total of nine days. At the end point, cells were stained with 0.5 % crystal violet. B) Crystal violet absorbance of each condition was then measured at 540 nm and results are plotted as Mean $\pm$ SD (n=3). IC50 values were calculated on GraphPad 8 software and are indicated in the table.

In the last decades, many studies have suggested that a population of cells that display stem properties, so-called cancer stem-like cells (CSCs), can drive progression and relapse of numerous tumours (Chen et al., 2016). Stemness is one of the key features of medulloblastoma relapse and MB resistance to therapy (Casciati et al., 2020). Therefore, targeting medulloblastoma cancer stem cells (MBSCs) represents a promising option for MB patients (Huang et al., 2016). Thus, the ability of tivantinib to affect medulloblastoma stemness was evaluated *in vitro* by assessing colony formation ability and production of medullospheres.

For colony formation ability, DAOY and ONS76 cell lines were treated with tivantinib for 24h and then seeded at low-density to evaluate the ability of single cells to grow into a colony after treatment. After 15 days of colony forming time, cells were stained with crystal violet and colony formation was assessed. In both cell lines, pre-treatment with tivantinib significantly impaired their ability to form colonies in a concentration-dependent manner when compared to untreated cells with the maximum effect at 1 $\mu$ M (Figure 24 A-B). Concomitantly, we also assessed the ability of tivantinib to suppress the efficiency of medulloblastoma cells to form medullospheres. In this case, DAOY and ONS76 cell lines were treated with tivantinib 0.1, 0.5 and 1 $\mu$ M concentrations for 24h; after treatment, single cells were seeded in low-attachment plate and 5 days later medullospheres were manually counted. Results showed that a single 24h pre-treatment with tivantinib caused a significant reduction of the ability of a single MB cell to behave like a CSC in a dose-dependent manner with the highest inhibitory effect at 1 $\mu$ M (Figure 25 A-B).

Taken together, these results suggested that tivantinib affects stemness properties in SHH MB cells and its use can support tumour eradication.

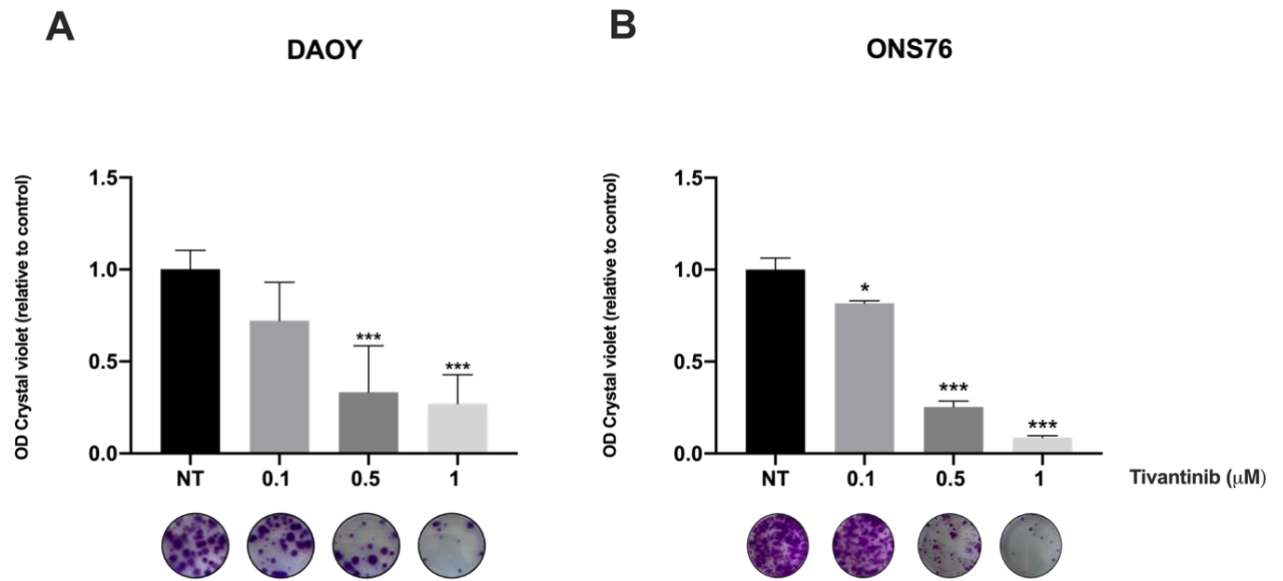


**Figure 24: Tivantinib effects on colony formation ability in DAOY and ONS76 cells**

A-B) Representative graphs and pictures of colony formation assays on DAOY and ONS76 cells. Cells were treated with tivantinib at 0.1, 0.5 and 1 $\mu\text{M}$  for 24 h. After a day, cells were detached, counted and seeded at low-density (200 cells/well) in a 6-well plate. 15 days later, colonies were stained with Crystal Violet 0.5%. Graphs show absorbance of Crystal Violet as Mean $\pm$ SD normalized to the untreated cells. Student's t-test was performed to assess the significance (n=3). ( $p \leq 0.05 = *$ ,  $p \leq 0.01 = **$ ,  $p \leq 0.001 = ***$ )

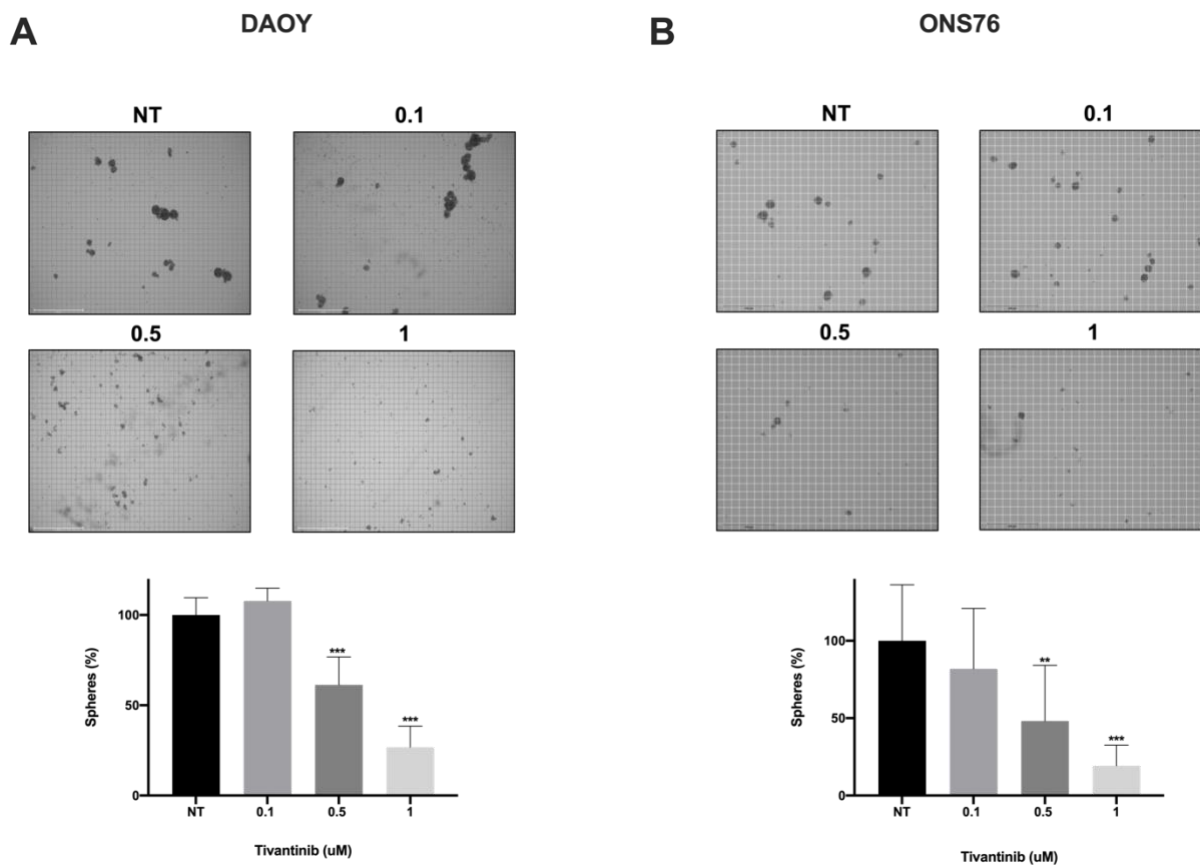


**Figure 25: Medullosphere formation upon tivantinib treatment in DAOY and ONS76 cells**

A-B) Representative graphs and pictures of DAOY and ONS76 medullospheres. Cells were treated with tivantinib at 0.1, 0.5 and 1 $\mu$ M for 24 h. After a day, cells were detached and counted. DAOY and ONS76 were seeded in low-attachment 6-well plate as single cells (5000 cells/well density). After 5 days, spheres above 50 $\mu$ m were manually counted. Percentage of spheres formation were normalized to the untreated cells and plotted as Mean $\pm$ SD. Student's t-test was performed to assess the significance ( $p \leq 0.05 = *$ ,  $p \leq 0.01 = **$ ,  $p \leq 0.001 = ***$ ) (n=2, each performed in triplicates).

## **4.8 Heterogeneous post-mitotic cell fate response to c-MET inhibitors in SHH MB cells**

Our observations showed that c-MET kinase inhibitors can impair SHH-MB cell proliferation with tivantinib exerting the more robust anti-proliferative activity. Interestingly, whilst tivantinib was induce a strong apoptotic response, other c-MET kinase inhibitors such as foretinib and crizotinib, although able to manifest an anti-proliferative effect against SHH MB cell lines, stimulated a G2/M arrest and did not trigger an apoptotic response. To better delineate the differences in the pharmacological responses of SHH-MB cells to the anti-proliferative activity of c-MET inhibitors, we challenged SHH-MB cells with tivantinib, foretinib and crizotinib and analysed the effects by high-throughput automated time-lapse light microscopy, investigating the cell fate profiles after treatment.

We initially established two cellular models of SHH MB cells expressing a GFP tagged version of the human H2B histone. These cellular models were used to visualise the different mitotic cell fates induced by treatments with c-MET inhibitors through the evaluation of changes in the nucleus and in the cellular morphology of MB cells (Kanda et al., 1998). Representative pictures of cells expressing H2B-GFP were taken every 10 minutes upon treatments with tivantinib or foretinib and, as shown in Figure 26, following mitosis, SHH cells were able to undergo three different cellular fates: initiate anaphase and divide in two daughter cells; exit mitosis without completing the cytokinesis, a phenomenon known as mitotic slippage; undergo cell death, either during interphase or during mitosis.

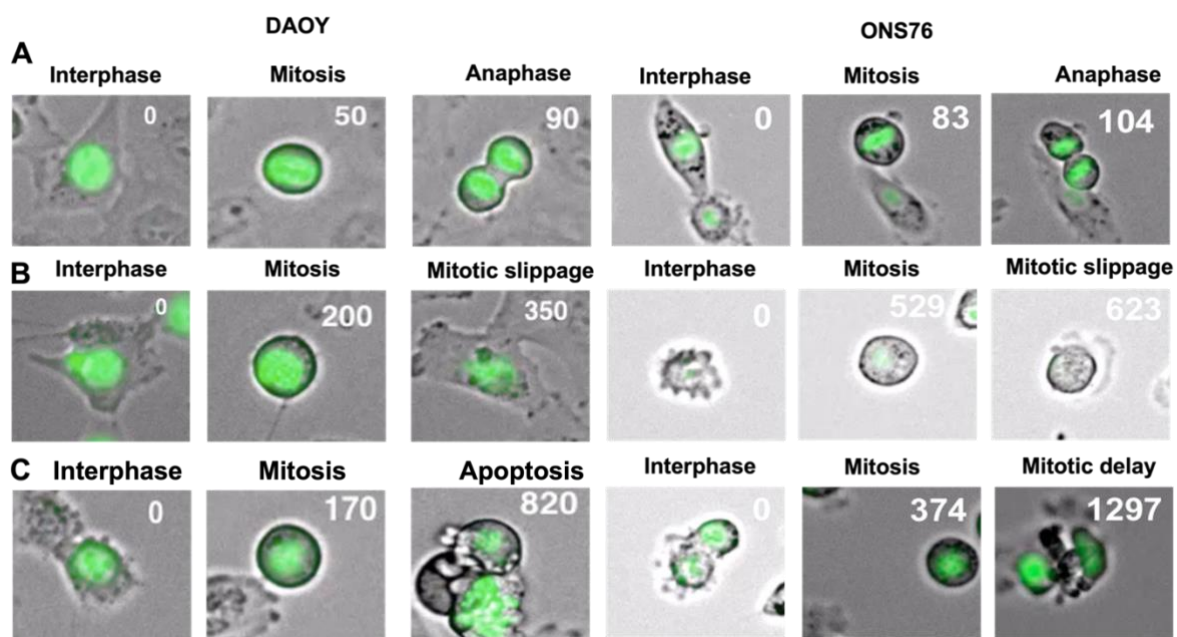


**Figure 26: Representative pictures of cell fate response visualized in H2B-GFP expressing DAOY and ONS76**

A-B-C) DAOY and ONS76 cells stably expressing H2B-GFP were either no treated (A) or treated with foretinib (B) and tivantinib (A) for 72h and subjected to time-lapse phase-contrast/fluorescence imaging to assess different cell fates. Cells were tracked until they entered in mitosis (round cells) and followed to assess difference in post-mitosis cell fates. Cells can initiate anaphase and divide (A), undergo mitotic slippage (B), undergo apoptotic death (C). Time (minutes) is indicated in white in the top-right corner.

We then performed the cell fate analysis by automated using time-lapse microscopy in bright field and cell fate profiles were constructed by tracking 40 unsynchronised cells for 72h after treatment with tivantinib, foretinib and crizotinib.

In the time frame chosen for the analysis, ~95% of untreated cells completed at least one full mitotic division and few events of death in mitosis or interphase were observed across all the three SHH cell lines (Figure 27A; Figure 28A; Supplementary 3). Interestingly, different SHH-MB cells displayed differences in the profiles of the cell fate when treated with the same drug. The extent of this variations is illustrated by the behavior of SHH cells in response to 0.5 $\mu$ M tivantinib. The majority of DAOY cells exhibited an extended mitosis (Figure 30), with 75% of them displaying a later death in mitosis (Figure 27 B-F). Similarly, the majority of UW228 died in mitosis after a prolonged arrest but 35% of cells exited mitosis and continued to cycle,

possibly due to the lower sensitivity of this cell line to tivantinib (Supplementary Figure 3). In stark contrast, all ONS76 cells exited mitosis after a prolonged arrest (Figure 30) and continued to cycle whilst only 10% of the cells died in mitosis (Figure 28 B-F). Once again, heterogeneity in the pharmacological response to the foretinib was also observed. DAOY cells displayed 52% of normal fates with multiple rounds of mitosis during the observation time; interestingly, 40% of the cells exhibited slippage with 22% of the cells entering again cell cycle and 18% dying in the following interphase or mitosis (Figure 27 C-G). Similarly, UW228 showed 45% of the cells undergoing mitotic slippage with most of the cells entering the cell cycle again and showing a prolonged mitosis (Supplementary 3; Supplementary 4).

However, ONS76 cells displayed dramatically different cell fate profiles when treated with foretinib with 92% of cells exited mitosis without completing cytokinesis. In addition, the majority of these cells entered again the cell cycle but, in the presence of the drug, continued to exit mitosis without dividing (Figure 28 C-G). To further address this, we performed light microscopy of DAOY and ONS76 cells treated with foretinib to measure variation in the cellular size; ONS76 cells showed an increase in cellular size with cells displaying an expanded cytoplasm and the presence of multinuclei structure related to the multiple rounds of slippage (Figure 29 A-B); in stark contrast, the majority of DAOY cells exhibited a round apoptotic appearance but we were able to still observe a small percentage of cells displaying an enhanced cell size (Figure 29 A-B), as expected from the number of DAOY cells that escaped cell death in mitosis or interphase after slippage (Figure 27 C-G).

Finally, we also evaluated the cell fate responses of DAOY and ONS76 cell lines to crizotinib. 48% of DAOY cells treated with crizotinib underwent two rounds of mitotic slippage; nonetheless, 40% of tracked cells died either in interphase or during mitosis after slippage (Figure 27 D-H). As previously reported for the foretinib, also crizotinib caused mitotic slippage in more than 92% of ONS76 cells and only 5% of the cells died after slippage either in interphase or mitosis (Figure 28 D-H).

It is well established that cell fates are dictated by the duration of the arrest in mitosis (Kops et al., 2005; Masuda et al., 2003; Rieder & Maiato, 2004; Tao et al., 2005). To this notion, we finally compared the mitotic period of cells treated with tivantinib, foretinib and crizotinib and their cellular fate (Figure 30). We observed that average mean mitotic time varied in response to different drugs, and we identified tivantinib as the drug able to induce the longest

mitotic arrest whilst foretinib and crizotinib having limited effects on mitotic delay. Overall, despite the presence of complex cellular fates with interline and intraline pharmacological heterogeneity to the c-MET inhibitors, these results confirmed the cytotoxic activity of tivantinib toward the *TP53*-mutant SHH MB cell lines and the cytostatic activity for both crizotinib and foretinib that, for the first time, were associated to the induction of mitotic slippage and the accumulation of polyploid cells.

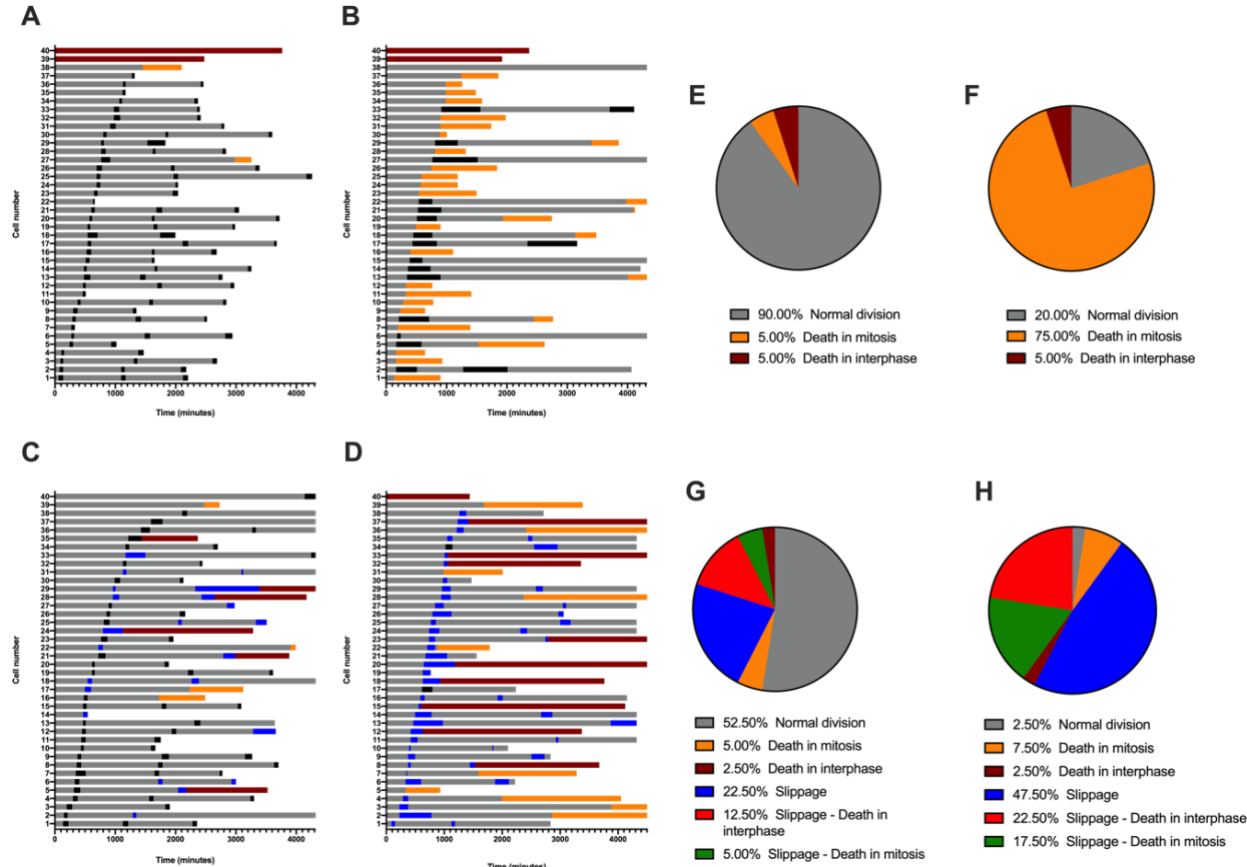


**Figure 27: Cell fate decisions upon c-MET inhibitors treatment in DAOY**

A-D) DAOY cells were either untreated (A) or treated with 0.5  $\mu\text{M}$  of tivatinib (B) and foretinib (C) or 2.5  $\mu\text{M}$  of crizotinib (D) and incubated in the Cytation 3 system (Biotek), at 37°C and 5% CO<sub>2</sub> where pictures were taken every 15 min for 72 hours at 10X magnification. 40 cells per condition were analysed and each horizontal bar in the graphs (on the left) indicates duration of each phase for a single cell (n=40 cells per condition). E-H) Pie charts representing percentages of all the different cell fate profiles observed upon treatment with tivatinib (F), foretinib (G) and crizotinib (H) compared to the untreated cells (E) (n=2)

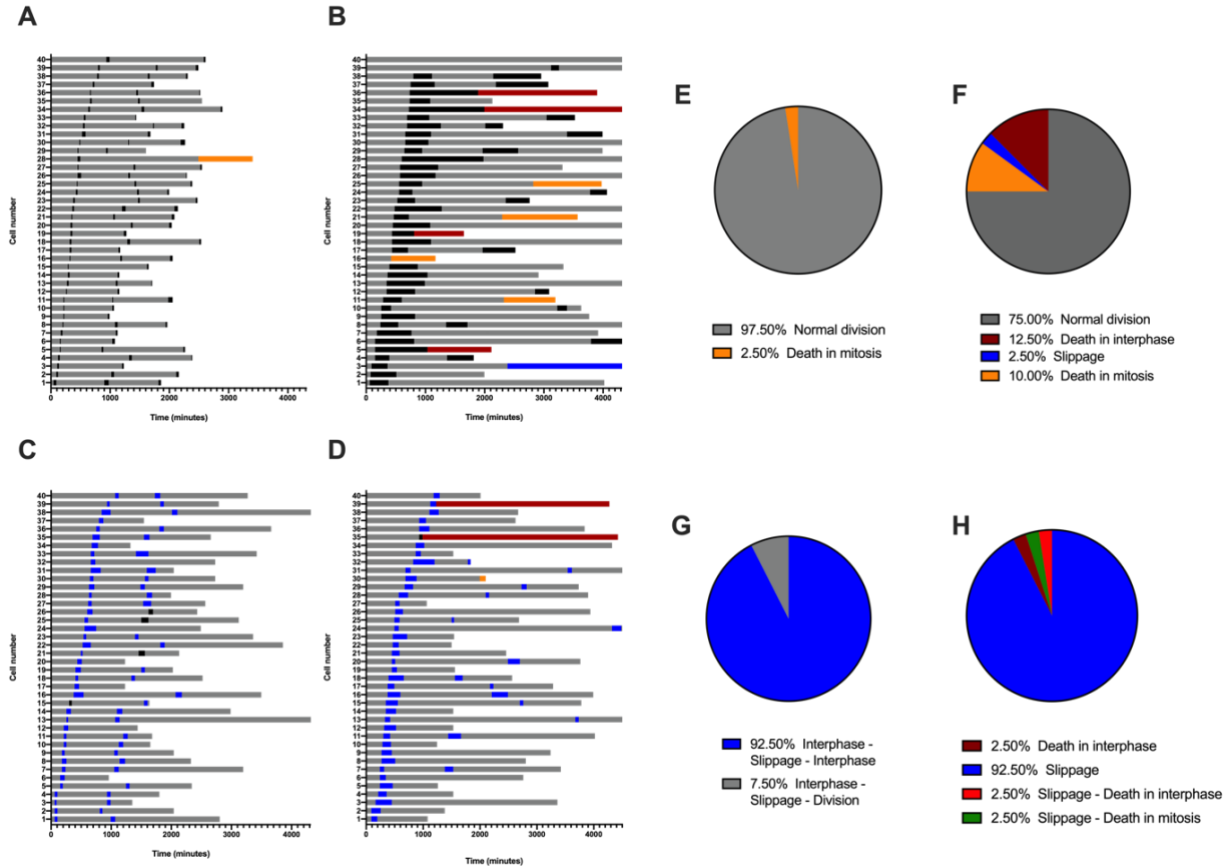


**Figure 28: Cell fate profiles upon c-MET inhibitors treatment in ONS76**

A-D) ONS76 cells were either untreated (A) or treated with 0.5 μM of tivantinib (B) and foretinib (C) or 2.5 μM of crizotinib (D) and incubated in the Cytation 3 system (Biotek), at 37°C and 5% CO<sub>2</sub> where pictures were taken every 15 min for 72 hours at 10X magnification. 40 cells per condition were analysed and each horizontal bar in the graphs (on the left) indicates duration of each phase for a single cell (n=40 cells per condition). E-H) Pie charts representing percentages of all the different cell fate profiles observed upon treatment with tivantinib (F), foretinib (G) and crizotinib (H) compared to the untreated cells (E) (n=2).

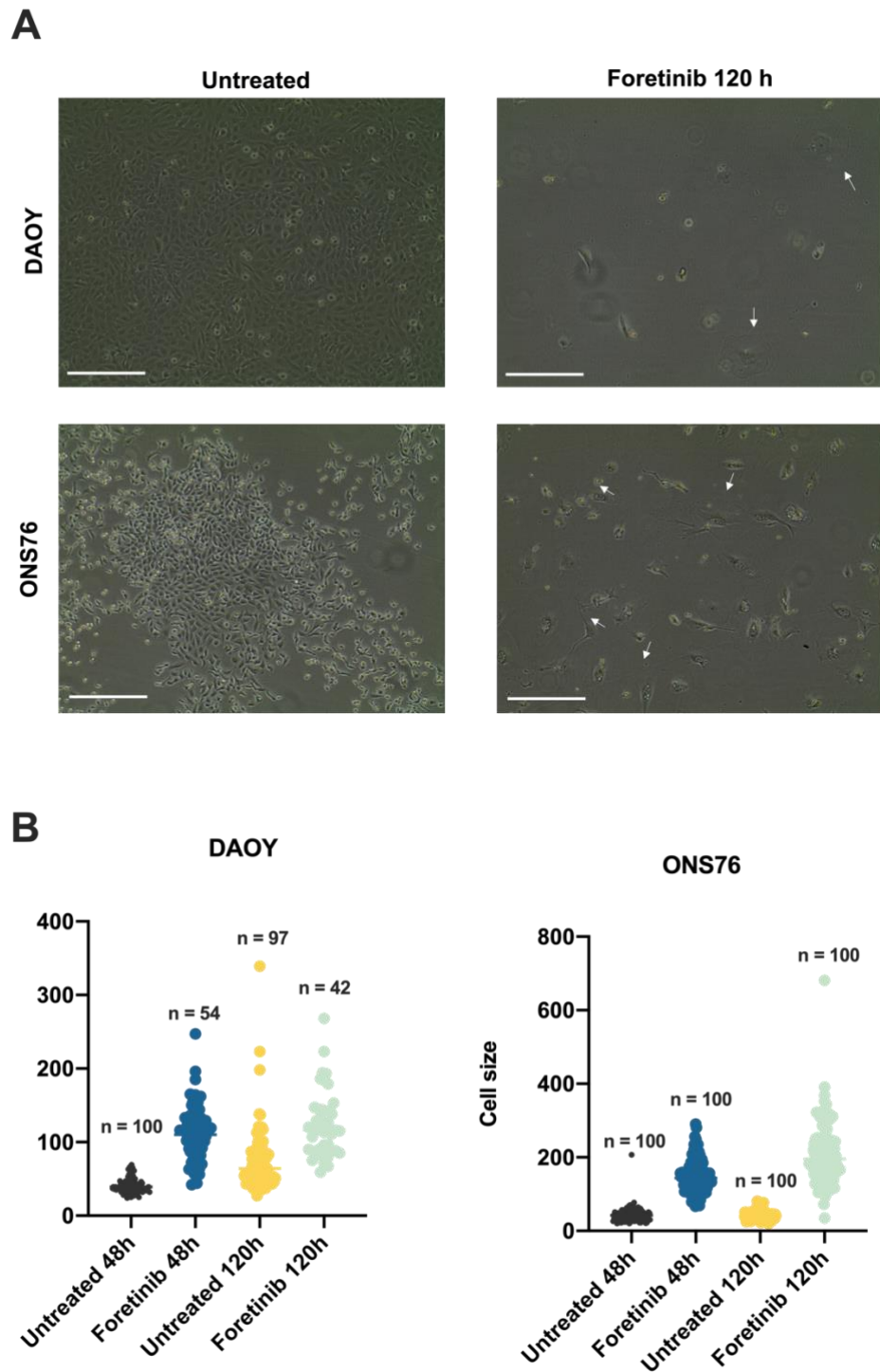


**Figure 29: DAOY and ONS76 cell sizes upon 120h treatment with foretinib**

A-B) DAOY and ONS76 cells were seeded in 96-well plates and treated with foretinib (1  $\mu$ M) for 48 and 120h. Representative pictures of DAOY and ONS76 at 120h either untreated or treated with foretinib were taken at 10X magnification using light microscopy (scale bar = 275 $\mu$ m). White arrows indicate cells with multinuclei. Size of each cell was calculated by drawing a line through the diameter of cells using ImageJ software. B) Plotted number of cells for each condition is indicated in the graphs. Graphs were generated on GraphPad Prism 8 Software.

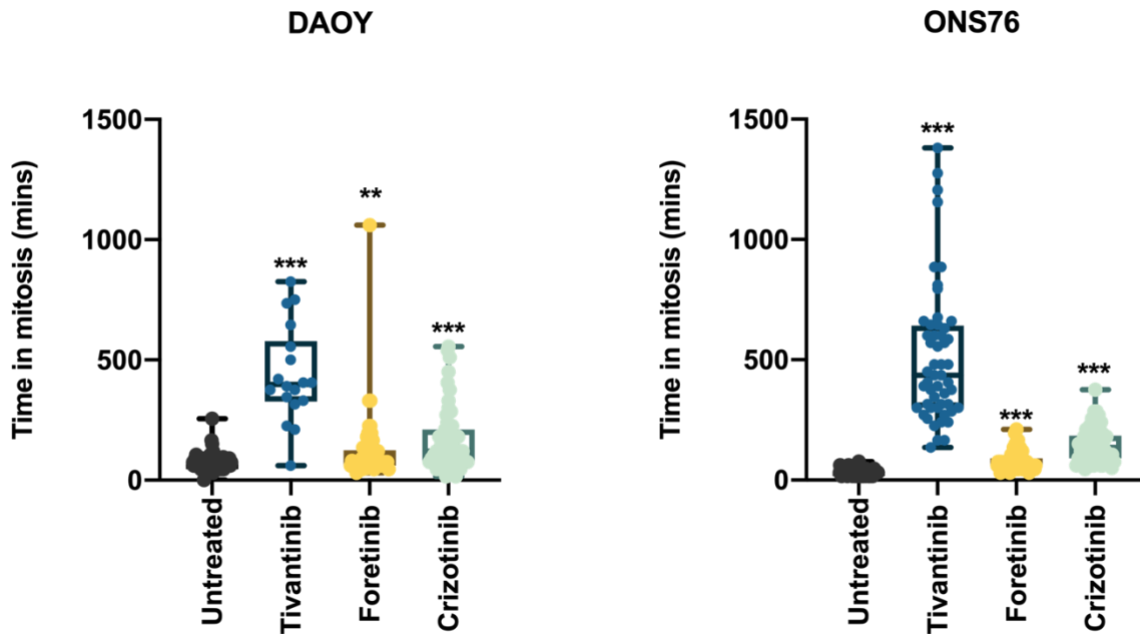


**Figure 30: Mitosis time length upon tivantinib, foretinib and crizotinib treatment**

Duration of mitosis (in minutes) was quantified by time-lapse microscopy. Box plots were generated with GraphPad Prism 8 software by plotting time spent in mitosis (minutes) by single cells upon treatment with tivantinib (0.5 $\mu$ M), foretinib (0.5 $\mu$ M), and crizotinib (2.5 $\mu$ M). Statistical comparison between the mitosis duration of untreated and treated cells was performed with Student's t-test ( $p \leq 0.05 = *$ ,  $p \leq 0.01 = **$ ,  $p \leq 0.001 = ***$ ).

#### **4.9 Tivantinib induces MCL-1 downregulation and PARP cleavage in DAOY cells**

It is well known that prolonged mitosis is the result of slow CCNB1 degradation that allows cells to “slip” not to “adapt” (Brito & Rieder, 2006); moreover, inhibition of caspase changes fate profiles denoting how the cellular fate is dictated by the balance between progression through mitosis driven by CCNB1 degradation and activation of apoptosis. To elucidate the molecular mechanism underlying the pharmacological heterogeneity of tivantinib, foretinib and crizotinib on SHH-MB cells, first western blot analyses were performed on protein extracts of DAOY and ONS76 cells treated for 24h with all drugs to investigate the balance between the apoptotic response and the progression through mitosis. To this aim, we assessed protein levels of: Poly (ADP-ribose) polymerase-1 or PARP plays a role in DNA repairs, and it is cleaved during apoptosis (Bressenot et al., 2009); CCNB1, essential component of the mitotic engine whose degradation triggers mitotic exit (Brito & Rieder,

2006); Myeloid cell leukemia protein (MCL1), an anti-apoptotic member of the BCL-2 family, whose modulation, either by degradation or overexpression, has been related to mitotic death and mitotic slippage respectively (Sloss et al., 2016). As shown in Figure 31A, PARP1 cleavage was increased by 2.5-fold in DAOY cells after 24h treatment with tivantinib while no cleavage was detected when DAOY cells were treated with foretinib or crizotinib (Figure 31A). In parallel, whilst MCL-1 was downregulated in DAOY cells exclusively after treatment with tivantinib, reduction of Cyclin B1 levels was observed in DAOY treated with foretinib and crizotinib, suggesting that these drugs induce mitotic slippage in these cells followed by death in the next interphase or mitosis (Figure 31A). In stark contrast, ONS76 cells treated with tivantinib showed no cleavage of PARP1, no consistent downregulation of MCL-1 or alteration in the levels of CCNB1 (Figure 31B) as expected by the limited apoptotic response we have observed with Caspase 3/7 assays and their ability to cycle with extended mitosis (Figure 21C; Figure 30). Despite the observation of mitotic slippage in most of the ONS76 cells treated with foretinib and crizotinib, CCNB1 levels were increased in these cells tipping off the balance between cell death and mitotic progression, allowing these cells to resume cell cycle and generate polyploid phenotype.

Altogether, these results confirmed that tivantinib specifically induces apoptotic death through the downregulation of MCL1 only in the *TP53*-mutant DAOY cells, which was also corroborated by western blot analysis of UW228 cells after treatment with tivantinib (Supplementary 5). Furthermore, treatment with tivantinib did not cause PARP cleavage or strong MCL-1 downregulation in ONS76 cells.

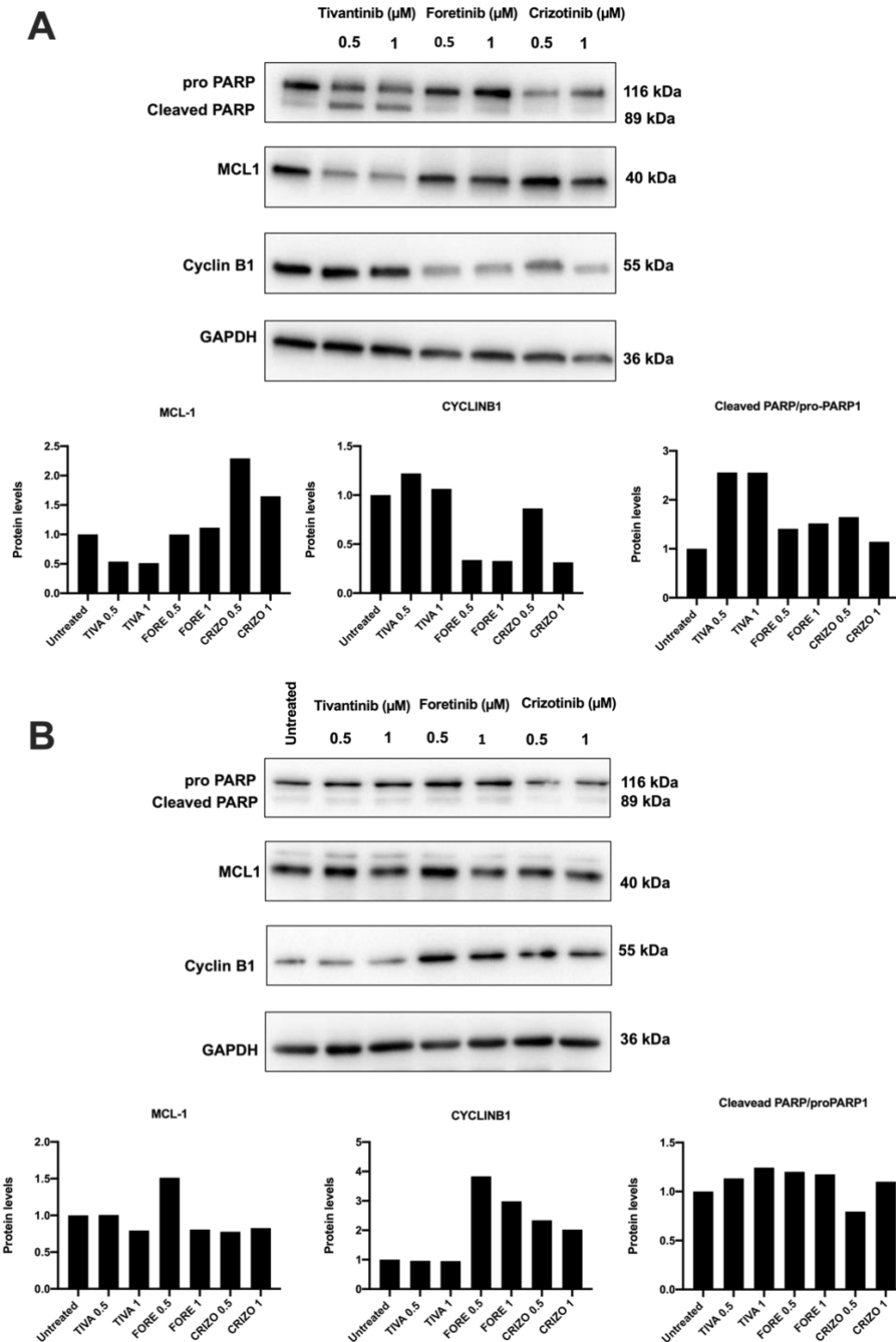


**Figure 31: c-MET kinase inhibitors effects on PARP1, MCL-1 and Cyclin B1 expression**

A-B) Representative western blot for DAOY (A) and ONS76 (B) of two independent experiments (n=2). Cells were treated with tivantinib, foretinib and crizotinib (0.5 and 1  $\mu\text{M}$ ) for 24h before protein extraction. Lysates (40  $\mu\text{g}$ ) were loaded in a poly-acrylamide gel and membranes were incubated with antibodies against each protein of interest. GAPDH was used as loading control and densitometric analysis was performed by normalizing each protein of interests with GAPDH. Proteins levels represented in the bar graphs are relative to the western presented and were generated on GraphPad Prism Software 8.

#### **4.10 c-MET signalling in DAOY cells after treatment with crizotinib and tivantinib**

Although, tivantinib has been developed as highly selective non-ATP competitive MET inhibitor, several articles suggest that the drug exhibits its anti-proliferative activity through other targets such as microtubule polymerisation or alpha catenin (Xiang et al., 2015). Thus, we aimed to clarify whether the inhibition of c-MET kinase by tivantinib is directly responsible for the effects observed on the SHH-MB cell lines. To this aim, we first evaluated the ability of tivantinib to suppress HGF-dependent activation of c-MET signalling pathway in SHH-MB cells. Treatment with tivantinib halted the ligand-dependent auto-phosphorylation of c-MET kinase in DAOY cells (Figure 32A). As shown by the moderate reduction in the phosphorylation levels of AKT and ERK, activation of the downstream signalling pathways of c-MET kinase was limitedly impaired by the treatment with tivantinib. When DAOY cells were treated with crizotinib, c-MET signalling pathways was potently inhibited after the stimulation with HGF (Figure 32A). These data suggest that tivantinib has the capacity to mitigate HGF-dependent c-MET kinase activation but, due to the limited inhibition of the downstream pathways, its antiproliferative effect on SHH-MB cells may be linked to other pathways.

To further explore the connection between c-MET kinase and the viability effects that we observed in SHH-MB cells, we performed a siRNA-mediated knockdown of c-MET in HGF-stimulate DAOY cells and assessed the levels of MCL-1 and CCNB1 that were both modulated when SHH-MB cells were treated with c-MET inhibitors. Whether MCL-1 levels were induced upon HGF stimulation, c-MET knockdown mitigated this increase after 6h of ligand stimulation and caused a 50% reduction in its levels after 24h (Figure 32 B). Then, we evaluated changes in CCNB1. As expected by G1 arrested cells, serum starved DAOY cells showed an accumulation of CCNB1 when compared to cycling cells (Supplementary Figure 5). Concomitantly, knockdown of c-MET delayed early degradation of the CCNB1 but, after 24h of HGF stimulation, no differences were evident with the siRNA control (Figure 32B).

Finally, to clarify whether knockdown of c-MET phenocopied the cell prolife caused by tivantinib or foretinib, we constructed by time-lapse microscopy the fate profile after c-MET knockdown in DAOY cells. This preliminary experiment showed that 25% of DAOY cells died in mitosis when c-MET kinase was knocked-down (Figure 33B). Conversely, death in

interphase affected the 22.5% of control cells compared to 12.5% of the cells dying in interphase with c-MET knockdown. A single event of mitotic slippage was observed in both samples (2.5%). Although time in mitosis was on average longer for c-MET knockdown compared to control (siMET= 50.83 mins vs siCTRL= 46.3 mins) (Figure 33C), no significance was reached. Altogether, these results revealed that MET knockdown mimics in part the cellular and biochemical effects observed by tivantinib thus other possible targets should be considered to fully describe its effects.

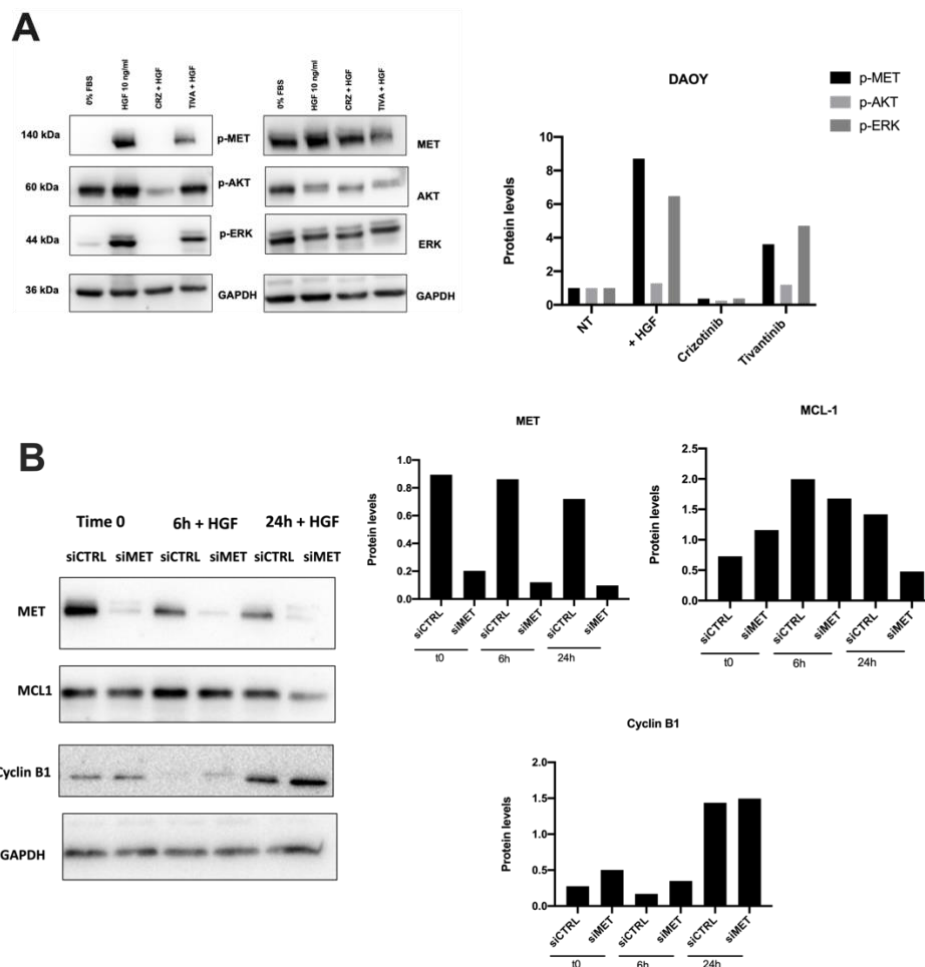


**Figure 32: c-MET kinase role in tivantinib-induced effects on DAOY cells**

A-B) Representative western blot images. A) DAOY were starved for 24h and then cells were either pre-treated 2 hours with crizotinib and tivantinib (1  $\mu$ M) and stimulated with HGF (10ng/ml) or stimulated with HGF alone. 40  $\mu$ g of lysates was loaded, and membranes were incubated with the indicated antibodies; GAPDH was used as loading control. Densitometric analysis was performed with ImageJ software and proteins levels of phosphorylated proteins were plotted as bar graphs on GraphPad Prism 8 Software (n=3). B) DAOY were transfected with siRNA against c-MET for 72h. After 48h transfected cells were serum-starved for 24h and then stimulated with HGF for 6 and 24h before protein extraction. 40  $\mu$ g of protein lysates was loaded. Densitometric analyses are referred to the western presented in the figures.

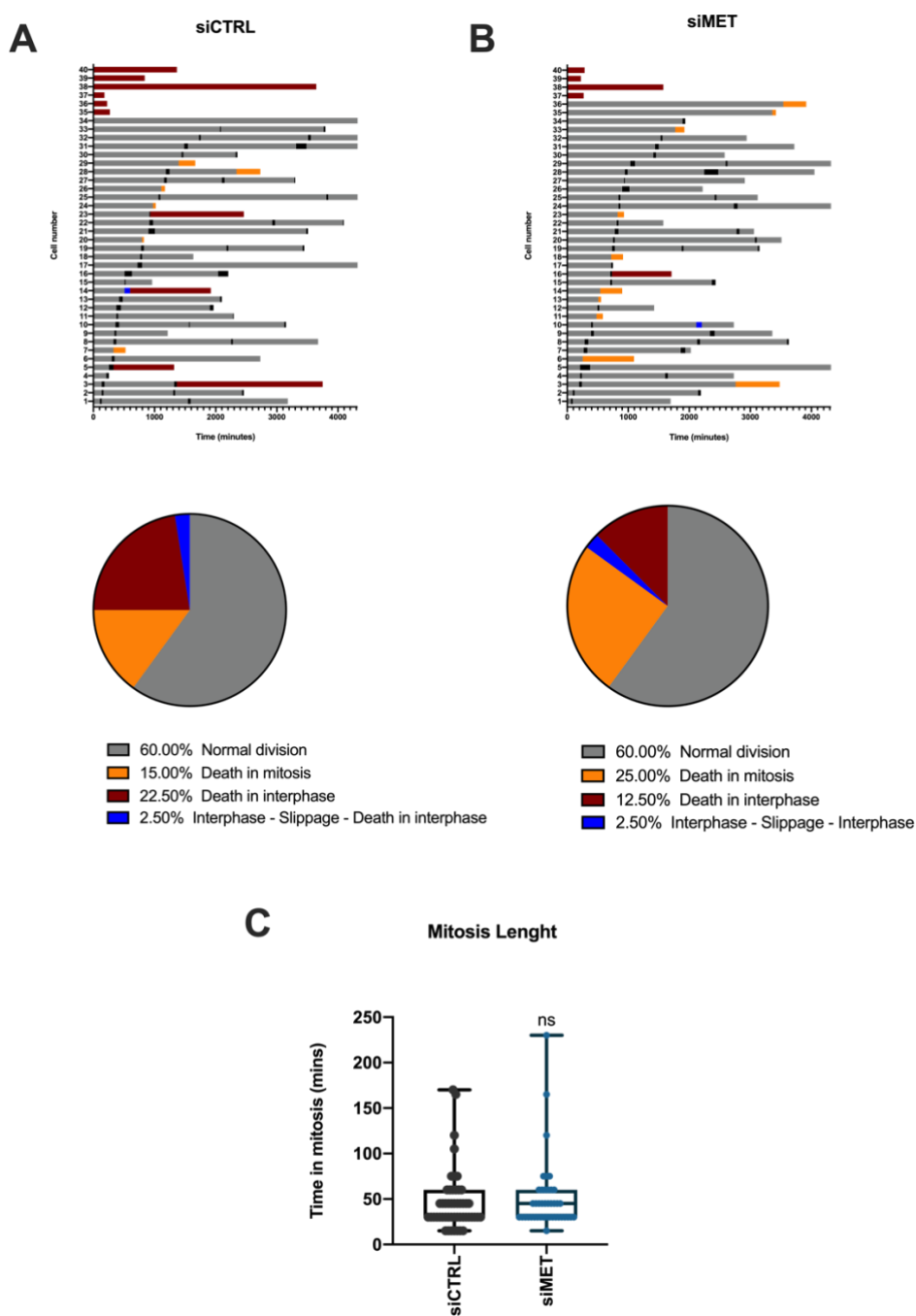


**Figure 33: Cell fate profiles upon c-MET kinase knockdown in DAOY**

A-C) DAOY cells were transfected with both scramble siRNA control (siCTRL) (A) and siRNA against c-MET (siMET) (B) and incubated in the Cytation 3 system (Biotek), at 37°C and 5% CO<sub>2</sub> where pictures were taken every 15 min for 72 h at 10X magnification. 40 cells per condition were analysed and each horizontal bar in the graphs (indicates duration of each phase for a single cell (n=40 cells per condition) (A-B). For each condition, percentages of each cell fates were calculated by dividing the number of cells that underwent a certain cell fate by the total number of cells analysed. Pie charts based on the different fates of the cells were generated with GraphPad 8 Software. C) Duration of mitosis (in minutes) was quantified by time-lapse microscopy. Box plots were generated with GraphPad Prism 8 software by plotting time spent in mitosis (minutes) by single cells either transfected with siMET or

scramble control siRNAs. Statistical comparison between untreated and treated cells were performed with Student's t-test ( $p \leq 0.05 = *$ ,  $p \leq 0.01 = **$ ,  $p \leq 0.001 = ***$ , ns= non-significant).

#### **4.11 Tivantinib synergises with vincristine in the killing of DAOY cells**

First-line treatment of medulloblastoma comprises chemotherapeutic drugs, such as vincristine, a well-known antimetabolic drug, that inhibits microtubule polymerization and causes block in mitosis (Jordan, 2002). Previous results in this study highlighted that tivantinib strongly induces mitotic death in DAOY cells and significant mitotic delay in ONS76 cells (Figure 27B; Figure 28B). Combined with the observation that tivantinib exerts anti-tumour effects via microtubule inhibition with a mechanism of action that seems to be different from the classical anti-mitotic drugs (Katayama et al., 2013; Xiang et al., 2015), we decided to assess the ability of tivantinib to enhance the cytotoxic effects of vincristine.

To this aim, combination treatments of vincristine and tivantinib were performed on DAOY and ONS76 cell lines by using linear dilutions of vincristine coupled with five concentrations of tivantinib spanning the  $IC_{50}$  of the drug on the two cell lines. Cells were treated with the drug combination for 72h and then subjected to MTT proliferation assay to compare the % of viability to single drug treatments (Figure 34 A-C). Combined treatments of vincristine/tivantinib significantly inhibited the growth of both SHH-MB cell lines compared to single treatments. Analysis of the  $IC_{50}$  values for the combinatorial strategy in DAOY cells demonstrated superior efficacy when tivantinib was added to vincristine at concentration lower than  $0.6\mu M$  (Figure 34 A-C). Consistently, ONS76 cells showed benefits from the combination vincristine/tivantinib but only when tivantinib was used at concentration of  $0.01$  and  $0.04\mu M$ .

Combination Index (CI) were calculated by using the Chou-Talalay matrix (CI=1 indicates additive effect, CI < 1 indicates synergism and C > 1 antagonism) (Chou, 2010), and used to assess the synergistic interaction of the two drugs. Analysis of the combination indexes confirmed that the addition of tivantinib chemosensitised SHH-MB cells to vincristine with ONS76 cells showing the highest degree of synergy for low concentration of vincristine and tivantinib (Figure 34 B-D). To further confirm these results, we decided to assess the apoptotic activation after drug combination by measuring the activation of PARP1. DAOY and ONS76

cells were treated with the combination of tivantinib and vincristine for 24h and then PARP1 cleavage was assessed by western blots. Consistently with previous results, DAOY cells showed a robust induction of PARP1 cleavage when compared to single drug treatments (Figure 35A). Unfortunately, minimal or irrelevant induction of PARP cleavage was observed when *TP53* wild-type ONS76 cells were treated with combinations of vincristine and tivantinib (Figure 35B). This suggested that the combination tivantinib/vincristine, although promoting a potent anti-proliferative effect possibly related to an extended time in mitosis, will be unable to activate the apoptotic programme and contribute to the eradication of this specific cell type of MB.

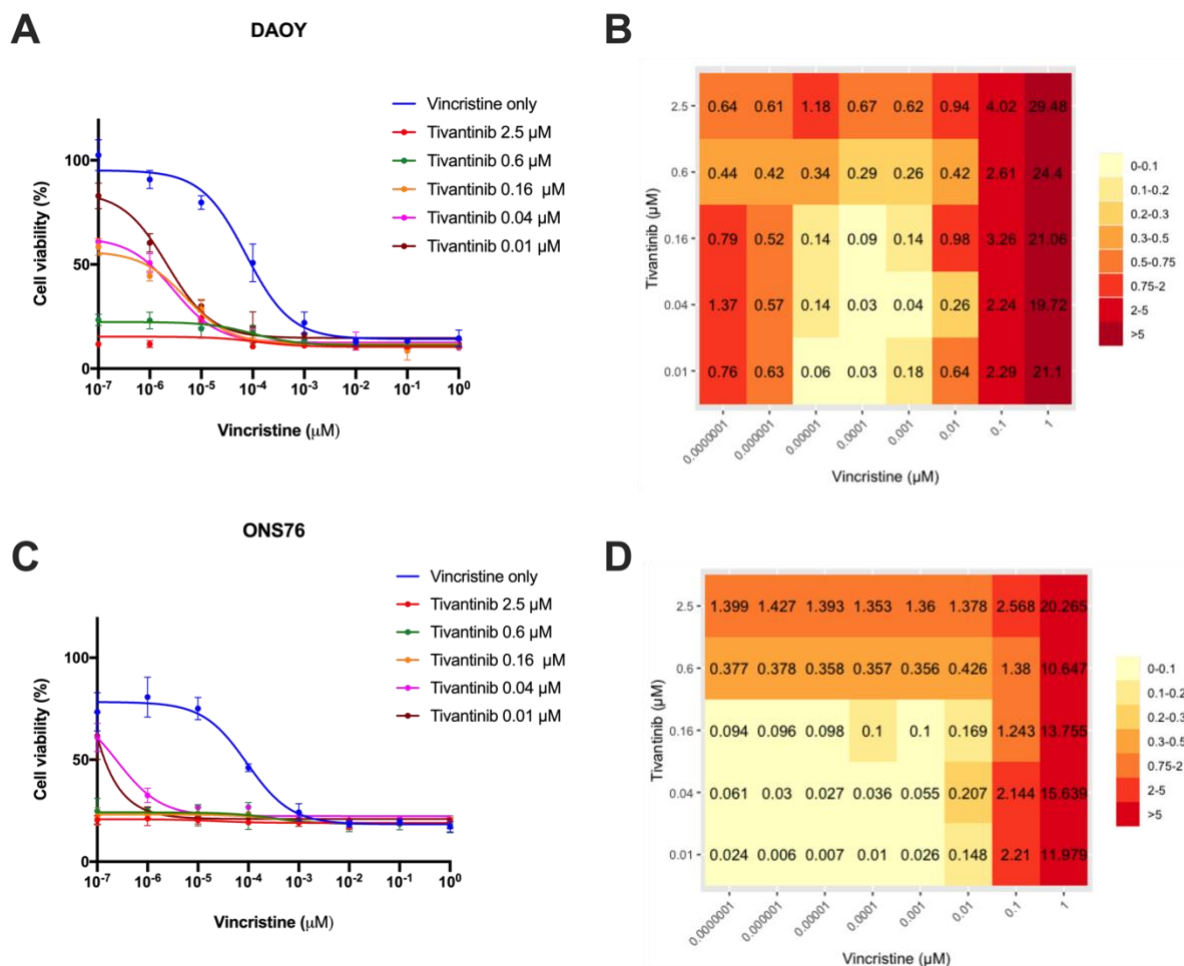


**Figure 34: Synergistic effects of tivantinib and vincristine on DAOY and ONS76 cell proliferation**

A) DAOY and ONS76 cells were treated with Vincristine and/or Tivantinib at increasing concentrations of vincristine (Fold dilution 1:10- starting from 1  $\mu\text{M}$ ) and with fixed concentration of tivantinib (0.01-0.04-0.6-2.5  $\mu\text{M}$ ) for 72h. Cell viability was assessed using MTT assay and absorbance data were

normalized to the untreated cells. Graphs represent Mean $\pm$ SD (n=3) and were plotted with GraphPad 8.0 software B) Combination index values were calculated with Compusyn software (CI=1 additive effect; CI < 1 synergism; C > 1 antagonism) and representative CI values are presented as heatmaps generated with R software.

The synergistic effects of combinatorial treatment vincristine/tivantinib was further investigated in the 3-D culture system with DAOY cells. The chemotherapeutic regimen was similar to the one we used for the PARP1 cleavage assay, but spheroids were treated for 9 days, and drugs refreshed every 3 days. Combination index analysis was used again to establish whether the two drugs acted synergistically to impair spheroids growth. As shown in Figure 36A, measurements of the spheroid volumes confirmed the enhanced activity of tivantinib and vincristine in suppressing the proliferation of DAOY cells after combined treatments, compared to single agent treatments. The lowest CI value (CI = 0.04), indicating the highest synergistic effect was observed when spheroids were treated at concentration of 0.01 $\mu$ M for both vincristine and tivantinib (Figure 36B).

Concomitantly, we also tested the induction of apoptotic programme by measuring the caspase 3/7 activation after 24h of combinatorial treatment with tivantinib and vincristine (0.01 $\mu$ M VCR + 0.01 $\mu$ M TIVA). In this pilot experiment, results of fluorescence intensity analysis showed that caspase 3/7 enzyme was activated with vincristine treatment alone (0.01 $\mu$ M) but not with tivantinib (0.01 $\mu$ M). However, we found that fluorescence signal was enhanced when spheroids were treated with both drugs compared to both untreated and single agents (Figure 37).

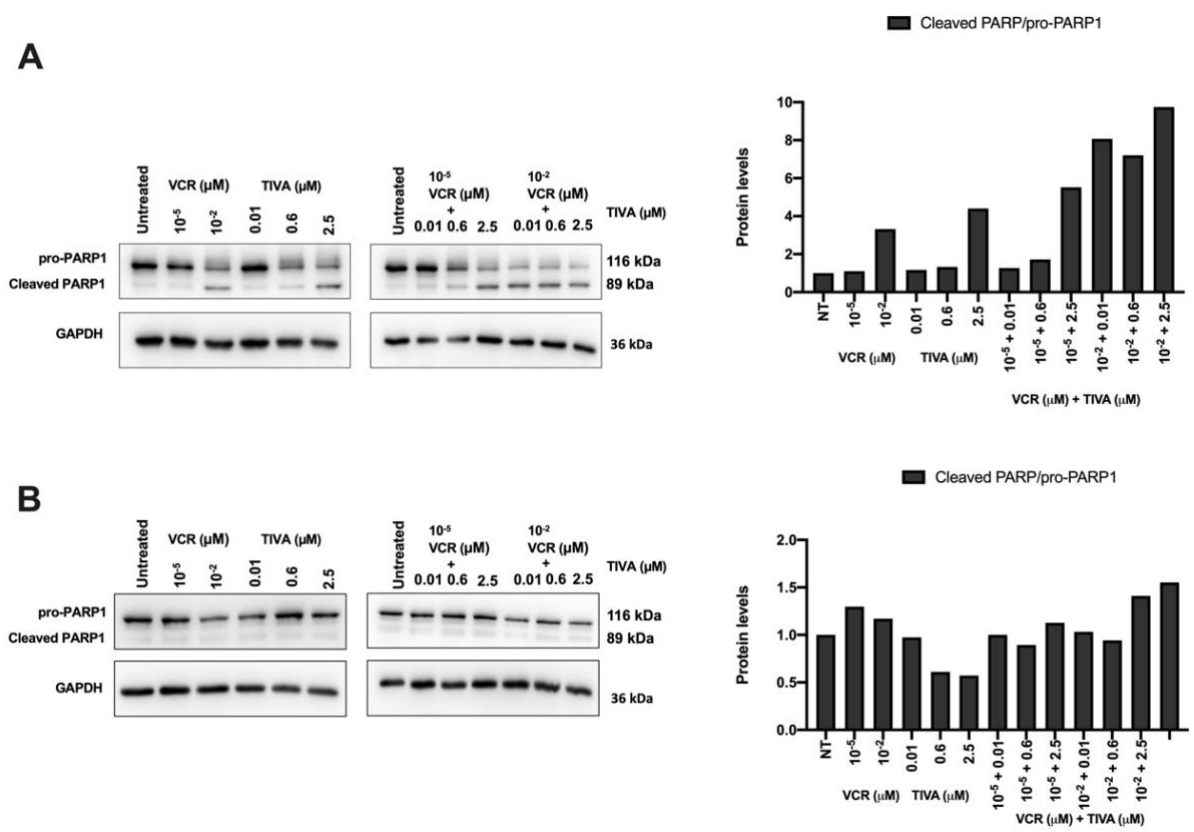


**Figure 35: PARP1 cleavage upon combination treatment with vincristine and tivantinib**

A-B) DAOY (A) and ONS76 (B) representative western blot images. PARP analysis after vincristine and tivantinib combination treatment DAOY and ONS76 were treated for 24h with vincristine (VCR) and tivantinib (TIVA) as single agents and with drug combination. Two concentrations were chosen for vincristine (0.01 and 0.00001 $\mu$ M) and three for tivantinib (2.5-0.6-0.01 $\mu$ M). After protein extractions, 40  $\mu$ g of each sample were loaded, and western blot was performed. GAPDH was used as loading control. Densitometric analysis is provided on the left and it is referred to the images presented (n=3).

Overall, we observed that vincristine and tivantinib exhibited a synergistic potential in killing DAOY cells, as suggested by combination index values in both 2D and 3D cultures and assessment of levels of PARP1 cleavage, which infers that the dual treatment could be a beneficial approach for MB treatment. In contrast, although treatment of ONS76 cells showed synergistic effects in impairing cell viability upon 72h treatment with combination of vincristine and tivantinib, 24h treatment with both drugs did not cause any significant cleavage in PARP1, likely due the possibility that these cells are delayed in mitosis and not dying with the same extent as DAOY cells, as suggested by cell fate analysis (Figure 28B).

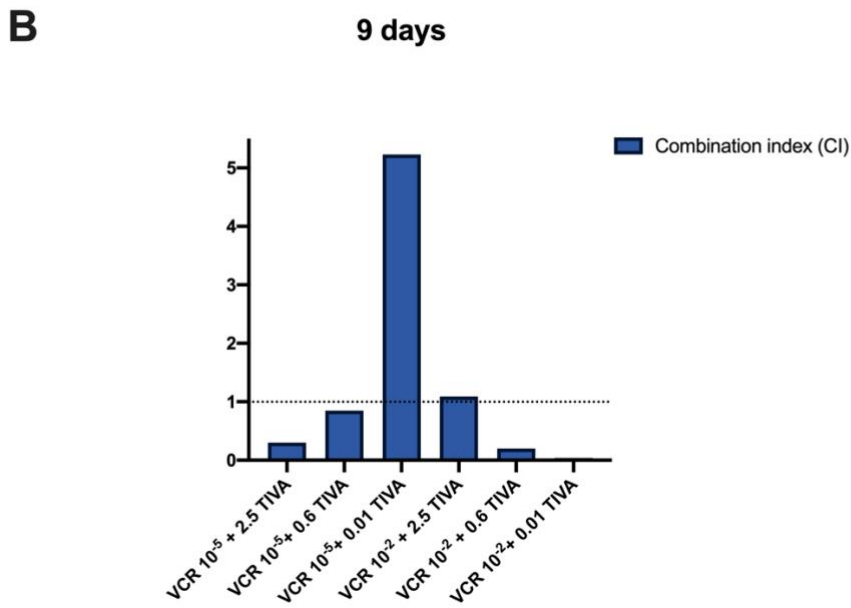
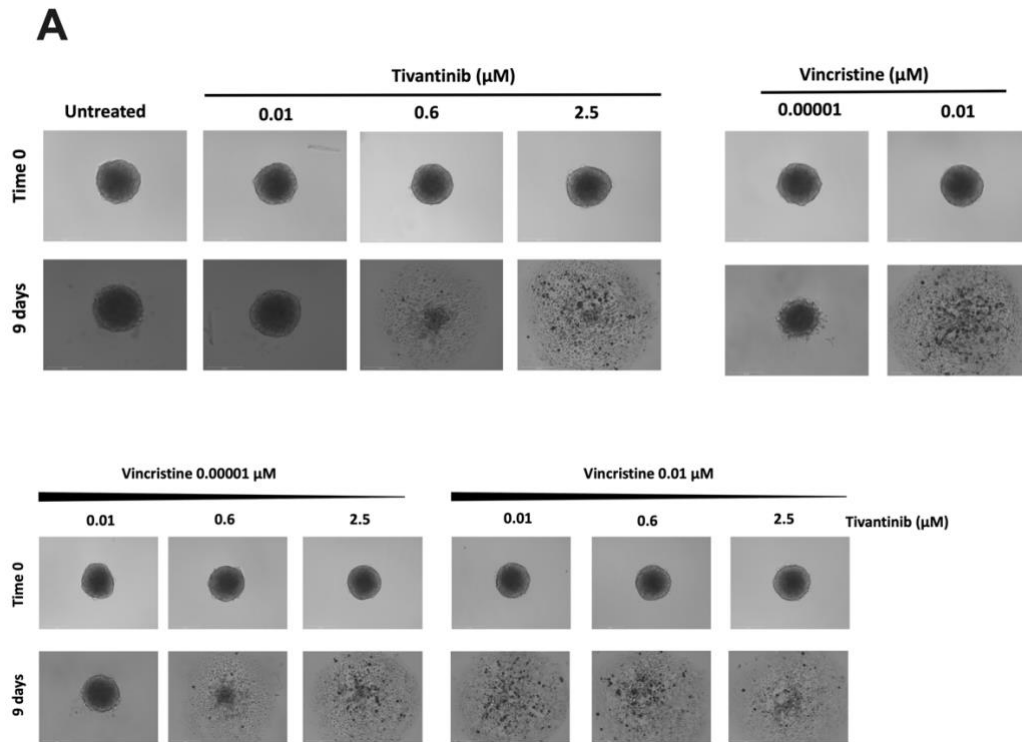


**Figure 36: Combination treatment with vincristine and tivantinib on DAOY 3D spheroids**

A-B) 5 days after seeding, DAOY 3D spheroids were treated with either vincristine (0.01 and 0.00001 $\mu\text{M}$ ) and tivantinib (2.5, 0.6, 0.01 $\mu\text{M}$ ) alone or with combinatorial treatments using the two drugs. Treatments were replaced every 3 days for a total of 9 days. Pictures were taken at the end point (9 days) with Evos Auto 2 microscope (scale bar = 275 $\mu\text{m}$ ) (n=2, each done in triplicates) C) CI values were calculated with Compusyn software (CI=1 additive effect; CI < 1 synergism; C > 1 antagonism) and representative CI values were plotted as bar graph on GraphPad 8 software.

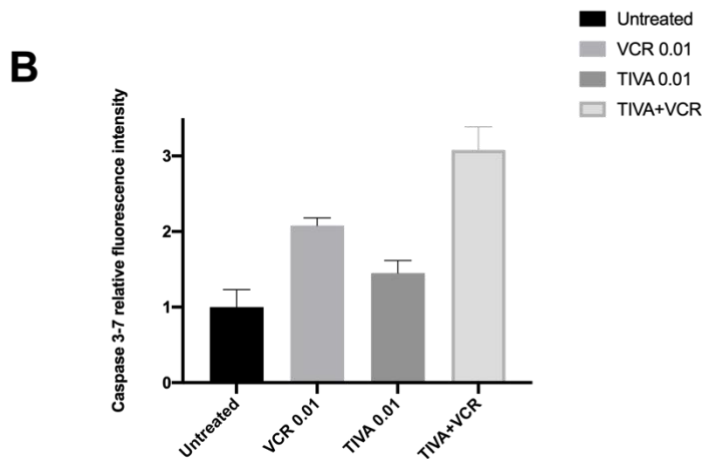
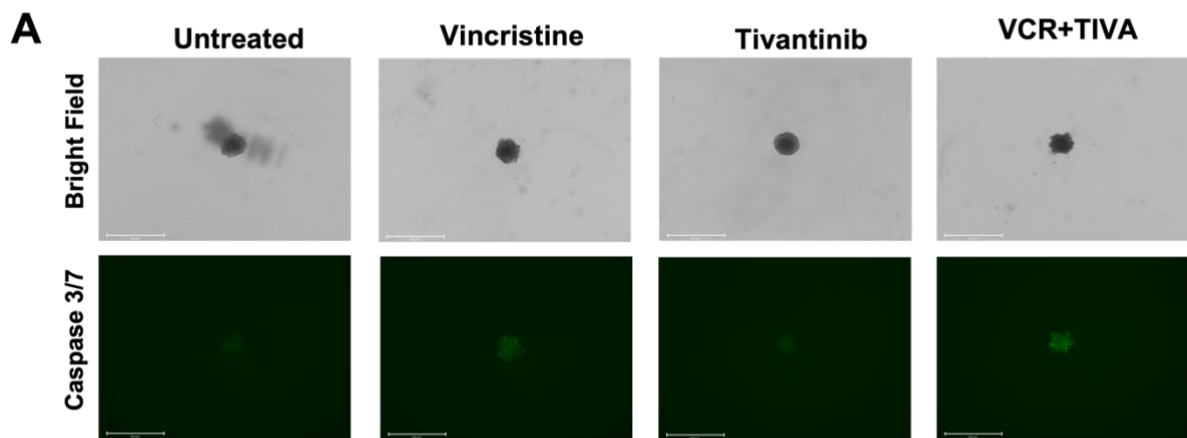


**Figure 37: Caspase 3/7 activation in DAOY spheroids treated with vincristine and tivantinib combination**

DAOY spheroids were treated with vincristine and tivantinib alone at 0.01  $\mu$ M concentration for 24h. Apoptotic activation was assessed by adding CellEvent Caspase 3/7 detection reagent. Apoptotic cells in the spheroids are showed in green. Pictures were taken with Evos FL Auto 2 microscope (scale bar = 650  $\mu$ m). Fluorescence intensity data are plotted as Mean $\pm$ SD of two technical replicates.

## 4.12 Targeting BCL-2 family induces death in foretinib-treated cells

When cancer exhibit a prolonged arrest in mitosis, due for example to anti-mitotic drugs, they can either died in mitosis or undergo slippage (Ghelli Luserna Di Rorà et al., 2019). This decision is dictated by a balance between two contrasting signalling networks: one gradually activating an apoptotic signal that, regulated mainly by the BCL-2 family proteins, coordinates the death of the cancer cells; the other which is controlled by the degradation of CCNB1 and may pushes cancer cells into slippage (Brito & Rieder, 2006). Following slippage, a cancer cell can generally arrest in the next interphase, go into senescence or die; but if the cell resumes the cell cycle, then chromosomal instability can be fuelled, inducing tumour progression and resistance to therapy (Brito & Rieder, 2006; Sinha et al., 2019; Sloss et al., 2016). The observation that foretinib or crizotinib induce slippage when used against DAOY or ONS76 (Figure 27 C; Figure 28 C) cells supported the idea that initial balance in these treated cells is tilted toward a pro-survival fate, allowing slow degradation of CCNB1 and induction of slippage (Topham & Taylor, 2013). To redirect the balance toward cell death, we decided to reinforce the apoptotic trigger by using BCL2-related inhibitors in combination with these classical c-MET inhibitors.

To this aim, we decided to test the efficacy of maritoclax (MCL-1) inhibitor and navitoclax (broad BCL-2 family protein inhibitor) either in combinatorial or sequential treatments with foretinib in both DAOY and ONS76 cell lines. DAOY and ONS76 cells were initially challenged with linear dilution of foretinib combined with either navitoclax or maritoclax at four different concentrations (0.01-0.1-1-10 $\mu$ M) (Figure 38 A-H) spanning the IC<sub>50</sub> previously calculated (Buzzetti et al., 2021). MTT assays were performed 72h after treatment to assess cell viability; we observed that combinations between foretinib and navitoclax or maritoclax were synergistic in both cell lines but at concentrations of both drugs too high to be clinically relevant. Combination index analysis confirmed the synergistic effects between foretinib and navitoclax or maritoclax at the concentration of 10 $\mu$ M for both cell lines. Generally lower concentration of foretinib together with low concentrations of navitoclax and maritoclax, showed the least synergistic effects in both cell lines with major extent in ONS76 cells (Figure 37 C-D, D-H).

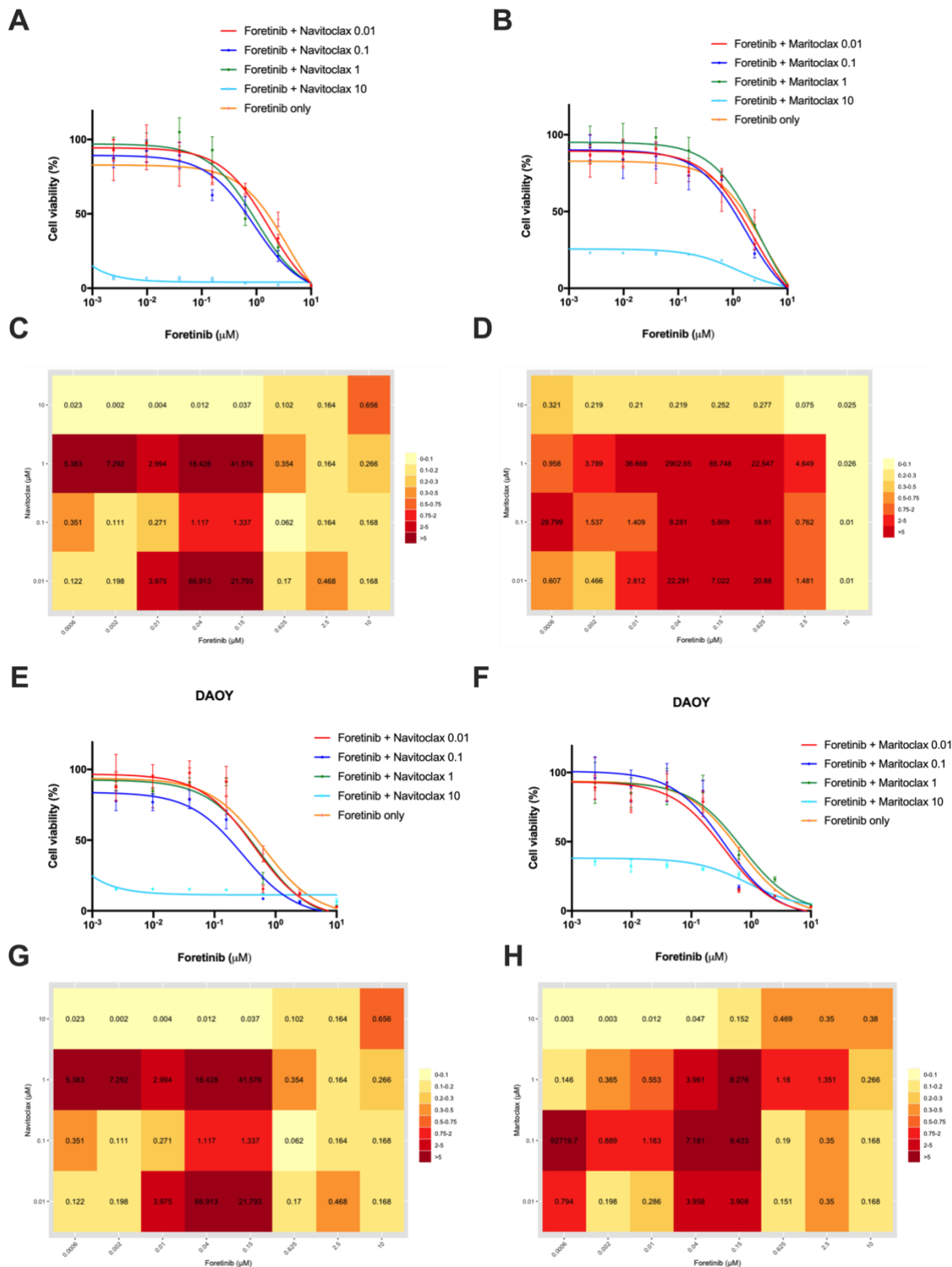


**Figure 38: BH3-mimetics in combination with foretinib in ONS76 and DAOY cells**

A-H) ONS76 (E-F) and DAOY (G-H) cells were treated with foretinib and/or navitoclax or maritoclax at increasing concentrations of foretinib (Fold dilution 1:2.5; starting from 1 μM) and with fixed concentration of maritoclax or navitoclax (0.01-0.1-1-10 μM) for 72h. Cell viability was assessed using

MTT assay and absorbance data were normalized to the untreated cells. Graphs were plotted with GraphPad 8.0 software are represented as Mean $\pm$ SD (n=3) B) Representative CI values were calculated with Compusyn software (CI=1 additive effect; CI < 1 synergism; C > 1 antagonism) and are shown as heatmap generated on R software.

Next, we aimed to investigate whether navitoclax and maritoclax can induce cell death in DAOY and ONS76 after mitotic slippage caused by pre-treatment with foretinib.

To this aim, DAOY and ONS76 cells were treated for 72h with foretinib and, after assessing formation of multinucleated cells by light microscopy as shown in Figure 29, treatments with maritoclax and navitoclax were performed to investigate whether mitotic 'slipped' cells were more sensitive to the inhibition of anti-apoptotic proteins. Results showed that navitoclax was the most effective drug in impairing viability of ONS76 cells previously treated with foretinib when compared to navitoclax or foretinib as single agents (Figure 39A). Even though DAOY cells were already sensitive to foretinib, sequential treatment with navitoclax further impaired cell viability (Figure 39B). In contrast, while mono-treatment with maritoclax affected cell viability in both DAOY and ONS76 cells, we did not observe any significant enhanced effects when the drug was used in a sequential treatment with foretinib. Moreover, single agent treatment with navitoclax did not show any anti-proliferative activity against both cell lines (Figure 39 A-B). Crystal violet staining of ONS76 cells showed the efficacy of navitoclax in a sequential treatment with foretinib pre-treated cells when compared to both foretinib and navitoclax effects as single agents (Figure 39C). To further assess the ability of navitoclax in causing cell death, PARP analysis was performed by western blot (Figure 40). To this aim, DAOY and ONS76 were treated with foretinib (1  $\mu$ M) for 48h and then navitoclax (2  $\mu$ M) was added for 24h. Cells treated only with foretinib were used as comparison. As shown in Figure 40, levels of cleaved PARP/proPARP1 ratio increased in both cell lines after navitoclax treatment compared to untreated and foretinib treated cells.

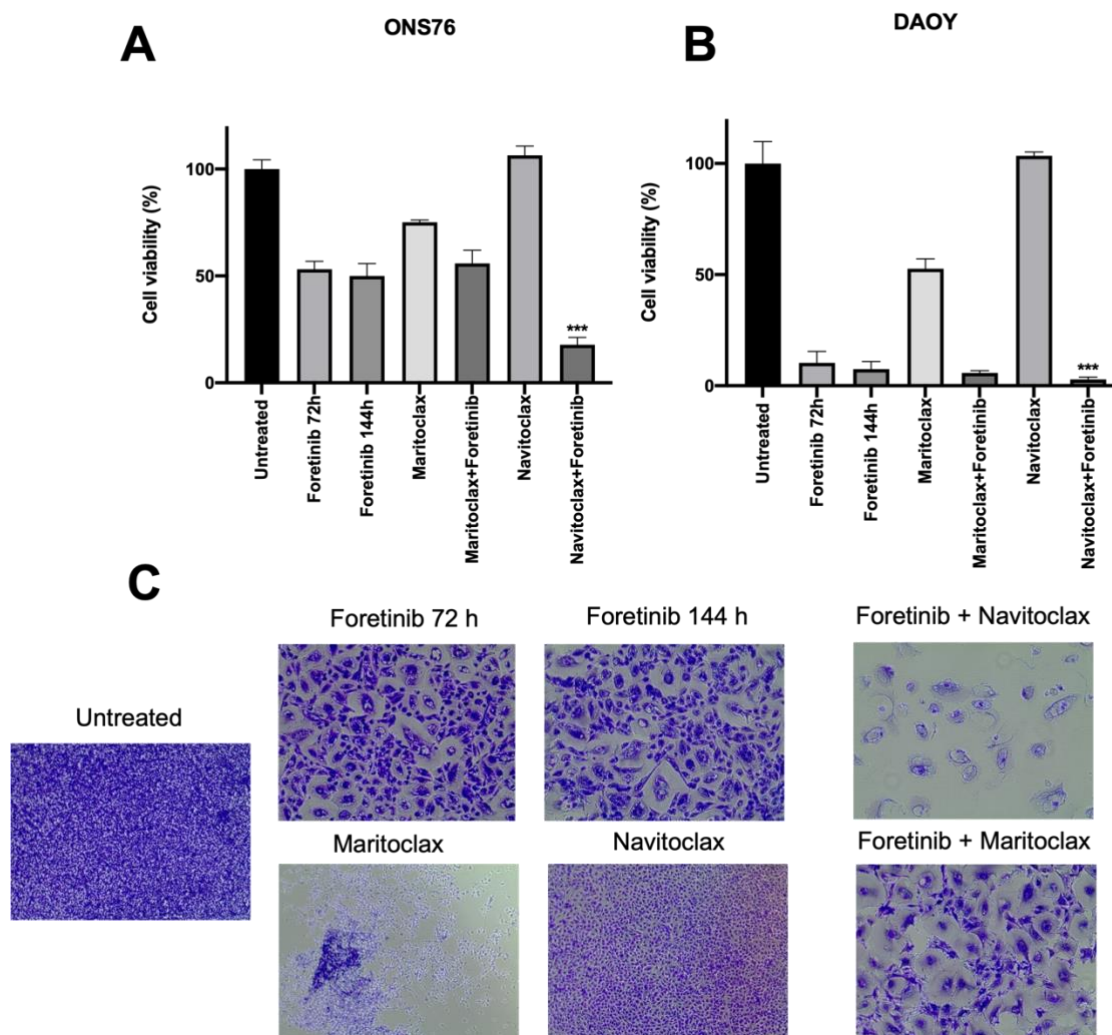


**Figure 39: Anti-proliferative effects of BCL-2 family inhibitors on foretinib-treated DAOY and ONS76**

A) ONS76 cells were subjected for 48h and 120h with foretinib treatment (1  $\mu$ M), p DAOY (A) and ONS76 (B) cells were firstly treated with foretinib (1  $\mu$ M) for 72h. After, foretinib pre-treated cells were subjected to 72h treatment with navitoclax and maritoclax (2  $\mu$ M). Drug withdrawal, second treatment with foretinib and treatment with navitoclax and maritoclax as single agents were performed as controls together with the untreated cells. MTT results are showed as Mean $\pm$ SD (n=3). Statistical analysis was performed with Student's t-test ( $p \leq 0.05 = *$ ,  $p \leq 0.01 = **$ ,  $p \leq 0.001 = ***$ ) between foretinib 72h treatment and navitoclax and maritoclax treatments following foretinib treatment. C) Representative pictures of Crystal Violet staining on ONS76 treated with foretinib (72 and 144h), navitoclax and maritoclax (2 $\mu$ M) as single agents, and sequential treatment after foretinib with both BH3-mimetics.

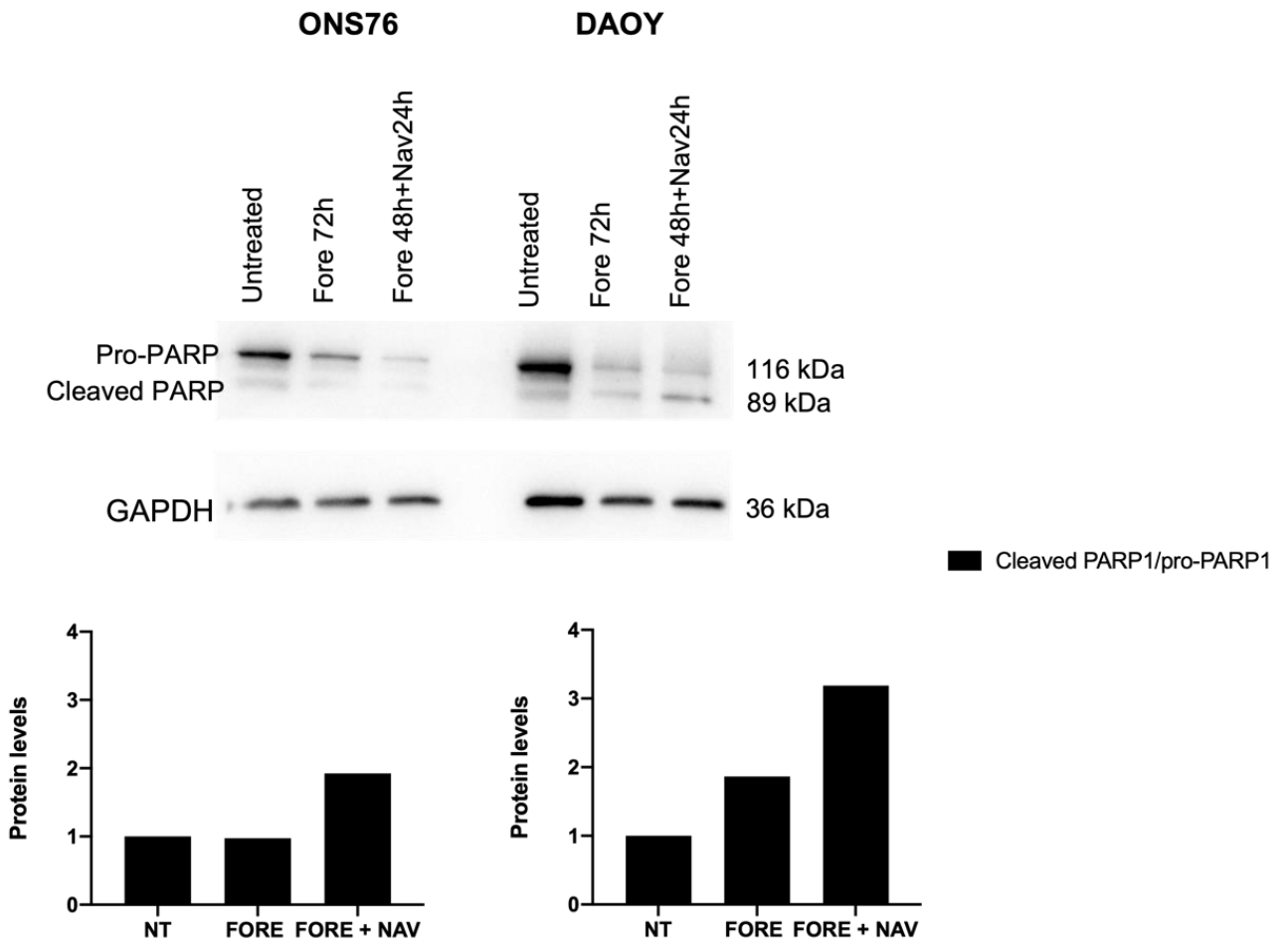


**Figure 40: PARP cleavage upon treatment with navitoclax in DAOY and ONS76 pre-treated with foretinib**

Representative western blot images for DAOY and ONS76 treated with foretinib (48h) plus navitoclax (24h) to assess PARP cleavage. After 48h of foretinib treatment navitoclax was added (2 $\mu$ M) and proteins were extracted to perform western blot analysis. 40  $\mu$ g of proteins were loaded for all the samples and GAPDH was used as loading control. Densitometric analysis show the ratio between cleaved PARP1 and pro-PARP1

#### 4.13 Enhanced MET signalling in vincristine-resistant MB cells

Chemotherapy belongs to the standard care regimen for patients diagnosed with medulloblastoma; however, tumour recurrence in infant patients (< 3 years old), where chemotherapy represents the main strategy, is worryingly frequent and often associated with drug-resistance and limited efficacy of this therapeutic strategy (Othman et al., 2014). Thus, identifying new mechanisms underlying drug resistance in recurrent medulloblastoma is crucial. It has been well established that overexpression of c-MET receptor is related to the development of resistance mechanisms to small-molecule targeted strategies, such as inhibitors of EGFR (Engelman et al., 2007). Nonetheless, numerous studies suggested that SF-HGF/c-MET kinase pathway activation plays a role in resistance to chemotherapy in cancer cells mainly through inhibition of apoptosis, stimulation of cell proliferation and maintenance stemness properties in CSCs (Delitto et al., 2014; Wood et al., 2021). As mentioned in the first chapter, c-MET pathway activates downstream proteins such as ERK and AKT which promote cell survival and proliferation. In chemo resistant cells, activation of c-MET causes increase in cell viability by inhibiting pro-apoptotic proteins, mainly regulated by AKT activation, and enhanced cell proliferation by ERK activation and mitogen signals (Wood et al., 2021). Overexpression of *MET* and enhanced c-MET signalling pathway was observed in concomitance with cisplatin resistance in both ovarian and osteosarcoma cancer cells; moreover, use of c-MET inhibitors reversed cisplatin resistance and enhanced apoptotic response in resistant cells through inhibition of PIK3/AKT signalling (Li et al., 2016; Wang et al., 2012).

To this regard, here c-MET kinase pathway activation was investigated in vincristine (VCR) resistant DAOY cells (previously generated in the laboratory) in comparison with DAOY parental cells. Western blot analysis was performed upon HGF stimulation and pre-treatment with crizotinib. As shown in Figure 41, c-MET kinase signalling resulted more activated in response to HGF stimulation in vincristine resistant cells compared to the parental cells. However, crizotinib was effective in decreasing phosphorylation in both cell types.

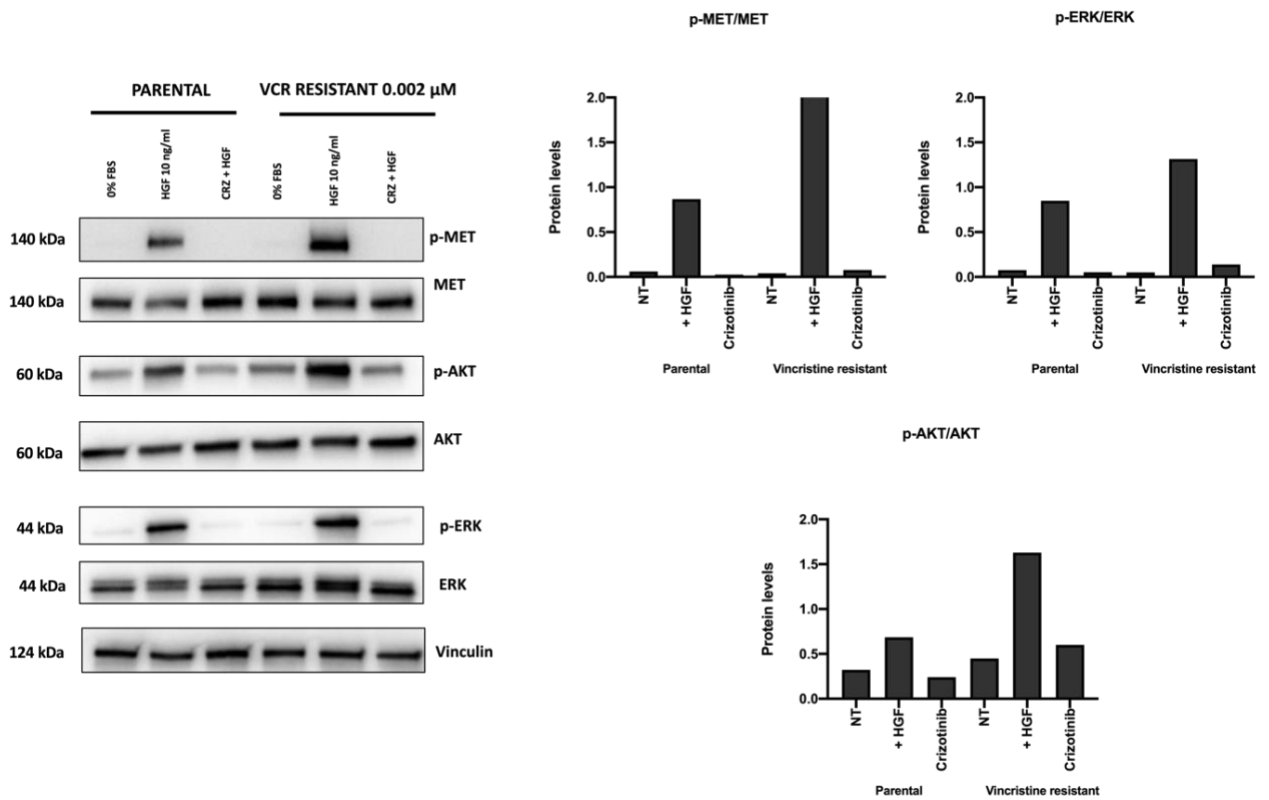


**Figure 41: c-MET kinase pathway activation in vincristine resistant DAOY**

Vincristine-resistant DAOY and parental DAOY were subjected to western blot analysis. Cells were starved for 24h before performing pre-treatment with 1 $\mu$ M crizotinib (2h) and stimulation with 10ng/ml HGF (30mins). Protein lysates were loaded on polyacrylamide gel (40 $\mu$ g for each sample) and membranes were incubated with the indicated antibodies. Vinculin was used as loading control and densitometric analysis is referred to the western presented in the figure.

Due to the increased level of c-MET signalling pathway, we decided to subject vincristine resistant DAOY cells with tivantinib, foretinib and crizotinib treatments for 72h to assess whether development of resistance to vincristine sensitize cells to c-MET inhibitors. Firstly, treatment with vincristine was performed to confirm the resistance to the drug. As shown in Figure 42A, DAOY vincristine-resistant cells showed an  $IC_{50}$  value 10-fold higher compared to the parental cells, confirming the acquisition of the chemoresistance phenotype to the vincristine. Although,  $IC_{50}$  values showed that treatments with crizotinib and foretinib (Figure 42 C-D) were significantly less effective (Figure 42 E) in vincristine resistant cells compared to parental cells, treatments with tivantinib were still effective in suppressing the efficacy of vincristine resistant cells when compared to parental cells (Figure 42B). Altogether, these results suggested that c-MET signalling may be implicated in the mechanism of resistance of MB cells to the anti-mitotic drugs such as vincristine. The unexpected decrease in the sensitivity to foretinib and crizotinib of vincristine resistant cells highlighted the possibility that these two c-MET inhibitors share a similar mechanism of action with vincristine in altering the mitotic progression of cancer cells (Gortany et al., 2021; Megiorni et al., 2015). Therefore, it will be highly unreasonable to use these drugs in therapy for MB patients that have been already treated with vincristine. In contrast, since tivantinib is an atypical c-MET inhibitor and it was observed to exert an anti-mitotic effect through the inhibition of the microtubule polymerisation by binding the colchicine binding site without affecting the vincristine binding to the tubulin (Katayama et al., 2013), we may hypothesise that tivantinib can be a viable option as second line therapy for recurrent MB patients.

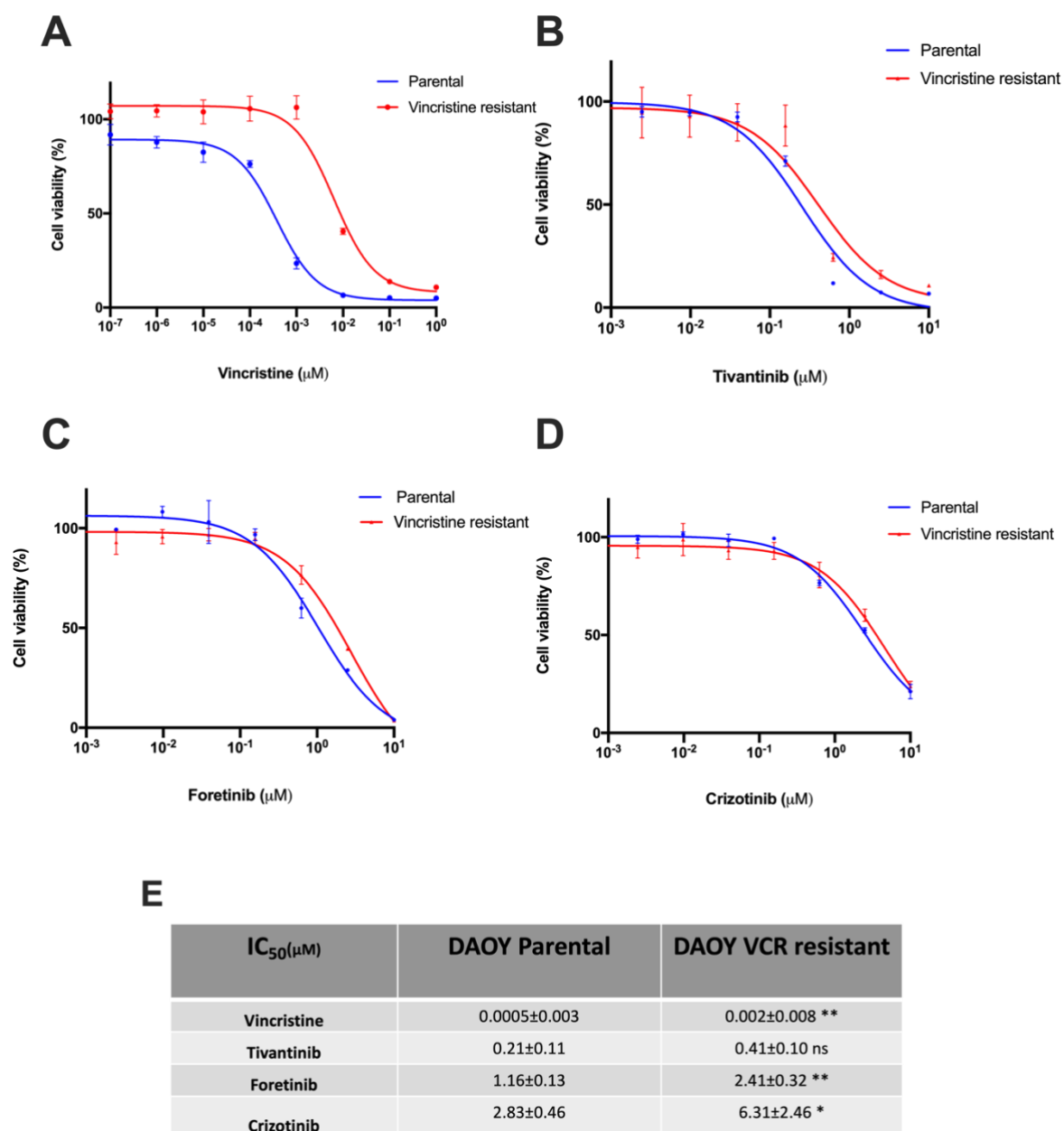


**Figure 42: c-MET kinase inhibitors effects on DAOY vincristine resistant**

A-D) Vincristine resistant DAOY and parental DAOY were treated for 72h with vincristine (A), tivantinib (B), foretinib (C) and crizotinib (D) at scalar concentration starting from 10  $\mu\text{M}$  for MET inhibitors and 1  $\mu\text{M}$  for vincristine (Fold dilution 1:10). MTT assay was performed to determine cell viability. Data are shown as Mean $\pm$ SD (n=3) E)  $\text{IC}_{50}$  values were calculated with GraphPad 8 software and are shown as Mean $\pm$ SD of three independent replicates. Statistical comparison between parental and vincristine resistant was performed by Student's t-test ( $p \leq 0.05 = *$ ,  $p \leq 0.01 = **$ ,  $p \leq 0.001 = ***$ , ns= non-significant) on three independent experiments.

#### 4.14 Tivantinib and mTOR inhibitors synergistically affect DAOY proliferation

The PI3K/AKT/mTOR pathway is an intracellular signalling pathway which plays a fundamental role in cellular growth, proliferation and metabolism (Zou et al., 2020) and its genetic and epigenetic alterations are strictly associated with tumour initiation and progression, including medulloblastoma (Dimitrova & Arcaro, 2015). For this reason, inhibition of PI3K/AKT/mTOR signalling pathway has been thoroughly evaluated in MB context; for instance, inhibition of PI3K with the inhibitor LY294002 strongly induced apoptotic response in medulloblastoma cell lines and more importantly, this inhibitor showed even more promising effects when used to treat medulloblastoma CD133<sup>+</sup> cancer stem cells (Frasson et al., 2015), suggesting its promising role as therapeutic target in recurrent medulloblastomas.

Furthermore, mTOR inhibitors showed promising effects when used in combination with the BET protein bromodomain inhibitor JQ1 in medulloblastoma cell lines (Chaturvedi et al., 2020). Recent observations by Wu et al. (2019) have shown that tivantinib can inhibit glioblastoma cell proliferation through block of the PI3K/AKT/mTOR pathway (Wu et al., 2019).

Therefore, here we aimed to investigate the efficacy of tivantinib to suppress cell SHH MB cell proliferation when subjected to combinatorial regimen with dual ATP-competitive PI3K and mTOR inhibitor BEZ235 or the FDA approved mTOR inhibitor everolimus. Initially, we challenged DAOY cells for 72h treatments with linear dilutions of the two inhibitors and we observed that DAOY cells were highly sensitive to nanomolar concentrations of the dual inhibitor BEZ235 (Figure 43A) whilst 25 $\mu$ M concentration of everolimus were needed to reach the 50% inhibitory effects (IC<sub>50</sub>) (Figure 43B). Next, DAOY cells were treated with tivantinib in combination with BEZ235 at three different concentrations (0.003-0.03-0.3 $\mu$ M) or everolimus (2-20 $\mu$ M). MTT proliferation assays showed that combinatorial treatment with both BEZ235 and everolimus drugs caused a significant decrease in cell proliferation compared to tivantinib alone (Figure 43C-D).

Combination index value analysis suggested that drugs potentially act in synergy to cause anti-proliferative effects (Figure 43E-F). CI values < 1 were mainly observed at 0.6 and 2.5 $\mu$ M of tivantinib in combination with all the three concentrations tested for BEZ235. Generally,

DAOY cells resulted more sensitive to combination treatments with tivantinib and everolimus compared to BEZ235, as suggested by lower CI values (Figure 43F).

Next, DAOY 3-D spheroids model were generated again to test the ability of these combinations to hamper spheroids cell growth. To this aim, we chose 2.5 and 0.6  $\mu\text{M}$  concentration of tivantinib for treating spheroids in combination with either BEZ235 (0.03 $\mu\text{M}$ ) or everolimus (20 $\mu\text{M}$ ) over a period of 9 days. We showed that spheroids growth was strongly impaired when they were treated with both BEZ235 and everolimus, but we did not observe evidence of structure dissociation when spheroids were treated with mTOR inhibitors as a single agent. Treatment with tivantinib was confirmed again to be effective in inhibiting spheroids growth as well as in disrupting their structures (Figure 44A). When DAOY 3-D spheroids were treated with the combination of BEZ235 and tivantinib, no significant advantages in impairing spheroids growth were not evident when compared to tivantinib alone (Figure 44B-C). Interestingly, everolimus in combination with tivantinib 0.6 $\mu\text{M}$  showed to be slightly but significantly more effective in inhibiting spheroids growth compared to single agents. Overall, we observed that both BEZ235 and everolimus elicit anti-proliferative effects in DAOY cells which resulted importantly more sensitive to the dual inhibition of PI3K/AKT/ mTOR when compared to the mTOR inhibitor everolimus. Combination treatment with either BEZ234 and everolimus and tivantinib have synergistically effects on DAOY cells proliferation; however, when 3D spheroid models were challenged with similar regimen no significant effects were observed, likely due the need to use higher concentration to elicit an effect in such a complex structure.

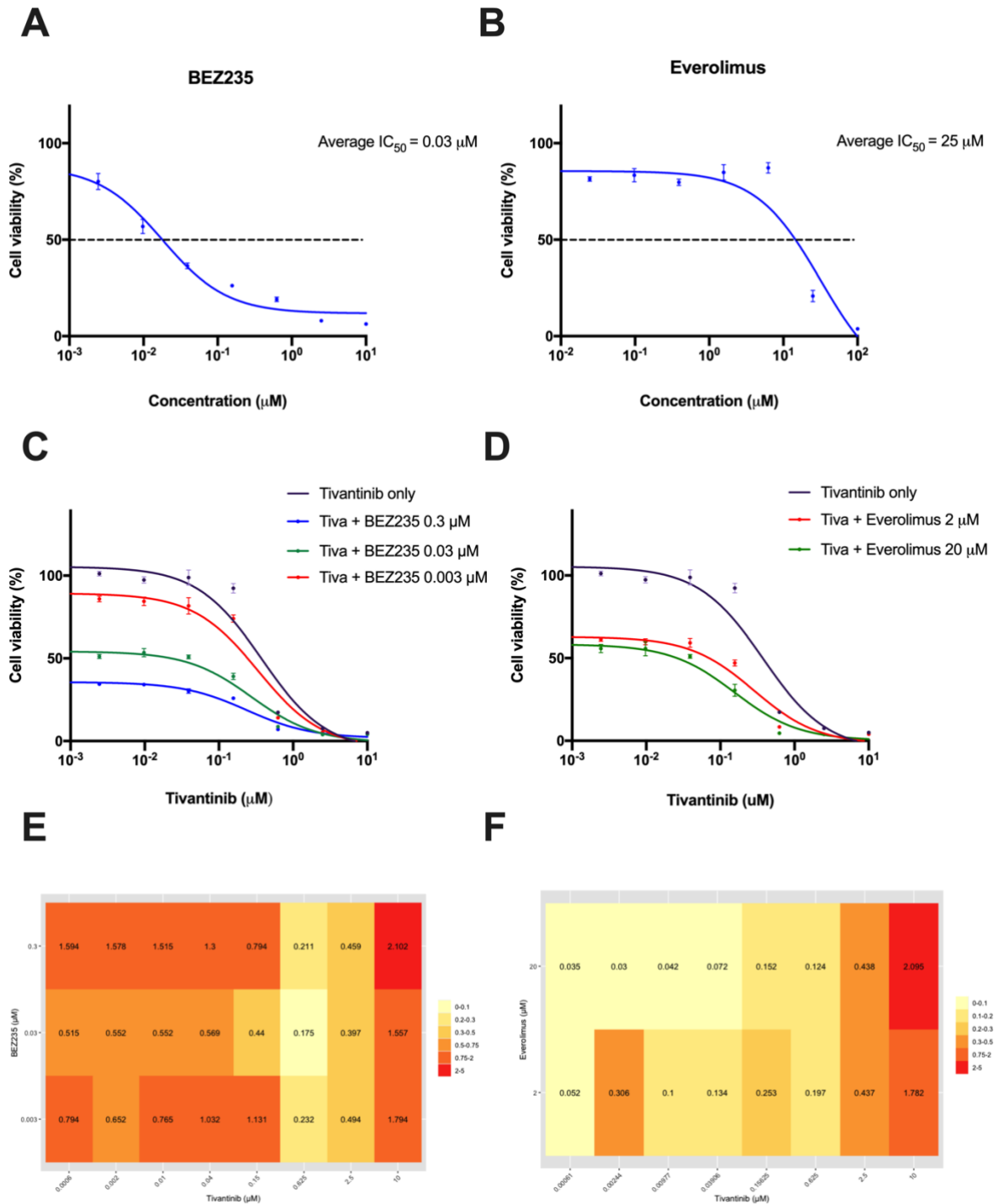


**Figure 43: Tivantinib and BEZ235 synergistic effects on DAOY cell proliferation**

A-B) DAOY cells were treated with tivantinib alone at increasing concentrations (Fold dilution 1:4 - starting from 10 μM) and with fixed concentration of BEZ235 (0.003-0.03-0.3 μM) (A) and Everolimus (2-20 μM) (B) for 72h. Cell viability was assessed using MTT assay and absorbance data were normalized to the untreated cells. Graphs were plotted with GraphPad 8.0 software. Data are represented as Mean±SD (n=3). B-D) CI values were calculated with Compusyn software (CI=1 additive effect; CI < 1 synergism; C > 1 antagonism) and were plotted as heatmaps generated with R software.

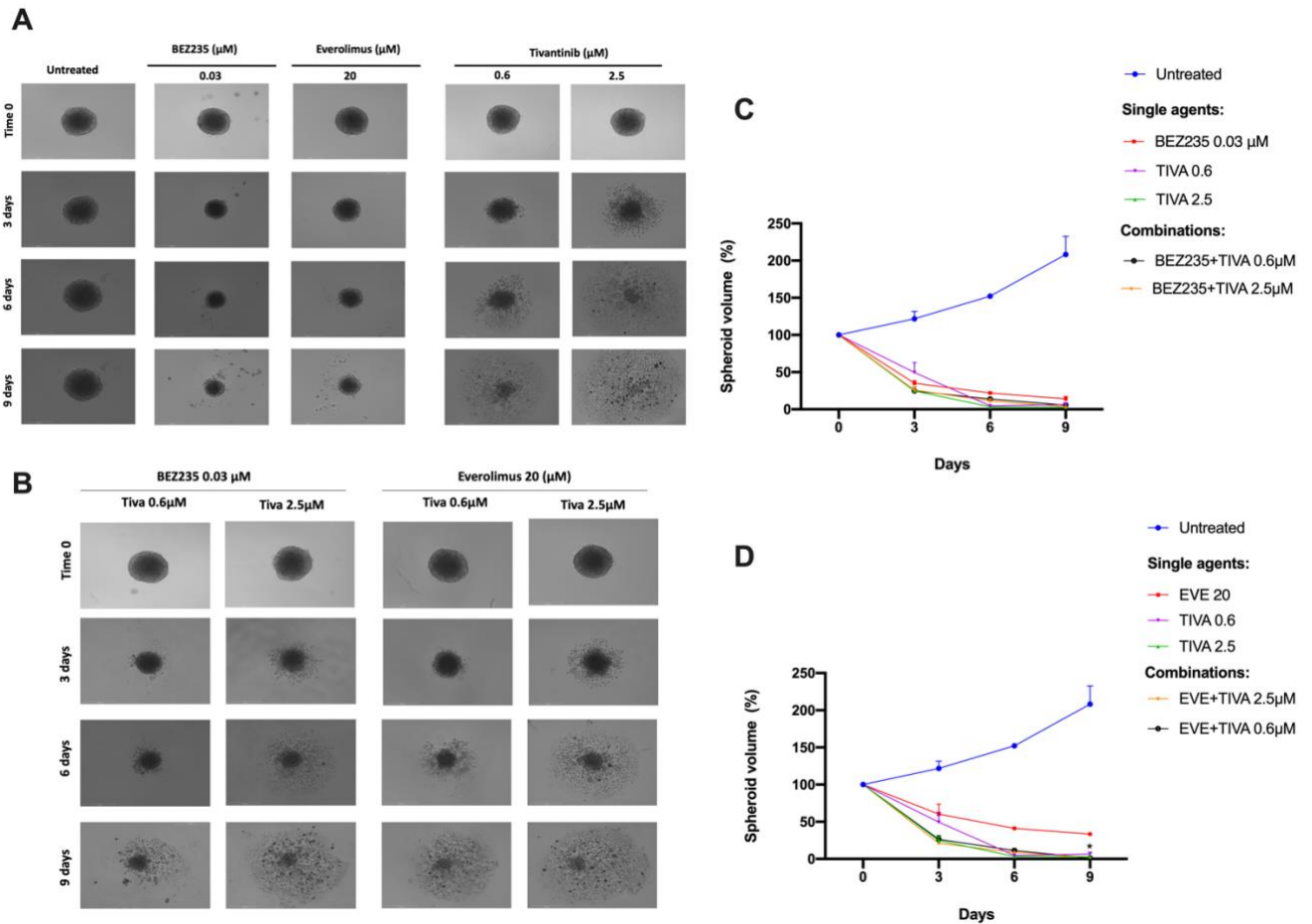


**Figure 44: Effects of dual combination with mTOR inhibitors and tivantinib in 3D spheroids**

A-B) 5 days after seeding, DAOY 3D spheroids were treated with tivantinib (0.6 and 2.5 $\mu\text{M}$ ) with either BEZ235 (0.03 $\mu\text{M}$ ) or everolimus (20 $\mu\text{M}$ ) alone (A) or with combinatorial treatments using the two drugs (B). Treatments were replaced every 3 days for a total of 9 days. Pictures were taken at the end point (9 days) with Evos Auto 2 microscope (scale bar = 275 $\mu\text{m}$ ) C) Volume of each spheroid was calculated at the end point and results were normalized to time 0 spheroids to determine the growth over time. Student's t-test ( $p \leq 0.05 = *$ ,  $p \leq 0.01 = **$ ,  $p \leq 0.001 = ***$ ) was performed to statistically compared volume at time 0 vs volume at 3, 6, and 9 days for each treatment (n=2, each done in quadruplicates).

## ***CHAPTER 5: Discussion***

## 5.1 General discussion

Targeting SF-HGF/c-MET signalling pathway has been shown as a valid therapeutic approach for treating numerous cancers, including MB (Y. Li et al., 2005; Tong et al., 2004). Medulloblastoma is one of the most common brain tumours during childhood, and it accounts for almost 20% of all the diagnosed paediatric brain tumours (Millard & De Braganca, 2016). Due to MB peculiar and high heterogeneity, in the post-genomic era, MB has been widely studied and dissected; to date MB is classified in four distinct subgroups based on different molecular signatures (WNT, SHH, Group 3 and Group 4) (Louis et al., 2021; Taylor et al., 2012). Many genes have been correlated with the pathogenesis of different MB subgroups and among those, the SF-HGF/c-MET pathway was found to play a role in the SHH-MB progression and dissemination (Binning et al., 2008; Y. Li et al., 2005; Provencal et al., 2010). Relying on these findings, inhibitors of c-MET kinase were tested both *in vitro* and *in vivo* MB models, providing promising insights into their potential use for treatment of medulloblastoma (Guessous et al., 2010; Kongkham et al., 2010). Interestingly, a phase 1 study is now recruiting patients with recurrent MB to test the efficacy of the highly selective c-MET inhibitor savolinitib as monotherapy.

Here, we initially interrogated the latest transcriptional study performed on 763 MB primary tumour samples (Cavalli et al., 2017) and we confirmed that, as previously shown by other groups (Faria et al., 2015; Onvani et al., 2012), c-MET kinase is highly expressed in SHH MB compared to the other subgroups (Figure 9B); moreover, Cavalli *et al.* provided an additional classification for MB subgroups in different subtypes within subgroups, which are correlated to different prognoses and outcomes (Cavalli et al., 2017). Among the subtypes, SHH- $\alpha$ , which harbours genomic aberrations associated with poor survival, such as *TP53* or *MYCN* mutations, showed the highest expression of c-MET kinase compared to the other subtypes (Figure 9C). Although, our analysis of MB patients' survival in correlation with c-MET expression did not reveal a significant difference in overall survival between high-MET and low-MET patients across the cohort, it is crucial to consider that biomarkers of c-MET activity, such as phosphorylation of the kinase, were not evaluated in this instance. Study of phosphorylation status of c-MET kinase represent an essential proof to establish activation of the c-MET in tumour samples and lack of its evaluation, as biomarker for patient stratification

and recruitment, has been often correlated with failures of clinical trials that aimed to evaluate c-MET inhibitors (Hughes & Siemann, 2019).

The high expression of *MET* gene in SHH MB primary tumours, together with the evidence already found in the literature regarding its role in MB, provided the basis for exploring the effects of a panel of seven different commercially available c-MET kinase inhibitors, both selective and non-selective for the c-MET receptor, in *in vitro* SHH MB cell lines. Since the extreme heterogeneity, within subgroups and subtypes, of MB is the hardest challenge when it comes to decide the most proper treatment for patients, we aimed to provide most of the results on SHH MB cell lines representative of both SHH-*TP53* mutated (DAOY and UW228) and SHH-*TP53* wildtype (ONS76) (Ivanov et al., 2016).

Firstly, in line with previous studies (Faria et al., 2015; Li et al., 2008; Santhana Kumar et al., 2015), we observed that c-MET kinase was activated by receptor autophosphorylation (Tyr1234/1235) in our SHH cell lines in response to HGF stimulation (Figure 12). Moreover, we observed that proliferation of the *TP53*-mutated DAOY significantly increased after 24 hours of HGF (10ng/ml) (Figure 13) stimulation and that DAOY cells proliferation was affected by *MET* knockdown (Figure 14), suggesting that inhibition of the kinase influences MB cells growth.

When we challenged SHH MB cell lines for 72 h with c-MET kinase inhibitors, we observed that the highly selective non-ATP competitive c-MET inhibitor tivantinib showed the highest efficacy across the three SHH MB cell lines, being the most effective in hampering cell proliferation in these cells. Foretinib (non-selective ATP competitive) and crizotinib (non-selective ATP competitive) ranked, respectively, as second and third most effective drugs among the ones tested (Figure 15D), consistently with previous studies (Endersby et al., 2021; Faria et al., 2015; Zomerman et al., 2015). Outperformance by tivantinib when compared to foretinib and crizotinib was confirmed also in DAOY 3-D cultures, used to mimic as close as possible the tumour geometry, suggesting the ability of tivantinib to elicit its effects in more complex structures compared to 2D cultures.

Based on our viability assays, we decided to mainly use two different concentrations of the different drugs (0.5 and 1 $\mu$ M) based on the different time-point on which the following assays were performed. For instance, we showed, through cell cycle analysis by flow cytometry, that

24 hours treatment with tivantinib significantly caused accumulation in Sub-G1 in SHH cell lines, with major extent in the SHH-*TP53* mutated DAOY cells (Figure 20 A-B) compared to *TP53* wild-type ONS76, while the SHH-*TP53* mutated UW228 cells showed to be arrested in G2/M phase but still a 20% of gated cells were accumulated in Sub-G1 (Figure 20 C). However, analyses of caspase 3/7 activation in both 2D and 3D cultures, confirmed the strong apoptotic response upon tivantinib treatment in DAOY (Figure 20A; Figure 21) and UW228 cells (Figure 20B) while no significant activation was observed in the ONS76 upon tivantinib treatment (Figure 20C).

In contrast, we showed that treatment with foretinib caused a significantly major G2/M arrest (Figure 19A-C) in our SHH cell lines which has not been previously described in MB cells (Faria et al., 2015). On the other hand, cells treated with crizotinib did not show any major change in terms of cell cycle distribution, likely due to the need of using higher concentrations of this drug when treating SHH MB cell lines, as suggested by the IC<sub>50</sub> values (Table 6). Moreover, no prominent apoptotic activation was observed across SHH MB cell lines after 24h of foretinib and crizotinib treatments when compared to tivantinib. Interestingly, ability of the foretinib to induce G2/M arrest and apoptotic death was recently shown, and associated with c-MET inhibition, in glioblastoma cells; however, to observe significant cell death in glioblastoma cells, very high concentrations of foretinib were needed (10 and 20 $\mu$ M) (Gortany et al., 2021).

Next, cell fates analysis provided more detailed information on the inhibitory mechanism of tivantinib, foretinib and crizotinib. We observed that tivantinib largely caused mitotic cell death in *TP53*-mutated DAOY cells (Figure 27 B-F), as suggested by cell cycle analysis and apoptotic assays; cell fate profiles analysed after tivantinib treatment in UW228 confirmed its ability of causing death during mitosis (Supplementary 3). Furthermore, western blot analyses showed that tivantinib induces mitotic cell death in DAOY and UW228 cells (Figure 26B; Supplementary 3) through down-regulation of MCL-1 (Figure 30A; Supplementary 5), as previously shown in different cancer cell lines (Lu et al., 2015), implying that mitochondrial apoptotic pathway is triggered in these cells.

In contrast, effects of tivantinib on ONS76 cells resulted in a major mitotic delay (Figure 27 B-F; Figure 29) with no downregulation of MCL-1 observed after treatment with tivantinib in this cell line. We then speculated that the higher sensitivity to the drug can be correlated to the loss of p53 protein. Nonetheless, further experiments are required to clarify this point.

However, long-term effects with 9 days tivantinib treatment revealed that all the three SHH MB cell lines, including ONS76 cells, became more sensitive to the drug's effects, suggesting that ONS76 may only require longer treatment to be strongly affected by tivantinib. Moreover, our results also confirmed that 24 hours treatments with tivantinib is significantly able to affect colony forming ability and formation of DAOY and ONS76-derived medullospheres, which suggests tivantinib's ability to also affect the cancer stem cells population, which are often responsible for medulloblastoma recurrence and drug resistance (Singh et al., 2003).

Surprisingly, cell fate profiles analyses after treatment with foretinib showed that this drug mainly caused mitotic slippage and failure of cytokinesis in our *in vitro* SHH-MB models. Mitotic slippage is a well-known cause of chromosomal instability that may lead to drug resistance and cell survival (Ghelli Luserna Di Rorà et al., 2019; Huang et al., 2019). Moreover, similarly to foretinib, also treatment with crizotinib in DAOY and ONS76 cells induced mitotic slippage, suggesting that these two c-MET inhibitors may have similar mechanism of action in SHH MB cells. However, foretinib and crizotinib effects resulted to be again cell line-dependent; while a fraction of mitotic 'slipped' DAOY and UW228 cells died either in mitosis or in interphase, ONS76 cells treated with foretinib and crizotinib continued to undergo events of mitotic slippage over the 72 hours. At molecular level, compared to tivantinib, 24h treatment with foretinib and crizotinib were not able to induce either cleavage of PARP1 or MCL-1 down-regulation in both cell lines, suggesting that apoptotic pathway was not activated with these treatments, as also corroborated by Caspase 3/7 detection.

Moreover, we observed that levels of Cyclin B1 were decreasing in DAOY cells after foretinib and crizotinib treatment. This is in line with the idea that CNNB1 degradation is responsible for premature mitotic exit and slippage (Sloss et al., 2016). Nonetheless, Cyclin B1 levels increased in response to foretinib and crizotinib in ONS76 cells; we then hypothesize that such an effect is due to the tendency of this cells to re-start the cell cycle after the mitotic slippage, which it may require higher levels of CNNB1. This is only a speculation and experiments with synchronized cells are needed to better clarify this point (Sonoda, 2006).

Mitotic cell fates in response to drug treatment, mainly in the context of anti-mitotic drugs, are regulated by networks of death signals release and regulation of CNNB1 levels, two different pathways that compete to each other when prolonged mitotic arrest occurs.

Furthermore, boosting pro-apoptotic pathways is a valid approach to avoid mitotic slippage tipping the balance towards cell death (Topham & Taylor, 2013). It is well known that apoptosis is controlled by the BCL-2 family proteins including both pro-apoptotic (BAX, BAK, BIM) and anti-apoptotic (BCL-2, MCL-1, BCL-XL) proteins (Carrington et al., 2017). Here, we showed that pharmacological inhibition of BCL-2 and BCL-XL with the small molecules BH3-mimetic, navitoclax, significantly sensitize SHH MB cells to the effects of pre-treatment with foretinib when compared to their use as single agents. Besides, an increased ratio of cleaved PARP1/pro-PARP1 confirmed that sequential foretinib and navitoclax was more effective compared to foretinib treatment alone in triggering cell death in both DAOY and ONS76 cells. Interestingly, similar to what we have observed with foretinib in our SHH-MB cells, treatment with navitoclax was demonstrated to be extremely effective in triggering apoptosis in mitotic arrested cells after treatment with anti-mitotic drugs, by inhibition of MCL-1 and BCL-XL (Shi et al., 2011). It would be helpful to investigate the expression of these two anti-apoptotic proteins after sequential treatment with foretinib and navitoclax, to better explain molecular mechanisms underlying such effects. We showed for the first time in the MB context, that both foretinib and crizotinib, which were demonstrated to be promising candidates as c-MET kinase inhibitors for treatment of MB cells, induced premature mitotic exit without completing cytokinesis, potentially resulting in aneuploid cells, chromosomal instability and development of drug resistance (Sinha et al., 2019). However, pre-treatment with foretinib followed by treatment with BH-3 mimetics may represent a valid strategy to avoid survival of *slipped* cells. Nonetheless, we hypothesise that both foretinib and crizotinib should be carefully re-evaluated for their clinical relevance in MB context.

Next, we indicated tivantinib as the most promising c-MET inhibitors in affecting cell proliferation by inducing MCL-1 mediated mitotic cell death in our *in vitro* models of SHH MB. When evaluated in phase 2 clinical trial for treatment of hepatocellular carcinoma, tivantinib showed an advantage in the overall survival in patients with high expression of *MET* compared to patients expressing low *MET* (Santoro et al., 2013). However, *in vitro* studies showed that cytotoxic mechanisms of tivantinib were independent from c-MET inhibition and correlated to microtubules disruption (Basilico et al., 2013; Katayama et al., 2013; Xiang et al., 2015). Here, we observed that treatment with tivantinib inhibits autophosphorylation of c-MET kinase upon ligand stimulation but the modest inhibition of the downstream protein's

activation, AKT and ERK, may suggest that the robust cytotoxic effects observed in DAOY cells are also correlated to the inhibition of different processes (Michieli & Di Nicolantonio, 2013). Interestingly, mitotic cell death was observed when *MET* knockdown experiments were performed in DAOY cells; however further experiments are required due to the unhealthy state of cells transfected with scramble siCTRL.

MCL-1 protein which belongs to the downstream apoptotic pathway triggered by c-MET kinase activation, was downregulated when *MET* was silenced by siRNA in HGF-stimulated DAOY cells, again in line with observations in different cancer cell lines (Lu et al., 2015). However, we still recognize the need of considering different targets to fully explain the efficacy of tivantinib as candidate therapy for medulloblastoma.

We then considered that patients diagnosed with medulloblastoma younger than 3 years are currently treated with very-high doses of chemotherapeutic agents. This regimen comes with long-term and severe side effects during adulthood and thus, strategies to reduce toxicity and to use lower dose of the drugs are constantly under evaluation in clinic (Ayoub, 2021; Menyhárt & Gyórfy, 2020). In order to address this problem, we evaluated the potential of tivantinib, which in this study exhibited the most promising effects in causing MB cell death, in combination with vincristine, a first-line chemotherapeutic agent used in medulloblastoma (Kim et al., 2013). We observed that this combinatorial strategy had synergistic effects in hampering SHH MB cells in both 2D and 3D culture, suggesting the possibility of this approach for MB treatment.

Moreover, as mentioned before, one of the main obstacles in clinic is the onset of multi-drug resistance which has been related to multiple mechanisms, including enhanced activity of c-MET kinase pathway (Wood et al., 2021). Here, we showed that stimulation with HGF caused an increased phosphorylation of c-MET, AKT and ERK proteins in DAOY vincristine-resistant cells compared to parental cells, suggesting that c-MET activation has a role in chemoresistance in MB cells. When we challenged our vincristine resistant cells with tivantinib treatment, we observed that there was no significant difference between the anti-proliferative effects compared to the parental cells, suggesting that they may still be sensitive to the drug; this would be explained by the evidence that tivantinib acts on microtubule by binding the colchine-binding site and not the vincristine-binding site (Katayama et al., 2013). Unexpectedly, DAOY vincristine-resistant resulted to be significantly less sensitive to

crizotinib and foretinib treatment, suggesting that they may have been developing a parallel resistance to those two drugs. Together with the evidence that they cause mitotic slippage, which has been indicated as mechanism of resistance to anti-mitotic drugs (Cheng & Crasta, 2017), we hypothesise that both foretinib and crizotinib mechanisms of actions, independently from c-MET inhibition, in MB cells need to be carefully investigated. Possibly, high-selective c-MET inhibitors are required to overcome the resistance and, based on our data we assumed that first-line combinatorial treatments may still represent a better choice. Finally, we provide a small set of data to support the idea of using tivantinib in combination with other small-molecule inhibitors. Tivantinib has been investigated in multiple clinical trials for hepatocellular carcinoma and non-small lung cancers, both as single therapy and in combination with others tyrosine kinase inhibitors (Wu et al., 2020). Here, we considered that targeting PI3K-mTOR pathway has been recently suggested as a valid therapeutic strategy in medulloblastoma (Aldaregia et al., 2018; Chaturvedi et al., 2018; Eckerdt et al., 2019) and we aimed to provide an insight on the use of tivantinib in combination with the PI3K/mTOR dual inhibitor Dactolisib (BEZ235) and the mTOR inhibitor Everolimus. Our *in vitro* analysis demonstrated that targeting mTOR pathway in combination with tivantinib, had synergistic effects in hampering the proliferation of SHH MB cells DAOY in 2D. However, when we challenged 3D-spheroids models with combination treatments, we did not observe significant effects in DAOY 3D spheroids disaggregation when treated when tivantinib was combined with BEZ235. Potentially, higher concentration of BEZ235, due to the use of more complex structures compared to the 2D, are needed to observe significant effects. Nonetheless, explorations on the molecular mechanism underlying these anti-proliferative effects are needed.

## 5.2 Conclusions and future directions

Overall, we found that expression of c-MET kinase is positively correlated with SHH medulloblastoma subgroups and subtypes. Among seven different commercially available c-MET kinase inhibitors tested, only three were able to affect proliferation within 10  $\mu$ M concentration, which is roughly the accepted range for clinical relevance (Hughes et al., 2011), across our SHH MB cell lines. Nonetheless, we acknowledge that the small panel of c-MET inhibitors tested was a limit in this study and a broader selection of drugs, including more high-selective for c-MET kinase, may be required.

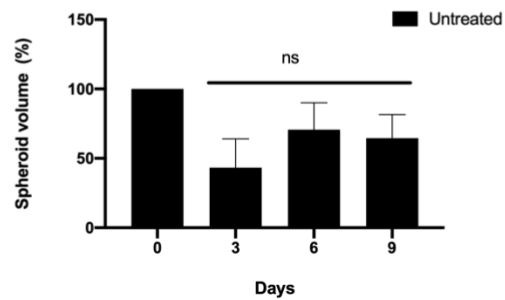
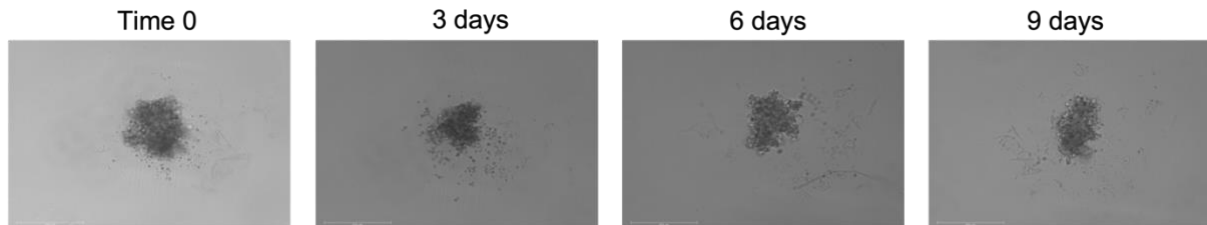
On one hand, tivantinib generally showed the ability to induce cell death more prominently in *TP53* mutated cell lines compared to *TP53* wildtype cells where it mainly caused mitotic delay. Nonetheless, further investigation is needed to understand the link between loss of p53 and the sensitivity to tivantinib as well as understanding potential molecular differences between these heterogeneous cells lines that may explain the observed effects. On the other hand, the other two c-MET kinase inhibitors evaluated in this study, foretinib and crizotinib, mainly caused mitotic slippage in our cell lines. To the best of our knowledge, we showed for the first time in the MB context, that both foretinib and crizotinib, which were demonstrated to be promising candidates as c-MET kinase inhibitors for treatment of MB cells, induced premature mitotic exit without completing cytokinesis, potentially resulting in aneuploid cells, chromosomal instability and development of drug resistance (Sinha et al., 2019). Nonetheless, we showed that the use of BH3-mimetic navitoclax induces potent cell death specifically in SHH MB cells pre-treated with foretinib suggesting that mitotic “slipped” cells are more sensitive to the inhibition of anti-apoptotic proteins. However, additional experiments to evaluate expression of BCL-2 family upon sequential treatment with foretinib are required. We acknowledged that more experiments are needed to better understand the exact molecular mechanisms which underlie such effects and whether those effects are strictly linked to c-MET inhibition. Furthermore, the promising results obtained with combination treatments with both vincristine and mTOR inhibitors need to be further explored, to fully understand molecular changes underlying the observed effects, and eventually to be validated in *in vivo* models to corroborate their potential as therapeutic approach in SHH-MB.

Understanding the mechanisms of action of drugs is crucial to successful clinical trials but many drugs showed promising safety profiles and efficacy during clinical trials and are approved by the FDA without precise knowledge of how they work. Therefore, characterizing mechanisms of action, especially in the context of target-therapy, is essential to better stratify and recruit patients in clinical trials and to avoid treatment failures ("Mechanism matters," 2010). Here, we provided a new insight on the heterogeneous response to c-MET kinase inhibition in SHH medulloblastoma cell lines, which may help in future for tailoring new therapies.

## ***Chapter 6: Supplementary***

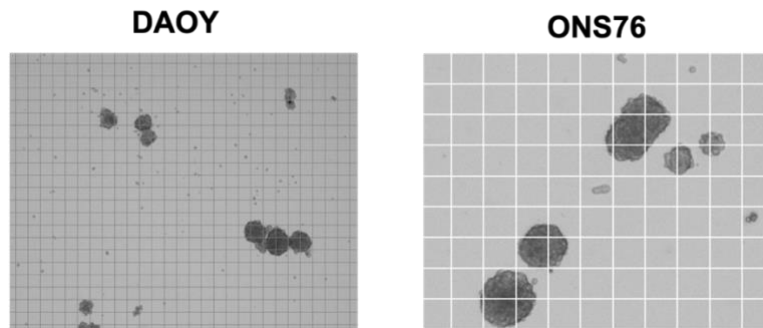
## Supplementary 1. Growth rate for ONS76-derived 3-D spheroids

ONS76 cells were seeded in U-bottom 96-well plate and left for 5 days to allow spheroids formation. Pictures were taken with the Evos FL Auto 2 microscope (Invitrogen) at 10X magnification (scale bar = 275  $\mu\text{m}$ ).



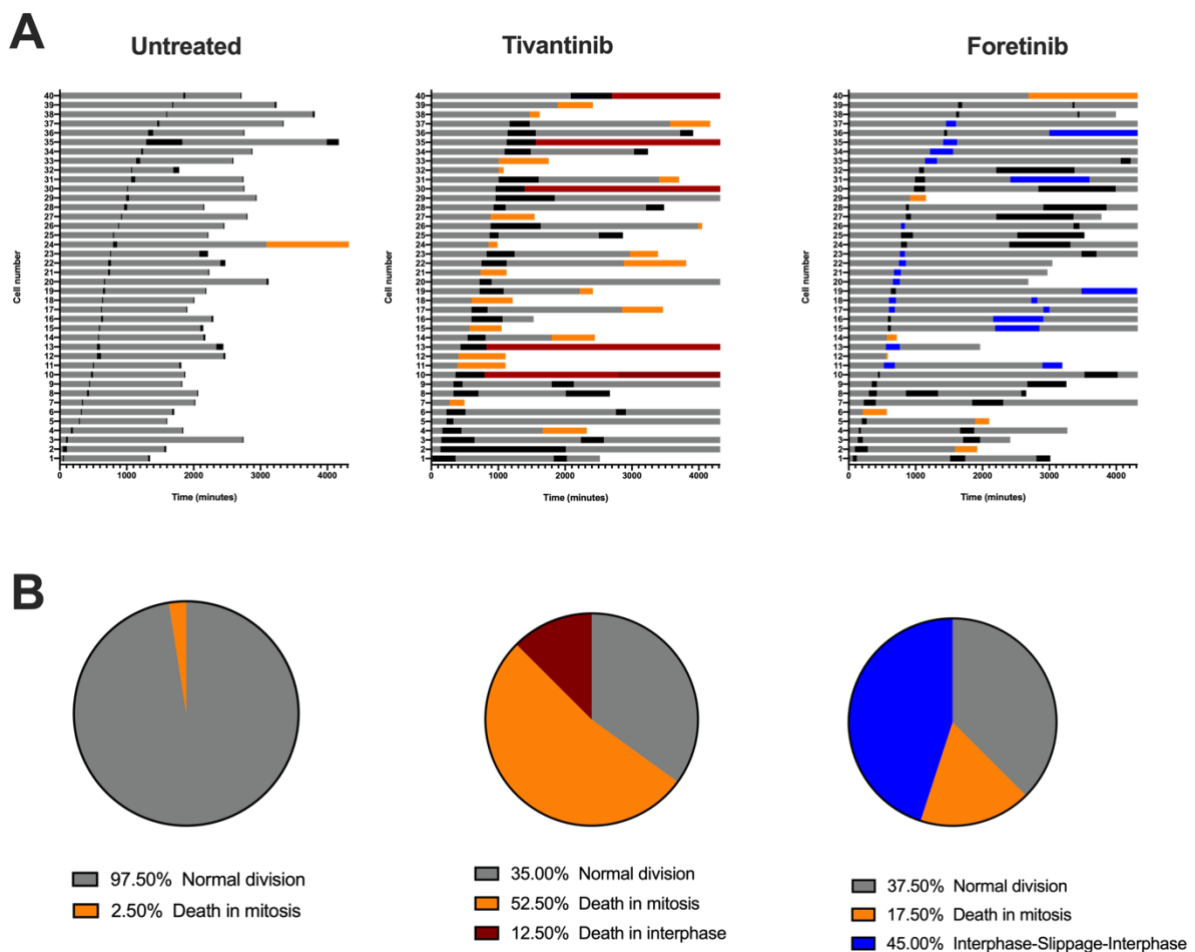
## Supplementary 2. Enlarged images for DAOY and ONS76 medullospheres

Representative pictures of untreated DAOY and ONS76-derived medullospheres after 5 days.



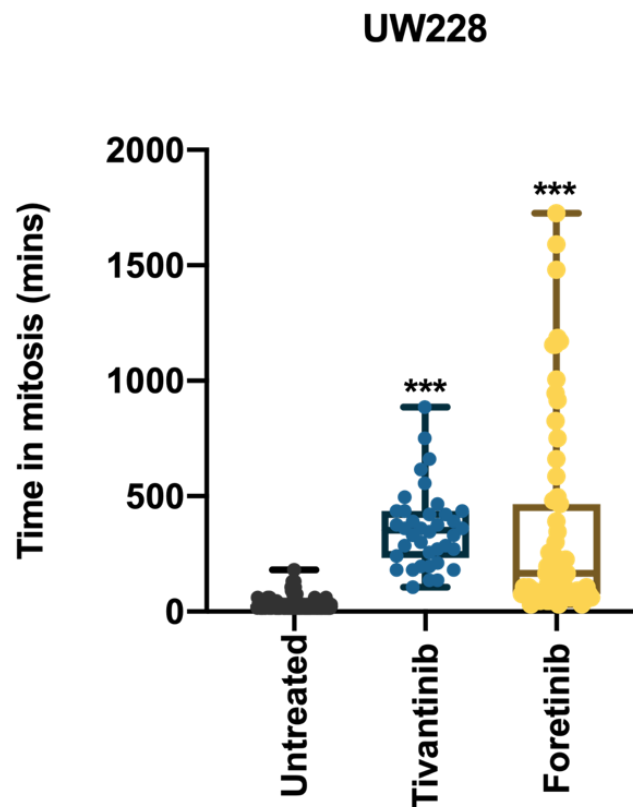
### Supplementary 3. Cell fate analysis on UW228 treated with tivantinib and foretinib

UW228 were subjected to 72h treatment with tivantinib and foretinib and cell fate profiles were analysed. Tivantinib majorly caused mitotic cell death while foretinib induced mitotic slippage. Those results sustained the idea that *TP53* mutated cells are more sensitive to tivantinib treatment compared to *TP53* wildtype cells (ONS76).



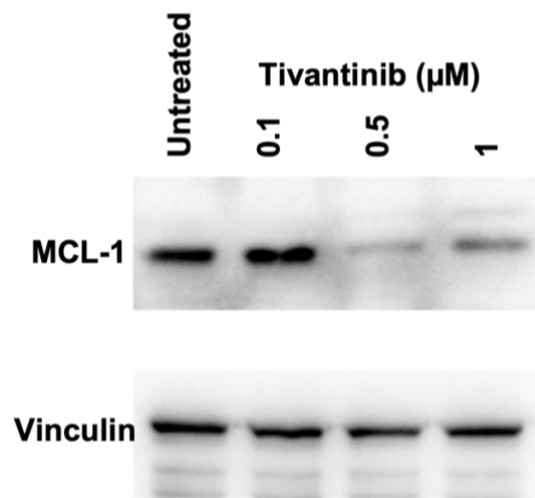
#### Supplementary 4. Mitosis length in UW228 upon foretinib and tivantinib treatments

Time (in minutes) spent in mitosis by UW228 after treatment with tivantinib and foretinib was quantified by time-lapse microscopy. Box plots were generated with GraphPad Prism 8 software by plotting time spent in mitosis (minutes) by single cells upon treatment with tivantinib and foretinib and statistical comparison between the mitosis duration of untreated and treated cells was performed with Student's t-test ( $p \leq 0.05 = *$ ,  $p \leq 0.01 = **$ ,  $p \leq 0.001 = ***$ )



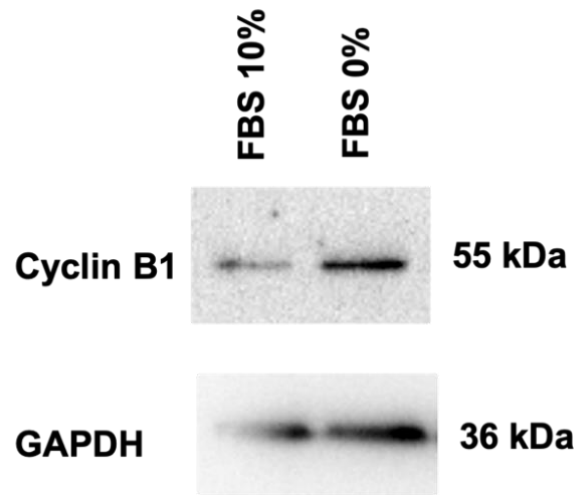
## Supplementary Figure 5: MCL-1 downregulation in UW228 cells after tivantinib treatment

Western blot analysis showing down-regulation of MCL-1 protein after 24h tivantinib treatment (0.1-0.5-1 $\mu$ M). 40 $\mu$ g was loaded for each sample and representative western images are provided below (N=2)



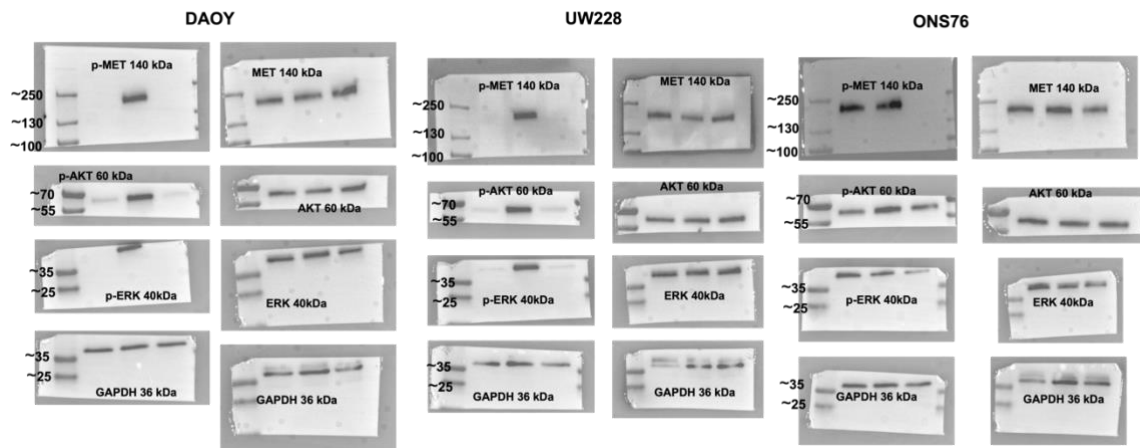
### Supplementary Figure 6. CyclinB1 levels in DAOY serum-starved cells

Western blot analysis showed Cyclin B1 protein levels in DAOY cells after 24h starvation compared to 10% FBS-serum.

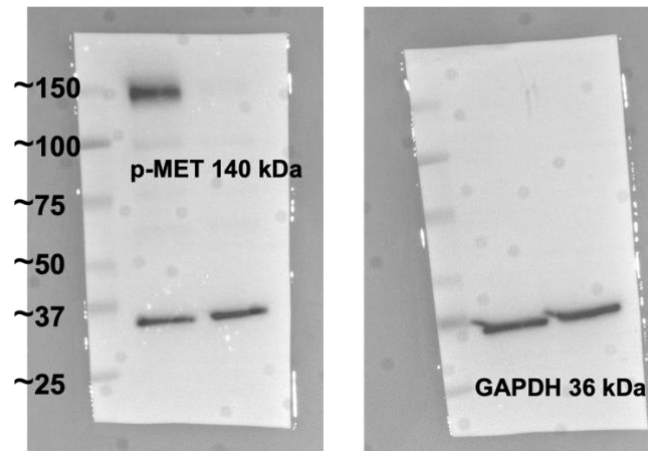


# Supplementary Figure 7. Unprocessed western blot showed in Figure 12

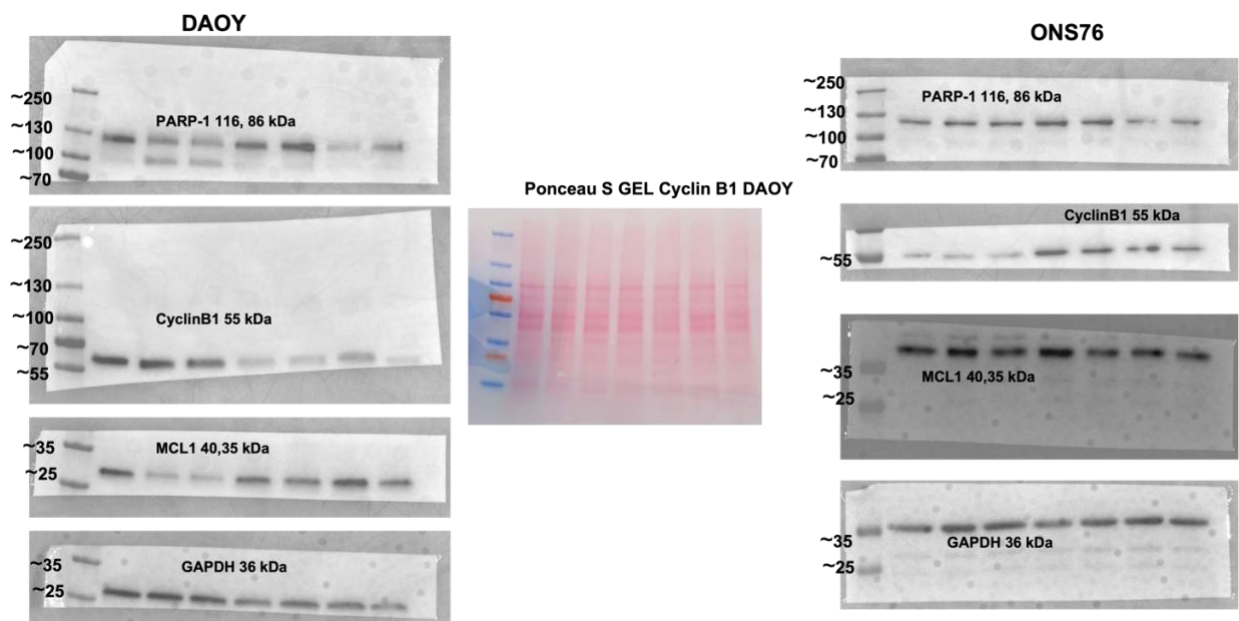
=



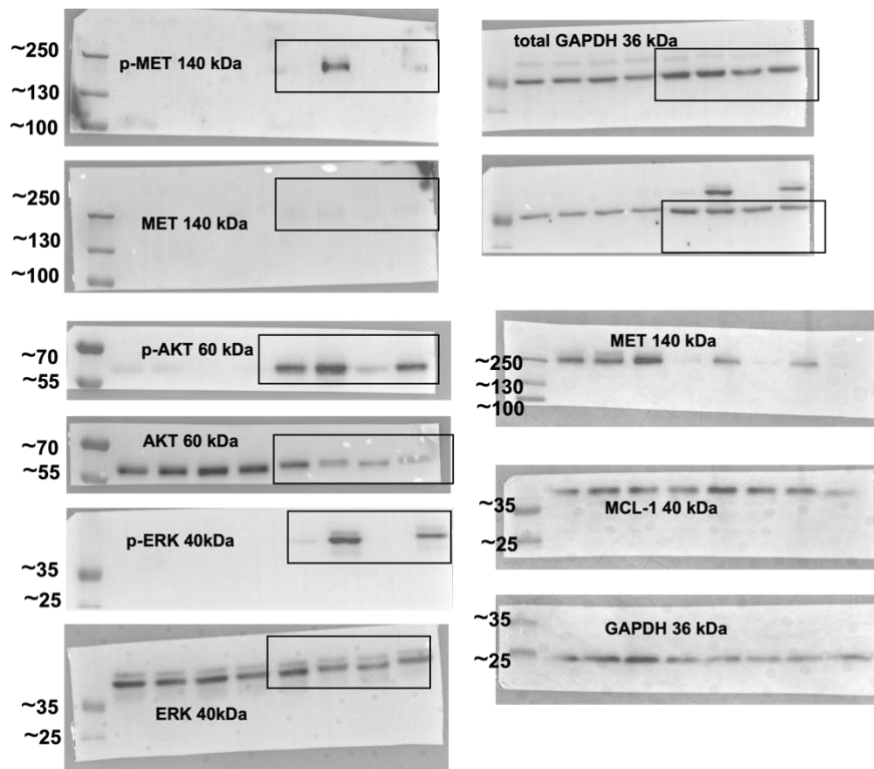
**Supplementary Figure 8. Unprocessed western blot showed in Figure 14**



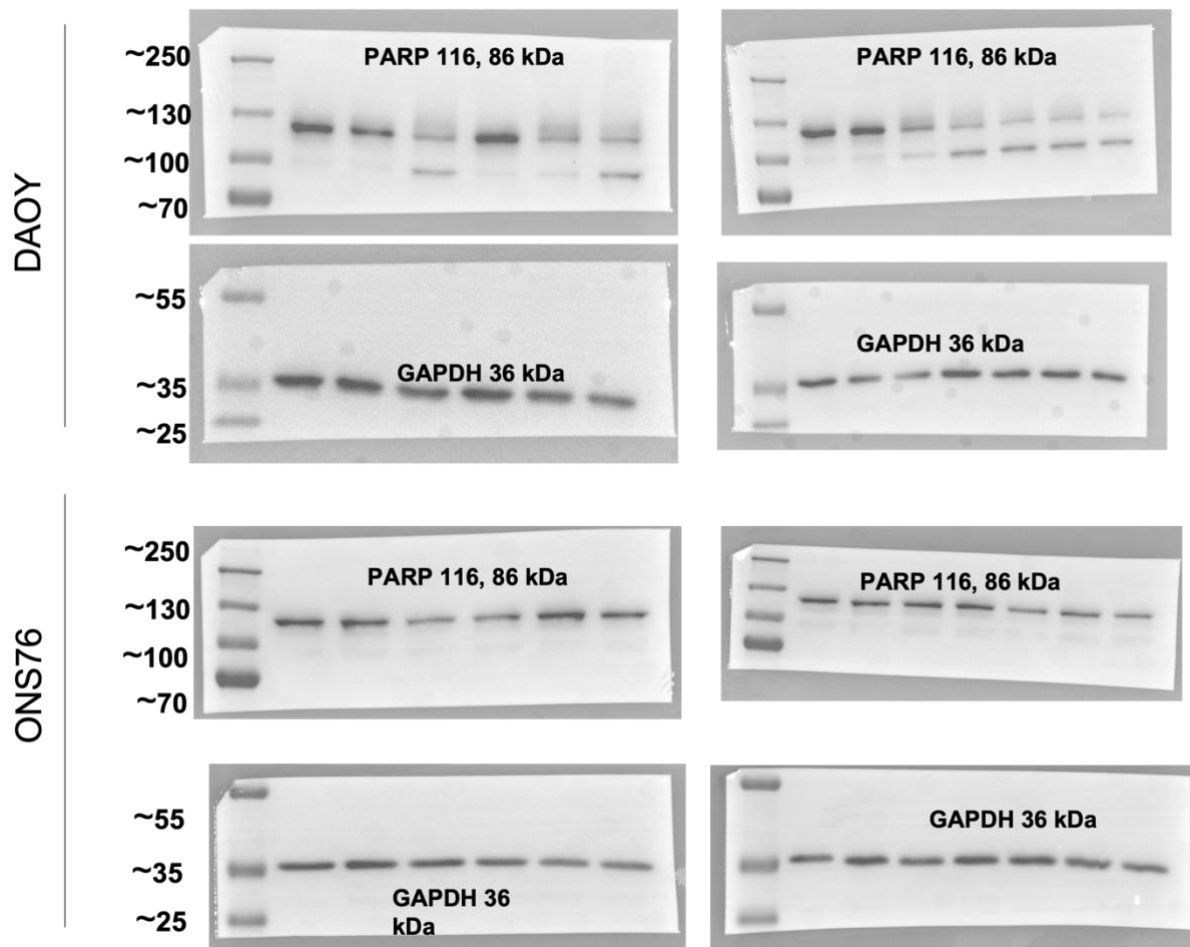
### Supplementary Figure 9. Unprocessed western blot showed in Figure 30



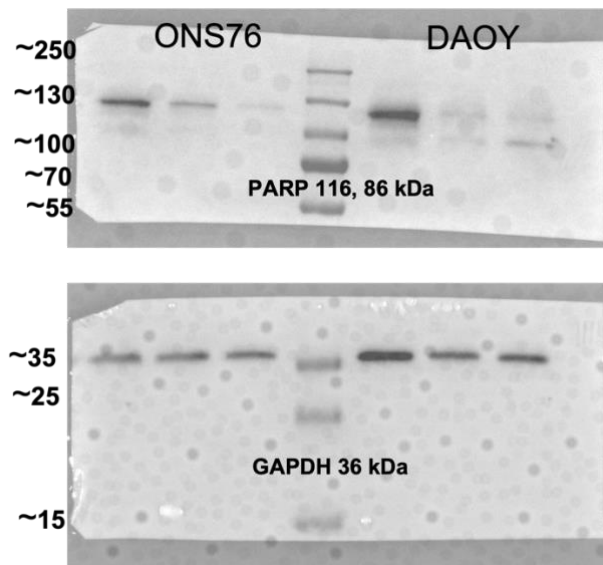
Supplementary Figure 10. Unprocessed western blot showed in Figure 31



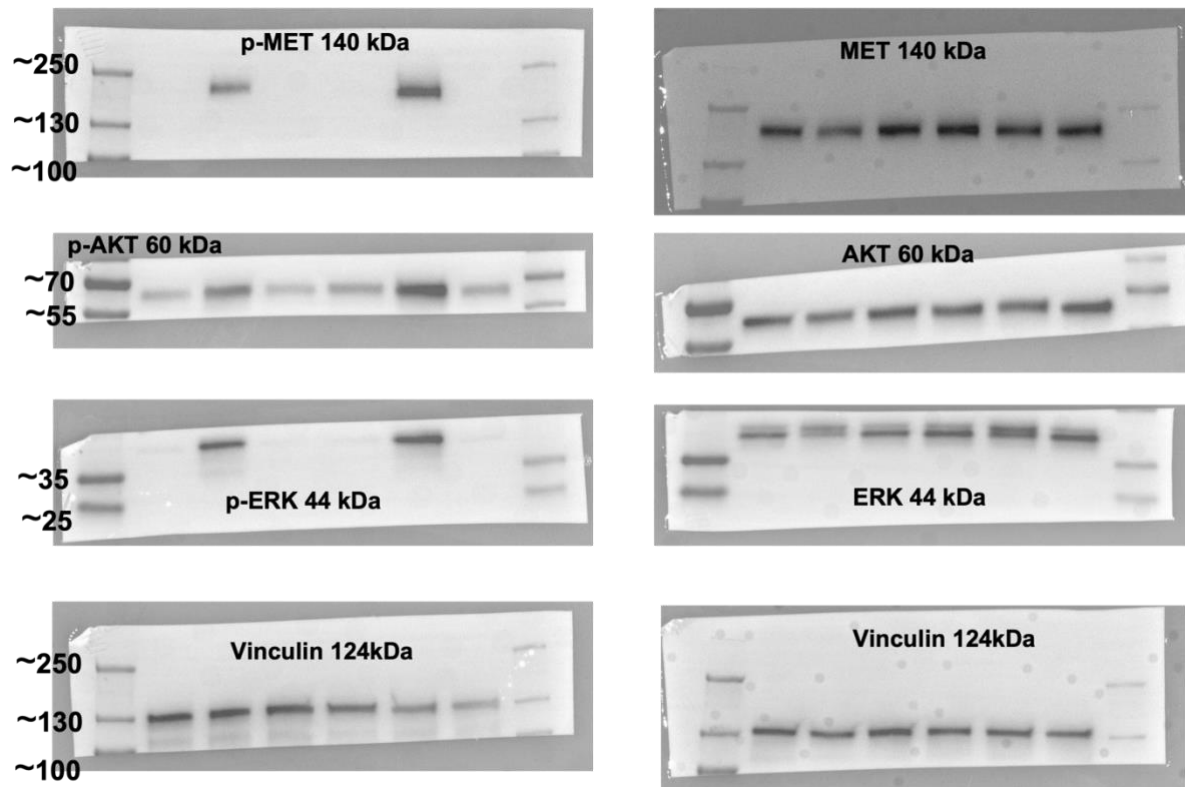
Supplementary Figure 11. Unprocessed western blot showed in Figure 37



**Supplementary Figure 11. Unprocessed western blot showed in Figure 35**



Supplementary Figure 12. Unprocessed western blot showed in Figure 40



# BIBLIOGRAPHY

- Aldaregia, J., Odriozola, A., Matheu, A., & Garcia, I. (2018). Targeting mTOR as a Therapeutic Approach in Medulloblastoma. *International Journal of Molecular Sciences*, 19(7), 1838. <https://doi.org/10.3390/ijms19071838>
- Alexander, P. B., & Wang, X.-F. (2015). Resistance to receptor tyrosine kinase inhibition in cancer: molecular mechanisms and therapeutic strategies. *Frontiers of Medicine*, 9(2), 134-138. <https://doi.org/10.1007/s11684-015-0396-9>
- Ariyawutyakorn, W., Saichaemchan, S., & Varella-Garcia, M. (2016). Understanding and Targeting MET Signaling in Solid Tumors - Are We There Yet? *J Cancer*, 7(6), 633-649. <https://doi.org/10.7150/jca.12663>
- Ayoub, N. M. (2021). Editorial: Novel Combination Therapies for the Treatment of Solid Cancers. *Front Oncol*, 11, 708943. <https://doi.org/10.3389/fonc.2021.708943>
- Azzarelli, R., Simons, B. D., & Philpott, A. (2018). The developmental origin of brain tumours: a cellular and molecular framework. *Development*, 145(10), dev162693. <https://doi.org/10.1242/dev.162693>
- Bailey, P., & Cushing, H. (1925). MEDULLOBLASTOMA CEREBELLI: A COMMON TYPE OF MIDCEREBELLAR GLIOMA OF CHILDHOOD. *Archives of Neurology & Psychiatry*, 14(2), 192-224. <https://doi.org/10.1001/archneurpsyc.1925.02200140055002>
- Bandopadhyay, P., Bergthold, G., Nguyen, B., Schubert, S., Gholamin, S., Tang, Y., Bolin, S., Schumacher, S. E., Zeid, R., Masoud, S., Yu, F., Vue, N., Gibson, W. J., Paoella, B. R., Mitra, S. S., Cheshier, S. H., Qi, J., Liu, K.-W., Wechsler-Reya, R., . . . Cho, Y.-J. (2014). BET Bromodomain Inhibition of MYC-Amplified Medulloblastoma. *Clinical Cancer Research*, 20(4), 912-925. <https://doi.org/10.1158/1078-0432.ccr-13-2281>
- Basilico, C., Pennacchietti, S., Vigna, E., Chiriaco, C., Arena, S., Bardelli, A., Valdembri, D., Serini, G., & Michieli, P. (2013). Tivantinib (ARQ197) displays cytotoxic activity that is independent of its ability to bind MET. *Clin Cancer Res*, 19(9), 2381-2392. <https://doi.org/10.1158/1078-0432.CCR-12-3459>
- Bhatia, S., Hirsch, K., Bukkapatnam, S., Baig, N. A., Oweida, A., Griego, A., Calame, D., Sharma, J., Donson, A., Foreman, N., Albanese, C., Venkataraman, S., Vibhakar, R., & Karam, S. D. (2017). Combined EphB2 receptor knockdown with radiation decreases cell viability and invasion in medulloblastoma. *Cancer Cell Int*, 17, 41. <https://doi.org/10.1186/s12935-017-0409-7>
- Bhullar, K. S., Lagarón, N. O., McGowan, E. M., Parmar, I., Jha, A., Hubbard, B. P., & Rupasinghe, H. P. V. (2018). Kinase-targeted cancer therapies: progress, challenges and future directions. *Molecular Cancer*, 17(1). <https://doi.org/10.1186/s12943-018-0804-2>

- Binning, M. J., Niazi, T., Pedone, C. A., Lal, B., Eberhart, C. G., Kim, K. J., Laterra, J., & Fults, D. W. (2008). Hepatocyte growth factor and sonic Hedgehog expression in cerebellar neural progenitor cells costimulate medulloblastoma initiation and growth. *Cancer Res*, *68*(19), 7838-7845. <https://doi.org/10.1158/0008-5472.CAN-08-1899>
- Birchmeier, C., Birchmeier, W., Gherardi, E., & Vande Woude, G. F. (2003). Met, metastasis, motility and more. *Nat Rev Mol Cell Biol*, *4*(12), 915-925. <https://doi.org/10.1038/nrm1261>
- Birchmeier, C., & Gherardi, E. (1998). Developmental roles of HGF/SF and its receptor, the c-Met tyrosine kinase. *Trends Cell Biol*, *8*(10), 404-410. [https://doi.org/10.1016/s0962-8924\(98\)01359-2](https://doi.org/10.1016/s0962-8924(98)01359-2)
- Blessing, M. M., & Alexandrescu, S. (2020). Embryonal Tumors of the Central Nervous System: An Update. *Surg Pathol Clin*, *13*(2), 235-247. <https://doi.org/10.1016/j.path.2020.01.003>
- Blume-Jensen, P., & Hunter, T. (2001). Oncogenic kinase signalling. *Nature*, *411*(6835), 355-365. <https://doi.org/10.1038/35077225>
- Bottaro, D. P., Rubin, J. S., Faletto, D. L., Chan, A. M., Kmieciak, T. E., Vande Woude, G. F., & Aaronson, S. A. (1991). Identification of the hepatocyte growth factor receptor as the c-met proto-oncogene product. *Science*, *251*(4995), 802-804. <https://doi.org/10.1126/science.1846706>
- Bressenot, A., Marchal, S., Bezdetnaya, L., Garrier, J., Guillemin, F., & Plenat, F. (2009). Assessment of apoptosis by immunohistochemistry to active caspase-3, active caspase-7, or cleaved PARP in monolayer cells and spheroid and subcutaneous xenografts of human carcinoma. *J Histochem Cytochem*, *57*(4), 289-300. <https://doi.org/10.1369/jhc.2008.952044>
- Brito, D. A., & Rieder, C. L. (2006). Mitotic checkpoint slippage in humans occurs via cyclin B destruction in the presence of an active checkpoint. *Curr Biol*, *16*(12), 1194-1200. <https://doi.org/10.1016/j.cub.2006.04.043>
- Buzzetti, M., Morlando, S., Solomos, D., Mehmood, A., Cox, A. W. I., Chiesa, M., D'Alessandra, Y., Garofalo, M., Topham, C. H., & Di Leva, G. (2021). Pre-therapeutic efficacy of the CDK inhibitor dinaciclib in medulloblastoma cells. *Sci Rep*, *11*(1), 5374. <https://doi.org/10.1038/s41598-021-84082-3>
- Caenepeel, S., Cooke, K., Wadsworth, S., Huang, G., Robert, L., Moreno, B. H., Parisi, G., Cajulis, E., Kendall, R., Beltran, P., Ribas, A., Coxon, A., & Hughes, P. E. (2017). MAPK pathway inhibition induces MET and GAB1 levels, priming BRAF mutant melanoma for rescue by hepatocyte growth factor. *Oncotarget*, *8*(11), 17795-17809. <https://doi.org/10.18632/oncotarget.14855>
- Carrington, E. M., Zhan, Y., Brady, J. L., Zhang, J.-G., Sutherland, R. M., Anstee, N. S., Schenk, R. L., Vikstrom, I. B., Delconte, R. B., Segal, D., Huntington, N. D., Bouillet, P., Tarlinton, D. M., Huang, D. C., Strasser, A., Cory, S., Herold, M. J., & Lew, A. M. (2017). Anti-apoptotic proteins BCL-2, MCL-1 and A1 summate collectively to maintain survival of immune cell populations both in vitro and in vivo. *Cell Death & Differentiation*, *24*(5), 878-888. <https://doi.org/10.1038/cdd.2017.30>

- Casciati, A., Tanori, M., Manczak, R., Saada, S., Tanno, B., Giardullo, P., Porcu, E., Rampazzo, E., Persano, L., Viola, G., Dalmay, C., Lalloue, F., Pothier, A., Merla, C., & Mancuso, M. (2020). Human Medulloblastoma Cell Lines: Investigating on Cancer Stem Cell-Like Phenotype. *Cancers (Basel)*, 12(1). <https://doi.org/10.3390/cancers12010226>
- Cavalli, F. M. G., Remke, M., Rampasek, L., Peacock, J., Shih, D. J. H., Luu, B., Garzia, L., Torchia, J., Nor, C., Morrissy, A. S., Agnihotri, S., Thompson, Y. Y., Kuzan-Fischer, C. M., Farooq, H., Isaev, K., Daniels, C., Cho, B.-K., Kim, S.-K., Wang, K.-C., . . . Taylor, M. D. (2017). Intertumoral Heterogeneity within Medulloblastoma Subgroups. *Cancer Cell*, 31(6), 737-754.e736. <https://doi.org/10.1016/j.ccell.2017.05.005>
- Chang, C. H., Housepian, E. M., & Herbert, C., Jr. (1969). An operative staging system and a megavoltage radiotherapeutic technic for cerebellar medulloblastomas. *Radiology*, 93(6), 1351-1359. <https://doi.org/10.1148/93.6.1351>
- Chaturvedi, N. K., Kling, M. J., Coulter, D. W., McGuire, T. R., Ray, S., Keshewani, V., Joshi, S. S., & Sharp, J. G. (2018). Improved therapy for medulloblastoma: targeting hedgehog and PI3K-mTOR signaling pathways in combination with chemotherapy. *Oncotarget*, 9(24), 16619-16633. <https://doi.org/10.18632/oncotarget.24618>
- Chaturvedi, N. K., Kling, M. J., Griggs, C. N., Keshewani, V., Shukla, M., McIntyre, E. M., Ray, S., Liu, Y., McGuire, T. R., Sharp, J. G., Band, H., Joshi, S. S., & Coulter, D. W. (2020). A Novel Combination Approach Targeting an Enhanced Protein Synthesis Pathway in MYC-driven (Group 3) Medulloblastoma. *Mol Cancer Ther*, 19(6), 1351-1362. <https://doi.org/10.1158/1535-7163.MCT-19-0996>
- Chen, Y. C., Ingram, P. N., Fouladdel, S., McDermott, S. P., Azizi, E., Wicha, M. S., & Yoon, E. (2016). High-Throughput Single-Cell Derived Sphere Formation for Cancer Stem-Like Cell Identification and Analysis. *Sci Rep*, 6, 27301. <https://doi.org/10.1038/srep27301>
- Cheng, B., & Crasta, K. (2017). Consequences of mitotic slippage for antimicrotubule drug therapy. *Endocr Relat Cancer*, 24(9), T97-T106. <https://doi.org/10.1530/ERC-17-0147>
- Cho, Y.-J., Tsherniak, A., Tamayo, P., Santagata, S., Ligon, A., Greulich, H., Berhoukim, R., Amani, V., Goumnerova, L., Eberhart, C. G., Lau, C. C., Olson, J. M., Gilbertson, R. J., Gajjar, A., Delattre, O., Kool, M., Ligon, K., Meyerson, M., Mesirov, J. P., & Pomeroy, S. L. (2011). Integrative Genomic Analysis of Medulloblastoma Identifies a Molecular Subgroup That Drives Poor Clinical Outcome. *Journal of Clinical Oncology*, 29(11), 1424-1430. <https://doi.org/10.1200/jco.2010.28.5148>
- Chou, T.-C. (2010). Drug Combination Studies and Their Synergy Quantification Using the Chou-Talalay Method. *Cancer Research*, 70(2), 440-446. <https://doi.org/10.1158/0008-5472.can-09-1947>
- Christensen, J. G., Burrows, J., & Salgia, R. (2005). c-Met as a target for human cancer and characterization of inhibitors for therapeutic intervention. *Cancer Letters*, 225(1), 1-26. <https://doi.org/10.1016/j.canlet.2004.09.044>
- Comoglio, P. M., Giordano, S., & Trusolino, L. (2008). Drug development of MET inhibitors: targeting oncogene addiction and expedience. *Nat Rev Drug Discov*, 7(6), 504-516. <https://doi.org/10.1038/nrd2530>
- Cooper, C. S., Park, M., Blair, D. G., Tainsky, M. A., Huebner, K., Croce, C. M., & Vande Woude, G. F. (1984). Molecular cloning of a new transforming gene from a chemically

- transformed human cell line. *Nature*, 311(5981), 29-33. <https://doi.org/10.1038/311029a0>
- Cui, J. J., Tran-Dube, M., Shen, H., Nambu, M., Kung, P. P., Pairish, M., Jia, L., Meng, J., Funk, L., Botrous, I., McTigue, M., Grodsky, N., Ryan, K., Padrique, E., Alton, G., Timofeevski, S., Yamazaki, S., Li, Q., Zou, H., . . . Edwards, M. P. (2011). Structure based drug design of crizotinib (PF-02341066), a potent and selective dual inhibitor of mesenchymal-epithelial transition factor (c-MET) kinase and anaplastic lymphoma kinase (ALK). *J Med Chem*, 54(18), 6342-6363. <https://doi.org/10.1021/jm2007613>
- De Braganca, K. C., & Packer, R. J. (2013). Treatment Options for Medulloblastoma and CNS Primitive Neuroectodermal Tumor (PNET). *Curr Treat Options Neurol*, 15(5), 593-606. <https://doi.org/10.1007/s11940-013-0255-4>
- Delitto, D., Vertes-George, E., Hughes, S. J., Behrns, K. E., & Trevino, J. G. (2014). c-Met signaling in the development of tumorigenesis and chemoresistance: potential applications in pancreatic cancer. *World J Gastroenterol*, 20(26), 8458-8470. <https://doi.org/10.3748/wjg.v20.i26.8458>
- Desole, C., Gallo, S., Vitacolonna, A., Montarolo, F., Bertolotto, A., Vivien, D., Comoglio, P., & Crepaldi, T. (2021). HGF and MET: From Brain Development to Neurological Disorders. *Front Cell Dev Biol*, 9, 683609. <https://doi.org/10.3389/fcell.2021.683609>
- DeSouza, R. M., Jones, B. R., Lowis, S. P., & Kurian, K. M. (2014). Pediatric medulloblastoma - update on molecular classification driving targeted therapies. *Front Oncol*, 4, 176. <https://doi.org/10.3389/fonc.2014.00176>
- Dimitrova, V., & Arcaro, A. (2015). Targeting the PI3K/AKT/mTOR signaling pathway in medulloblastoma. *Curr Mol Med*, 15(1), 82-93. <https://doi.org/10.2174/1566524015666150114115427>
- Ding, X., Ji, J., Jiang, J., Cai, Q., Wang, C., Shi, M., Yu, Y., Zhu, Z., & Zhang, J. (2018). HGF-mediated crosstalk between cancer-associated fibroblasts and MET-unamplified gastric cancer cells activates coordinated tumorigenesis and metastasis. *Cell Death & Disease*, 9(9). <https://doi.org/10.1038/s41419-018-0922-1>
- Drilon, A., Clark, J. W., Weiss, J., Ou, S. I., Camidge, D. R., Solomon, B. J., Otterson, G. A., Villaruz, L. C., Riely, G. J., Heist, R. S., Awad, M. M., Shapiro, G. I., Satouchi, M., Hida, T., Hayashi, H., Murphy, D. A., Wang, S. C., Li, S., Usari, T., . . . Paik, P. K. (2020). Antitumor activity of crizotinib in lung cancers harboring a MET exon 14 alteration. *Nat Med*, 26(1), 47-51. <https://doi.org/10.1038/s41591-019-0716-8>
- Du, Z., & Lovly, C. M. (2018). Mechanisms of receptor tyrosine kinase activation in cancer. *Molecular Cancer*, 17(1). <https://doi.org/10.1186/s12943-018-0782-4>
- Dufour, C., Beaugrand, A., Pizer, B., Micheli, J., Aubelle, M. S., Fourcade, A., Couanet, D., Laplanche, A., Kalifa, C., & Grill, J. (2012). Metastatic Medulloblastoma in Childhood: Chang's Classification Revisited. *Int J Surg Oncol*, 2012, 245385. <https://doi.org/10.1155/2012/245385>
- Eckerdt, F., Clymer, J., Bell, J. B., Beauchamp, E. M., Blyth, G. T., Goldman, S., & Platanius, L. C. (2019). Pharmacological mTOR targeting enhances the antineoplastic effects of selective PI3K $\alpha$  inhibition in medulloblastoma. *Sci Rep*, 9(1), 12822. <https://doi.org/10.1038/s41598-019-49299-3>

- Edmondson, R., Broglie, J. J., Adcock, A. F., & Yang, L. (2014). Three-Dimensional Cell Culture Systems and Their Applications in Drug Discovery and Cell-Based Biosensors. *ASSAY and Drug Development Technologies*, 12(4), 207-218. <https://doi.org/10.1089/adt.2014.573>
- Eid, A. M., & Heabah, N. A. E.-G. (2021). Medulloblastoma: clinicopathological parameters, risk stratification, and survival analysis of immunohistochemically validated molecular subgroups. *Journal of the Egyptian National Cancer Institute*, 33(1). <https://doi.org/10.1186/s43046-021-00060-w>
- Ellison, D. W. (2010). Childhood medulloblastoma: novel approaches to the classification of a heterogeneous disease. *Acta Neuropathol*, 120(3), 305-316. <https://doi.org/10.1007/s00401-010-0726-6>
- Ellison, D. W., Dalton, J., Kocak, M., Nicholson, S. L., Fraga, C., Neale, G., Kenney, A. M., Brat, D. J., Perry, A., Yong, W. H., Taylor, R. E., Bailey, S., Clifford, S. C., & Gilbertson, R. J. (2011). Medulloblastoma: clinicopathological correlates of SHH, WNT, and non-SHH/WNT molecular subgroups. *Acta Neuropathologica*, 121(3), 381-396. <https://doi.org/10.1007/s00401-011-0800-8>
- Endersby, R., Whitehouse, J., Pribnow, A., Kuchibhotla, M., Hii, H., Carline, B., Gande, S., Stripay, J., Ancliffe, M., Howlett, M., Schoep, T., George, C., Andradas, C., Dyer, P., Schluck, M., Patterson, B., Tacheva-Gigorova, S. K., Cooper, M. N., Robinson, G., . . . Gottardo, N. G. (2021). Small-molecule screen reveals synergy of cell cycle checkpoint kinase inhibitors with DNA-damaging chemotherapies in medulloblastoma. *Sci Transl Med*, 13(577). <https://doi.org/10.1126/scitranslmed.aba7401>
- Engelman, J. A., Zejnullahu, K., Mitsudomi, T., Song, Y., Hyland, C., Park, J. O., Lindeman, N., Gale, C. M., Zhao, X., Christensen, J., Kosaka, T., Holmes, A. J., Rogers, A. M., Cappuzzo, F., Mok, T., Lee, C., Johnson, B. E., Cantley, L. C., & Janne, P. A. (2007). MET amplification leads to gefitinib resistance in lung cancer by activating ERBB3 signaling. *Science*, 316(5827), 1039-1043. <https://doi.org/10.1126/science.1141478>
- Fabbro, D., Cowan-Jacob, S. W., & Moebitz, H. (2015). Ten things you should know about protein kinases: IUPHAR Review 14. *Br J Pharmacol*, 172(11), 2675-2700. <https://doi.org/10.1111/bph.13096>
- Faria, C. C., Golbourn, B. J., Dubuc, A. M., Remke, M., Diaz, R. J., Agnihotri, S., Luck, A., Sabha, N., Olsen, S., Wu, X., Garzia, L., Ramaswamy, V., Mack, S. C., Wang, X., Leadley, M., Reynaud, D., Ermini, L., Post, M., Northcott, P. A., . . . Rutka, J. T. (2015). Foretinib is effective therapy for metastatic sonic hedgehog medulloblastoma. *Cancer Res*, 75(1), 134-146. <https://doi.org/10.1158/0008-5472.CAN-13-3629>
- Ferlay, J., Colombet, M., Soerjomataram, I., Parkin, D. M., Pineros, M., Znaor, A., & Bray, F. (2021). Cancer statistics for the year 2020: An overview. *Int J Cancer*. <https://doi.org/10.1002/ijc.33588>
- Frasson, C., Rampazzo, E., Accordi, B., Beggio, G., Pistollato, F., Basso, G., & Persano, L. (2015). Inhibition of PI3K Signalling Selectively Affects Medulloblastoma Cancer Stem Cells. *BioMed Research International*, 2015, 1-11. <https://doi.org/10.1155/2015/973912>
- Gajjar, A., Chintagumpala, M., Ashley, D., Kellie, S., Kun, L. E., Merchant, T. E., Woo, S., Wheeler, G., Ahern, V., Krasin, M. J., Fouladi, M., Broniscer, A., Krance, R., Hale, G. A.,

- Stewart, C. F., Dauser, R., Sanford, R. A., Fuller, C., Lau, C., . . . Gilbertson, R. J. (2006). Risk-adapted craniospinal radiotherapy followed by high-dose chemotherapy and stem-cell rescue in children with newly diagnosed medulloblastoma (St Jude Medulloblastoma-96): long-term results from a prospective, multicentre trial. *Lancet Oncol*, 7(10), 813-820. [https://doi.org/10.1016/S1470-2045\(06\)70867-1](https://doi.org/10.1016/S1470-2045(06)70867-1)
- Gak, E., Taylor, W. G., Chan, A. M., & Rubin, J. S. (1992). Processing of hepatocyte growth factor to the heterodimeric form is required for biological activity. *FEBS Lett*, 311(1), 17-21. [https://doi.org/10.1016/0014-5793\(92\)81356-q](https://doi.org/10.1016/0014-5793(92)81356-q)
- Garcia-Lopez, J., Kumar, R., Smith, K. S., & Northcott, P. A. (2021). Deconstructing Sonic Hedgehog Medulloblastoma: Molecular Subtypes, Drivers, and Beyond. *Trends Genet*, 37(3), 235-250. <https://doi.org/10.1016/j.tig.2020.11.001>
- Ghelli Luserna Di Rorà, A., Martinelli, G., & Simonetti, G. (2019). The balance between mitotic death and mitotic slippage in acute leukemia: a new therapeutic window? *Journal of Hematology & Oncology*, 12(1). <https://doi.org/10.1186/s13045-019-0808-4>
- Gherardi, E., Birchmeier, W., Birchmeier, C., & Vande Woude, G. (2012). Targeting MET in cancer: rationale and progress. *Nat Rev Cancer*, 12(2), 89-103. <https://doi.org/10.1038/nrc3205>
- Giangaspero, F., Wellek, S., Masuoka, J., Gessi, M., Kleihues, P., & Ohgaki, H. (2006). Stratification of medulloblastoma on the basis of histopathological grading. *Acta Neuropathologica*, 112(1), 5-12. <https://doi.org/10.1007/s00401-006-0064-x>
- Gibson, P., Tong, Y., Robinson, G., Thompson, M. C., Currie, D. S., Eden, C., Kranenburg, T. A., Hogg, T., Poppleton, H., Martin, J., Finkelstein, D., Pounds, S., Weiss, A., Patay, Z., Scoggins, M., Ogg, R., Pei, Y., Yang, Z. J., Brun, S., . . . Gilbertson, R. J. (2010). Subtypes of medulloblastoma have distinct developmental origins. *Nature*, 468(7327), 1095-1099. <https://doi.org/10.1038/nature09587>
- Gilbertson, R. J., & Ellison, D. W. (2008). The origins of medulloblastoma subtypes. *Annu Rev Pathol*, 3, 341-365. <https://doi.org/10.1146/annurev.pathmechdis.3.121806.151518>
- Gortany, N. K., Panahi, G., Ghafari, H., Shekari, M., & Ghazi-Khansari, M. (2021). Foretinib induces G2/M cell cycle arrest, apoptosis, and invasion in human glioblastoma cells through c-MET inhibition. *Cancer Chemother Pharmacol*, 87(6), 827-842. <https://doi.org/10.1007/s00280-021-04242-0>
- Greenman, C., Stephens, P., Smith, R., Dalgliesh, G. L., Hunter, C., Bignell, G., Davies, H., Teague, J., Butler, A., Stevens, C., Edkins, S., O'Meara, S., Vastrik, I., Schmidt, E. E., Avis, T., Barthorpe, S., Bhamra, G., Buck, G., Choudhury, B., . . . Stratton, M. R. (2007). Patterns of somatic mutation in human cancer genomes. *Nature*, 446(7132), 153-158. <https://doi.org/10.1038/nature05610>
- Guessous, F., Zhang, Y., diPierro, C., Marcinkiewicz, L., Sarkaria, J., Schiff, D., Buchanan, S., & Abounader, R. (2010). An orally bioavailable c-Met kinase inhibitor potently inhibits brain tumor malignancy and growth. *Anticancer Agents Med Chem*, 10(1), 28-35. <https://doi.org/10.2174/1871520611009010028>
- Gurney, J. G., Kadan-Lottick, N. S., Packer, R. J., Neglia, J. P., Sklar, C. A., Punyko, J. A., Stovall, M., Yasui, Y., Nicholson, H. S., Wolden, S., McNeil, D. E., Mertens, A. C., & Robison, L.

- L. (2003). Endocrine and cardiovascular late effects among adult survivors of childhood brain tumors. *Cancer*, 97(3), 663-673. <https://doi.org/10.1002/cncr.11095>
- Hanahan, D. (2022). Hallmarks of Cancer: New Dimensions. *Cancer Discovery*, 12(1), 31-46. <https://doi.org/10.1158/2159-8290.cd-21-1059>
- Hanahan, D., & Weinberg, R. A. (2000). The hallmarks of cancer. *Cell*, 100(1), 57-70. [https://doi.org/10.1016/s0092-8674\(00\)81683-9](https://doi.org/10.1016/s0092-8674(00)81683-9)
- Hanahan, D., & Weinberg, R. A. (2011). Hallmarks of cancer: the next generation. *Cell*, 144(5), 646-674. <https://doi.org/10.1016/j.cell.2011.02.013>
- Hassanpour, S. H., & Dehghani, M. (2017). Review of cancer from perspective of molecular. *Journal of Cancer Research and Practice*, 4(4), 127-129. <https://doi.org/10.1016/j.icrpr.2017.07.001>
- Hossain, M. A., Russell, J. C., Gomes, R., & Lattera, J. (2002). Neuroprotection by scatter factor/hepatocyte growth factor and FGF-1 in cerebellar granule neurons is phosphatidylinositol 3-kinase/Akt-dependent and MAPK/CREB-independent. *Journal of Neurochemistry*, 81(2), 365-378. <https://doi.org/10.1046/j.1471-4159.2002.00837.x>
- Hovestadt, V., Ayrault, O., Swartling, F. J., Robinson, G. W., Pfister, S. M., & Northcott, P. A. (2020). Medulloblastomics revisited: biological and clinical insights from thousands of patients. *Nat Rev Cancer*, 20(1), 42-56. <https://doi.org/10.1038/s41568-019-0223-8>
- Huang, D., Roy, I. J., Murray, G. F., Reed, J., Zangle, T. A., & Teitell, M. A. (2019). Identifying fates of cancer cells exposed to mitotic inhibitors by quantitative phase imaging. *Analyst*, 145(1), 97-106. <https://doi.org/10.1039/c9an01346f>
- Huang, G. H., Xu, Q. F., Cui, Y. H., Li, N., Bian, X. W., & Lv, S. Q. (2016). Medulloblastoma stem cells: Promising targets in medulloblastoma therapy. *Cancer Sci*, 107(5), 583-589. <https://doi.org/10.1111/cas.12925>
- Hughes, J., Rees, S., Kalindjian, S., & Philpott, K. (2011). Principles of early drug discovery. *British Journal of Pharmacology*, 162(6), 1239-1249. <https://doi.org/10.1111/j.1476-5381.2010.01127.x>
- Hughes, V. S., & Siemann, D. W. (2018). Have Clinical Trials Properly Assessed c-Met Inhibitors? *Trends in Cancer*, 4(2), 94-97. <https://doi.org/10.1016/j.trecan.2017.11.009>
- Hughes, V. S., & Siemann, D. W. (2019). Failures in preclinical and clinical trials of c-Met inhibitors: evaluation of pathway activity as a promising selection criterion. *Oncotarget*, 10(2), 184-197. <https://doi.org/10.18632/oncotarget.26546>
- Ieraci, A., Forni, P. E., & Ponzetto, C. (2002). Viable hypomorphic signaling mutant of the Met receptor reveals a role for hepatocyte growth factor in postnatal cerebellar development. *Proc Natl Acad Sci U S A*, 99(23), 15200-15205. <https://doi.org/10.1073/pnas.222362099>
- Ivanov, D. P., Coyle, B., Walker, D. A., & Grabowska, A. M. (2016). In vitro models of medulloblastoma: Choosing the right tool for the job. *J Biotechnol*, 236, 10-25. <https://doi.org/10.1016/j.jbiotec.2016.07.028>

- Jensen, M. M., Jorgensen, J. T., Binderup, T., & Kjaer, A. (2008). Tumor volume in subcutaneous mouse xenografts measured by microCT is more accurate and reproducible than determined by 18F-FDG-microPET or external caliper. *BMC Med Imaging*, 8, 16. <https://doi.org/10.1186/1471-2342-8-16>
- Jiao, Q., Bi, L., Ren, Y., Song, S., Wang, Q., & Wang, Y. S. (2018). Advances in studies of tyrosine kinase inhibitors and their acquired resistance. *Mol Cancer*, 17(1), 36. <https://doi.org/10.1186/s12943-018-0801-5>
- Jordan, M. A. (2002). Mechanism of action of antitumor drugs that interact with microtubules and tubulin. *Curr Med Chem Anticancer Agents*, 2(1), 1-17. <https://doi.org/10.2174/1568011023354290>
- Juraschka, K., & Taylor, M. D. (2019). Medulloblastoma in the age of molecular subgroups: a review. *Journal of Neurosurgery: Pediatrics*, 24(4), 353-363. <https://doi.org/10.3171/2019.5.peds18381>
- Kabir, T. F., Kunos, C. A., Villano, J. L., & Chauhan, A. (2020). Immunotherapy for Medulloblastoma: Current Perspectives. *Immunotargets Ther*, 9, 57-77. <https://doi.org/10.2147/ITT.S198162>
- Kanda, T., Sullivan, K. F., & Wahl, G. M. (1998). Histone–GFP fusion protein enables sensitive analysis of chromosome dynamics in living mammalian cells. *Current Biology*, 8(7), 377-385. [https://doi.org/10.1016/s0960-9822\(98\)70156-3](https://doi.org/10.1016/s0960-9822(98)70156-3)
- Katayama, R., Aoyama, A., Yamori, T., Qi, J., Oh-hara, T., Song, Y., Engelman, J. A., & Fujita, N. (2013). Cytotoxic activity of tivantinib (ARQ 197) is not due solely to c-MET inhibition. *Cancer Res*, 73(10), 3087-3096. <https://doi.org/10.1158/0008-5472.CAN-12-3256>
- Kawauchi, D., Robinson, G., Uziel, T., Gibson, P., Rehg, J., Gao, C., Finkelstein, D., Qu, C., Pounds, S., David, Richard, & Martine. (2012). A Mouse Model of the Most Aggressive Subgroup of Human Medulloblastoma. *Cancer Cell*, 21(2), 168-180. <https://doi.org/10.1016/j.ccr.2011.12.023>
- Kim, H., Kang, H. J., Lee, J. W., Park, J. D., Park, K. D., Shin, H. Y., & Ahn, H. S. (2013). Irinotecan, vincristine, cisplatin, cyclophosphamide, and etoposide for refractory or relapsed medulloblastoma/PNET in pediatric patients. *Child's Nervous System*, 29(10), 1851-1858. <https://doi.org/10.1007/s00381-013-2163-z>
- Kongkham, P. N., Onvani, S., Smith, C. A., & Rutka, J. T. (2010). Inhibition of the MET Receptor Tyrosine Kinase as a Novel Therapeutic Strategy in Medulloblastoma. *Transl Oncol*, 3(6), 336-343. <https://doi.org/10.1593/tlo.10121>
- Kool, M., Korshunov, A., Remke, M., Jones, D. T. W., Schlanstein, M., Northcott, P. A., Cho, Y.-J., Koster, J., Schouten-Van Meeteren, A., Van Vuurden, D., Clifford, S. C., Pietsch, T., Von Bueren, A. O., Rutkowski, S., McCabe, M., Collins, V. P., Bäcklund, M. L., Haberler, C., Bourdeaut, F., . . . Pfister, S. M. (2012). Molecular subgroups of medulloblastoma: an international meta-analysis of transcriptome, genetic aberrations, and clinical data of WNT, SHH, Group 3, and Group 4 medulloblastomas. *Acta Neuropathologica*, 123(4), 473-484. <https://doi.org/10.1007/s00401-012-0958-8>
- Kops, G. J., Weaver, B. A., & Cleveland, D. W. (2005). On the road to cancer: aneuploidy and the mitotic checkpoint. *Nat Rev Cancer*, 5(10), 773-785. <https://doi.org/10.1038/nrc1714>

- Kumar, R., Liu, A. P. Y., & Northcott, P. A. (2020). Medulloblastoma genomics in the modern molecular era. *Brain Pathol*, 30(3), 679-690. <https://doi.org/10.1111/bpa.12804>
- Labbe, D., Provencal, M., Lamy, S., Boivin, D., Gingras, D., & Beliveau, R. (2009). The flavonols quercetin, kaempferol, and myricetin inhibit hepatocyte growth factor-induced medulloblastoma cell migration. *J Nutr*, 139(4), 646-652. <https://doi.org/10.3945/jn.108.102616>
- Lee, J. J. X., Chan, J. J., & Choo, S. P. (2015). Clinical Development of c-MET Inhibition in Hepatocellular Carcinoma. *Diseases*, 3(4), 306-324. <https://doi.org/10.3390/diseases3040306>
- Li, E., Hu, Z., Sun, Y., Zhou, Q., Yang, B., Zhang, Z., & Cao, W. (2016). Small molecule inhibitor of c-Met (PHA665752) suppresses the growth of ovarian cancer cells and reverses cisplatin resistance. *Tumour Biol*, 37(6), 7843-7852. <https://doi.org/10.1007/s13277-015-4318-x>
- Li, Y., Guessous, F., Johnson, E. B., Eberhart, C. G., Li, X. N., Shu, Q., Fan, S., Lal, B., Lattera, J., Schiff, D., & Abounader, R. (2008). Functional and molecular interactions between the HGF/c-Met pathway and c-Myc in large-cell medulloblastoma. *Lab Invest*, 88(2), 98-111. <https://doi.org/10.1038/labinvest.3700702>
- Li, Y., Lal, B., Kwon, S., Fan, X., Saldanha, U., Reznik, T. E., Kuchner, E. B., Eberhart, C., Lattera, J., & Abounader, R. (2005). The scatter factor/hepatocyte growth factor: c-met pathway in human embryonal central nervous system tumor malignancy. *Cancer Res*, 65(20), 9355-9362. <https://doi.org/10.1158/0008-5472.CAN-05-1946>
- Li, Y., Lal, B., Kwon, S., Fan, X., Saldanha, U., Reznik, T. E., Kuchner, E. B., Eberhart, C., Lattera, J., & Abounader, R. (2005). The Scatter Factor/Hepatocyte Growth Factor: c-Met Pathway in Human Embryonal Central Nervous System Tumor Malignancy. *Cancer Research*, 65(20), 9355-9362. <https://doi.org/10.1158/0008-5472.can-05-1946>
- Lin, C. Y., Erkek, S., Tong, Y., Yin, L., Federation, A. J., Zapatka, M., Haldipur, P., Kawauchi, D., Risch, T., Warnatz, H.-J., Worst, B. C., Ju, B., Orr, B. A., Zeid, R., Polaski, D. R., Segura-Wang, M., Waszak, S. M., Jones, D. T. W., Kool, M., . . . Northcott, P. A. (2016). Active medulloblastoma enhancers reveal subgroup-specific cellular origins. *Nature*, 530(7588), 57-62. <https://doi.org/10.1038/nature16546>
- Liu, K. W., Pajtler, K. W., Worst, B. C., Pfister, S. M., & Wechsler-Reya, R. J. (2017). Molecular mechanisms and therapeutic targets in pediatric brain tumors. *Sci Signal*, 10(470). <https://doi.org/10.1126/scisignal.aaf7593>
- Lokker, N. A., Mark, M. R., Luis, E. A., Bennett, G. L., Robbins, K. A., Baker, J. B., & Godowski, P. J. (1992). Structure-function analysis of hepatocyte growth factor: identification of variants that lack mitogenic activity yet retain high affinity receptor binding. *EMBO J*, 11(7), 2503-2510. <https://www.ncbi.nlm.nih.gov/pubmed/1321034>
- Longati, P., Bardelli, A., Ponzetto, C., Naldini, L., & Comoglio, P. M. (1994). Tyrosines1234-1235 are critical for activation of the tyrosine kinase encoded by the MET proto-oncogene (HGF receptor). *Oncogene*, 9(1), 49-57. <https://www.ncbi.nlm.nih.gov/pubmed/8302603>
- LoRusso, P. M., Rudin, C. M., Reddy, J. C., Tibes, R., Weiss, G. J., Borad, M. J., Hann, C. L., Brahmer, J. R., Chang, I., Darbonne, W. C., Graham, R. A., Zerivitz, K. L., Low, J. A., &

- Von Hoff, D. D. (2011). Phase I trial of hedgehog pathway inhibitor vismodegib (GDC-0449) in patients with refractory, locally advanced or metastatic solid tumors. *Clin Cancer Res*, 17(8), 2502-2511. <https://doi.org/10.1158/1078-0432.CCR-10-2745>
- Louis, D. N., Perry, A., Reifenberger, G., von Deimling, A., Figarella-Branger, D., Cavenee, W. K., Ohgaki, H., Wiestler, O. D., Kleihues, P., & Ellison, D. W. (2016). The 2016 World Health Organization Classification of Tumors of the Central Nervous System: a summary. *Acta Neuropathol*, 131(6), 803-820. <https://doi.org/10.1007/s00401-016-1545-1>
- Louis, D. N., Perry, A., Wesseling, P., Brat, D. J., Cree, I. A., Figarella-Branger, D., Hawkins, C., Ng, H. K., Pfister, S. M., Reifenberger, G., Soffiotti, R., von Deimling, A., & Ellison, D. W. (2021). The 2021 WHO Classification of Tumors of the Central Nervous System: a summary. *Neuro Oncol*, 23(8), 1231-1251. <https://doi.org/10.1093/neuonc/noab106>
- Lu, S., Torok, H. P., Gallmeier, E., Kolligs, F. T., Rizzani, A., Arena, S., Goke, B., Gerbes, A. L., & De Toni, E. N. (2015). Tivantinib (ARQ 197) affects the apoptotic and proliferative machinery downstream of c-MET: role of Mcl-1, Bcl-xl and Cyclin B1. *Oncotarget*, 6(26), 22167-22178. <https://doi.org/10.18632/oncotarget.4240>
- Luzzi, S., Giotta Lucifero, A., Brambilla, I., Semeria Mantelli, S., Mosconi, M., Foadelli, T., & Savasta, S. (2020). Targeting the medulloblastoma: a molecular-based approach. *Acta Biomed*, 91(7-S), 79-100. <https://doi.org/10.23750/abm.v91i7-S.9958>
- Maina, F., Hilton, M. C., Andres, R., Wyatt, S., Klein, R., & Davies, A. M. (1998). Multiple Roles for Hepatocyte Growth Factor in Sympathetic Neuron Development. *Neuron*, 20(5), 835-846. [https://doi.org/10.1016/s0896-6273\(00\)80466-3](https://doi.org/10.1016/s0896-6273(00)80466-3)
- Martincorena, I., & Campbell, P. J. (2015). Somatic mutation in cancer and normal cells. *Science*, 349(6255), 1483-1489. <https://doi.org/10.1126/science.aab4082>
- Masuda, A., Maeno, K., Nakagawa, T., Saito, H., & Takahashi, T. (2003). Association between Mitotic Spindle Checkpoint Impairment and Susceptibility to the Induction of Apoptosis by Anti-Microtubule Agents in Human Lung Cancers. *The American Journal of Pathology*, 163(3), 1109-1116. [https://doi.org/10.1016/s0002-9440\(10\)63470-0](https://doi.org/10.1016/s0002-9440(10)63470-0)
- Maulik, G., Shrikhande, A., Kijima, T., Ma, P. C., Morrison, P. T., & Salgia, R. (2002). Role of the hepatocyte growth factor receptor, c-Met, in oncogenesis and potential for therapeutic inhibition. *Cytokine Growth Factor Rev*, 13(1), 41-59. [https://doi.org/10.1016/s1359-6101\(01\)00029-6](https://doi.org/10.1016/s1359-6101(01)00029-6)
- McKinney, N., Yuan, L., Zhang, H., Liu, J., Cho, Y. J., Rushing, E., Schniederjan, M., & MacDonald, T. J. (2015). EphrinB1 expression is dysregulated and promotes oncogenic signaling in medulloblastoma. *J Neurooncol*, 121(1), 109-118. <https://doi.org/10.1007/s11060-014-1618-8>
- Mechanism matters. (2010). *Nature Medicine*, 16(4), 347-347. <https://doi.org/10.1038/nm0410-347>
- Megiorni, F., McDowell, H. P., Camero, S., Mannarino, O., Ceccarelli, S., Paiano, M., Losty, P. D., Pizer, B., Shukla, R., Pizzuti, A., Clerico, A., & Dominici, C. (2015). Crizotinib-induced antitumour activity in human alveolar rhabdomyosarcoma cells is not solely dependent on ALK and MET inhibition. *J Exp Clin Cancer Res*, 34, 112. <https://doi.org/10.1186/s13046-015-0228-4>

- Menyhárt, O., & Győrffy, B. (2020). Molecular stratifications, biomarker candidates and new therapeutic options in current medulloblastoma treatment approaches. *Cancer and Metastasis Reviews*, 39(1), 211-233. <https://doi.org/10.1007/s10555-020-09854-1>
- Metibemu, D. S., Akinloye, O. A., Akamo, A. J., Ojo, D. A., Okeowo, O. T., & Omotuyi, I. O. (2019). Exploring receptor tyrosine kinases-inhibitors in Cancer treatments. *Egyptian Journal of Medical Human Genetics*, 20(1). <https://doi.org/10.1186/s43042-019-0035-0>
- Michieli, P., & Di Nicolantonio, F. (2013). Targeted therapies: Tivantinib--a cytotoxic drug in MET inhibitor's clothes? *Nat Rev Clin Oncol*, 10(7), 372-374. <https://doi.org/10.1038/nrclinonc.2013.86>
- Millard, N. E., & De Braganca, K. C. (2016). Medulloblastoma. *J Child Neurol*, 31(12), 1341-1353. <https://doi.org/10.1177/0883073815600866>
- Miyazawa, K., Shimomura, T., Kitamura, A., Kondo, J., Morimoto, Y., & Kitamura, N. (1993). Molecular cloning and sequence analysis of the cDNA for a human serine protease responsible for activation of hepatocyte growth factor. Structural similarity of the protease precursor to blood coagulation factor XII. *J Biol Chem*, 268(14), 10024-10028. <https://www.ncbi.nlm.nih.gov/pubmed/7683665>
- Munshi, N., Jeay, S., Li, Y., Chen, C. R., France, D. S., Ashwell, M. A., Hill, J., Moussa, M. M., Leggett, D. S., & Li, C. J. (2010). ARQ 197, a novel and selective inhibitor of the human c-Met receptor tyrosine kinase with antitumor activity. *Mol Cancer Ther*, 9(6), 1544-1553. <https://doi.org/10.1158/1535-7163.MCT-09-1173>
- Nakamura, T., Matsumoto, K., Kiritoshi, A., Tano, Y., & Nakamura, T. (1997). Induction of hepatocyte growth factor in fibroblasts by tumor-derived factors affects invasive growth of tumor cells: in vitro analysis of tumor-stromal interactions. *Cancer Res*, 57(15), 3305-3313. <https://www.ncbi.nlm.nih.gov/pubmed/9242465>
- Naldini, L., Vigna, E., Narsimhan, R. P., Gaudino, G., Zarnegar, R., Michalopoulos, G. K., & Comoglio, P. M. (1991). Hepatocyte growth factor (HGF) stimulates the tyrosine kinase activity of the receptor encoded by the proto-oncogene c-MET. *Oncogene*, 6(4), 501-504. <https://www.ncbi.nlm.nih.gov/pubmed/1827664>
- Ng, J. M., & Curran, T. (2011). The Hedgehog's tale: developing strategies for targeting cancer. *Nat Rev Cancer*, 11(7), 493-501. <https://doi.org/10.1038/nrc3079>
- Northcott, P. A., Buchhalter, I., Morrissy, A. S., Hovestadt, V., Weischenfeldt, J., Ehrenberger, T., Grobner, S., Segura-Wang, M., Zichner, T., Rudneva, V. A., Warnatz, H. J., Sidiropoulos, N., Phillips, A. H., Schumacher, S., Kleinheinz, K., Waszak, S. M., Erkek, S., Jones, D. T. W., Worst, B. C., . . . Lichter, P. (2017). The whole-genome landscape of medulloblastoma subtypes. *Nature*, 547(7663), 311-317. <https://doi.org/10.1038/nature22973>
- Northcott, P. A., Robinson, G. W., Kratz, C. P., Mabbott, D. J., Pomeroy, S. L., Clifford, S. C., Rutkowski, S., Ellison, D. W., Malkin, D., Taylor, M. D., Gajjar, A., & Pfister, S. M. (2019). Medulloblastoma. *Nat Rev Dis Primers*, 5(1), 11. <https://doi.org/10.1038/s41572-019-0063-6>
- Northcott, P. A., Shih, D. J. H., Peacock, J., Garzia, L., Sorana Morrissy, A., Zichner, T., Stütz, A. M., Korshunov, A., Reimand, J., Schumacher, S. E., Beroukhi, R., Ellison, D. W.,

- Marshall, C. R., Lionel, A. C., Mack, S., Dubuc, A., Yao, Y., Ramaswamy, V., Luu, B., . . . Taylor, M. D. (2012). Subgroup-specific structural variation across 1,000 medulloblastoma genomes. *Nature*, 488(7409), 49-56. <https://doi.org/10.1038/nature11327>
- Onvani, S., Terakawa, Y., Smith, C., Northcott, P., Taylor, M., & Rutka, J. (2012). Molecular genetic analysis of the hepatocyte growth factor/MET signaling pathway in pediatric medulloblastoma. *Genes Chromosomes Cancer*, 51(7), 675-688. <https://doi.org/10.1002/gcc.21954>
- Othman, R. T., Kimishi, I., Bradshaw, T. D., Storer, L. C., Korshunov, A., Pfister, S. M., Grundy, R. G., Kerr, I. D., & Coyle, B. (2014). Overcoming multiple drug resistance mechanisms in medulloblastoma. *Acta Neuropathol Commun*, 2, 57. <https://doi.org/10.1186/2051-5960-2-57>
- Owusu, B., Galembo, R., Janetka, J., & Klampfer, L. (2017). Hepatocyte Growth Factor, a Key Tumor-Promoting Factor in the Tumor Microenvironment. *Cancers*, 9(12), 35. <https://doi.org/10.3390/cancers9040035>
- Packer, R. J., Gajjar, A., Vezina, G., Rorke-Adams, L., Burger, P. C., Robertson, P. L., Bayer, L., LaFond, D., Donahue, B. R., Marymont, M. H., Muraszko, K., Langston, J., & Spoto, R. (2006). Phase III study of craniospinal radiation therapy followed by adjuvant chemotherapy for newly diagnosed average-risk medulloblastoma. *J Clin Oncol*, 24(25), 4202-4208. <https://doi.org/10.1200/JCO.2006.06.4980>
- Packer, R. J., & Vezina, G. (2008). Management of and Prognosis With Medulloblastoma. *Archives of Neurology*, 65(11), 1419. <https://doi.org/10.1001/archneur.65.11.1419>
- Packer, R. J., Zhou, T., Holmes, E., Vezina, G., & Gajjar, A. (2013). Survival and secondary tumors in children with medulloblastoma receiving radiotherapy and adjuvant chemotherapy: results of Children's Oncology Group trial A9961. *Neuro Oncol*, 15(1), 97-103. <https://doi.org/10.1093/neuonc/nos267>
- Park, M., Dean, M., Cooper, C. S., Schmidt, M., O'Brien, S. J., Blair, D. G., & Vande Woude, G. F. (1986). Mechanism of met oncogene activation. *Cell*, 45(6), 895-904. [https://doi.org/10.1016/0092-8674\(86\)90564-7](https://doi.org/10.1016/0092-8674(86)90564-7)
- Park, M., Dean, M., Kaul, K., Braun, M. J., Gonda, M. A., & Vande Woude, G. (1987). Sequence of MET protooncogene cDNA has features characteristic of the tyrosine kinase family of growth-factor receptors. *Proceedings of the National Academy of Sciences*, 84(18), 6379-6383. <https://doi.org/10.1073/pnas.84.18.6379>
- Pei, Y., Colin, Wang, J., Alok, Eroshkin, A., Cho, Y.-J., Witt, H., Korshunov, A., Read, T.-A., Julia, Earlene, C, Anne, Roger, Thomas, Paul, Michael, Stefan, Phillip, & Robert. (2012). An Animal Model of MYC-Driven Medulloblastoma. *Cancer Cell*, 21(2), 155-167. <https://doi.org/10.1016/j.ccr.2011.12.021>
- Perreault, S., Ramaswamy, V., Achrol, A. S., Chao, K., Liu, T. T., Shih, D., Remke, M., Schubert, S., Bouffet, E., Fisher, P. G., Partap, S., Vogel, H., Taylor, M. D., Cho, Y. J., & Yeom, K. W. (2014). MRI Surrogates for Molecular Subgroups of Medulloblastoma. *American Journal of Neuroradiology*, 35(7), 1263-1269. <https://doi.org/10.3174/ajnr.a3990>
- Phoenix, T. N., Patmore, D. M., Boop, S., Boulos, N., Jacus, M. O., Patel, Y. T., Roussel, M. F., Finkelstein, D., Goumnerova, L., Perreault, S., Wadhwa, E., Cho, Y. J., Stewart, C. F., &

- Gilbertson, R. J. (2016). Medulloblastoma Genotype Dictates Blood Brain Barrier Phenotype. *Cancer Cell*, 29(4), 508-522. <https://doi.org/10.1016/j.ccell.2016.03.002>
- Pievsky, D., & Pysopoulos, N. (2016). Profile of tivantinib and its potential in the treatment of hepatocellular carcinoma: the evidence to date. *J Hepatocell Carcinoma*, 3, 69-76. <https://doi.org/10.2147/JHC.S106072>
- Piguet, A. C., Medova, M., Keogh, A., Gluck, A. A., Aebersold, D. M., Dufour, J. F., & Zimmer, Y. (2015). Impact of MET targeting on tumor-associated angiogenesis and growth of MET mutations-driven models of liver cancer. *Genes Cancer*, 6(7-8), 317-327. <https://doi.org/10.18632/genesandcancer.74>
- Ponzetto, C., Bardelli, A., Zhen, Z., Maina, F., dalla Zonca, P., Giordano, S., Graziani, A., Panayotou, G., & Comoglio, P. M. (1994). A multifunctional docking site mediates signaling and transformation by the hepatocyte growth factor/scatter factor receptor family. *Cell*, 77(2), 261-271. [https://doi.org/10.1016/0092-8674\(94\)90318-2](https://doi.org/10.1016/0092-8674(94)90318-2)
- Porta, C., Paglino, C., & Mosca, A. (2014). Targeting PI3K/Akt/mTOR Signaling in Cancer. *Front Oncol*, 4, 64. <https://doi.org/10.3389/fonc.2014.00064>
- Provencal, M., Berger-Thibault, N., Labbe, D., Veitch, R., Boivin, D., Rivard, G. E., Gingras, D., & Beliveau, R. (2010). Tissue factor mediates the HGF/Met-induced anti-apoptotic pathway in DAOY medulloblastoma cells. *J Neurooncol*, 97(3), 365-372. <https://doi.org/10.1007/s11060-009-0041-z>
- Puccini, A., Marin-Ramos, N. I., Bergamo, F., Schirripa, M., Lonardi, S., Lenz, H. J., Loupakis, F., & Battaglin, F. (2019). Safety and Tolerability of c-MET Inhibitors in Cancer. *Drug Saf*, 42(2), 211-233. <https://doi.org/10.1007/s40264-018-0780-x>
- Purzner, T., Purzner, J., Buckstaff, T., Cozza, G., Gholamin, S., Rusert, J. M., Hartl, T. A., Sanders, J., Conley, N., Ge, X., Langan, M., Ramaswamy, V., Ellis, L., Litzemberger, U., Bolin, S., Theruvath, J., Nitta, R., Qi, L., Li, X. N., . . . Scott, M. P. (2018). Developmental phosphoproteomics identifies the kinase CK2 as a driver of Hedgehog signaling and a therapeutic target in medulloblastoma. *Sci Signal*, 11(547). <https://doi.org/10.1126/scisignal.aau5147>
- Qian, F., Engst, S., Yamaguchi, K., Yu, P., Won, K. A., Mock, L., Lou, T., Tan, J., Li, C., Tam, D., Loughheed, J., Yakes, F. M., Bentzien, F., Xu, W., Zaks, T., Wooster, R., Greshock, J., & Joly, A. H. (2009). Inhibition of tumor cell growth, invasion, and metastasis by EXEL-2880 (XL880, GSK1363089), a novel inhibitor of HGF and VEGF receptor tyrosine kinases. *Cancer Res*, 69(20), 8009-8016. <https://doi.org/10.1158/0008-5472.CAN-08-4889>
- Ramaswamy, V., Northcott, P. A., & Taylor, M. D. (2011). FISH and chips: the recipe for improved prognostication and outcomes for children with medulloblastoma. *Cancer Genet*, 204(11), 577-588. <https://doi.org/10.1016/j.cancergen.2011.11.001>
- Ramaswamy, V., Remke, M., Bouffet, E., Bailey, S., Clifford, S. C., Doz, F., Kool, M., Dufour, C., Vassal, G., Milde, T., Witt, O., von Hoff, K., Pietsch, T., Northcott, P. A., Gajjar, A., Robinson, G. W., Padovani, L., Andre, N., Massimino, M., . . . Pomeroy, S. L. (2016). Risk stratification of childhood medulloblastoma in the molecular era: the current consensus. *Acta Neuropathol*, 131(6), 821-831. <https://doi.org/10.1007/s00401-016-1569-6>

- Ransohoff, K. J., Sarin, K. Y., & Tang, J. Y. (2015). Smoothened Inhibitors in Sonic Hedgehog Subgroup Medulloblastoma. *J Clin Oncol*, 33(24), 2692-2694. <https://doi.org/10.1200/JCO.2015.62.2225>
- Rao, G., Pedone, C. A., Coffin, C. M., Holland, E. C., & Fufts, D. W. (2003). c-Myc enhances sonic hedgehog-induced medulloblastoma formation from nestin-expressing neural progenitors in mice. *Neoplasia*, 5(3), 198-204. [https://doi.org/10.1016/S1476-5586\(03\)80052-0](https://doi.org/10.1016/S1476-5586(03)80052-0)
- Rensing Rix, L. L., Kuenzi, B. M., Luo, Y., Remily-Wood, E., Kinose, F., Wright, G., Li, J., Koomen, J. M., Haura, E. B., Lawrence, H. R., & Rix, U. (2014). GSK3 alpha and beta are new functionally relevant targets of tivantinib in lung cancer cells. *ACS Chem Biol*, 9(2), 353-358. <https://doi.org/10.1021/cb400660a>
- Rieder, C. L., & Maiato, H. (2004). Stuck in Division or Passing through. *Developmental Cell*, 7(5), 637-651. <https://doi.org/10.1016/j.devcel.2004.09.002>
- Robertson, P. L., Muraszko, K. M., Holmes, E. J., Sposto, R., Packer, R. J., Gajjar, A., Dias, M. S., Allen, J. C., & Children's Oncology, G. (2006). Incidence and severity of postoperative cerebellar mutism syndrome in children with medulloblastoma: a prospective study by the Children's Oncology Group. *J Neurosurg*, 105(6 Suppl), 444-451. <https://doi.org/10.3171/ped.2006.105.6.444>
- Robinson, D. R., Wu, Y.-M., & Lin, S.-F. (2000). The protein tyrosine kinase family of the human genome. *Oncogene*, 19(49), 5548-5557. <https://doi.org/10.1038/sj.onc.1203957>
- Robinson, G. W., Orr, B. A., Wu, G., Gururangan, S., Lin, T., Qaddoumi, I., Packer, R. J., Goldman, S., Prados, M. D., Desjardins, A., Chintagumpala, M., Takebe, N., Kaste, S. C., Rusch, M., Allen, S. J., Onar-Thomas, A., Stewart, C. F., Fouladi, M., Boyett, J. M., . . . Gajjar, A. (2015). Vismodegib Exerts Targeted Efficacy Against Recurrent Sonic Hedgehog-Subgroup Medulloblastoma: Results From Phase II Pediatric Brain Tumor Consortium Studies PBTC-025B and PBTC-032. *J Clin Oncol*, 33(24), 2646-2654. <https://doi.org/10.1200/JCO.2014.60.1591>
- Rodig, S. J., & Shapiro, G. I. (2010). Crizotinib, a small-molecule dual inhibitor of the c-Met and ALK receptor tyrosine kinases. *Curr Opin Investig Drugs*, 11(12), 1477-1490. <https://www.ncbi.nlm.nih.gov/pubmed/21154129>
- Rong, S., Segal, S., Anver, M., Resau, J. H., & Vande Woude, G. F. (1994). Invasiveness and metastasis of NIH 3T3 cells induced by Met-hepatocyte growth factor/scatter factor autocrine stimulation. *Proc Natl Acad Sci U S A*, 91(11), 4731-4735. <https://doi.org/10.1073/pnas.91.11.4731>
- Santhana Kumar, K., Tripolitsioti, D., Ma, M., Grahlert, J., Egli, K. B., Fiaschetti, G., Shalaby, T., Grotzer, M. A., & Baumgartner, M. (2015). The Ser/Thr kinase MAP4K4 drives c-Met-induced motility and invasiveness in a cell-based model of SHH medulloblastoma. *Springerplus*, 4, 19. <https://doi.org/10.1186/s40064-015-0784-2>
- Santoro, A., Rimassa, L., Borbath, I., Daniele, B., Salvagni, S., Van Laethem, J. L., Van Vlierberghe, H., Trojan, J., Kolligs, F. T., Weiss, A., Miles, S., Gasbarrini, A., Lencioni, M., Cicalese, L., Sherman, M., Gridelli, C., Buggisch, P., Gerken, G., Schmid, R. M., . . . Porta, C. (2013). Tivantinib for second-line treatment of advanced hepatocellular carcinoma:

- a randomised, placebo-controlled phase 2 study. *Lancet Oncol*, 14(1), 55-63. [https://doi.org/10.1016/S1470-2045\(12\)70490-4](https://doi.org/10.1016/S1470-2045(12)70490-4)
- Sattler, M., & Salgia, R. (2009). The MET axis as a therapeutic target. *Update on Cancer Therapeutics*, 3(3), 109-118. <https://doi.org/10.1016/j.uct.2009.01.001>
- Scagliotti, G. V., Novello, S., & von Pawel, J. (2013). The emerging role of MET/HGF inhibitors in oncology. *Cancer Treat Rev*, 39(7), 793-801. <https://doi.org/10.1016/j.ctrv.2013.02.001>
- Schlessinger, J. (2000). Cell Signaling by Receptor Tyrosine Kinases. *Cell*, 103(2), 211-225. [https://doi.org/10.1016/S0092-8674\(00\)00114-8](https://doi.org/10.1016/S0092-8674(00)00114-8)
- Schüller, U., Heine, V. M., Mao, J., Kho, A. T., Dillon, A. K., Han, Y.-G., Huillard, E., Sun, T., Ligon, A. H., Qian, Y., Ma, Q., Alvarez-Buylla, A., McMahon, A. P., Rowitch, D. H., & Ligon, K. L. (2008). Acquisition of Granule Neuron Precursor Identity Is a Critical Determinant of Progenitor Cell Competence to Form Shh-Induced Medulloblastoma. *Cancer Cell*, 14(2), 123-134. <https://doi.org/10.1016/j.ccr.2008.07.005>
- Schwalbe, E. C., Lindsey, J. C., Nakjang, S., Crosier, S., Smith, A. J., Hicks, D., Rafiee, G., Hill, R. M., Iliasova, A., Stone, T., Pizer, B., Michalski, A., Joshi, A., Wharton, S. B., Jacques, T. S., Bailey, S., Williamson, D., & Clifford, S. C. (2017). Novel molecular subgroups for clinical classification and outcome prediction in childhood medulloblastoma: a cohort study. *The Lancet Oncology*, 18(7), 958-971. [https://doi.org/10.1016/S1470-2045\(17\)30243-7](https://doi.org/10.1016/S1470-2045(17)30243-7)
- Sharma, T., Schwalbe, E. C., Williamson, D., Sill, M., Hovestadt, V., Mynarek, M., Rutkowski, S., Robinson, G. W., Gajjar, A., Cavalli, F., Ramaswamy, V., Taylor, M. D., Lindsey, J. C., Hill, R. M., Jager, N., Korshunov, A., Hicks, D., Bailey, S., Kool, M., . . . Clifford, S. C. (2019). Second-generation molecular subgrouping of medulloblastoma: an international meta-analysis of Group 3 and Group 4 subtypes. *Acta Neuropathol*, 138(2), 309-326. <https://doi.org/10.1007/s00401-019-02020-0>
- Shi, J., Zhou, Y., Huang, H.-C., & Mitchison, T. J. (2011). Navitoclax (ABT-263) Accelerates Apoptosis during Drug-Induced Mitotic Arrest by Antagonizing Bcl-xL. *Cancer Research*, 71(13), 4518-4526. <https://doi.org/10.1158/0008-5472.can-10-4336>
- Shi, Y. (2004). Caspase activation, inhibition, and reactivation: a mechanistic view. *Protein Sci*, 13(8), 1979-1987. <https://doi.org/10.1110/ps.04789804>
- Singh, S. K., Clarke, I. D., Terasaki, M., Bonn, V. E., Hawkins, C., Squire, J., & Dirks, P. B. (2003). Identification of a cancer stem cell in human brain tumors. *Cancer Res*, 63(18), 5821-5828. <https://www.ncbi.nlm.nih.gov/pubmed/14522905>
- Sinha, D., Duijf, P. H. G., & Khanna, K. K. (2019). Mitotic slippage: an old tale with a new twist. *Cell Cycle*, 18(1), 7-15. <https://doi.org/10.1080/15384101.2018.1559557>
- Skoda, A. M., Simovic, D., Karin, V., Kardum, V., Vranic, S., & Serman, L. (2018). The role of the Hedgehog signaling pathway in cancer: A comprehensive review. *Bosnian Journal of Basic Medical Sciences*, 18(1), 8-20. <https://doi.org/10.17305/bjbm.2018.2756>
- Sloss, O., Topham, C., Diez, M., & Taylor, S. (2016). Mcl-1 dynamics influence mitotic slippage and death in mitosis. *Oncotarget*, 7(5), 5176-5192. <https://doi.org/10.18632/oncotarget.6894>

- Sonoda, E. (2006). Synchronization of cells. *Subcell Biochem*, 40, 415-418. [https://doi.org/10.1007/978-1-4020-4896-8\\_37](https://doi.org/10.1007/978-1-4020-4896-8_37)
- Steeghs, N., Nortier, J. W., & Gelderblom, H. (2007). Small molecule tyrosine kinase inhibitors in the treatment of solid tumors: an update of recent developments. *Ann Surg Oncol*, 14(2), 942-953. <https://doi.org/10.1245/s10434-006-9227-1>
- Stratton, M. R., Campbell, P. J., & Futreal, P. A. (2009). The cancer genome. *Nature*, 458(7239), 719-724. <https://doi.org/10.1038/nature07943>
- Straussman, R., Morikawa, T., Shee, K., Barzily-Rokni, M., Qian, Z. R., Du, J., Davis, A., Mongare, M. M., Gould, J., Frederick, D. T., Cooper, Z. A., Chapman, P. B., Solit, D. B., Ribas, A., Lo, R. S., Flaherty, K. T., Ogino, S., Wargo, J. A., & Golub, T. R. (2012). Tumour micro-environment elicits innate resistance to RAF inhibitors through HGF secretion. *Nature*, 487(7408), 500-504. <https://doi.org/10.1038/nature11183>
- Suda, K., Onozato, R., Yatabe, Y., & Mitsudomi, T. (2009). EGFR T790M Mutation: A Double Role in Lung Cancer Cell Survival? *Journal of Thoracic Oncology*, 4(1), 1-4. <https://doi.org/10.1097/jto.0b013e3181913c9f>
- Takeuchi, K., & Ito, F. (2011). Receptor Tyrosine Kinases and Targeted Cancer Therapeutics. *Biological and Pharmaceutical Bulletin*, 34(12), 1774-1780. <https://doi.org/10.1248/bpb.34.1774>
- Tao, W., South, V. J., Zhang, Y., Davide, J. P., Farrell, L., Kohl, N. E., Sepp-Lorenzino, L., & Lobell, R. B. (2005). Induction of apoptosis by an inhibitor of the mitotic kinesin KSP requires both activation of the spindle assembly checkpoint and mitotic slippage. *Cancer Cell*, 8(1), 49-59. <https://doi.org/10.1016/j.ccr.2005.06.003>
- Tartarone, A., & Lerosé, R. (2015). Clinical approaches to treat patients with non-small cell lung cancer and epidermal growth factor receptor tyrosine kinase inhibitor acquired resistance. *Ther Adv Respir Dis*, 9(5), 242-250. <https://doi.org/10.1177/1753465815587820>
- Taylor, M. D., Northcott, P. A., Korshunov, A., Remke, M., Cho, Y.-J., Clifford, S. C., Eberhart, C. G., Parsons, D. W., Rutkowski, S., Gajjar, A., Ellison, D. W., Lichter, P., Gilbertson, R. J., Pomeroy, S. L., Kool, M., & Pfister, S. M. (2012). Molecular subgroups of medulloblastoma: the current consensus. *Acta Neuropathologica*, 123(4), 465-472. <https://doi.org/10.1007/s00401-011-0922-z>
- ten Donkelaar, H. J., Lammens, M., Wesseling, P., Thijssen, H. O., & Renier, W. O. (2003). Development and developmental disorders of the human cerebellum. *J Neurol*, 250(9), 1025-1036. <https://doi.org/10.1007/s00415-003-0199-9>
- Tomita, Y., Tatsugami, K., Nakaigawa, N., Osawa, T., Oya, M., Kanayama, H., Nakayama Kondoh, C., Sassa, N., Nishimura, K., Nozawa, M., Masumori, N., Miyoshi, Y., Kuroda, S., Tanaka, S., Kimura, A., & Tamada, S. (2020). Cabozantinib in advanced renal cell carcinoma: A phase II, open-label, single-arm study of Japanese patients. *Int J Urol*, 27(11), 952-959. <https://doi.org/10.1111/iju.14329>
- Tong, C. Y., Hui, A. B., Yin, X. L., Pang, J. C., Zhu, X. L., Poon, W. S., & Ng, H. K. (2004). Detection of oncogene amplifications in medulloblastomas by comparative genomic hybridization and array-based comparative genomic hybridization. *J Neurosurg*, 100(2 Suppl Pediatrics), 187-193. <https://doi.org/10.3171/ped.2004.100.2.0187>

- Topham, C. H., & Taylor, S. S. (2013). Mitosis and apoptosis: how is the balance set? *Curr Opin Cell Biol*, 25(6), 780-785. <https://doi.org/10.1016/j.ceb.2013.07.003>
- Tripolitsiotti, D., Kumar, K. S., Neve, A., Migliavacca, J., Capdeville, C., Rushing, E. J., Ma, M., Kijima, N., Sharma, A., Pruschy, M., McComb, S., Taylor, M. D., Grotzer, M. A., & Baumgartner, M. (2018). MAP4K4 controlled integrin beta1 activation and c-Met endocytosis are associated with invasive behavior of medulloblastoma cells. *Oncotarget*, 9(33), 23220-23236. <https://doi.org/10.18632/oncotarget.25294>
- Trusolino, L., Bertotti, A., & Comoglio, P. M. (2010). MET signalling: principles and functions in development, organ regeneration and cancer. *Nat Rev Mol Cell Biol*, 11(12), 834-848. <https://doi.org/10.1038/nrm3012>
- Varkaris, A., Gaur, S., Parikh, N. U., Song, J. H., Dayyani, F., Jin, J.-K., Logothetis, C. J., & Gallick, G. E. (2013). Ligand-independent activation of MET through IGF-1/IGF-1R signaling. *International Journal of Cancer*, 133(7), 1536-1546. <https://doi.org/10.1002/ijc.28169>
- Vieira, W. A., Weltman, E., Chen, M. J., da Silva, N. S., Cappellano, A. M., Pereira, L. D., Goncalves, M. I., Ferrigno, R., Hanriot, R. M., Nadalin, W., Odone Filho, V., & Petrilli, A. S. (2014). Ototoxicity evaluation in medulloblastoma patients treated with involved field boost using intensity-modulated radiation therapy (IMRT): a retrospective review. *Radiat Oncol*, 9, 158. <https://doi.org/10.1186/1748-717X-9-158>
- von Bueren, A. O., von Hoff, K., Pietsch, T., Gerber, N. U., Warmuth-Metz, M., Deinlein, F., Zwiener, I., Faldum, A., Fleischhack, G., Benesch, M., Krauss, J., Kuehl, J., Kortmann, R. D., & Rutkowski, S. (2011). Treatment of young children with localized medulloblastoma by chemotherapy alone: results of the prospective, multicenter trial HIT 2000 confirming the prognostic impact of histology. *Neuro Oncol*, 13(6), 669-679. <https://doi.org/10.1093/neuonc/nor025>
- Voskamp, M. J., Li, S., van Daalen, K. R., Crnko, S., Ten Broeke, T., & Bovenschen, N. (2021). Immunotherapy in Medulloblastoma: Current State of Research, Challenges, and Future Perspectives. *Cancers (Basel)*, 13(21). <https://doi.org/10.3390/cancers13215387>
- Wang, K., Zhuang, Y., Liu, C., & Li, Y. (2012). Inhibition of c-Met activation sensitizes osteosarcoma cells to cisplatin via suppression of the PI3K-Akt signaling. *Arch Biochem Biophys*, 526(1), 38-43. <https://doi.org/10.1016/j.abb.2012.07.003>
- Wang, Q., Yang, S., Wang, K., & Sun, S. Y. (2019). MET inhibitors for targeted therapy of EGFR TKI-resistant lung cancer. *J Hematol Oncol*, 12(1), 63. <https://doi.org/10.1186/s13045-019-0759-9>
- Weiner, H. L., Bakst, R., Hurlbert, M. S., Ruggiero, J., Ahn, E., Lee, W. S., Stephen, D., Zagzag, D., Joyner, A. L., & Turnbull, D. H. (2002). Induction of medulloblastomas in mice by sonic hedgehog, independent of Gli1. *Cancer Res*, 62(22), 6385-6389. <https://www.ncbi.nlm.nih.gov/pubmed/12438220>
- Wood, G. E., Hockings, H., Hilton, D. M., & Kermorgant, S. (2021). The role of MET in chemotherapy resistance. *Oncogene*, 40(11), 1927-1941. <https://doi.org/10.1038/s41388-020-01577-5>
- Wood, K. C. (2015). Mapping the Pathways of Resistance to Targeted Therapies. *Cancer Research*, 75(20), 4247-4251. <https://doi.org/10.1158/0008-5472.can-15-1248>

- Wu, Y., Li, Z., Zhang, L., & Liu, G. (2019). Tivantinib Hampers the Proliferation of Glioblastoma Cells via PI3K/Akt/Mammalian Target of Rapamycin (mTOR) Signaling. *Med Sci Monit*, 25, 7383-7390. <https://doi.org/10.12659/MSM.919319>
- Wu, Z. X., Yang, Y., Teng, Q. X., Wang, J. Q., Lei, Z. N., Wang, J. Q., Lusvardi, S., Ambudkar, S. V., Yang, D. H., & Chen, Z. S. (2020). Tivantinib, A c-Met Inhibitor in Clinical Trials, Is Susceptible to ABCG2-Mediated Drug Resistance. *Cancers (Basel)*, 12(1). <https://doi.org/10.3390/cancers12010186>
- Xiang, Q., Zhen, Z., Deng, D. Y., Wang, J., Chen, Y., Li, J., Zhang, Y., Wang, F., Chen, N., Chen, H., & Chen, Y. (2015). Tivantinib induces G2/M arrest and apoptosis by disrupting tubulin polymerization in hepatocellular carcinoma. *J Exp Clin Cancer Res*, 34, 118. <https://doi.org/10.1186/s13046-015-0238-2>
- Yap, T. A., Olmos, D., Brunetto, A. T., Tunariu, N., Barriuso, J., Riisnaes, R., Pope, L., Clark, J., Futreal, A., Germuska, M., Collins, D., deSouza, N. M., Leach, M. O., Savage, R. E., Waghorne, C., Chai, F., Garmey, E., Schwartz, B., Kaye, S. B., & de Bono, J. S. (2011). Phase I trial of a selective c-MET inhibitor ARQ 197 incorporating proof of mechanism pharmacodynamic studies. *J Clin Oncol*, 29(10), 1271-1279. <https://doi.org/10.1200/JCO.2010.31.0367>
- Zahnreich, S., & Schmidberger, H. (2021). Childhood Cancer: Occurrence, Treatment and Risk of Second Primary Malignancies. *Cancers (Basel)*, 13(11). <https://doi.org/10.3390/cancers13112607>
- Zhang, Y., Farenholtz, K. E., Yang, Y., Guessous, F., Dipierro, C. G., Calvert, V. S., Deng, J., Schiff, D., Xin, W., Lee, J. K., Purow, B., Christensen, J., Petricoin, E., & Abounader, R. (2013). Hepatocyte growth factor sensitizes brain tumors to c-MET kinase inhibition. *Clin Cancer Res*, 19(6), 1433-1444. <https://doi.org/10.1158/1078-0432.CCR-12-2832>
- Zhang, Y., Xia, M., Jin, K., Wang, S., Wei, H., Fan, C., Wu, Y., Li, X., Li, X., Li, G., Zeng, Z., & Xiong, W. (2018). Function of the c-Met receptor tyrosine kinase in carcinogenesis and associated therapeutic opportunities. *Molecular Cancer*, 17(1). <https://doi.org/10.1186/s12943-018-0796-y>
- Zhang, Y. W., Su, Y., Volpert, O. V., & Vande Woude, G. F. (2003). Hepatocyte growth factor/scatter factor mediates angiogenesis through positive VEGF and negative thrombospondin 1 regulation. *Proc Natl Acad Sci U S A*, 100(22), 12718-12723. <https://doi.org/10.1073/pnas.2135113100>
- Zhong, L., Li, Y., Xiong, L., Wang, W., Wu, M., Yuan, T., Yang, W., Tian, C., Miao, Z., Wang, T., & Yang, S. (2021). Small molecules in targeted cancer therapy: advances, challenges, and future perspectives. *Signal Transduct Target Ther*, 6(1), 201. <https://doi.org/10.1038/s41392-021-00572-w>
- Zomerman, W. W., Plasschaert, S. L., Diks, S. H., Lourens, H. J., Meeuwse-de Boer, T., Hoving, E. W., den Dunnen, W. F., & de Bont, E. S. (2015). Exogenous HGF Bypasses the Effects of ErbB Inhibition on Tumor Cell Viability in Medulloblastoma Cell Lines. *PLoS One*, 10(10), e0141381. <https://doi.org/10.1371/journal.pone.0141381>
- Zou, Z., Tao, T., Li, H., & Zhu, X. (2020). mTOR signaling pathway and mTOR inhibitors in cancer: progress and challenges. *Cell & Bioscience*, 10(1). <https://doi.org/10.1186/s13578-020-00396-1>

